ACTIVATION OF SMALL MOLECULES FOR CYCLOADDITION AND COUPLING REACTIONS OVER TRANSITION METAL CATALYSTS

A THESIS

SUBMITTED TO THE

UNIVERSITY OF PUNE

FOR THE DEGREE OF

DOCTOR OF PHILOSOPHY

IN

CHEMISTRY

BY

RAJENDRA SRIVASTAVA

CATALYSIS DIVISION

NATIONAL CHEMICAL LABORATORY

PUNE - 411 008, INDIA

AUGUST 2005

DEDICATED TO MY BELOVED PARENTS

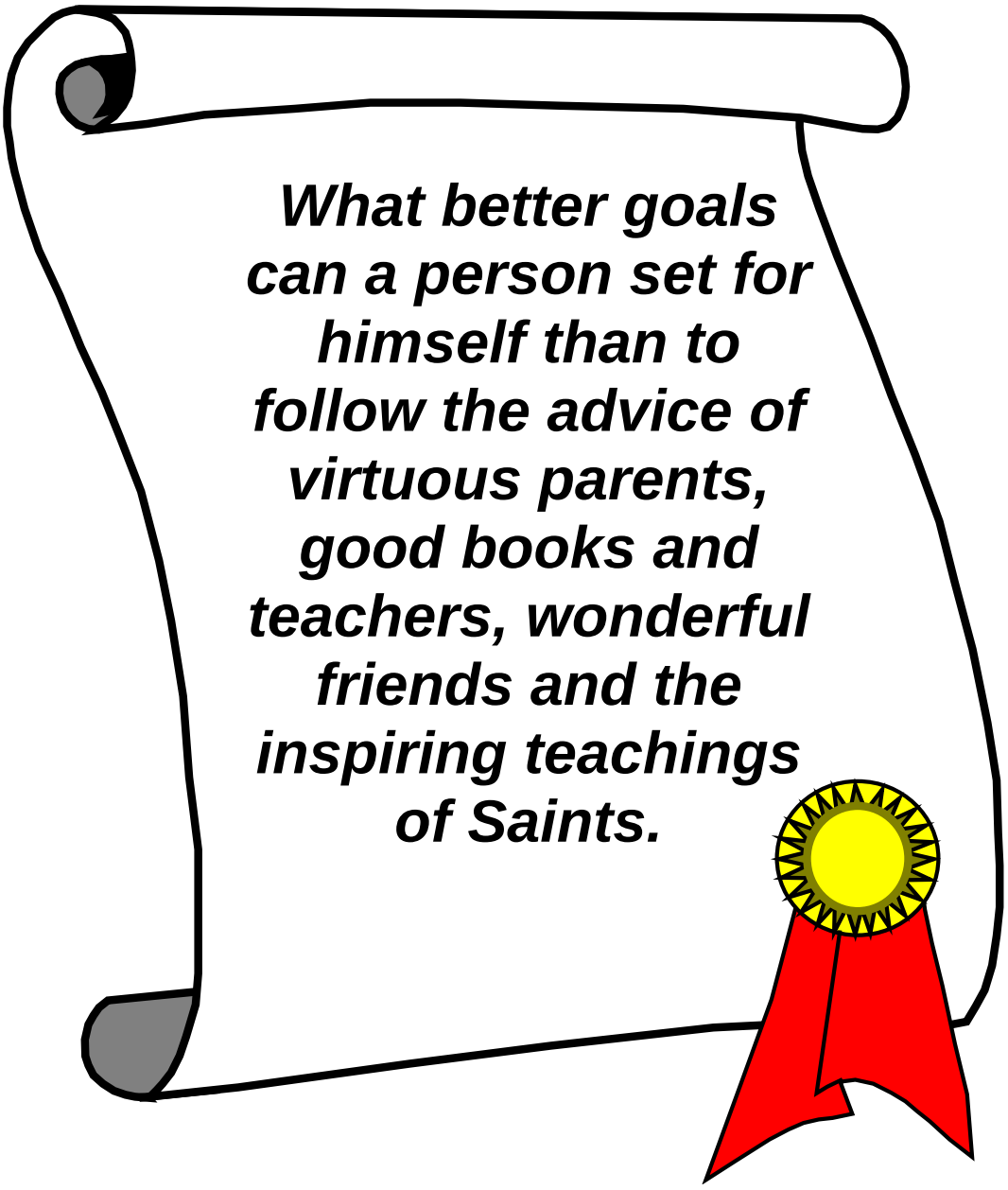

CERTIFICATE

It is certified that the work incorporated in the thesis entitled "**Activation of Small Molecules for Cycloaddition and Coupling Reactions over Transition Metal Catalysts**", submitted by **Mr. Rajendra Srivastava,** for the degree of **Doctor of Philosophy in Chemistry**, was carried out by the candidate under my supervision in the Catalysis Division, National Chemical Laboratory, Pune – 411 008, India. Materials obtained from other sources have been duly acknowledged in the thesis.

Dr. D. Srinivas

Research Guide

Acknowledgments

I acknowledge with respect the valuable guidance and support given by Dr. D. Srinivas, National Chemical Laboratory, Pune during the course of this work. His continuous inspiration and constructive guidance has helped me profoundly during the course of my work. The work presented in this thesis would not have been accomplished without his unfailing attention, constant encouragement and wise counsel.

I wish to express my sincere gratitude and indebtedness to Dr. Paul Ratnasamy, Former Director, National Chemical Laboratory, Pune for his thought provoking discussions and the help rendered throughout the course of this investigation without which I would not have completed this work successfully.

I offer my sincere thanks to Dr. S. Sivasanker, Former Head, Catalysis Division for providing me all the facilities and the kindness extended during my stay at NCL. I thank Dr. Rajiv Kumar, present Head, Catalysis Division for his valuable support. I place on record my gratitude to Dr. S. Sivaram, Director, NCL, Pune for permitting me to carry out research at NCL.

I am grateful to Dr. Mrs. A. J. Chandwadkar, Dr. P. Manikandan, Dr. C. Ramesh, Dr. S. B. Halligudi, Dr. S. A. Pardhy, Dr. C. V. V. Satyanarayana, Dr. A. P. Singh, Dr. V. Ramaswamy, Dr. C. S. Gopinath, Dr. Agashe, Dr. S. V. Awate, Dr. A. A. Belhekar, Dr. S. Umbarkar, Mrs. Violet, N. E. Jacob, Dr. S. P. Mirajkar, Mrs. Renu Pasricha, Mr. Ratnesh Jha, Mr. Katti, Mr. Madu, Mr. Milind and all other scientific and non-scientific staff of catalysis division for their help and cooperation given to me in completing my research work successfully.

It is my pleasure to thank my friends Vasu, Bennur, Suresh, Lakshi, Manju, Pai, Reddy, Sachin, Vaneet, Mahesh, Dr. Venkatathri, Surekha, Smita, Preeti, Dhanashri, Maitri, Sanmitra, Prashant, Sankar, Rohit, Shanbaug, Deu, Vijay, Biju, Thomas, Shiju, Shaylesh, Pranjal, Sonu, Amit, Chidambaram, Surendran, Satyendra, Keshri, Dharmendra, and many others from whom I have received valuable help and friendly working environment.

I am extremely grateful to my parents, sister Madhavi and Mamta, brother-in-laws Suresh and Anand, brother, bhabhi and Pallavi for their love, total support and valuable blessings.

Finally I thank Council of Scientific and Industrial Research, New Delhi and University Grants Commission, New Delhi for financial assistance.

Rajendra Srivastava

CONTENTS

Chapter – 1

General Introduction

1.1. Introduction

Cycloaddition and coupling (C—C, C—O, C—N, C—S etc., for example) are two important classes of atom-efficient reactions available to chemists for the synthesis of a variety of organic compounds of fine and pharmaceutical interest. Transition metals play an important role as catalysts in such organic reactions. They adsorb and activate the reactant molecules prior to formation of cyclized and coupled products. In recent times, there has been a growing concern to carry out organic reactions on solid, heterogeneous catalyst surfaces, as the surfaces have properties that are not duplicated in the solution or gas phase, entirely new chemistry may occur. Additionally, reactions over solid heterogeneous catalysts have the following advantages features: (1) it is often easy to isolate the product and separate the catalyst, and (2) the product selectivity is, often, higher over heterogeneous catalysts than on the related homogeneous catalysts. For these reasons, there has been a considerable interest in the design and development of efficient heterogeneous catalysts and benign catalytic processes. In this thesis, emphasis is given on discovering novel, solid catalysts for (1) cyclic / organic carbonates and carbamates synthesis utilizing carbon dioxide, and (2) carbon-carbon coupling Heck reactions.

1.2. CO_2 - Greenhouse Effect

Carbon dioxide (CO_2) forms 0.034% of the air by volume. The total quantity of carbon present as CO_2, carbonates and hydrogen carbonates in the earth's atmosphere, hydrosphere and lithosphere has been estimated to be 10^{16} tons [1]. Part of the CO_2 is subjected to natural circulation processes that are influenced to some extent by man. Carbon dioxide and water are converted into carbohydrates and oxygen in plant chloroplasts; this photosynthetic process forms organic compounds from low-energy carbon dioxide by utilizing sunlight. A rough estimate has indicated that ca. 200

billion tons of biomass is produced in this way per year. In terms of chemical throughput, photosynthesis is by far the most important synthetic process. The respiration of man and animals and the decomposition of organic substances return CO_2 to the atmosphere in comparable quantities and an equilibrium is, thus, set up [2]. This equilibrium has, however, been considerably shifted in recent years by the activities of man. The increasing demand for energy and the industrial revolution has led to increased combustion of fossil fuels (coal, oil and gas), forming carbon dioxide. No one can be sure to what extent this increased CO_2 emission will affect our environment. There are many indications that the higher CO_2 concentration in the atmosphere can alter the earth's radiation balance and thus, the world climate [3]. The CO_2 levels in the atmosphere have risen by ca., 31% over the last 250 years and these concentrations may double or even triple in the next century.

Greenhouse effect is the phenomenon in which earth's atmosphere traps the heat from the sun and prevents it from escaping into the outer sphere. Earth's atmosphere allows most of the sunlight falls on it to pass through and heat the surface. But the heat radiated from the heated surface cannot pass freely into space, because certain gases called "greenhouse gases" (such as CO_2, CH_4, O_3, CFCs and H_2O vapor) in the atmosphere absorb it. Thus they add to the heating of the atmosphere. The increasing levels of CO_2 (1 ppm per year) are expected to increase the average temperature of the earth by about 2.5 K. This doesn't sound like much, but it could be enough for climatic changes.

1.3. CO_2 Utilization in Chemicals Synthesis

Carbon dioxide recovered from flue stacks and oil wells can be sequestered in oceans in an effort to mitigate CO_2. Alternatively, recovered CO_2 can be used in value-added chemicals synthesis. Presently, CO_2 is used in beverage industry, fire

extinguisher technology, refrigeration, enhanced oil recovery and supercritical CO_2 extraction and cleaning. In inorganic chemical industry, it is used to manufacture Na_2CO_3 or $NaHCO_3$ (the Solvay process), $CaCO_3$, and other carbonates. CO_2 is also used as an acid for the purification of water and in neutralization process. Totally, only 0.7-1.0% of the produced CO_2 is used, and the consumption of chemical industries is about 0.1%. There are several motivations for producing chemicals from CO_2 whenever possible.

(1) CO_2 is a cheap, non-toxic feedstock that can frequently replace toxic chemicals such as phosgene or isocyanates.

(2) CO_2 is a totally renewable feedstock compared to oil or coal.

(3) The production of chemicals from CO_2 can lead to totally new materials such as polymers.

(4) New routes to existing chemical intermediates and products could be more efficient and economical than current methods.

(5) The production of chemicals from CO_2 could have a small but some positive impact on the global carbon balance.

As fossil fuels are being depleted and global warming is becoming severe, renewable energy (solar, electric, wind, hydroelectric, geothermal and biomass) and nuclear energy will become our primary energy sources. Of these future energy sources, only biomass produces fuels directly. The reduction of CO_2 to methanol and methane and other carbon-based fuels using renewable energy sources or nuclear energy would provide a future energy distribution system based on high energy density liquid and gaseous fuels and without any net increase in atmospheric CO_2. This would have a significant impact on future CO_2 emissions, especially from the transportation sector.

CO_2 is generally considered to be a green or environmentally benign solvent. It is relatively non-toxic, non-flammable and naturally abundant. As such, CO_2 has been suggested as a suitable replacement for organic solvents in a number of chemical processes [4].

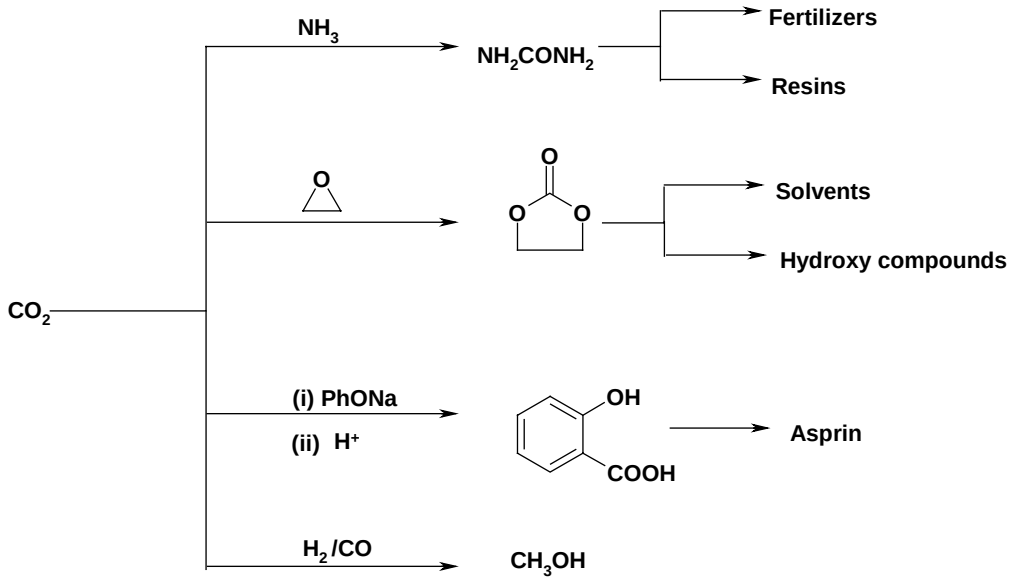

Scheme 1.1. CO_2-based commercial process in current practice.

Approximately 110 megatons of CO_2 are currently used for chemical synthesis annually [5]. There are only four industrial processes that are utilizing CO_2: (1) urea, (2) salicylic acid, (3) cyclic carbonate & polycarbonate, and (4) methanol (Scheme 1.1). The largest of these uses is urea production, which reached approximately 90 million metric tons per year in 1997. Next pilot plant scale based utilization of CO_2 is the production of methanol**.** In addition to these commercial processes (Scheme 1.1) using CO_2 there are a number of reactions currently under study in various laboratories that hold promises (Scheme 1.2). These reactions differ in the extent to which CO_2 is reduced during the chemical transformation [6]. Details of cycloaddition of CO_2 to epoxide in the synthesis of cyclic carbonates and coupling reaction of CO_2 to amines and alkyl halides in the synthesis of carbamates are discussed below in more detail.

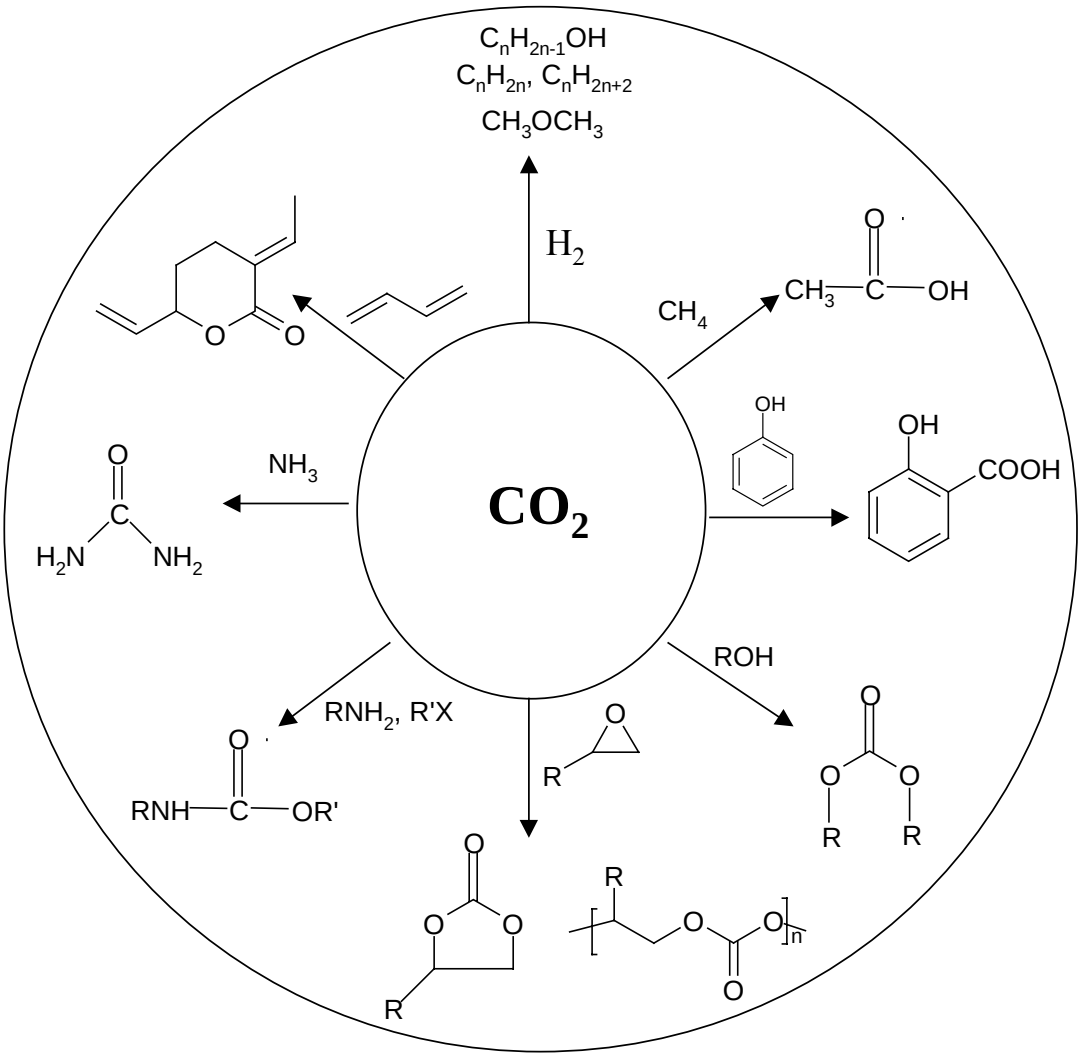

Scheme 1.2. Chemicals synthesized from CO_2.

1.4. Synthesis of Organic Carbonates

There are many possibilities for carbon dioxide to be used as a safe and cheap C_1 component to produce useful organic compounds (Scheme 1.2). Organic carbonates may be divided into two groups *viz.*, cyclic carbonates and linear carbonates. Organic carbonates have a large market value (1.8 Mt/year), as they can be used as solvents, selective reagents, intermediates (for the synthesis of pharmaceutical and agrochemicals), fuel additives and monomers for polymers [7]. These carbonates are commercially synthesized by the following methods.

Phosgenation method. In this method hydroxy compounds dissolved in large excess amount of anhydrous, inert solvent (*ca.*, dichloromethane) are reacted with phosgene ($COCl_2$) in the presence of excess pyridine at or below room temperature. Pyridine acts as an acid acceptor and reacts with phosgene forming an ionic adduct [8]. Nearly all the organic carbonates can be prepared by this method (Scheme 1.3). Symmetrical carbonates are obtained in one step, whereas unsymmetrical (alkyl aryl or substituted alkyl aryl) carbonates are obtained by a two-step reaction. Aromatic hydroxy compounds are much slower to react with phosgene than aliphatic hydroxy compounds [9]. The more acidic hydroxy compounds are less reactive toward phosgene.

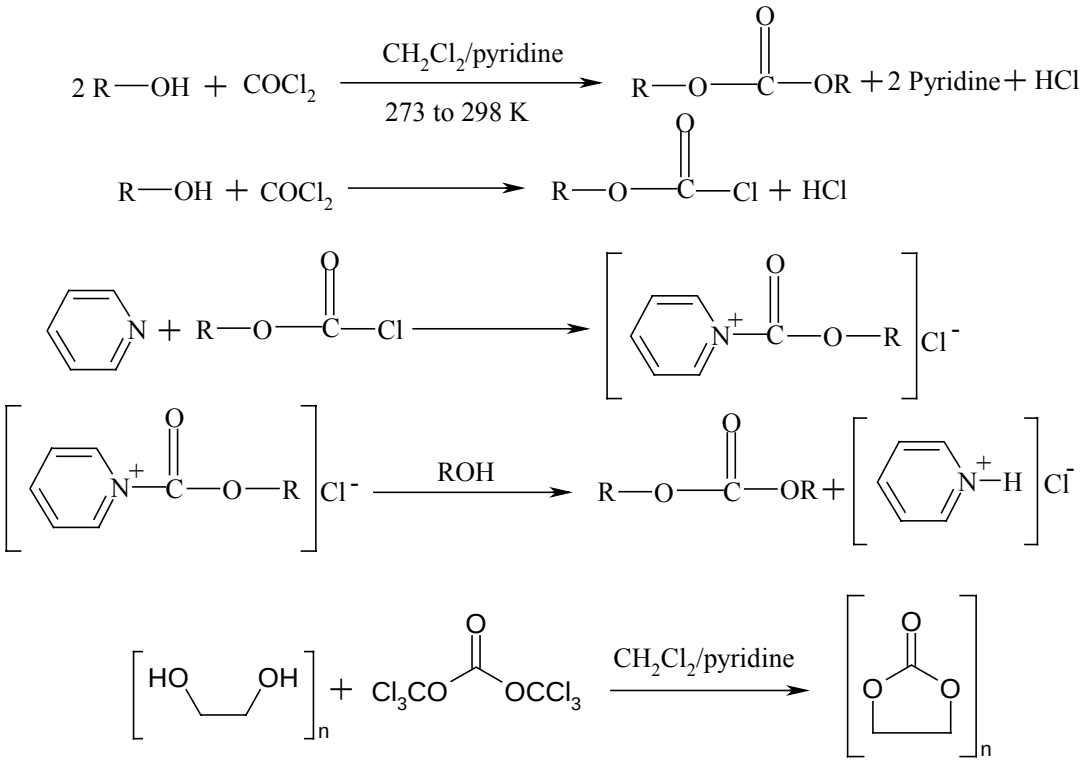

Scheme 1.3. Phosgenation method for cyclic carbonate synthesis

For the preparation of cyclic carbonates from diol, phosgene can be substituted by compounds such as chloroformic acid, trichloromethyl ester (diphosgene) and bis(trichloromethyl) carbonate. For example, 1, 2- and 1, 3-diols are easily converted to

cyclic carbonates with triphosgene in CH_2Cl_2 and pyridine at 343 K [10]. Bisphenol-A is selectively converted to corresponding carbonates under pseudo-high-dilution conditions employing triethylamine catalyst [11]. A variety of carbonates useful as monomers for the preparation of high molecular weight polymers can be synthesized in very high yields by this method. However, the major drawback of this method of carbonates synthesis is that the process involves the use of highly toxic and hazardous chemicals like phosgene and pyridine. At the end of the reaction pyridine has to be neutralized and disposal of the byproduct salt is another major issue.

Oxidative Carbonylation of Alcohols. Dialkyl carbonates can be synthesized by oxidative carbonylation of alcohols in the presence of transition metal compounds (in particular palladium, mercury, and copper) and post-transition metal compounds [12]. In the case of palladium and mercury, however, the reaction does not seem to be selective and involves reduction of the metal, which cannot be reoxidized directly. The reactivity of copper is of greater interest. Romano et al. [13] explored the synthesis of dimethyl carbonate by oxidative carbonylation of methanol using a copper salt such as copper chloride as catalyst. The reaction takes place in two steps, in which cuprous chloride is oxidized to cupric methoxy chloride and this is reduced with carbon monoxide to form dimethyl carbonate; cuprous chloride is regenerated (Scheme 1.4).

$$2\ CuCl + 2CH_3OH + 1/2\ O_2 \longrightarrow 2(CH_3OCu)^+Cl^- + H_2O$$

$$2(CH_3OCu)^+Cl^- + H_2O + CO \longrightarrow (CH_3)_2CO + 2CuCl$$

Scheme 1.4

Dimethyl carbonate is also produced by a continuous gas phase reaction of alkyl nitrites (RONO) with CO in the presence of a catalyst comprised of a platinum halide or a complex with alkali metal or alkaline earth metal halides [14]. Dimethyl carbonate

was produced in 70-80% yield with a selectivity in the range of 80-90%. Dimethyl carbonate is produced industrially by oxidative carbonylation of methanol by Enichem [15], Dow Chemical [16], and Ube Industries Ltd. Enichem synthesis produces dimethyl carbonate at 8800 tons/year [17].

Oxidative carbonylation of phenols with carbon monoxide and molecular oxygen is carried out in the presence of catalysts containing palladium compounds, alkyl ammonium halide, and an organic or inorganic base under a pressure of 4 - 30 MPa, at 373 – 473 K, for 1 - 13 h (Scheme 1.5). Diphenyl carbonate is obtained in 4 - 30% yield with 90 - 96% selectivity [18]. Use of molecular sieves is also found to have favorable effect on yield and selectivity [19]. Diphenyl carbonate, in 39.5% yield, with 99% selectivity, is produced by a continuous process, in a multistage distillation column, in which water formed in the reaction is removed as steam by distillation [20].

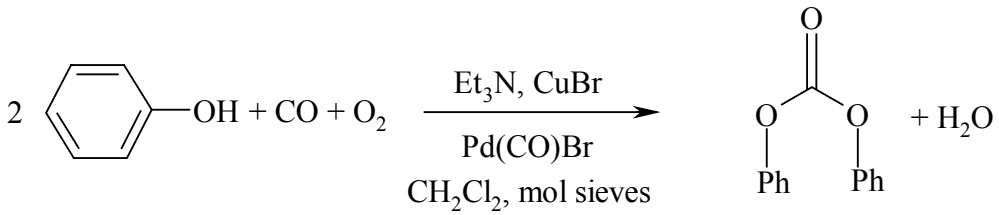

Scheme 1.5

Lower basicity of phenols, expensive catalysts, low yields, and low catalyst turnover efficiencies precluded a commercial process based on oxidative carbonylation of phenols. In this context, it is generally acknowledged that the discovery of a convenient and less expensive route to diaryl carbonates would be a revolutionary development.

Cycloaddition of CO_2 to Epoxides - A Phosgene-free Synthetic Route. An efficient, eco-friendly route for the synthesis of cyclic carbonates involves cycloaddition of CO_2 to epoxides (Scheme 1.6). This reaction is highly atom efficient.

There are several homogeneous and heterogeneous catalyst systems, which catalyze this cycloaddition reaction.

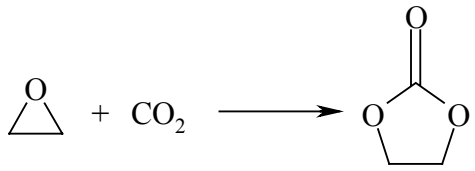

Scheme 1.6

(a) Quaternary ammonium salt, phosphonium salt and group I metal salts-based catalysts. Simple quaternary salts such as alkyl ammonium and phosphonium halides are effective for cyclic carbonate formation from epoxide and CO_2 [21]. Simple metal salts such as KCl and NaOH also catalyze this reaction. In the course of heterogenizing the catalysts, quaternary salts have been immobilized on resins and used as catalysts. BASF [22] and Chimei-Asahi Corporation (Taiwan) have recently announced commercial production based on these heterogeneous catalysts [23]. However, with the commercial quaternary ammonium salt catalyst, the reaction had to be carried out at high temperatures / pressures (30–80 bar) for high carbonate yields.

Rokicki et al. [24] have studied a variety of alkali metal salts alone and in conjunction with crown ether to catalyze the reaction of epoxides and CO_2 to form cyclic carbonates. High yields of cyclic carbonates were detected. Polycarbonates did not form even after 24 h, at 393 K, and 40 bar of CO_2.

(b) M(II) Alkoxide and Carboxalate Catalysts. Among the group 12 metals, Zn(II) complexes have been the most studied [25]. In the light of initial success of a variety of Zn(II) species to catalyze the reaction of epoxide and CO_2 to form polycarbonates, the bulk of research focused on Zn(II) chemistry. A variety of metal carboxalate or alkoxides were reported to catalyze polycarbonate synthesis at relatively mild temperatures (373 K) [26]. Coates et al [27, 28] reported asymmetric alternating

copolymerization with a well-defined Zn-imine oxazoline and β-diiminate zinc methoxide complexes, which showed higher activity under mild conditions. These complexes offer new opportunities for control of molecular weight and block co-polymer synthesis owing to the living nature of the copolymerization. A well-characterized Et_2Zn-amino alcohol complex was also studied for the copolymerization reaction [29]. Various proline derivatives with various substituents have a great effect on the catalytic activity and steroselectivity, suggesting that further optimization of the ligand structure would lead to an achievement of the improved catalyst [30].

(c) Schiff Base Complexes. Metal salen complexes catalyzed the cycloaddition reaction of CO_2 to epoxides in the presence of organic bases like N-MeIm. Among several salen complexes, Cr(III)(salen)Cl, showed high activity and yielded both cyclic carbonate and polycarbonate depending upon the reaction conditions [31]. IR spectroscopy has differentiated these different carbonate compounds. Characteristic IR peak for cyclic carbonate was observed at 1800 cm^{-1} and for polycarbonates at 1750 cm^{-1}. Although weakly active compared to Cr(salen)Cl and Zn-imine complexes, Co(salcy)(OAc) catalyzes polycarbonate formation (with high polymer selectivity and excellent regio-selectivity) by alternative copolymerization of CO_2 to epoxides even in the absence of a co-catalyst [32].

(d) Porphyrine and Phthalocyanine Complexes. Tetraphenylporphinato aluminum methoxide, (TPP)AlOMe, in the presence of 1-methyl imidazole (1-MeIm) activates CO_2 at room temperature and reacts with epoxide to afford corresponding alkylene carbonates [33]. In addition, there have been a variety of other metals, which have been, to a lesser extent, investigated as potential catalysts for the coupling reaction to afford cyclic and polycarbonates. [34]. Co(III)TPP(Cl) showed 50 times higher activity than Co(II)TPP [35].

Metallophthalocyanines, which have similar structural characteristics to that of metalloporphyrinates, also showed high activity for cyclic carbonates synthesis in the presence of Lewis bases such as tributylamine, 1-methylimidazole and triphenylphosphine [36].

(e) Heterogeneous Catalyst Systems. There have been some efforts to develop solid catalysts for this reaction. Below are listed the solid catalysts reported so far for this reaction and their performance.

Mg-Al mixed oxides (with Mg/Al = 5) obtained by calcination of hydrotalcites (673 K) showed high activity for the addition of CO_2 to various epoxides under mild reaction conditions (CO_2 pressure = 5 atm, reaction temperature = 373 K) [37]. Al and Mg act as acid-base sites and the catalyst is reusable. However, the reaction requires longer duration and large amount of catalyst. Additionally it requires solvent like DMF. MgO while retaining the stereoselectivity (99% ee) produced cyclic carbonate in 70% yield in the presence of DMF solvent [38]. Kim et al [39] reported the synthesis of ethene carbonate and propene carbonate over poly(4-vinylpyridine)-supported zinc bromides and iodides, however, the yields were only 30 – 60% (ethene carbonate) and 8 – 10% (propene carbonate), respectively. He et al [40] reported the application of Al phthalocyanine covalently bonded to silica. Polymer-supported chromium porphyrin [41] has been reported as a recyclable catalyst for alternative copolymerization of cyclohexene and carbon dioxide. There has been a report on the use of guanidine anchored to MCM-41 [42]. Although, these catalysts were reusable they exhibited lower activity than the homogeneous analogues [43].

(f) Ionic Liquids. Recently, the use of room temperature ionic liquids as environmentally benign media for catalytic processes or chemical extractions has become widely recognized and accepted. Room temperature ionic liquids have

negligible vapor pressure, excellent thermal stability and special characteristics in comparison with conventional organic and inorganic solvents. Several approaches were made to use them in cyclic carbonate synthesis [44, 45].

Synthesis of Dimethyl Carbonate from CO_2. Direct synthesis of dimethyl carbonate (DMC) from CO_2 and methanol has been reported (Scheme 1.6). Organometallic complexes [46], and modified ZrO_2 [47] have been employed as catalysts for this reaction. This method of DMC synthesis by a non-phosgene route utilizing CO_2 is highly eco-friendly. However, thermodynamics limits the conversion of this reaction. DMC can also be synthesized from CO_2 and ortho-esters [48] or acetals [120]. The disadvantage of this route is the high cost of the raw materials.

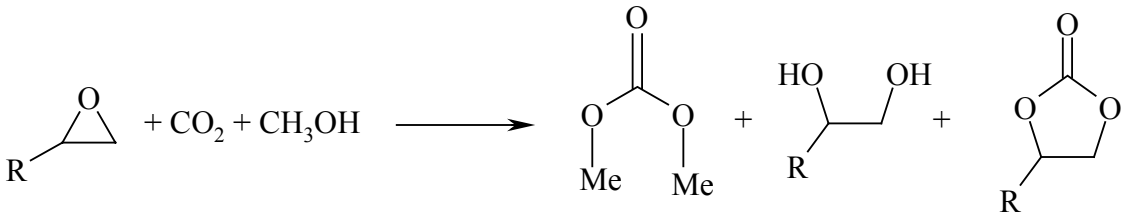

Scheme 1.7

Alternatively, DMC can be synthesized in one-pot, directly from epoxides, methanol and CO_2 (Scheme 1.7). Bhanage et al [49] reported the synthesis of DMC over various metal oxides and obtained propene oxide conversion of 96-99% but DMC selectivity was only 28% (at 8 MPa CO_2 pressure and 423 K). On Mg-smectite [50] the selectivity improved from 28% to 36%. DMC synthesis from supercritical CO_2, ethene oxide (EO) / propene oxide (PO), and methanol over different solid catalysts has been explored [51]. KI supported on ZnO showed high catalytic activity. The activity improved when K_2CO_3 was also present. Very high conversions of epoxides (96-99 %) and DMC selectivity (55-58 %) were obtained over K_2CO_3-KI-ZnO system [52]. Supercritial CO_2 acts as reactant as well as a solvent. Efforts are still in progress to

develop more efficient catalysts for DMC synthesis from CO_2 in a one-pot synthesis reaction.

1.5. Synthesis of Carbamates

The organic carbamates represent an important class of compounds. The carbamate group –(OC(O)NH)- constitutes a typical structural feature of certain classes of natural products. Furthermore, -OC(O)NHR and related groups have frequently been used as control elements in the synthesis of natural products and their precursors. Carbamates find growing interest due to their broad application in several fields such as agrochemical industry [53], pharmaceutical industry [54] and polymer industry [55]. In agrochemical industry, carbamates are used as herbicides, fungicides and pesticides because they are rapidly detoxified and eliminated in animal urine and not concentrated in fat or secreted in the butter, fat or milk. More than billion pounds of polyurethanes are sold annually and they are used in the applications such as foams, coatings, adhesives, plastics and fibers. Of all the preparative methods evolved during the long history of carbamate chemistry, only the following have reached any commercial importance.

Amination of Alkyl Chloroformate. The ammonolysis of an alkyl chloroformate is an excellent general laboratory method for the preparation of carbamate esters (Eqs. (1) and (2)).

$$ROH + COCl_2 \rightarrow ROCOCl + HCl \qquad (1)$$

$$ROCOCl + 2\ NH_3 \rightarrow ROCONH_2 + NH_4Cl \qquad (2)$$

In the presence of a base, most of the alcohols react with phosgene to give the chloroformic ester, which reacts with ammonia or amine to form a desired carbamate. Another method is through the formation of isocyanate as an intermediate (Eqs. (3) and (4)) [56].

$$RNH_2 + COCl_2 \rightarrow RNCO + 2\ HCl \quad (3)$$

$$RNCO + R'OH \rightarrow RNHCO_2R' \quad (4)$$

Reductive Carbonylation of Nitro Aromatics. Even though this route (Eq. (5)) gave promising results, only one third of CO could be used efficiently, and the separation of CO from CO_2 would increase the operation cost. Also, the presence of co-catalyst gives rise to the corrosion problems and makes recovery of the catalyst difficult. [57].

$$RNO_2 + 3\ CO + R'OH \rightarrow RNHCO_2R' + 2\ CO_2 \quad (5)$$

Oxidative Carbonylation of Amines. The reaction (Eq. (6)) is a costly process together with safety problems. The hazards in handling carbon monoxide and oxygen at high pressure make this route difficult to execute [58].

$$RNH_2 + CO + O_2 + R'OH \rightarrow RNHCO_2R' + H_2O \quad (6)$$

Miscellaneous Methods. The commercial production of the urethanes is almost exclusively based on phosgene/isocyanate technology. However, due to the worldwide awareness of pollution hazards of phosgene and pollution prevention laws adapted by governmental agencies, it is most essential to substitute the existing technology by environmentally benign routes. Efforts have continuously been made for the replacement of phosgene route. The following show some promises.

Carbamate synthesis has also been accomplished by several pot-reaction methods.

(1) Hoffmann rearrangement from amides (Eq. (7)) [59]

$$RCONH_2 + R'OH \rightarrow RCO_2NHR' \quad (7)$$

(2) Reaction of chloroformates and amines catalyzed by zinc (Eq. (8)) [60]

$$RNH_2 + ClCOOR' \rightarrow RNHCOOR' \quad (8)$$

Coupling Reaction of Amine, CO_2 and Alkyl Halide. Recently, the use of CO_2 to replace phosgene has been attracting attention of research workers mainly due to its non-hazardous nature in handling under pressure. This method lies on the production of carbamate anion from the reaction of CO_2 with primary amine (Scheme 1.8). Reaction of this anion with various alkyl halides can yield the corresponding carbamate (Scheme 1.8).

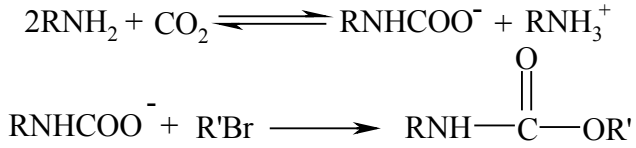

Scheme 1.8

Strong organic bases, crown ethers and onium salts have been found to stabilize the carbamate anion [61]. In addition, ionic liquids and solid bases such as $CsCO_3$ and K_2CO_3 have also been claimed to catalyze the carbamate synthesis through the anion route [62]. However, due to their lower activity very large quantity of such catalysts has to be used. Hence, there still exists a need for an efficient, solid catalyst for the phosgene-free synthesis of organic carbamates.

1.6. Transesterfication

Transesterification is a classic organic reaction frequently used by chemists for the preparation of esters. On some occasions, transesterification is more advantageous than ester synthesis from carboxylic acid and alcohols. For instance, some organic carboxylic acids are sparingly soluble in organic solvents and accordingly, difficult to subject to homogeneous esterification whereas esters are commonly soluble in organic solvents. The ester-to-ester transformation is particularly useful when the parent carboxylic acids are labile and difficult to isolate. Some esters especially methyl and

ethyl esters, are readily or commercially available and thus they serve conveniently as starting materials in transesterification.

Transesterification is a crucial step in several industrial processes such as (i) production of higher acrylates from methylmethacrylate (for applications in resins and paints), (ii) polyethylene terephthalate (PET) from dimethyl terephthalate (DMT) and ethylene glycol (in polyester manufacturing), (iii) intramolecular transesterifications leading to lactones and macrocycles, (iv) alkoxy esters (bio-diesel) from vegetable oils, and (v) co-synthesis of dimethyl carbonate (an alkylating agent, octane booster and precursor for polycarbonates) and ethylene glycol from ethylene carbonate and methanol [63].

Transesterification is a process where an ester is transformed into another through interchange of alkoxy moiety. Since the reaction is an equilibrium process, the transformation occurs essentially by simple mixing of two components. Transesterification reactions are accelerated by acid and base catalysts [64]. The reaction under the acidic or basic conditions does not always meet requirements of modern synthetic chemistry, which need to be highly efficient and selective. It is thus natural that efforts are in progress in search of new catalysts. This section describes the synthesis of dialkyl carbonates, fatty acid esters etc., by transesterification reactions over different solid catalysts.

1.6.1. Dialkyl Carbonates

As discussed in the previous section, dimethyl carbonate (DMC) can be synthesized directly from CO_2 in a one-pot reaction. However, its synthesis by transesterification of cyclic carbonates with alcohols (Scheme 1.9) is more efficient [65].

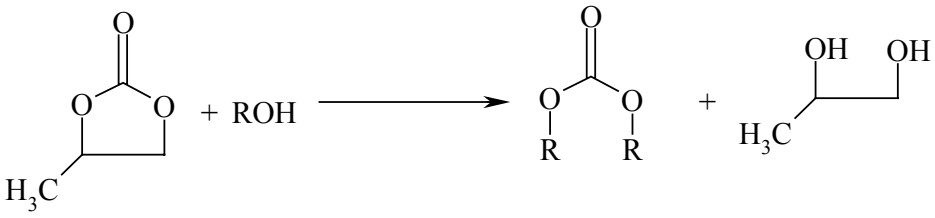

Scheme 1.9

In fact, this method of dimethyl carbonate synthesis is currently practiced by Ashahi Co., Taiwan in their bis-phenol-A-carbonate (BPC) manufacturing process (Scheme 1.10). BPC are conventionally synthesized by phosgene route (interfacial polycondensation). Various heterogeneous catalysts have been reported for DMC synthesis via transesterification route [66]. But these catalysts have not met the industrial requirements. Thus efforts are still in progress to develop selective transesterification catalysts.

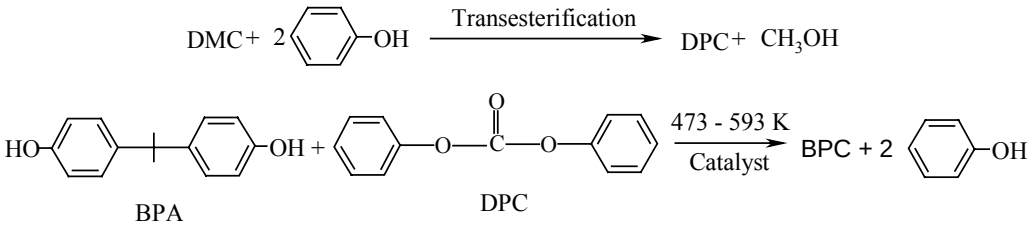

Scheme 1.10

1.6.2. Fatty Acid Alkyl Esters - Biofuel

In recent times, the world has been confronted with energy crisis due to depletion of resources and increased environmental problems. The situation has led to search for an alternative fuel, which should be not only sustainable but also environment friendly. As per an estimate, India consumed about 40.34 million tons of diesel in 2000–2001, which was 43.2% of the total consumption of petroleum products, and two-thirds of the demand was met by import costing about 200 billion rupees [67].

Of the alternative fuels, bio-diesel obtained from vegetable oils holds good promises as an eco-friendly alternative to diesel fuel.

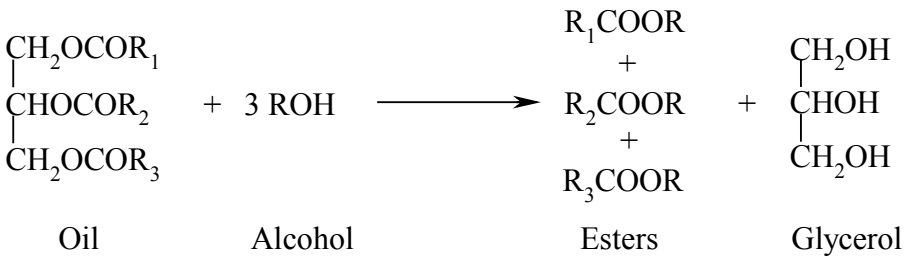

Scheme 1.11

Fatty acid methyl esters, known as bio-diesel, derived from trigycerides by transesterification with methanol have received much attention in recent years (Scheme 1.11) [68]. Vegetable oils are widely available from a variety of sources. Unlike hydrocarbon-based fuels, the sulfur content of vegetable oils is close to zero and hence the environmental damage caused by sulfuric acid is reduced. The main advantages of using bio-diesel are its renewability, better quality exhaust gas emission, biodegradability and given that all the organic carbon present is photosynthetic in origin, it does not contribute to a rise in the level of CO_2 in the atmosphere and consequently to the greenhouse effect.

Vegetable oils, also known as triglycerides, comprise of 98% triglycerides and small amounts of mono- and diglycerides. Triglycerides are esters of three molecules of fatty acids and one molecule of glycerol and contain substantial amounts of oxygen in their structure. The fatty acids vary in their carbon chain length and in the number of double bonds. Different types of oils have different types of fatty acids.

Several processes for bio-diesel fuel production have been developed, among which transesterification using homogeneous alkali-catalysts gives high levels of conversion of triglycerides to their corresponding methyl esters in short reaction times [69]. This process has therefore been widely utilized for bio-diesel fuel production in a

number of countries. Recently, enzymatic transesterification using lipase has become more attractive for bio-fuel production, since the glycerol produced as a by-product can easily be recovered and the purification of fatty methyl esters is simple to accomplish [70]. The main hurdle to commercialize this system is the cost of lipase production. A variety of homogeneous catalysts [71] and alkali loaded heterogeneous catalysts [72] were reported for the production of fatty acid methyl esters. Efforts are still in progress to develop an effective heterogeneous catalyst for bio-diesel and bio-lubricants production.

1.7 . C-C Coupling (Heck) Reactions

Transition metal catalyzed carbon-carbon (C-C) bond formation reactions are among the most important reactions in synthetic organic chemistry. Palladium catalyzed coupling reactions such as Heck reaction [73], Suzuki coupling [74] and Sonogashira reaction [75] are versatile methods practiced in various chemical syntheses in both academic research and chemical industry. Generally, these reactions involve the use of homogeneous palladium catalysts containing *phosphine ligands* to couple (i) aryl or alkyl halides with vinyl functionality (Heck reaction), (ii) aryl halides with aryl boronic acids (Suzuki coupling) and (iii) aryl halides with acetylene (Sonogashira reaction). Heck reaction (Scheme 1.12) is generally catalyzed in solution by palladium species generated from either Pd(0) compounds, such as $[Pd(PPh_3)_4]$ and $[Pd_2(dba)_3]$ or Pd(II) salts, such as the acetate and chloride.

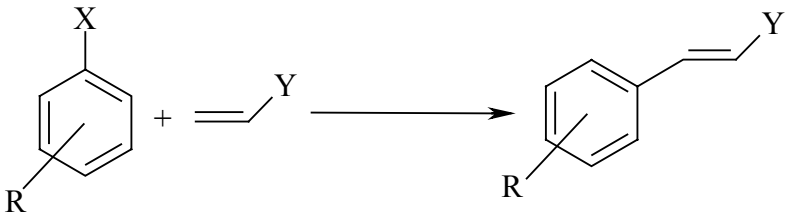

X= I, Br, Cl Y = Ph, OR, COOR', CN.....

R = H, NO_2, CHO, COR, Alkyl, Halide

Scheme 1.12

Some of the recent applications of Heck reactions include the manufacture of Novartis' Prosulfuron^{TM}- an agrochemical, octyl-p-methoxycinnamate - a sunscreen agent, Albemarle's naproxen - an antibiotic and Singulair - an antiasthma drug [76]. The palladium-catalyzed reactions are tolerant to a large number of functional groups and hence, can be employed in a wide range of applications. Most of the reports of Pd-catalyzed coupling described the use of organic bromide, iodide and triflates as substrate. Organic chlorides are the uncommon partners despite the fact that among the halides, chlorides are cheaper and easily available [77]. The low reactivity of chlorides is usually due to the strength of C-Cl bond (bond dissociation energies for Ph-X: Cl = 96 kcal/mol, Br = 81 kcal/mol and I = 65 kcal/mol) which leads to reluctance by aryl chlorides to oxidatively add to Pd(0) centers, a critical step in the palladium-catalyzed coupling reactions. Developing new catalyst systems for aryl chloride activation is a challenging task. Additionally, development of solid catalysts for this reaction would still be more beneficial for the reasons described earlier. Some of the catalysts systems and their performances reported in recent times are as follows.

Davison et al. [78] were the first to describe significant success in the coupling of a non-activated aryl chloride (chloro benzene) with styrene in presence of a Pd-1,2-

bis(diphenylphosphanyl)ethane complex (Pd-dppe) in moderate yields (53%). A lower yield (45%) was obtained when PPh_3 was employed instead of dppe [79]. Among heterogeneous catalysts, Pd/C was employed in the coupling of 4-methoxy bromobenzene with octylacrylate for the industrial production of octylmethoxycinnamate, a common UV-absorber utilized in the manufacture of sunscreen lotions [80]. When graphite was used in place of carbon the reaction required a relatively high amount of Pd (37 mol% with respect to halide) and worked only with iodobenzene and not with bromobenzene [81]. Kaneda et al. [82] reported the activation of chlorobenzene in the coupling with styrene (in methanol at 423 K using Na_2CO_3 as base) in presence of Pd/MgO catalyst. Ying and co-workers reported studies using Nb-MCM-41 [83]. A series of palladium catalysts obtained by ion-exchanging Na or H-zeolite with $[Pd(NH_3)_4]Cl_2$ have also been investigated [84].

1.8. Activation and Mode of CO_2 Coordination

In gaseous state, CO_2 is a linear tri-atomic molecule with $D_{\infty h}$ symmetry. The difference in the electronegativity of carbon (2.5) and oxygen (3.5) generates negative polarization on the oxygen atom and partial positive charge on the central carbon atom. Thus, carbon dioxide is the molecule with multiple reactive sites: the carbon is a Lewis acid center (or electrophilic center) and oxygens are weak Lewis bases (or nucleophilic centers). Upon coordination to metals it adopts a bent structure with O-C-O angle varying from 101^0 to 136^0 [85]. Different modes of CO_2 coordination have been proposed (Scheme 1.13) and some of them have been experimentally (X-ray) confirmed [86]. Due to the instability of metal-CO_2 adduct, it may not always be possible to determine the single crystal X-ray structure of the CO_2-adduct. Optical spectroscopy (Infrared and Raman) provides a great deal of information about the mode

of CO_2 coordination. This technique can be applied even for weakly the stable metal-CO_2 adducts.

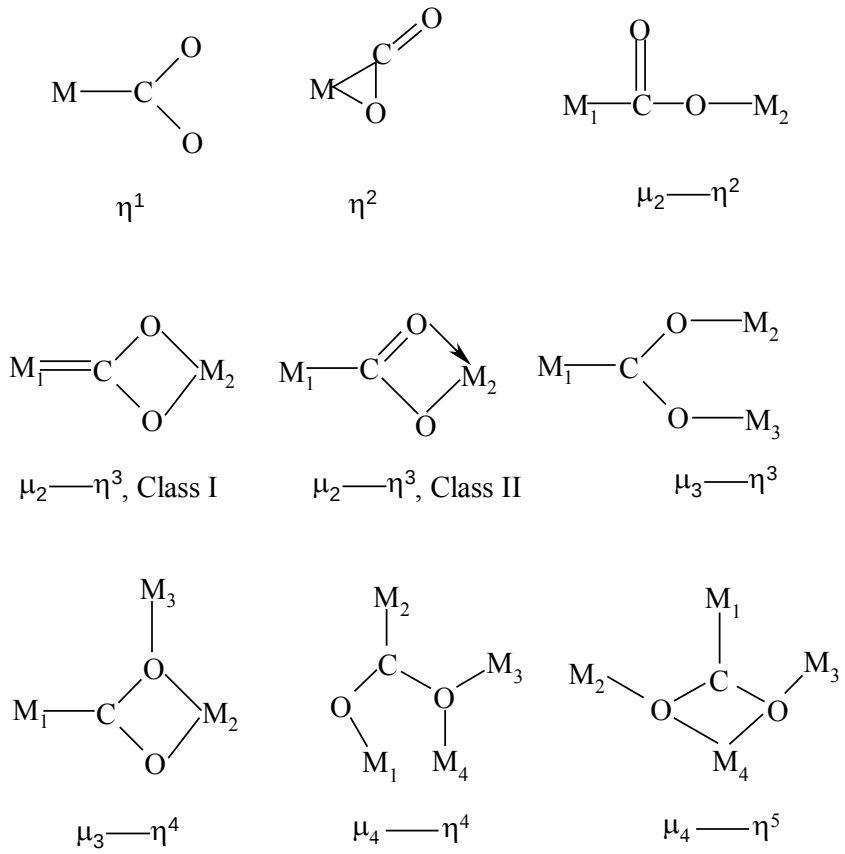

Scheme 1.13. Various modes of CO_2 coordination

A linear tri-atomic CO_2 molecule has three fundamental modes of vibration (ν_1, ν_2 and ν_3) (Scheme 1.14). By convention, ν_1 and ν_3 are referred to as symmetric and asymmetric C—O stretching modes whereas ν_2 is a degenerate C—O deformational mode. The centro-symmetrical nature of free CO_2 molecules leads to mutual exclusion restriction on the vibrational activities and as a result ν_1 is Raman active and ν_2 and ν_3 are IR active. Gaseous CO_2 molecules shows vibrational bands at 1285 and 1388 cm^{-1} due to ν_1, 667 cm^{-1} due to ν_2 and 2349 cm^{-1} due to ν_3. Apart from the weak bands due to natural abundance $^{13}CO_2$ and overtone combination bands, a classic Fermi-resonance between ν_1 and $2\nu_2$ at 1285/1388 cm^{-1} is observed in the Raman spectrum. A

chemisorbed or complexed CO_2 molecule shows asymmetric (ν_3) and symmetric (ν_1) C—O stretching vibration bands at 1750 – 1500 and 1350 – 1150 cm^{-1}, respectively, depending on the mode of CO_2 coordination. The position and number of vibrational bands indicate a marked decrease in both the C—O bond order and the symmetry of the tri-atomic species upon complexation.

The position of the C—O stretching band is sensitive to the mode of coordination. For η^1–C coordination, the asymmetric stretching band (ν_{asym} or ν_3) occurs in the range 1650-1750 cm^{-1} and symmetric stretching band (ν_{sym} or ν_1) occurs in the range 1280-1180 cm^{-1}. For η^1–O coordination, IR bands are observed at 1751, 1221, 739 and 611 cm^{-1}. The η^2-coordination, the ν_{asym} band is observed at much higher values and ν_{sym} band at lower values. The IR bands for a typical η^2-coordinated adduct are observed at 1780-1620, 1300-1100, 900-800 and 600-400 cm^{-1} [87]. For η^1–C coordination, ν_3 - ν_1 is less than or equal to 400 cm^{-1}, for η^2–(C, O) coordination, this splitting is more than 500 cm^{-1}. For penta-coordinated metal complexes ν_3 - ν_1 is a little greater than 400 cm^{-1} while for the hexa-coordinated complexes this difference is less than or equal to 300 cm^{-1} [88]. Hence, based on the difference between ν_3 and ν_1 values in optical spectroscopy, the mode of CO_2 coordination can be estimated. However, a caution is needed in the structural estimation based on optical spectroscopy.

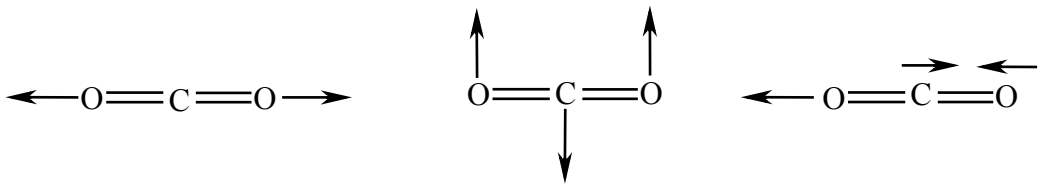

ν_1 (Raman active) (1285, 1388 cm^{-1})

ν_2 (IR active) (667 cm^{-1})

ν_3 (IR activee) (2349 cm^{-1})

Scheme 1.14. Vibrational stretching modes of CO_2

1.9. Acid-Base Properties – Solid Catalysts

Acidity of solid catalysts is of two types: (a) Lewis acidity and (b) Brönsted acidity. If the active metal sites are capable of accepting a lone pair of electrons from the substrate molecules and activate them for further reaction, such acidic sites are said to be Lewis acidic sites. Brönsted acid sites, in particular in zeolites, are created because of the substitution of Al^{3+} for Si^{4+} ions in the zeolite framework. The strength, type and amount of acidity can be determined using probe molecules by temperature programmed desorption (TPD) and infrared (IR) spectroscopy techniques.

In a TPD technique, basic, volatile, probe molecules such as NH_3, pyridine, quinoline and n-butylamine are initially allowed to adsorb on an activated solid catalyst at a defined temperature. The adsorbed molecules are then allowed to desorb by heating the catalyst material in a programmable manner. The amount of desorbed gas is detected and analyzed. Based on the amount of base molecules desorbed the total acidity and the relative strength of the acid sites can be determined.

IR spectroscopy of ammonia and pyridine adsorbed on solid surfaces distinguishes Brönsted and Lewis acid sites [89]. In the case of IR studies of adsorbed pyridine, H-bonded pyridine groups show characteristic IR peaks at around 1595 and 1445 cm^{-1}. Pyridine-coordinated to weak Lewis acid sites show bands at 1580 and 1485 cm^{-1} and strong Lewis acid sites show IR bands at 1623 and 1455 cm^{-1}. The Brönsted acid sites can be clearly differentiated by their characteristic pyridine IR bands at 1639 and 1546 cm^{-1} [89].

Basic properties to solids can be imparted by alkali and alkaline metal oxides/hydroxides deposition on the surfaces. Alternatively, the basic sites (on silica, for example) can be created by surface modifications with basic organic molecules (N-bases). CO_2, an acid molecule, can be used as a probe to determine the strength and

amount of basic sites. TPD of CO_2 and diffuse reflectance infrared Fourier transform (DRIFT) spectroscopy provide valuable information on basic sites.

In CO_2-TPD studies, CO_2 is adsorbed on an activated catalyst surface and then its desorption characteristics as a function of temperature are determined. CO_2 activated on the catalysts surface forms various activated CO_2 species such as carbonates, carbamates and bicarbonates. Depending on their mode of coordination (mono / bidentate), characteristic IR peaks are observed in DRIFT spectroscopy.

1.10. Scope and Objectives of the Present Work

As noted from the earlier sections, activation and utilization of CO_2 in chemicals synthesis is of great importance and is an area of contemporary research in catalysis. Syntheses of organic carbonates (alkylene carbonate precursors of polycarbonates) and alkyl / aryl carbamates (precursors of polyurethanes) are particularly more interesting as CO_2 can be used as a replacement for phosgene in their synthesis. The CO_2-based manufacturing processes of carbonates and carbamates are eco-friendly and non-hazardous. Additionally, they lead to the most efficient way of CO_2 utilization. Use of solid, heterogeneous catalysts, makes the process still more eco-friendly. Although, there have been efforts toward using solid catalysts, a majority of the synthetic processes face draw backs of requirement of a large amount of catalyst, additional co-catalysts, solvents, high temperatures, high pressures and long reaction times. Hence, there is a need to develop more efficient, reusable, solid catalysts for the CO_2-based organic transformations. This requires a detailed understanding of the adsorption of CO_2 and other substrate molecules and the sites for CO_2 activation.

While dialkyl carbonates (dimethyl carbonate, for example) can be synthesized in a one-pot reaction directly from CO_2, their synthesis by transesterification of cyclic carbonates with alcohols is more efficient. This method of organic carbonates synthesis

is again eco-friendly and a phosgene-free process. However, one of the challenges is to develop an efficient, reusable, solid catalyst that can result high dialkyl carbonate yields.

Bio-fuel produced from vegetable feedstocks by transesterificaiton reaction is more environmental friendly than the conventional pertroleum-based fuel. There are already some commercial plants in Europe for bio-diesel production. However, there is a need to develop more efficient, solid catalyst for this reaction.

By now it is established that chemicals synthesis by C-C coupling (Heck reaction, for example) is an atom-efficient route. A majority of the reports employ homogeneous metal complexes as catalysts for this reaction. Further, activated halides like iodobenzene and to some extent bromobenzene are used as coupling agents for C-C bond formation with olefins. However, major challenges in this area to make the synthesis more economical lies in the development of efficient, heterogeneous catalysts that activate cheaper chloroarenes.

Accordingly, the objective of the present study is to develop efficient, solid catalysts (1) to activate CO_2 for its utilization in the synthesis of cyclic carbonates and alkyl/aryl carbamates by reactions with epoxides and amines, respectively, (2) for the synthesis of dialkyl carbonates by transesterification of cyclic carbonates with alcohols, (3) for the synthesis of fatty acid alkyl esters (bio-fuel) by transesterification of vegetable oils with alcohols and (4) for activation of aryl chlorides for C-C forming reactions with olefins. It is also an objective to investigate active sites on various solid catalysts for CO_2 activation using spectroscopic and TPD techniques. In other words, the work conducted in this thesis aims to contribute towards green and sustainable catalytic processes.

1.11. Organization of the Thesis

The thesis is divided into seven chapters including Chapter 1 on general introduction.

Chapter 2 describes synthetic methodologies of various catalysts used in the present study and their characterization by various physicochemical techniques. The various catalysts investigated in the present work include:

(1) Titanosilicate molecular sieves (microporous TS-1, mesoporous Ti-MCM-41 and Ti-SBA-15 and amorphous TiO_2-SiO_2),

(2) Zeolite-Y-encapsulated metal phthalocyanines (MPc-Y; M = Cu^{2+}, Ni^{2+}, Co^{2+} and Al^{3+}),

(3) Organic-inorganic hybrids (as-synthesized H-Al-beta and Si-MCM-41),

(4) Organo-functionalized, ordered mesoporous materials (amine-, imidazole-, guanine- and adenine-functionalized (Ti/Al)-SBA-15),

(5) Pd-loaded silicoaluminophosphates (Pd-SAPO-31, Pd-SAPO-11 and Pd-SAPO-41),

(6) Homogeneous copper complexes of cyclic and acyclic ligands (Cu-phenanthroline, Cu-bipyridine, Cu-salen, Cu-phthalocyanine, Cu-tetraphenylporphyrin), and

(7) Solid double metal cyanide catalysts of Fe and Zn.

Chapter 3 deals with the phosgene-free synthesis of cyclic carbonate precursors of polycarbonates over the above-mentioned catalysts. Cyclic carbonates including chloropropene carbonate, propene carbonate, styrene carbonate and n-butene carbonate were synthesized at mild reaction conditions by cycloaddition reaction of CO_2 with the oxirane ring of corresponding epoxides *viz.,* epichlorohydrin, propene oxide, styrene

oxide and *n*-butene oxide, respectively. The active sites for CO_2 and epoxide activation over these catalyst systems were investigated.

Chapter 4 reports the synthesis of alkyl and aryl carbamates over solid catalyst systems. A variety of carbamates were synthesized by reacting amines (butyl amine, hexylamine, octylamine, dodecyl amine, cyclohexyl amine, benzylamine, aniline, 2,4,6-trimethylaniline and cyclododecylamine), CO_2 and *n*-butyl halide (n-BuX, X = Cl and Br). Catalytic activities of titanosilicates, encapsulated metal phthalocyanines, organo-inorganic hybrids and organo-functionalized mesoporous silica for this reaction were investigated. Influence of reaction parameters (temperature, pressure, solvent, amount of catalyst, amine to bromide ratio etc.) on catalytic activity was examined.

Chapter 5 describes the synthesis of a variety of dialkyl carbonates by transesterification reaction of cyclic carbonates with different alcohols. Titanosilicates and double metal cyanides (Fe-Zn) were used as catalysts. The activity of double metal cyanide catalysts for the transesterification of triglycerides of vegetable oils into fatty acid esters for bio-diesel and lubricant applications was also investigated. Vegetable oils such as coconut oil, sunflower oil, soyabean oil, margarine oil were transesterified with C1 to C8-alcohols.

Chapter 6 reports activation of olefins and aryl chlorides for C-C coupling (Heck) reaction over Pd/Cu/Ni-loaded silicoaluminophosphates. SAPO-31, SAPO-11 and SAPO-41 with varying pore dimensions and acidity are used as supports.

Chapter 7 provides an overall summary and conclusion of the work presented in the thesis.

By and large, the thesis reports novel, solid catalyst systems for benign, phosgene-free synthesis of cyclic carbonate precursors of polycarbonates and carbamates precursors of polyurethanes. Efficient catalysts are reported also for several

transesterification reactions. Reusable catalysts are developed for carbon-carbon coupling reactions. The work presented in the thesis contributes to the area of green chemistry and sustainable technology.

1.12. References

1. E. Hillenbrand, in Ullmanns Encyclopedia for Technical Chemistry Vol 14, 4th Eds. Verlag Chemie, Weinheim 1977, p 569.
2. W.C. Clark, Carbon dioxide review, university press, Oxford, 1982.
3. (a) J. Lemons, J. Environ. Sci. 28 (1985) 60. (b) T. M. L Wigley, P. D. Jones, Nature (london) 292 (1981) 205.
4. P. T. Anatas, T.C. Williamson, Green Chemistry, ACS Symposium Series 626, Am. Chem. Soc.,Washington, DC, 1996, p-1.
5. M. Aresta, Rucadi, Recovery and utilization of carbon dioxide, EU-Report, 1999.
6. H. Arakawa, M. Aresta, J. N. Armor, M. A. Barteau, E. J. Beckman, A. T. Bell, J. E. Bercaw, C. Creutz, E. Dinjus, D. A. Dixon, K. Domen, D. L. DuBois, J. Eckert, E. Fujita, D. H. Gibson,W. A. Goddard, D. W. Goodman, J. Keller, G. J. Kubas, H. H. Kung, J. E. Lyons, L. E. Manzer, T. J. Marks, K. Morokuma, K. M. Nicholas, R. Periana, L. Que, J. RostrupNielson, W. M. H. Sachtler, L. D. Schmidt, A. Sen, G. A. Somorjai, P. C.Stair, B. R. Stults, W. Tumas, Chem. Rev. 101 (2001) 953.
7. K. Biggadike, R.M. Angell, C.M. Burgess, R.M. Farrekk, A.P. Hancick, A.J. Harker, A.J. Irving, W.R. Irving, C. Ioannou, P.A. Procopiou, R.E. Shaw, Y.E. Solanke, O.M.P. Singh, M.A. Snowden, R. Stubbs, S. Walton, H.E. Weston, J. Med. Chem. 43 (2000) 19.
8. Ger. Patent 116, 386 (Chemische Fabrick Von Heyden) 1900 Friedl, 1904, 6, 1160
9. H. Schnell, (Farbenfabriken Bayer AG) Chemistry and Physics of Polycarbonates; Interscience Publishers, New York 9 (1964) 91.
10. (a) A. R. Chopin, J. W. Roger, J. Am. Chem. Soc. 70 (1948) 2967. (b) R. M. Burk, M. B. Roof, Tetrahedron Lett. 34 (1993) 395.
11. D. J. Brunelle, T. G. Shannon, Macromolecules 24 (1991) 3035.
12. (a) D. M. Fenton, P. J. Steinwand, J. Org. Chem. 39 (1974) 701. (b) M. Graziani, P. Uguagliati, G. Carturan, J. Organomattalic Chem. 27 (1971) 275.
13. U. Romano, R. Tssei, M. M. Massi, P. Rebora, Ind. Eng. Chem. Prod. Res. Dev.

19 (1980) 396.

14. (a) K. Nishihira, S. Tanaka, K. Kodama, T. Kaneko, (Ube Ind. Ltd.) Eur. Pat. Appl. EP. 501,507, 1992; Chem. Abstr. (1992) 117, 194021k. (b) H. Landscheidth, A. Klausener, E. Wolters, H. Blank, U. Birkenstock, (Bayer AG) Eur. Pat. Appl. EP. 523,508, 1991; Chem. Abstr. 1993, 118, 147196g. (c) S. Fukuoka, (Asahi Chem. Ind. Co. Ltd.) Jap. Pat. 04,257,546, 1992; Chem. Abstr. 1993, 118, 38598u.
15. M. M. Mauri, U. Romano, Chim. Oggi. 1983, October, 33.
16. Chem. Eng. News 1987, Sept. 28, 26.
17. Eur. Chem. News 1989, Nov. 13, 44.
18. (a) J. E. Hallgren, (General Electric Co.) U.S. Pat. 4,096,168, 1978; Chem. Abstr. 1978, 89, 42830p. (b) J. E. Hallgren, (General Electroc Co.) U.S. Pat. 4,349,485, 1982; Chem. Abstr. 1981, 94, 180263k. (c) T. C. T. Chang, (General Electric Co.) EP-A 3 50 700, 1988; Chem. Abstr. 1990, 113, 40168u. (d) R. P. Joyce, J. A. King (Jr.), E. J. Pressman, (General Electric Co.) U.S. Pat. 5,231,210, 1993; Chem. Abstr. 1993, 119, 252566w.
19. S. Fukuoka, H. Ogawa, T. Watanabe (Asahi Chem. Ind. Co. Ltd.) Jap. Pat. 01 16 551, 1989; Chem. Abstr. 1990, 112, 76618j.
20. J. A. King (Jr.), P. D. Mckenzie, E. J. Pressman, (General Electric Co.) PCT Int. Appl. WO 93 03,000, 1993; U.S. Appl. Pat.737, 109, 1991; Chem. Abstr. 1993, 119, 183316a.
21. (a) A. Behr, Carbon Dioxide Activation by Metal Complexes, VCH Publishers, 1988. p-91. (b) N. Kihara, N. Hara, T. Endo, J. Org. Chem. 58 (1993) 6198.
22. Filtration Industry Analyst 1999 (Issue No. 27, June 1999) 2.
23. S. Fukuoka, M. Kawamura, K. Komiya, M. Tojo, H. Hachiya, K. Hasegawa, M. Aminaka, H. Okamoto, I. Fukawa, S. Konno, Green Chem. 5 (2003) 497.
24. A. Rokicki, W. Kuran, B.P. Marcinick, Monatsch. Chem. 115 (1984) 205.
25. D. J. Darensbourg, M. W. Holtcamp, B. Khandelwal, K. K. Klausmeyer, J. H. Reibenspies, J. Am. Chem. Soc. 117 (1995) 538.
26. (a) W. Kuran, T. Listos, Macromol. Chem. Phys., 195 (1994) 977. (b) D. J. Darensbourg, J. R. Wildeson, J. C. Yarbourgh, Inorg. Chem. 41 (2002) 973.
27. M. Cheng, N. A. Darling, E. B. Lobkovsky, G. W. Coates, Chem. Commun. (2000) 2007.
28. M. Cheng, D. R. Moore, J. J. Reczek, B. M. Chamberlain, E. B. Lobkovsky, G. W.

Coates, J. Am. Chem. Soc. 123 (2001) 8738.

29. K. Nakano, K. Nozaki, T. Hiyama, J. Am. Chem. Soc. 125 (2003) 5501.
30. R. L. Paddock, S. T. Nguyen, J. Am. Chem. Soc. 123 (2001) 11498.
31. Z. Qin, C. M. Thomas, S. Lee, G. W. Coates, Angew. Chem. Int. Ed. 42 (2003) 5484.
32. J. H. Jung, M. Ree, T. Chang, J. Polymer Science: Polym. Chem. 37 (1999) 3329.
33. W. J. Kruper, D. D. Dellar, J. Org. Chem. 60 (1995) 725.
34. (a) R. l. Paddock, Y. Hiyama, J.M. Mckay, S. T. Nguyen, Tetrahedron Lett. 45 (2004) 2023. (b) X-B Lu, Y. Wang, Angew Chem. Int. Ed. 43 (2004) 3574.
35. (a) K. Kasuga, T. Kato, N. Kabata, M. Handa, Bull. Chem. Soc. Jp. 69 (1996) 2885. (b) D. Ji, X Lu, R He, Appl. Catal. A: Gen. 203 (2000) 329.
36. K. Yamaguchi, K. Ebitani, T. Yoshida, H. Yoshida, K. Kaneda, J. Am. Chem. Soc. 121 (1999) 4526.
37. T. Yano, H. Matsui, T. Koike, H. Ishiguro, H. Fujihara, M. Yoshihara, T. Maeshima, Chem. Commun. (1997) 1129.
38. H.S. Kim, J.J. Kim, H.N. Kwon, M.J. Chung, B.G. Lee, H.G. Jang, J. Catal. 205 (2002) 226.
39. X.-B. Lu, H. Wang, R. He, J. Mol. Catal. A: Chem. 186 (2002) 33.
40. L. M. Stamp, S. A. Mang, A. B. Holmes, K. A. Knights, Y. R. de Miguel, I. F. McConey, Chem. Commun. (2001) 2502.
41. A. Barbarini, R. Maggi, A. Mazzacani, G. Mori, G. Sartori, R. Sartorio, Tetrahedron. Lett. 44 (2003) 2931.
42. (a) J. Peng, Y. Deng, New J. Chem. 25 (2001) 639. (b) H. Kawanami, A. Sasaki, K. Matsui, Y. Ikushima, Chem. Commun. (2003) 896. (c) H.S. Kim, J.J. Kim, H. Kim, H.G. Jang, J. Catal. 220 (2003) 44.
43. J. Sun, S-I Fujita, B. M Bhanage, M. Arai, Catal. Commun. 5 (2004) 83.
44. (a) J.C. Choi, T. Sakakura, T. Sako, J. Am. Chem. Soc. 121 (1999) 3793. (b) S.I. Fujita, B.M. Bhanage, Y. Ikushima, M. Arai, Green Chem. 32001) 87.
45. (a) K.T. Jung, A.T. Bell, Top. Catal. 20 (2002) 97. (b) J.C. Choi, L.N. He, H. Yasuda, T. Sakakura, Green Chem. 4 (2002) 230. (c) K. Tomishige, K. Kunimori, Appl. Catal. A: Gen. 237 (2002) 103.
46. N.S. Isaacs, B. O'Sullivan, C. Verhaelen, Tetrahedron 55 (1999) 11949.
47. T. Sakakura, J.C. Choi, Y. Saito, T. Masuda, T. Sako, T. Oriyama, J. Org. Chem.

64 (1999) 4506.

48. B.M. Bhanage, S-I Fujita, Y. Ikushima, K. Torii, M. Arai, Appl. Catal. A: Gen. 219 (2001) 259.
49. B.M. Bhanage, S-I Fujita, Y. Ikushima, K. Torii, M. Arai, Green Chem. 5 (2003) 71.
50. Y. Chang, T.J. Jiang, B. Han, Z. Liu, W. Wu, L. Gao, J. Li, H. Gao, G. Zhao, J. Huang, Appl. Catal. A.: Gen. 263 (2004) 179.
51. (a) T-T Wu, J. Huang, N. D. Arrington, G. M. Dill, J. Agric Food. Chem. 35 (1987) 817. (b) T. Kato, K. Suzuki, J. Takahashi, K. Kamoshita, J. Pesticide Sci. 9 (1984) 489.
52. (a) P. Adomes, F. A. Baron, Chem. Rev. 65 (1965) 567. (b) R. G. Karki, V. M. Kulkarni, Bioorg. Med. Chem. 9 (2001) 3153.
53. T.-T. Wu, J. Huang, N.D. Arrington, G.M. Dill, J. Agric. Food. Chem. 35 (1987) 817.
54. (a) D. P. N Satchell, R. S. Satchell, Chem. Soc. Rev. 4 (1975) 231. (b) S. Raucher, D. S. Jones, Synth. Commun. 15 (1985) 1025.
55. (a) E. Alessio, G. Mestroni, J. Organomet. Chem. 291 (1985) 117. (b) A. Bassoli, R. Rindone, S. Tollari, J. Mol. Catal. 61 (1990) L15. (c) F. Ragini, S. Cenini, J. Mol. Catal. A: Chem. 161 (2000) 31.
56. (a) F. Shi, Y. Deng, T. Sima, H. Yang, J. Catal. 203 (2001) 525. (b) B. Chen, S. S. C. Chuang, J. Mol. Catal. A: Chem. 195 (2003) 37. (C) S. Fukuoka, M. Chono, M. Kohno, J. Org. Chem. 49 (1984) 1458.
57. Y. Matsumura, T. Maki, Y. Satoh, Tetrahedron Lett. 38 (1997) 8878.
58. J.S. Yadav, G. Reddy, M. Reddy, H. Meshram, Tetrahedron Lett. 39 (1998) 3259.
59. (a) W. McGhee, D. Riley, K. Christ, Y. Pan, B. Parnas, J. Org. Chem. 60 (1995) 2820. (b) F. Shi, J. Peng, Y. Deng, J. Catal. 219 (2003) 372. (c) M. Yoshida, N. Hara, S. Okuyama, J. Chem. Soc., Chem. Commu. (2000) 151. (d) A. Inesi, V. Mucciante, L. Rossi, J. Org. Chem. 63 (1998) 1337. (e) M. Aresta, E. Quaranta, Tetrahedron 48 (1992) 1515.
60. (a) I. Vauthey, F. Valot, C. Gozzi, F. Fache, M. Lamaire, Tetrahedron Lett. 41 (2000) 6347. (b) F. Shi, Y. Deng, J. Catal. 211 (2002) 548. (c) A. Wolf, F. Schuth, Appl. Catal. A 226 (2002) 1.
61. U. Schuchardt, R. Sercheli, R.M. Vargas, J. Braz. Chem. Soc. 9 (1998) 199.

62. J. Otera, Chem. Rev. 93 (1993) 1449.

63. Y. Ono, Pure and Appl. Chem. 68 (1996) 367.

64. T. Tatsumi, Y. Watanabe, K.A. Koyano, Chem. Commun. (1996) 2281. (b) X. Ma, G. Guo, S. Wang, Y. Sun, Fuel. Proc. Tech. 83 (2003) 275.

65. B. K. Barnawal, M. P. Sharma, Renew. Sustain. Ener. Rev. 9 (2005) 363.

66. E. H. Pryde, J. Am. Oil. Chem. Soc. 60 (1983) 1557.

67. H. Noureddini, D. Zhu, J. Am. Oil. Chem. Soc. 74 (11) 1997.

68. (a) M. M. Soumanou, U. T. Bornscheuer, Enzym. Microbial Tech. 33 (2003) 97. (b) Y. Shimada, Y. Watanabe, A. Sugihara, Y. Tominaga, J. Mol. Catal. B: Enzym. 17 (2002) 133.

69. (a) G. Vicente, M. Martinez, J. Aracil, Bioresource Tech. 92 (2004) 297. (b) F. R. Abreu, M. B. Alves, C. C. S Macedo, L. F. Zara, P. A. Z. Suarez, J. Mol. Catal. A: Chem. 227 (2005) 263. (c) F. R. Abreu, D. G. Lima, E. H. Hamu, C. Wolf, P. A. Z. Suaraz, J. Mol. Catal. A: Chem. 209 (2004) 29.

70. (a) H-J Kim, B-S Kang, M-J Kim, Y. M. Park, D-K Kim, J-S Lee, K-Y Lee, Catal. Today 93-95 (2004) 315. (b) S. Furuta, H. Matsuhashi, K. Arata, Catal. Commun. 5 (2004) 721. (c) G. J. Suppes, M. A. Dasari, E. J. Doskocil, P. J. Mankidy, M. J. Goff, Appl. Catal. A: Gen. 257 (2004) 213.

71. (a) R.F. Heck, Acc. Chem. Soc. 12 (1979) 146. (b) A. De Meijer, F. E. Meyer, Angew. Chem. Int. Ed. Engl. 33 (1994) 2379.

72. (a) M. G. Andreu, A. Zapf, M. Beller, Chem. Commun. (2000) 2475. (b) C. R. LeBlond, A. T. Andrews, Y. Sun, J.R. Sowa, Org. Lett. 3 (2001) 1555.

73. K. Sonogashira, Y. Tohda, N. Hagihara, Tetrahedron Lett. (1975) 4467. (b) R. A. Sheldon, M. Wallau, I. W. C. E. Arends, U. Schuchardt, Acc. Chem. Res. 31 (1998) 485.

74. (a) J. G. De Uries, Can. J. Chem. 79 (2001) 1086. (b) R. A. Sheldon, J. Mol. Catal. A: Chem. 107 (1996) 75.

75. A. F. Littke, G. C. Fu, Angew. Chem. Int. Ed. 41 (2002) 4176.

76. J. B. Davison, N. M. Simon, S. A. Sojka, J. Mol. Catal. 22 (1984) 349.

77. (a) W. A. Herrmann, C. Brossmer, K. Oofele, C-P. Reisinger, T. Prriermeier, M. Beller, H. Fisher, Angew. Chem. Int. Ed. Engl. 34 (1995) 1844. (b) M. T. Reetz, G. Lohmer, R. Schwickardi, Angew. Chem. Int. Ed. Engl. 37 (1998) 481. (c) A. F. Littke, G. C. Fu, J. Org Chem. 64 (1999) 10.

78. R. L. Augustine, S. T. O'leary, J. Mol. Catal. 72 (1992) 229.
79. D. Savoia, C. Trombini, A. U. Ronchi, G. Verardo, J. Chem. Soc. Chem. Commun. (1981) 541.
80. K. Kaneda, M. Higuchi, T. Imanaka J. Mol. Catal. A: Chem. 63 (1990) L33.
82. R. L. Augustine, S. T. O' Leary, J. Mol. Catal. A: Chem. 95 (1995) 277.
83. L. Djakovitch, K. Kohler, J. Mol. Catal. A: Chem. 142 (1999) 275.
84. (a) S. Bhatia, "Zeolite Catalysis: Principles and Applications", CRC Press Inc., Boca Raton, Florida, (1990). (b) D. H. Olson, J. Phys. Chem. 74 (1970) 2758.
85. (a) W. Leitner, Coord. Chem. Rev. 153 (1996) 257. (b) D.H. Gibson, Chem. Rev. 96 (1996) 2063.
86. D. H. Gibson, Coord. Chem. Rev. 185-186 (1999) 335.
87. E. Fujita, C. Creutz, N. Sutin, B.S. Brunschwig, Inorg. Chem. 32 (1993) 2657.
88. (a) C. Jegat, M. Fouassier, J. Mascetti, Inorg. Chem. 30 (1991) 1521. (b) C. Jegat, M. Fouassier, M. Tranquille, J. Mascetti, Inorg. Chem. 30 (1991) 1529.
89. B. Chakraborthy, B. Viswanathan, Catal. Today 49 (1999) 253.

Chapter – 2

Materials Preparation and Characterization

2.1. Introduction

This chapter describes the synthesis methodologies of various catalysts investigated in the present study. It also presents the characterization of the catalyst materials by various physicochemical techniques. As described in Chapter-1, the objective of the thesis is to develop efficient catalyst systems for (1) CO_2 utilization in cyclic carbonates and carbamates synthesis, (2) transesterification of cyclic carbonates to dialkyl carbonates and triglycerides to fatty acid alkyl esters, and (3) C—C coupling Heck reactions. In this endeavor the following catalyst systems have been studied:

(1) Homogeneous copper complexes of acyclic and cyclic ligands,

(2) Zeolite-Y-encapsulated metal phthalocyanine complexes,

(3) Titanosilicate molecular sieves,

(4) Organo-functionalized, ordered mesoporous materials,

(5) Organic-inorganic hybrids,

(6) Solid double metal cyanide catalysts of Fe and Zn, and

(7) Pd-loaded silicoaluminophosphates.

A large number of metal complexes have been known to activate CO_2 and catalyze cyclic carbonate synthesis (see Chapter-1: Section 1.5). However, a systematic study on the influence of ligand structure (both molecular and electronic) on CO_2 activation and catalytic activity has not been investigated so far. In view of this, a variety of acyclic and cyclic ligand systems have been chosen in the present study. Metal phthalocyanines mimic the active sites of enzymes and chloroplasts. They are rugged molecules. Their size is a perfect fit for encapsulation in the supercages of zeolite-Y. It is known that

zeolite imposes restrictions on the stereochemistry of phthalocyanine molecules and as a consequence they exhibit distorted molecular geometries and unusual catalytic properties.

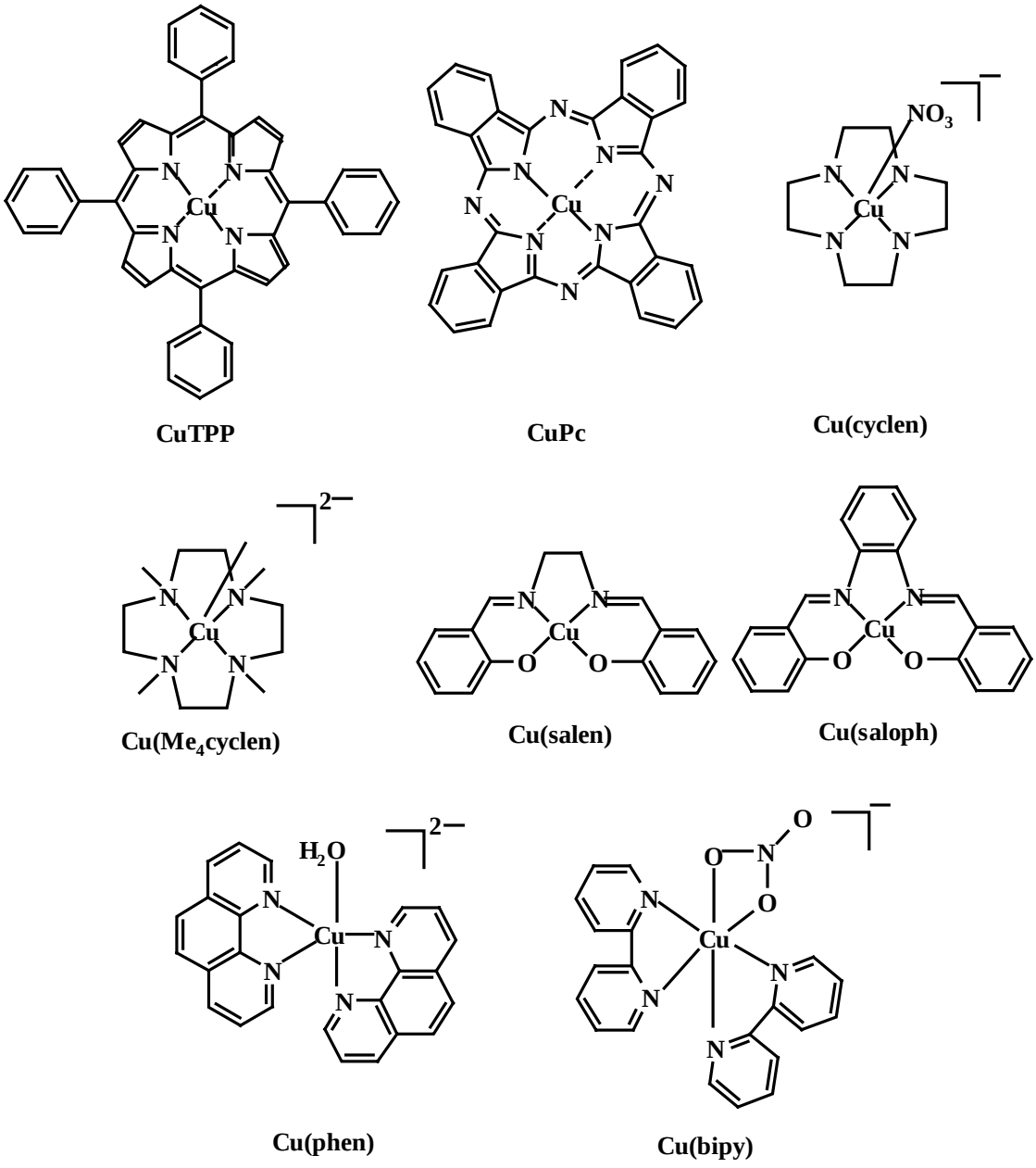

Scheme 2.1. Homogeneous Cu-complexes used in the present study.

Hence, these systems are chosen for CO_2 activation in the present study. Further, the effect of central metal ion on carbonate synthesis activity from CO_2 is examined. Titanosilicate catalysts have been widely known for their remarkable catalytic oxidation activity. Ti isomorphously substituted for Si in the framework site is a Lewis acid. Catalytic activity of titanosilicates in acid-catalyzed reactions has not been widely investigated. In this study, titanosilicate catalysts are used, for the first time, in CO_2 utilization reactions. Organo-functionalized, mesoporous, ordered silica materials and organic-inorganic hybrids act as bifunctional (acid-base) catalysts. Their catalytic activity for the above mentioned reactions is investigated, for the first time, in this study. Pd-loaded silicoaluminophosphates efficiently catalyze the Heck C—C coupling reaction. Detailed synthesis procedure and characterization of various catalysts are described in the following sections.

2.2. Materials

The solvents methanol, dichloromethane, chloroform, N, N-dimethylformamide (DMF), acetonitrile, ethanol, isopropanol, toluene etc., used in the present study were of A.R. grade and procured from Merck, India. The solvents were purified and dried according to standard purification procedures [1].

2.3. Synthesis and Characterization of Homogeneous Cu Complexes of Acyclic and Cyclic Ligands

Metal complex catalyzed reactions are already established as an important part of synthetic chemistry involving various organic transformations. As described in Chapter-1 (Section 1.4), a variety of metal complexes are known to activate and utilize CO_2 in cycloaddition with epoxides to form the cyclic carbonates. In the present study, the ligand

structure of the metal complex is systematically varied and its influence on cyclic carbonate synthesis is investigated. Cu(II) complexes coordinated to acyclic Schiff bases, 1,10-phenanthroline (phen) and 2,2'-bipyridine (bipy) and cyclic tetraphenyl porphyrine (TPP), phthalocyanine (Pc) and peraza macrocyclic ligands have been investigated (Scheme 2.1). Among the cyclic ligands, TPP and Pc belong to the category of a 16-membered unsaturated ring system and cyclen to a 12-membered saturated ring system. Delocalization of electron density is more in the case of Schiff base saloph than in salen. The structure of the copper complexes is varied from tetracoordinated square planar to pentacoordinated square pyramidal to hexacoordinated octahedral. Phthalocyanine was procured from Aldrich Co., and used as received. TPP, salen, saloph and cyclen ligands were prepared according to reported procedures. Phen and bipy ligands were purchased from Merck, India.

2.3.1. Cu(salen)

N,N-ethylenebis(salicylideneiminate) (salenH_2) was prepared first [2-3], by reacting an ethanolic solution (40 ml) of ethylenediamine (Merck.. India) (20 mmol, 1.33 ml) with salicylaldehyde (SRL, India Ltd.) (40 mmol, 4.26 ml). The mixture was heated to reflux for 1 h, the bright yellow crystalline solid salenH_2 formed was collected by filtration. In the synthesis of Cu(salen) complex, salenH_2 ligand (5 mmol) was taken in 20 ml of methanol and $Cu(CH_3COO)_2.H_2O$ (SRL, India Ltd.) (5 mmol) dissolved in 15 ml of methanol was added slowly to it, over a period of 30 min, while heating at 323 K. The reaction mixture was refluxed for 3 - 4 h and allowed to cool to room temperature (298 K). The solid, microcrystalline, green complex, thus obtained, was filtered and recrystallized from methanol/chloroform.

Analysis: SalenH_2 - Yield: 92% (4.98 g); m. p.: 401 K. Anal. (wt %): Found - C: 71.2, H: 6.0, N: 10.3. Calc. C: 71.6, H: 6.0, N: 10.4. ^{1}H NMR ($CDCl_3$), δ_{ppm}: 3.73 (s, 4H), 6.47-7.20 (m, 8H), 8.07 (s, 2H), 12.0 (br s, 2H). IR (KBr) cm^{-1}: 2854-2924, 1633, 1577, 1417, 1375, 1282, 1197, 1150, 1020, 1041, 975, 858.

Analysis: Cu(Salen) - Anal. (wt %): Found - C: 56.0, H: 4.7, N: 7.5. Calcd. - C: 56.4, H: 5.0, N: 7.4. IR (Nujol) cm^{-1}: 2854-2924, 1647, 1629, 1597, 1541, 1377, 1304, 1190, 1140, 980.

2.3.2. Cu(saloph)

N,N'-*o*-phenylenebis(salicylidenaminate) (salophH_2) was prepared in a similar manner [2] to that of salenH_2 except that *o*-phenylenediamine (S. D. Fine India Ltd.) and salicylaldehyde were reacted. Cu(saloph) was prepared from salophH_2 (5 mmol) and $Cu(CH_3COO)_2.H_2O$ (5 mmol) dissolved in methanol [2-3]. Recrystallization of the crude product was done from methanol/chloroform to obtain a brownish green product.

Analysis: SalophH_2 - Yield: 88 %; m. p.: 434 K. Anal. (wt %): Found - C: 75.0, H: 5.1, N: 8.9. Calcd. - C: 75.9, H: 5.0, N: 8.8. ^{1}H NMR ($CDCl_3$) δ_{ppm}: 6.47-7.22 (m, 12H), 8.3 (s, 2H), 12.2 (br s, 2H). IR (KBr) cm^{-1}: 2854-2924, 1649, 1560, 1375, 1275, 1191, 1149, 1103, 908.

Cu(saloph) - Anal. (wt %): Found - C: 62.0, H: 4.4, N: 7.2. Calcd. - C: 62.4, H: 4.1, N: 7.1. IR (Nujol) cm^{-1}: 2926, 1608, 1577, 1521, 1460, 1339, 1284, 1188, 1145, 1126, 920, 856.

2.3.3. $[Cu(NO_3)(2,2'\text{-bipy})_2](NO_3).H_2O$

To an ethanolic solution (50 ml) of $Cu(NO_3)_2.2.5\ H_2O$ (Merck India Ltd.; 1 g, 5.23 mmol), 1.67 g of 2,2' bipyridine (Loba Chem. India; 10.67 mmol) was added [4].

The solution was refluxed for 30 min and then cooled slowly to room temperature to get a blue crystalline product. Recrystallization of the compound was done from ethanol.

Analysis: Yield - 85%; m. p.: 563 K. Anal. (wt %): Found - C: 46.47, H: 3.59, N: 16.35. Calcd. - C: 46.02, H: 3.45, N: 16.1. IR (KBr) cm^{-1}: 3571, 3080, 1597, 1562, 1369, 1154, 1101, 1014, 898, 828, 769, 729, 647.

2.3.4. $[Cu(H_2O)(phen)_2](NO_3)_2$

In a typical synthesis, $Cu(NO_3)_2.2.5\ H_2O$ (1 g, 5.23 mmol) was dissolved in 50 ml of absolute ethanol. To it, 2.11 g of 1,10-phenanthroline (Merck. India) (10.67 mmol) was added. The solution was stirred overnight at room temperature. The green precipitate formed was filtered and washed with ethanol [4].

Analysis: Yield - 89 %. Anal. (wt %): Found - C: 50.97, H: 4.21, N: 14.91. Calcd. - C: 50.57, H: 3.16, N: 14.74. IR (KBr) cm^{-1}: 3542, 3053, 1626, 1585, 1380, 1142, 1101, 857, 717, 641.

2.3.5. CuTPP

TPP was prepared according to the reported procedure [5]. A freshly distilled pyrrole (SRL India Ltd.) (7.46 g, 0.112 mol) and benzaldehyde (Merk India) (10.66 g, 0.1 mol) were taken in 400 ml of propionic acid (Merck India) and refluxed for 30 min. The solid formed was separated using a sintered funnel and washed first with methanol and then with hot water. The resulting purple, crystalline product ($TPPH_2$) was dried under vacuum. TPP (0.3 g, 0.488 mmol) thus prepared was taken in 100 ml of DMF and brought to reflux temperature over an oil bath. Then four-fold excess of anhydrous $Cu(CH_3COO)_2$ (Aldrich Co.) (0.443 g, 1.95 mmol) was added in one proportion and continued the reaction for 5 h under reflux condition. After completion of the reaction,

the mixture was allowed to stand at room temperature and 400 g of chilled water was added to it. The purple precipitate obtained was filtered and air-dried [6].

Analysis: $TPPH_2$: Yield - 19%. Anal. (wt %): Found - C: 83.7, H: 5.8, N: 10.3. Calc. C: 85.9, H: 4.9, N: 9.2. ^{1}H NMR ($CDCl_3$), δ_{ppm}: -2.73 (s, 2H), 7.70-7.80 (m, 12H), 8.22 (dd, 8H), 8.84 (s, 8H). IR (KBr) cm^{-1}: 2854-2924, 1633, 1577, 1417, 1375, 1282, 1197, 1150, 1020, 1041, 975, 858.

CuTPP: Yield - 97 %. Anal. (wt %): Found - C: 75.7, H: 4.61, N: 9.50. Calcd. - C: 78.0, H: 4.2, N: 8.4. IR (KBr) cm^{-1}: 3058, 3018, 2919, 2843, 1661, 1585, 1439, 1376, 1334, 1068, 1003, 787, 729, 694,519.

2.3.6. [Cu(cyclen)(NO_3)]ClO_4

Cyclen ligand was prepared first by coupling of disodium salt of tritosylated diethylenetriamine with tritosylated diethanolamine [7, 8]. Then it was complexed with Cu(II) ions to get the desired complex. A detailed procedure for the synthesis of the different reactant intermediates, cyclen ligand and copper complex is given below.

(I) Preparation of N,N',N"-tris(p-toluenesulfonyl)diethylenetriamine (a)

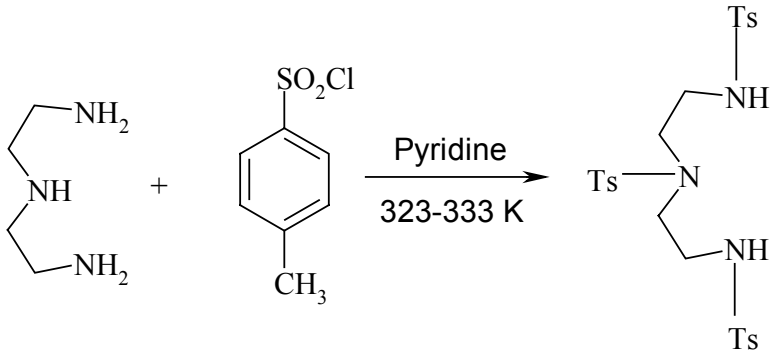

Diethylenetriamine *p*-tolunesulphonylchloride (Ts) (a)

A solution of diethylenetriamine (Merk India) (3.01 g, 30 mmol) in pyridine (30 ml) was added slowly to a solution of toluene-*p*-sulfonyl chloride (Merk India) (17.2 g,

90 mmol) in pyridine (30 ml) with constant stirring and cooling so as to keep the temperature below 323 K. When the addition was complete, the reaction mixture was heated at 323 – 333 K for an additional 4 h and was then poured into a beaker containing 300 g of ice and stirred well. The solid obtained was filtered, washed repeatedly with water and then with cold 50% aqueous ethanol and dried at 373 K to obtain a pale yellow solid. The solid was purified by recrystallization from acetonitrile.

Analysis: Yield - 93% (15.8 g); m.p.: 450-451 K. Anal. (wt%): Found - C: 52.8, H: 5.3, N: 7.3, S: 16.9. Calcd.; C: 53.0, H: 5.3, N: 7.4, S: 16.9. ^{1}H NMR ($CDCl_3$) δ_{ppm}: 2.43 (s, 9H), 3.16 (s, 8H), 3.33(br, 2H), 7.29 (d, 6H, J = 8 Hz), 7.59 (d, 2H, J = 10 Hz), 7.74 (d, 4H, J = 8 Hz). IR (Nujol) cm^{-1}: 3288, 2926, 1596, 1446, 1323, 1157, 1089, 913, 725.

(II) Preparation of 1,4,7-tritosyl-1,7-disodium-1,4,7-triazaheptane (b)

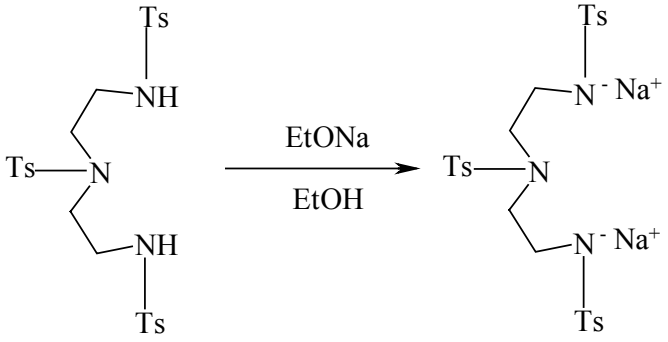

(a) (b)

A solution of sodium ethoxide (prepared from 0.92 g of sodium in 30 ml of dry ethanol) was added under dry condition to a slurry of N,N',N"-tris(p-toluenesulfonyl)diethylenetriamine (11.3 g, 20 mmol) prepared as above, at 353 K and stirred for 0.5 h at that temperature. Then the reaction mixture was left at room

temperature overnight to get 98% (11.9 g) yield of crystalline 1,4,7-tritosyl-1,7-disodium-1,4,7-triazaheptane (b), which is highly hygroscopic; m.p. >573 K.

(III) Preparation of N,O,O'-tris(p-tolylsulfonyl)diethanolamine (c)

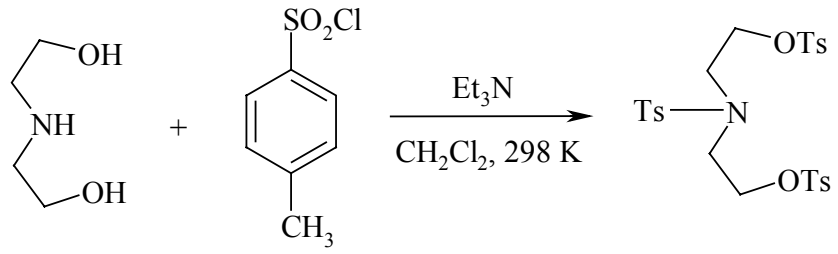

Diethanolamine *p*-tolunesulphonylchloride (Ts) (c)

To a stirred solution of toluene-*p*-sulfonyl chloride (8.5 g, 45 mmol) in dichloromethane (40 ml) was added diethanolamine (Merk India) (1.58 g, 15 mmol) and triethylamine (Loba Chem India) (7.5 ml, 54 mmol) drop-wise with constant stirring and cooling to 273 K under dry conditions. The reaction mixture was stirred overnight. The white precipitate obtained during the reaction was filtered off and washed with dichloromethane. The dichloromethane layer was washed with water, 1 N HCl, 1 N $NaHCO_3$ and brine and dried over Na_2SO_4. After solvent evaporation, the thick viscous liquid was allowed to stand several hours to obtain a solid that was crystallized from ethanol.

Analysis: Yield - 94% (8.0 g); m.p.:336 K. ^{1}H NMR ($CDCl_3$) δ_{ppm}: 2.42 (s, 6H), 2.45 (s, 3H), 3.36 (t, 4H J = 6Hz), 4.10 (t, 4H, J = 6 Hz), 7.34 (d, 6H, J = 8 Hz), 7.58 (d, 2H, J = 8 Hz), 7.73 (d, 4H, J = 8 Hz). IR (Nujol) cm^{-1}: 2924-2854, 1598, 1456, 1361, 1093, 1176,1159, 1097, 979, 813.

(IV) Preparation of 1,4,7,10-Tetratosyl-1,4,7,10-tetraazacyclododecane (d)

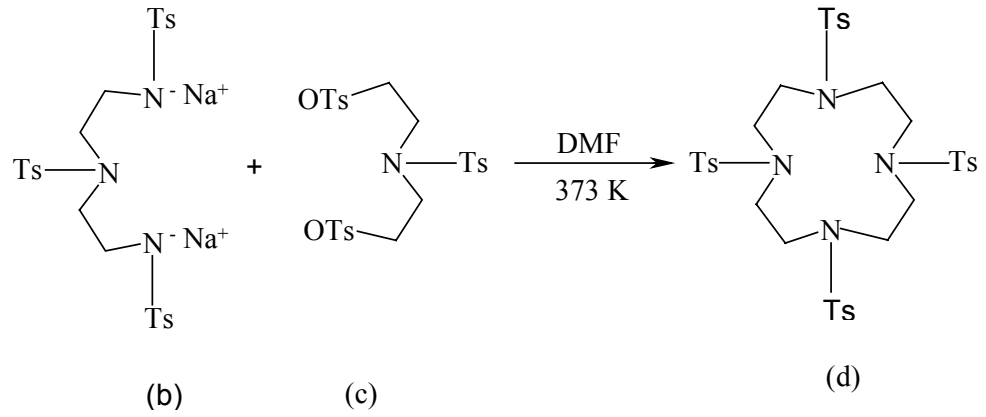

(b) (c) (d)

To a solution of 1,4,7-tritosyl-1,7-disodium-1,4,7-triazaheptane (b) (6.09 g, 10 mmol) in dry DMF (30 ml) heated to 373 K was added a solution of N,O,O'-tris(*p*-tolylsulfonyl)diethanolamine (c) (5.7 g, 10 mmol) in dry DMF (20 ml) slowly with stirring through a syringe over a period of 2 h. After the addition was complete, heating was continued for another 5 h and then the reaction mixture was cooled to room temperature. The solution was added to vigorously stirred water (400 ml), the precipitate was filtered-off, washed with water (50 ml), dried at 373 K and crystallized from acetone/ethanol (1:1).

Analysis: Yield - 89% (7.0 g); m.p. : 562 K. Anal. (wt %): Found - C: 54.8, H: 5.6, N: 7.3, S: 16.6. Calcd. C: 54.8, H: 5.6, N: 7.1, S: 16.4. ^{1}H NMR ($CDCl_3$) δ_{ppm}: 2.43 (s, 12H), 3.42 (s, 16H), 7.30 (d, 8H, J = 8 Hz), 7.65 (d, 8H, J = 8.3 Hz). IR (Neat) cm^{-1}: 2954-2924, 1597, 1460, 1336,1160,1081, 975, 902, 715.

(V) Preparation of 1,4,7,10-Tetraazacyclododecane (cyclen) (e)

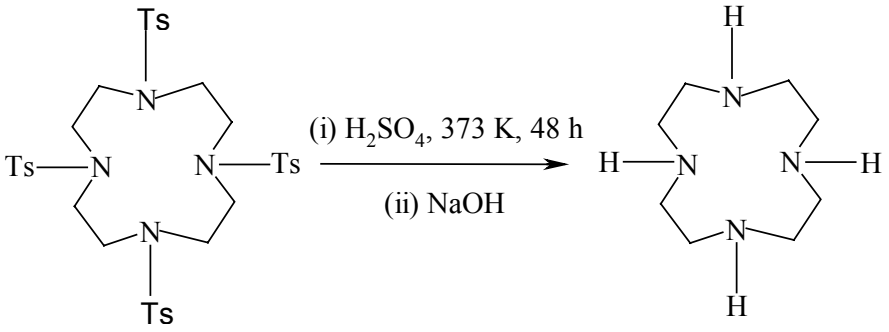

(d) (e)

1,4,7-tritosyl-1,7-disodium-1,4,7-triazaheptane (b) (4.0 g, 5 mmol; prepared as above) was dissolved in conc. H_2SO_4 (5 ml) and stirred at 373 K for 48 h. The mixture was cooled to 273 K and 20-30 ml of diethyl ether was added slowly with constant stirring. The brown solid obtained was filtered, dissolved in a minimum amount of water and the pH was adjusted to 10 with 10 N NaOH at 273 K (sodium sulfate precipitated was filtered out). The cyclen ligand in the solution was extracted repeatedly with equal volumes of chloroform (6 x 10 ml). The extracts were dried over Na_2SO_4 and evaporated to get a light yellow solid of cyclen (e).

Analysis: Yield - 68.5 % (0.65 g), m.p.:376 K. ^{1}H NMR ($CDCl_3$) δ_{ppm}: 2.68 (s, 16H), 2.39(br, 4H). IR (Neat) cm^{-1}: 3280, 2852-2924, 1560, 1350, 1110, 1036, 941, 759. MS: M^{+} 170, 153, 136, 121, 104, 85, , 80, 56, 44 (base peak).

(VI) Preparation of [Cu(cyclen)(NO_2)](ClO_4)

To a methanolic solution (3 ml) of cyclen (1 mmol) were added a solution of $Cu(NO_3)_2.2.5\ H_2O$ (1 mmol) in 3 ml of methanol and $NaClO_4$ (1.5 mmol) simultaneously while stirring at 298 K for 2 h. The reaction mixture was heated at 333 K

for 1 h. The solid obtained was filtered, washed with cold methanol (1-2 ml) and recrystallized from methanol to get bluish green crystals.

Analysis: [Cu(cyclen)(NO_2)](ClO_4): Yield - 42 %. Anal. (wt%): Found - C: 24.2, H: 6.3, N: 11.3. Calcd. - C: 24.0, H: 5.7, N: 11.2. IR (Nujol) cm^{-1}: 3240, 2854-2960, 1305, 1244,1012, 974, 624.

2.3.7. [Cu(tmcyclen)(CH_3CN)](ClO_4)$_2$

N,N',N",N"'-tetramethyl-1,4,7,10-tetraazacyclododecane (tmcyclen) was procured from Aldrich Co. [Cu(tmcyclen)(CH_3CN)](ClO_4)$_2$ was prepared in a similar manner to that of [Cu(cyclen)(NO_2)](ClO_4).

Analysis: Yield - 66% (crystallized from acetonitrile/chloroform). Anal. (wt%): Found - C: 28.3, H: 6.3, N: 11.0. Calcd. - C: 29.3, H: 5.7, N: 11.4. IR (Nujol) cm^{-1}: 2854-2960, 1350, 1294, 1278, 1018, 966, 756, 623.

2.4. Zeolite-Y-Encapsulated Metal Phthalocyanines

Metal phthalocyanine (MPc) complexes have been extensively studied as enzyme mimics [9]. They catalyze the oxidation of hydrocarbons [10] and epoxidation of olefins [11]. These complexes are easy to prepare. They are not sensitive to air and moisture. It is known that in solutions, MPc complexes agglomerate and hence, exibit lower catalytic activity [12]. Encapsulation of MPc complexes inside the cages of zeolites and zeolitic materials enhances their catalytic activity. A generalized procedure for the preparation of zeolite-Y-encapsulated metal phthalocyanines (denoted as MPc-Y, where M = Cu^{2+}, Ni^{2+}, Co^{2+} and Al^{3+}) is shown in Scheme 2.2. Initially metal ion-exchanged zeolite-Y was prepared from NH_4Y and then it was used in the preparation of MPc-Y catalysts.

2.4.1. Synthesis

2.4.1.1. Preparation of Metal Ion-Exchanged Zeolite Y (CuY, NiY, CoY and AlY)

Zeolite HY (Si/Al = 24) was prepared from NH_4Y by calcining the latter at 823 K for 24 h in static-air. HY was treated with 1 N aqueous NaCl solution at 353 K for 8 h, filtered, washed thoroughly with water and dried at 373 K. This procedure was repeated thrice to obtain (Na-Y) (1.8 wt%). To prepare Cu exchanged zeolite-Y (CuY), 250 mg of $Cu(CH_3COO)_2.H_2O$ was dissolved in 100 ml of distilled water. To this, 5 g of NaY was added and stirred for 12 h at 353 K. The solid was filtered and washed repeatedly with distilled water. Cu-Y thus obtained by the ion exchange method was dried at 393 K for 12 h. NiY was prepared in a similar manner using NaY and $Ni(CH_3COO)_2.4H_2O$. CoY and AlY were prepared using $Co(CH_3COO)_2.4H_2O$ and $Al_2(SO_4)_3.18H_2O$ as source of Co and Al, respectively. The metal ion content was estimated by atomic absorption spectroscopy (AAS): Cu - 0.41 wt%, Co - 0.58 wt%, Ni - 0.49%.

2.4.1.2. Preparation of MPc-Y

Zeolite-Y-encapsulated MPc complexes (MPc-Y, M = Cu, Co, Ni and Al) were prepared by the "*in situ* ligand synthesis" method using metal ion-exchanged Y and 1,2-dicyanobenzene (DCB) (Scheme 2.2) [13-15]. In the preparation of zeolite-Y-encapsulated MPc complexes, 3 g of MY was degassed for 8 h at 373 K and then exposed to the vapors of DCB (10 g) at 533 K for 24 h in a specially designed glass reactor. Nitrogen was used as a carrier gas. Unreacted DCB, uncomplexed phthalocyanine and other organic matter on the surface of the zeolite were removed by Soxhlet extraction with different solvents: acetone (for 12 h), pyridine (for 12 h), acetonitrile (for 12 h to

remove the residual pyridine and organics from the sample) and once again with acetone (for 12 h). Finally, the sample was dried at 373 K for 8 - 10 h.

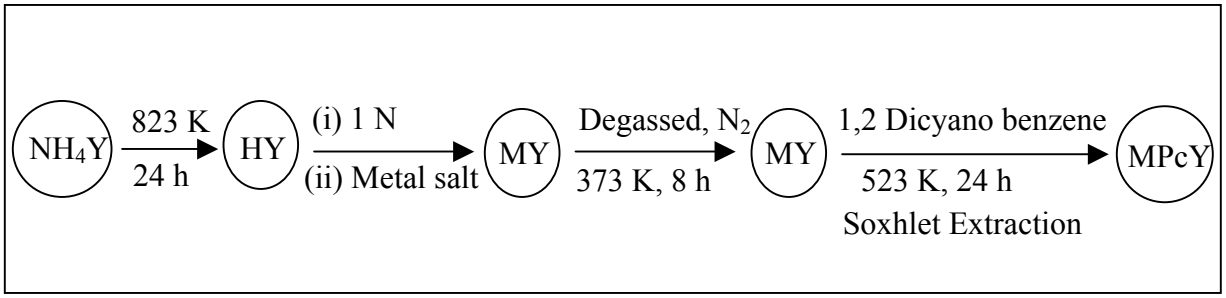

Scheme 2.2. Procedure for the preparation of MPc-Y.

For comparison studies a sample of CuPc supported on SiO_2 (denoted as CuPc-SiO_2) was prepared as follows. 250 mg of CuPc (obtained from Aldrich Co.) was dissolved in 100 ml of pyridine and to it 5 g of fumed silica (Aldrich Co.) was added. The suspension was stirred at 333 K for 8 h and the solid was separated by filtration and dried at 353 K. Loosely bound CuPc complexes on silica were removed by Soxhlet extraction as described above. Finally, the solid was dried at 373 K (Cu = 0.52 wt%).

2.4.2. Characterization

The materials were characterized by X-ray diffraction (XRD), N_2-adsorption studies, elemental composition, FT-IR, diffuse reflectance UV-visible (DRUV-Visible) and electron paramagnetic resonance (EPR) techniques.

2.4.2.1. XRD

XRD profiles of HY, NaY and MPc-Y are shown in Fig. 2.1. Metal complexes encapsulation doesn't cause any structural damage of zeolite-Y. No peaks corresponding

to occluded/bulk MPc were detected. MPc is isolated and possibly encapsulated in side the super cages of zeolite-Y.

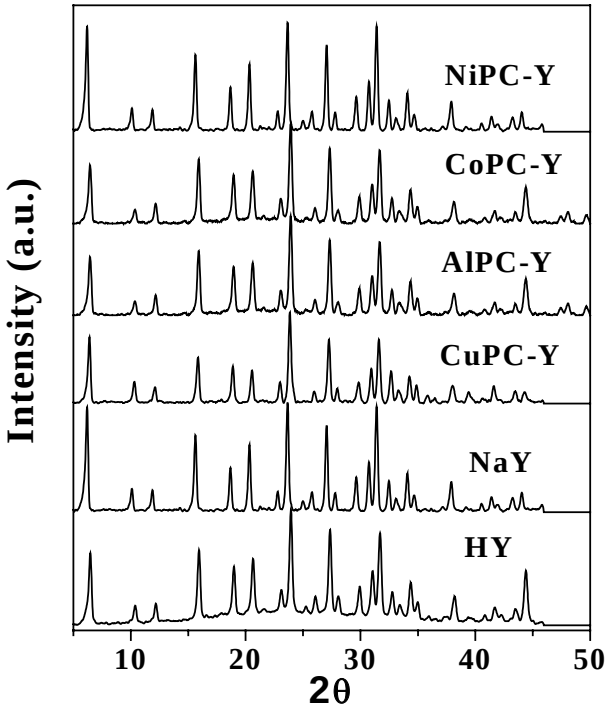

Fig. 2.1. XRD patterns Mc-Y.

2.4.2.2. N_2 Adsorption

The specific surface area (S_{BET}) values for HY and NaY obtained from N_2-adsorption isotherms are 712 and 679 m^2/g, respectively. Upon encapsulation of MPc, S_{BET} of zeolite-Y decreased markedly to 482 m^2/g (for CuPc-Y), 432 m^2/g (for NiPc-Y), 415 m^2/g (for CoPc-Y) and 437 m^2/g (for AlPc-Y), respectively. This large decrease in surface area with a small amount of phthalocyanine content (0.41 (for CuPc), 0.49 (for NiPc) and 0.58 wt% (for CoPc)) suggests that encapsulation occurs mainly in the more accessible cages at the periphery of the crystallites and perhaps not uniformly throughout the bulk of the crystallites.

2.4.2.3. FT-IR

Representative FT-IR spectra of "neat" MPc and MPc-Y are shown in Fig. 2.2. The bands at 1460 and 1089 cm^{-1} are attributed to the stretching modes of C=N and C-N, respectively. The band at 1375 cm^{-1} is due to the stretching mode of C=C and that at 1120 cm^{-1} corresponds to the bending C-H mode. Upon encapsulation a marginal shift of C=N and C=C bands to 1465 cm^{-1} and 1379 cm^{-1}, respectively was observed. Similarities in the spectral features provide evidence for the formation of macrocyclic MPc molecules in the supercages of zeolite-Y and indicate the influence of encapsulation on the structure.

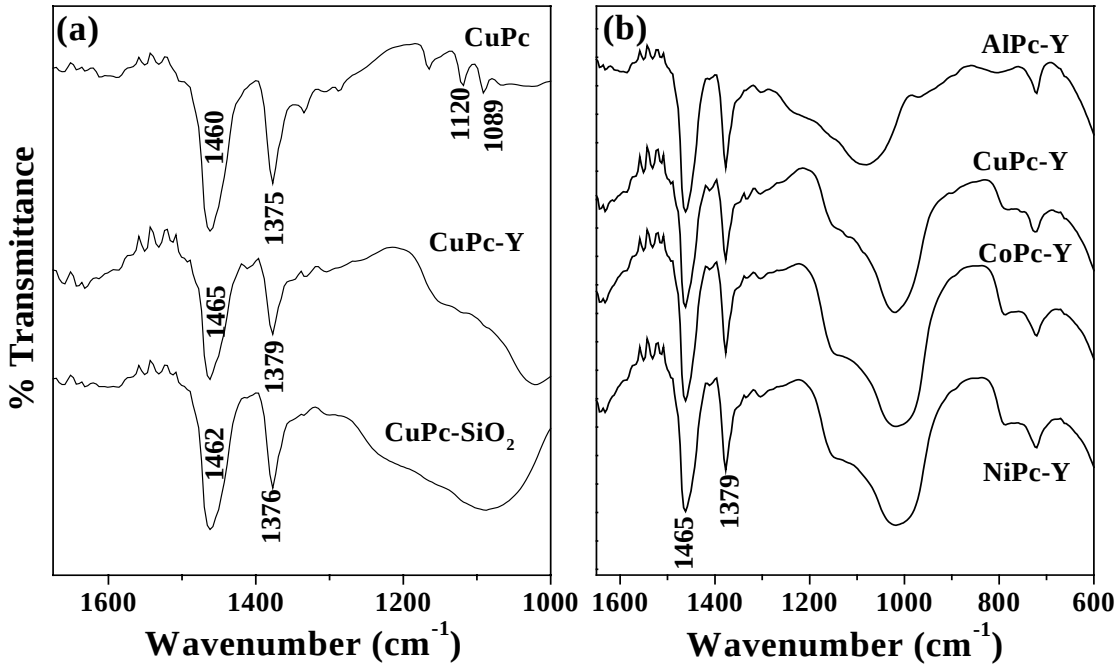

Fig. 2.2. FT-IR spectra (KBr pellet): (a) "neat" CuPc, CuPc-Y and CuPc-SiO_2, (b) zeolite-Y-encapsulated MPc complexes - AlPc-Y, CuPc-Y, CoPc-Y and NiPc-Y.

2.4.2.4. DRUV-Visible

The phthalocyanine complexes exhibited two characteristic ligand-based π–π^* transitions referred to as Q bands in the visible region (Fig. 2.3). For symmetry lower

than D_{4h}, these bands further split and show vibrational overtones Q(0,1) and Q(1,1) as shoulders or resolved bands [16]. The materials under consideration exhibit the Q-bands in the region 550 – 760 nm. The Q-bands for MPc-Y have red shifted on encapsulation. The red shift and change in the relative intensities are probably due to changes in the molecular structure from planar to a puckered geometry and isolation of the molecules. The resolved bands in MPc-Y compared to those in "neat" and supported complexes indicate that the active sites (complex molecules) are isolated in the former type of catalyst samples. In addition to the Q-bands, Soret band appeared around 342 nm. The position of the Soret and Q-bands are sensitive to central metal ion and its coordination.

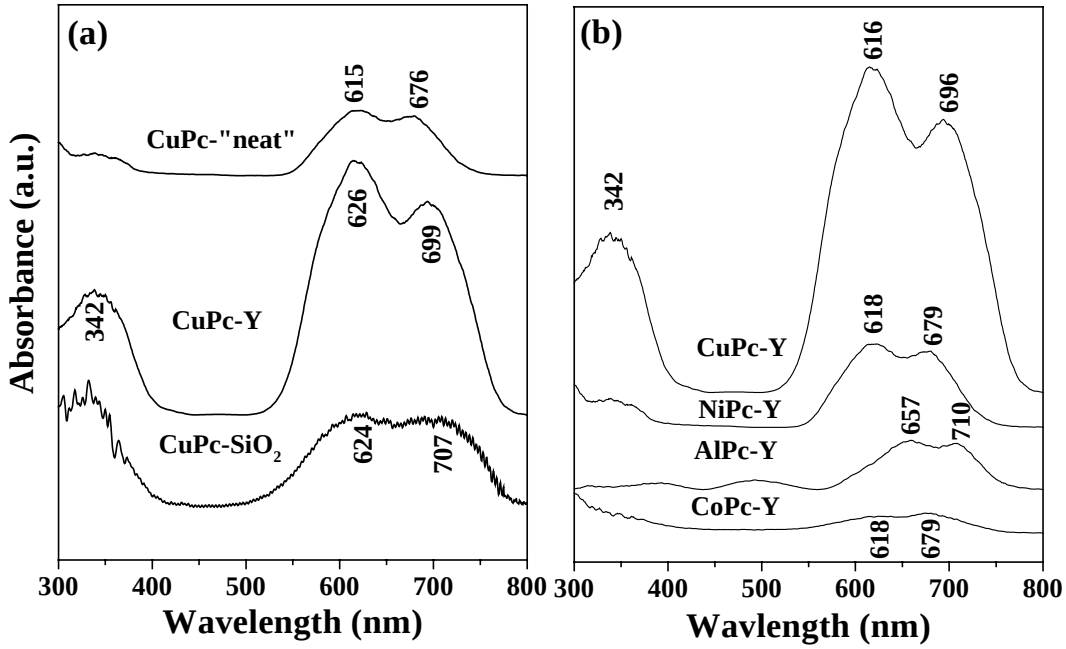

Fig. 2.3. DRUV-Visible spectra of (a) "neat"-CuPc, CuPc-Y and CuPc-SiO_2. (b) encapsulated MPc complexes - CuPc-Y, CoPc-Y, NiPc-Y and AlPc-Y.

2.4.2.5. EPR

The EPR spectra of "neat"-CuPc, CuPc-SiO_2, CuPc-Y and CuY at 100 K are shown in Fig. 2.4. In the "neat" complex the signals were broad and copper hyperfine

features were not resolved ($g_{\|}$ = 2.120, $g_{\perp}$ = 2.055) consistent with intermolecular interactions and agglomeration of CuPc molecules. CuPc-SiO_2 also did not show resolved Cu hyperfine features ($g_{\|}$ = 2.162, $g_{\perp}$ = 2.057). In contrast, zeolite-encapsulated CuPc (CuPc-Y), showed resolved, parallel hyperfine features ($g_{\|}$ = 2.311, $g_{\perp}$ = 2.057, $A_{\|}$ = 166.5 G) that are different from the ones exhibited by the uncomplexed Cu^{2+} ions in CuY ($g_{\|}$ = 2.402, $g_{\perp}$ = 2.087, $A_{\|}$ = 126.4 G) and characteristic of isolated CuPc molecules. These findings also reveal the isolation and confinement of CuPc complexes in the cavities of zeolite-Y. At very low CuPc loading, superhyperfine features from the N atoms of the phthalocyanine ligand were also observed.

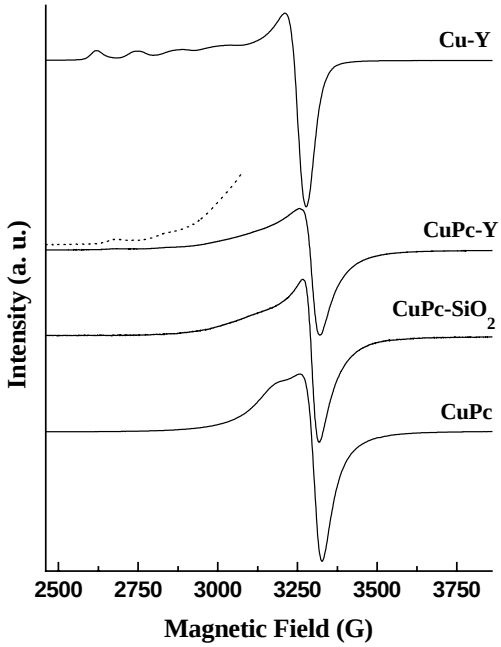

Fig 2.4. EPR spectra of "neat" CuPc, silica supported CuPc, CuPc-Y and Cu-Y.

2.5.Titanosilicate Molecular Sieves

Incorporation of Ti in silicalite framework generates Lewis acidity. Although titanosilicates have been widely investigated as oxidation catalysts [17], their activity in

acid catalyzed reactions is not much explored. The activity of titanosilicates in cycloaddition reaction is investigated, for the first time, in the present study. A variety of titanosilicates (microporous to mesoporous) were prepared and used as acid catalysts for cycloaddition and transesterification reactions.

2.5.1. Synthesis

2.5.1.1. TS-1

TS-1 ((Si/Ti = 36 (XRF); S_{BET} = 400 m^2/g) [18] was supplied by Catalysis Pilot Plant, National Chemical Laboratory, Pune.

2.5.1.2. Ti-MCM-41

Ti-MCM-41 was prepared by direct synthesis method [19] from the gel of molar composition: TEOS:0.25 CTMABr:0.3 TMAOH:0.0303 TBOT:40 H_2O:5 CH_3OH.

In a typical synthesis, 10.9 g of tetramethylammonium hydroxide (25 wt.% TMAOH, 99% Aldrich) was taken in 72 g of distilled water. To that, 8.75 g of cetyltrimethylammonium bromide (CTMABr, S. D. Fine Chem. Ltd., India) was added. Then, 20.8 g of tetraethylorthosilicate (TEOS, Aldrich) in 16 g of methanol was added drop-wise over a period of 20 min. To the resultant solution, 1.03 g of titanium tetrabutoxide (TBOT, Aldrich) in 10 ml of isopropanol was added over a period of 10 min. The resultant gel was stirred for further 4 h at 298 K and then transferred into a Teflon-lined stainless steel autoclave and heated to 373 K for 72 h. The solid product was filtered, washed with distilled water, dried at 353 K and finally calcined at 813 K for 6 h (Si/Ti (output) = 35; S_{BET} = 1055 m^2/g; pore volume = 0.77 cm^3; average pore diameter = 2.94 nm.

2.5.1.3. Amorphous TiO_2–SiO_2

Amorphous TiO_2–SiO_2 was prepared from the gel of molar composition: TEOS:0.55 CTMABr:0.33 TMAOH:0.0303 TBOT:60 H_2O.

In a typical synthesis, 12.0 g of 25 wt% TMAOH was taken in 108 g of distilled water. To it, 20 g of CTMABr was added. Then, 20.8 g of TEOS was added drop-wise over a period of 20 min. Subsequently, 1.03 g of TBOT dissolved in 10 ml isopropanol was added in 10 min. The resultant gel was stirred for 2 h at 298 K and then transferred to a Teflon-lined stainless steel autoclave and heated to 383 K for 5 days. The solid product was filtered, washed with distilled water, dried at 353 K and finally calcined at 813 K for 6 h. The minor changes in the synthetic procedure from that of Ti-MCM-41 have resulted in an amorphous TiO_2–SiO_2 solid (Si/Ti (output) = 37; S_{BET} = 273 m^2/g).

2.5.1.4. Ti-SBA-15

SBA-15 was synthesized first and then Ti was introduced into the mesoporous structure by post-synthesis method. Mesoporous silica SBA-15 was synthesized according to the reported procedure [20]. In a typical synthesis, 10 g of amphiphilic triblock copolymer, poly(ethylene glycol)-block-poly(propylene glycol)-block-poly(ethylene glycol) (average molecular weight = 5800, Aldrich Co.), was dispersed in 75 ml of water and 300 ml of 2 M HCl solution while stirring. Followed by that, 21.25 g of tetraethyl orthosilicate (TEOS, Aldrich Co.) was added to it**.** This gel was continuously stirred at 313 K for 24 h, and finally crystallized in a Teflon-lined autoclave at 373 K for 2 days. After crystallization, the solid product was centrifuged, filtered, washed with deionized water, and dried in air at room temperature. The material was calcined in air at

823 K for 24 h to decompose the triblock copolymer and to obtain a white SBA-15 powder.

Ti-incorporated SBA-15, designated as Ti-SBA-15, was prepared by the post-synthesis method using tetrabutyl orthotitanate (95wt % TBOT, Wako) as a Ti source [21]. In a typical preparation, a certain amount of TBOT was hydrolyzed in 40 ml of glycerol (99 wt%, Wako) containing 7.5 ml of tetrapropylammonium hydroxide (TPAOH; 20 wt), to obtain a homogeneous solution. To the above solution was added 2 g of SBA-15 without any pretreatment, and the mixture was heated statically to induce titanation at 373 K for 72 h. The amount of TBOT added was varied to give Si/Ti atomic ratios of 5.7-200. After the titanation, Ti-SBA-15 was filtered and washed with deionized water, and the organic species were burnt off at 773 K for 4 h.

2.5.2. Characterization

2.5.2.1. XRD

TS-1 belongs to MFI topology. Fig. 2.5 (a) shows the XRD pattern of TS-1**.** The typical XRD pattern characteristic of orthorhombic symmetry is indicative of Ti in the silicalite-1 framework. Upon calcination TS-1 retained the orthorhombic symmetry while silicalite changes its symmetry to monoclinic [22]. The replacement of Si by the larger Ti ions in the tetrahedral zeolite framework causes an expansion of the unit cell. XRD pattern of Ti-MCM-41 (Fig. 2.5 (b)) shows a very intense, low-angle peak (2.43°) assigned to (100) reflection and three additional peaks with very low intensities appearing at 4.14° (110), 4.68° (200) and 6.37° (210), respectively [19]. Amorphous TiO_2-SiO_2, on the contrary, showed weakly intense signals indicating mesoporous short-range ordering (broad (100) reflection at 2.95; barely seen higher 2θ reflections). However, the XRD

pattern and peak intensity reveal that this material was mainly amorphous in nature. The d_{100} and lattice parameters for Ti-MCM-41 were estimated to be 3.6 nm and 4.2 nm, respectively.

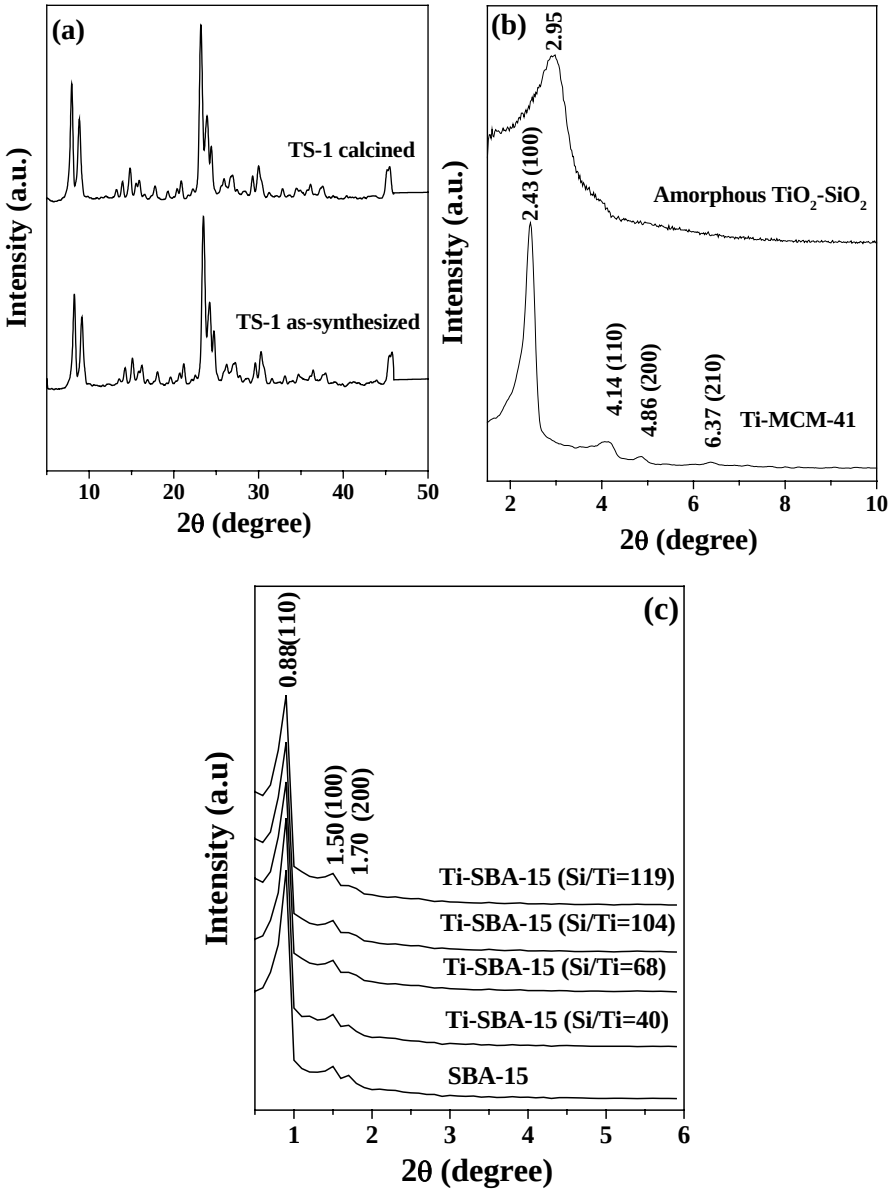

Fig. 2.5. XRD profiles of (a) TS-1, (b) Ti-MCM-41 and Amorphous TiO_2-SiO_2, and (c) SBA-15 and Ti-SBA-15.

Fig. 2.5 (c) shows the XRD pattern of SBA-15 and Ti-SBA-15 (Si/Ti = 30, 68, 104, 113). All the samples exhibited very similar pattern. Three well-resolved diffraction

peaks due to (100), (110) and (200) reflections were observed at 0.88, 1.50 and 1.70°, respectively [20]. Ti incorporation did not alter the long-range ordering of the mesoporous structure. Interplanar spacing (d_{100}) and unit cell parameter (a_0) of various Ti-SBA-15 materials are listed in Table 2.1.

Table 2.1. Composition and structural parameters of Ti-SBA-15 and Ti-MCM-41

Sample	SiO_2/TiO_2 molar ratio		d_{100} (nm)	a_0 (nm)	Pore diameter (nm)	Wall thickness (nm)
	Gel	Product (XRF)				
SBA-15	-	-	9.8	11.3	7.2	4.1
Ti-SBA-15 (40)	20	40	10.3	11.8	6.5	5.3
Ti-SBA-15 (68)	30	68	10.1	11.6	6.7	4.9
Ti-SBA-15 (104)	40	104	10.1	11.6	6.5	5.1
Ti-SBA-15 (119)	50	119	10.0	11.5	6.5	5.1
Ti-MCM-41	20	35	4.1	3.6	2.9	0.5

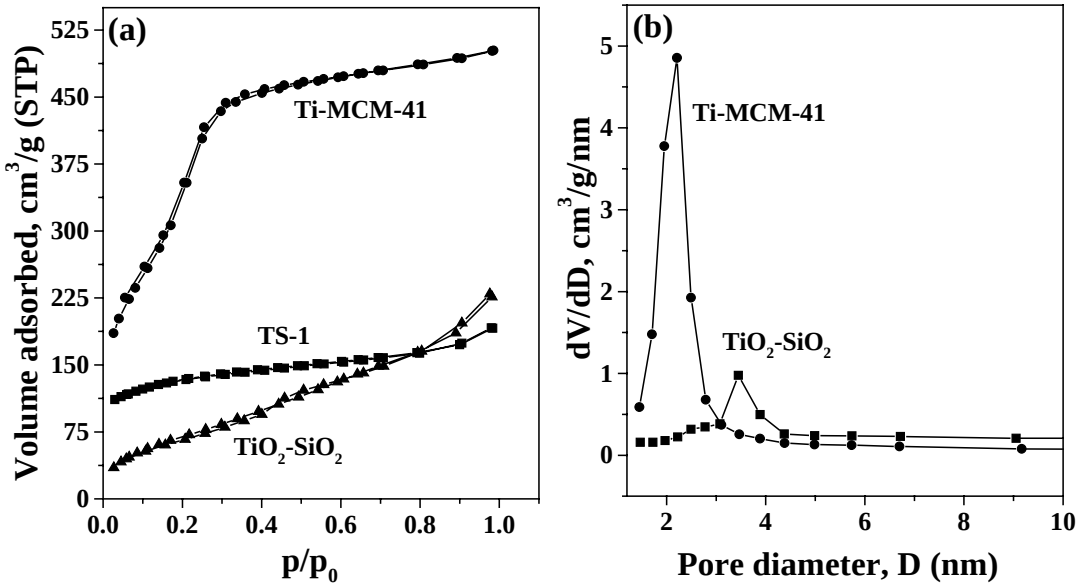

Fig. 2.6. (a) N_2-adsorption/desorption isotherms of TS-1, Ti-MCM-41 and TiO_2-SiO_2; (b) Pore size distribution of Ti-MCM-41 and TiO_2-SiO_2.

2.5.2.2. N_2 Adsorption

Fig. 2.6 shows the N_2-adsorption/desorption isotherms of TS-1, Ti-MCM-41 and TiO_2-SiO_2. The isotherm for TS-1 is characteristic of a microporous material. In the case of Ti-MCM-41, the inflection in the adsorption isotherm at P/P_0 = 0.29 indicates mesopore filling [19]. The textural parameters (S_{BET} and pore volume) of TS-1, Ti-MCM-41 and amorphous TiO_2-SiO_2 are given in Table 2.2.

Table 2.2. Physicochemical characteristics of titanosilicate molecular sieves

Sample	S_{BET} (m^2/g)	Pore diameter (nm)	Total pore volume (cm^3/g)	Mesopore volume (cm^3/g)	Micropore volume (cm^3/g)
SBA-15	871	7.2	1.55	1.44	0.11
Ti-SBA-15 (40)	662	6.5	1.07	0.99	0.08
Ti-SBA-15 (68)	770	6.7	1.29	1.19	0.10
Ti-SBA-15 (119)	794	6.5	1.29	1.19	0.10
Ti-MCM-41 (40)	1055	2.9	0.77	0.61	0.11
TS-1	400	-	-	-	-
TiO_2-SiO_2	273.2	5.1	0.355	0.31	0.041

The nitrogen adsorption/desorption isotherms of SBA-15 are of Type IV nature (Fig. 2.7) and exhibit a H1 hysteresis loop, which is typical of mesoporous solids [21]. Furthermore, the adsorption branch of each isotherm showed a sharp inflection at a relative pressure value of about 0.68. This is characteristic of capillary condensation within uniform pores. The position of the inflection point indicates mesopore structure, and the sharpness of these steps indicates the uniformity of the mesopore size distribution. A good match between the points of inflection on the adsorption branch of

each isotherm suggests that all of the samples have similar pore sizes (~ 6.5 nm) (Fig. 2.7). Furthermore, a narrow pore size distribution is observed for all of the samples.

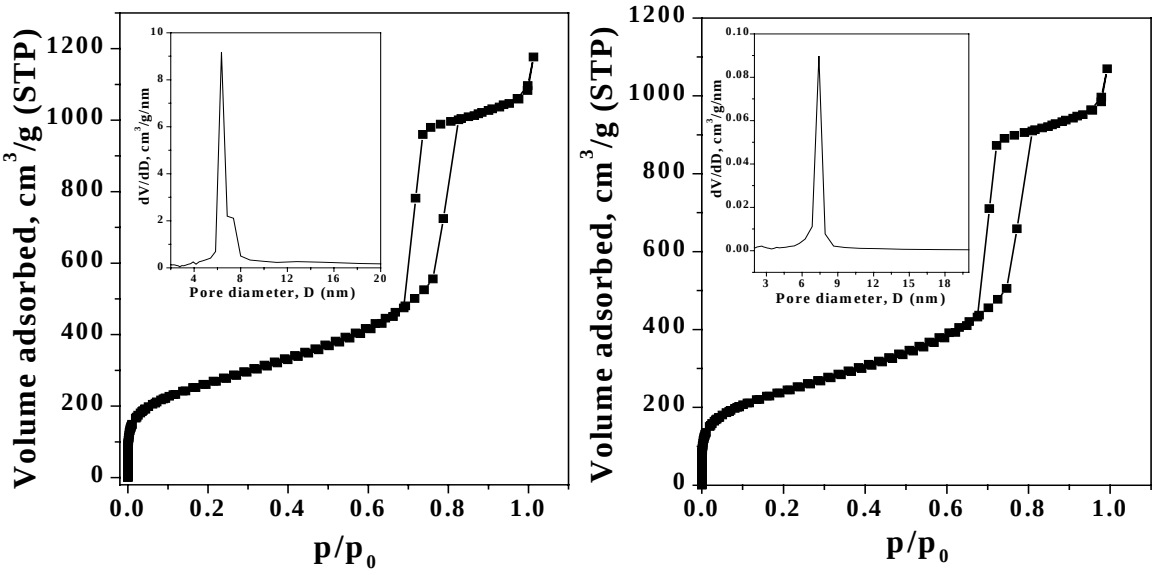

Fig. 2.7. N_2 adsorption/desorption isotherms. Left panel: SBA-15, right panel: Ti-SBA-15 and inset shows pore size distribution.

2.5.2.3. FT-IR

Figs. 2.8 (a) and (b) show the FTIR spectra of TS-1, Ti-MCM-41 and amorphous TiO_2-SiO_2. In all these samples, in addition to the characteristic 960 cm^{-1} band, 1125 cm^{-1} band is also present representing the symmetric stretching of TiO_4 tetrahedron [22]. Bands at 3417 and 3676 cm^{-1} are due to Si-OH and Ti-OH stretching modes [23]. These bands are weakly intense in the case of TS-1 than in Ti-MCM-41 and amorphous TiO_2-SiO_2 indicating that the concentration of hydroxyl groups is low in the former than in the latter samples. Fig. 2.8 (c) shows the FT-IR spectra of SBA-15 samples in the region 1400-400 cm^{-1}. The samples showed characteristic absorption bands at 458, 806 and 957 cm^{-1} assigned to δ(Si-O-Si), ν_s(Si-O-Si) and ν_{as}(Si-O-Ti), respectively.

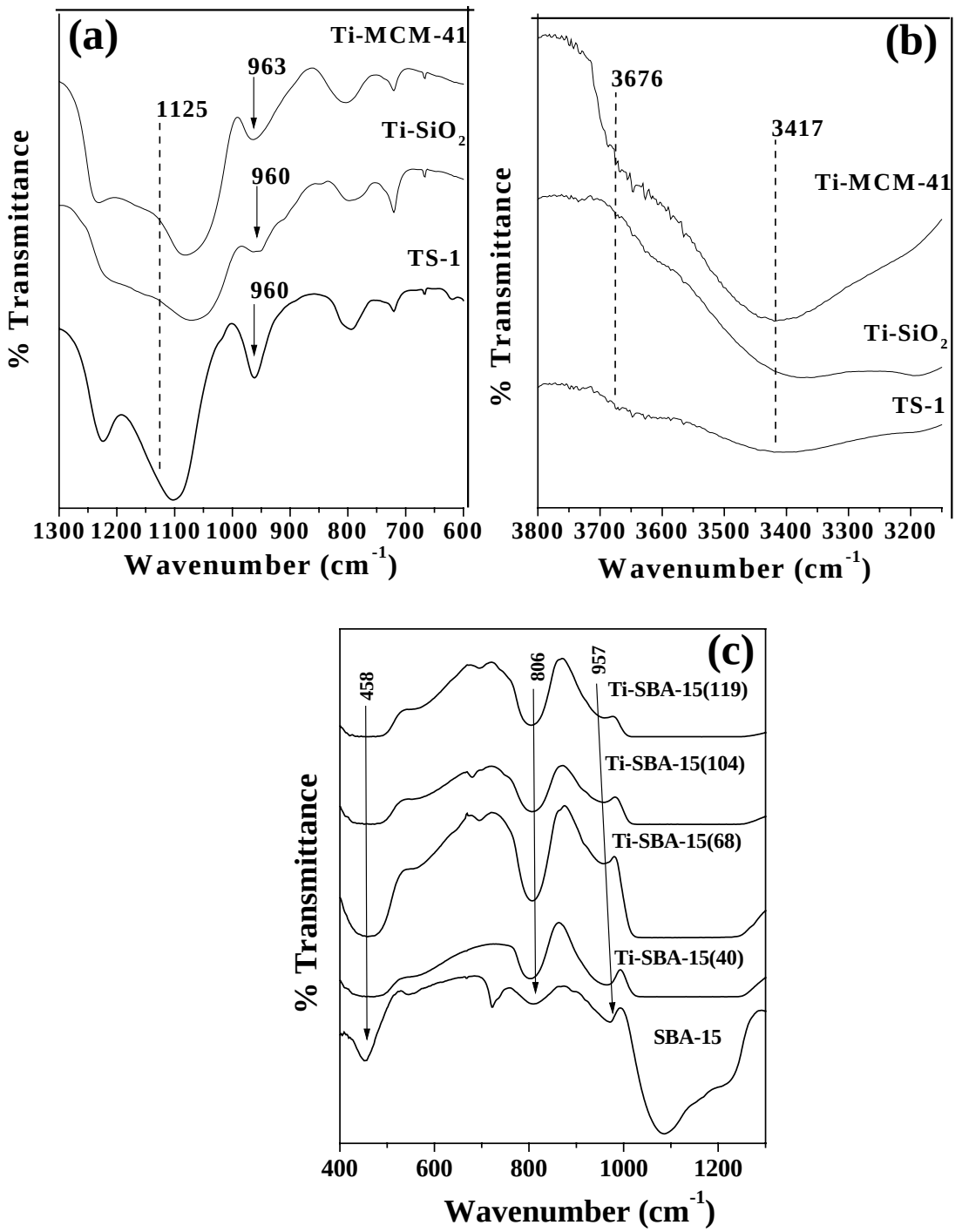

Fig. 2.8. FT-IR spectra of TS-1, Ti-MCM-41 and amorph. TiO_2-SiO_2: spectral region – (a) 600 – 1300 cm^{-1} and (b) 3050 – 3800 cm^{-1}. (c) FT-IR spectra of Ti-SBA-15 samples. Spectral region 400 – 1300 cm^{-1}.

2.5.2.4. DRUV-Visible

Additional evidence for isolated Ti ions in tetrahedral locations in the silicate lattice comes from the DRUV-Visible spectroscopy [24]. DRUV-Visible spectroscopy shows a characteristic band at 206 nm for TS-1 and at 215 nm for Ti-MCM-41 and Ti-SBA-15. This band arises from a charge transfer process from the ligand oxygen to an unoccupied orbital of Ti in isolated $Ti(OSi)_4$ or $Ti(OSi)_3(OH)$ units. In addition to a major tetrahedral Ti species, Ti-MCM-41 possesses also a small quantity of penta- and hexa-coordinated Ti species as shown by weak absorptions at 265 and 310 nm, respectively in Fig. 2.9 (a) [24]. Anatase titania phase is completely absent in all the titanosilicate samples investigated in the present work.

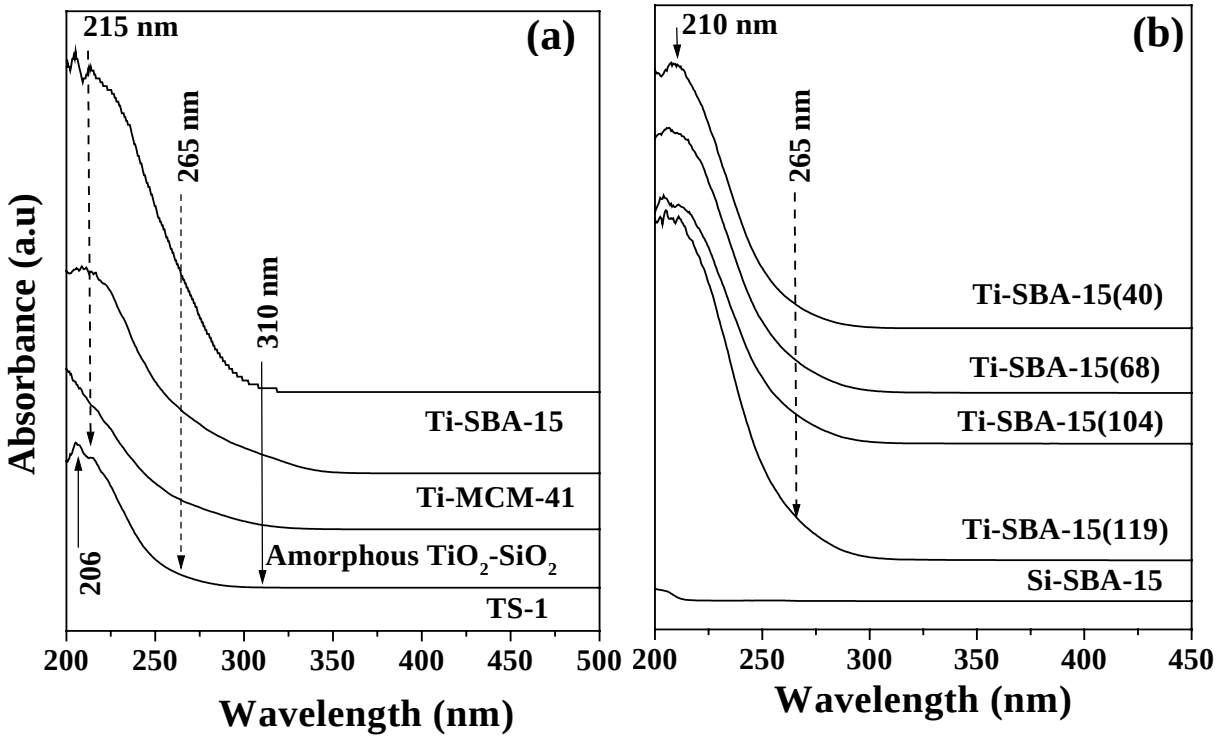

Fig. 2.9. DRUV-Visible spectra of different titanosilicate molecular sieves.

2.5.2.5. EPR

Titanosilicates are diamagnetic and EPR inactive indicating that Ti is in +4 oxidation state. Upon reaction with hydrogen peroxide, paramagnetic superoxide species $Ti(O_2^{\bullet-})$ are generated (Fig. 2.10) [25]. When TS-1 was contacted with H_2O_2, two type of superoxides are identified, a major species (designated as A) with g_{zz} = 2.0236, g_{yy} = 2.0100 and g_{xx} = 2.0091, and a minor species (designated as B) differing only in its g_{zz} value which is 2.027 in contrast to 2.0236. The A type species are assigned to those superoxides arising from the framework Ti sites and the B type species arising from the defect Ti sites such as $Ti(OSi)_3(OH)$. When amorphous TiO_2-SiO_2 was contacted with H_2O_2, it also showed two types of superoxide signals but the B type superoxo-Ti is more predominant.

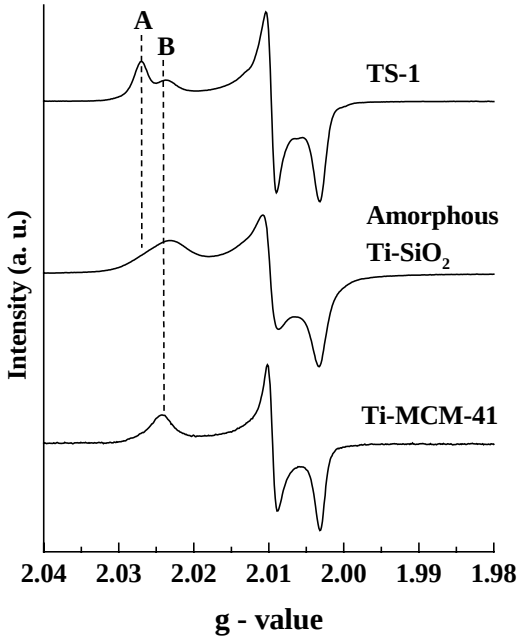

Fig. 2.10. EPR spectra of titaniosilicates interacted with aqueous H_2O_2 at 210 K.

2.5.2.6. TEM

TEM studies established the 2D hexagonal pore arrays and mesostructure of SBA-15 materials (Fig. 2.11). The pore diameter estimated form the TEM measurements (~8 nm) agrees well with that obtained (7.2 nm and 6.7 nm) from nitrogen adsorption (BJH) method for SBA-15 and Ti-SBA-15 samples. The samples investigated in the present study show a curved arrangement of the channels in the mesoscopic range consistent with the high TEOS to template (EO_{20}-PO_{70}-EO_{20}) ratio in the samples during their synthesis [26].

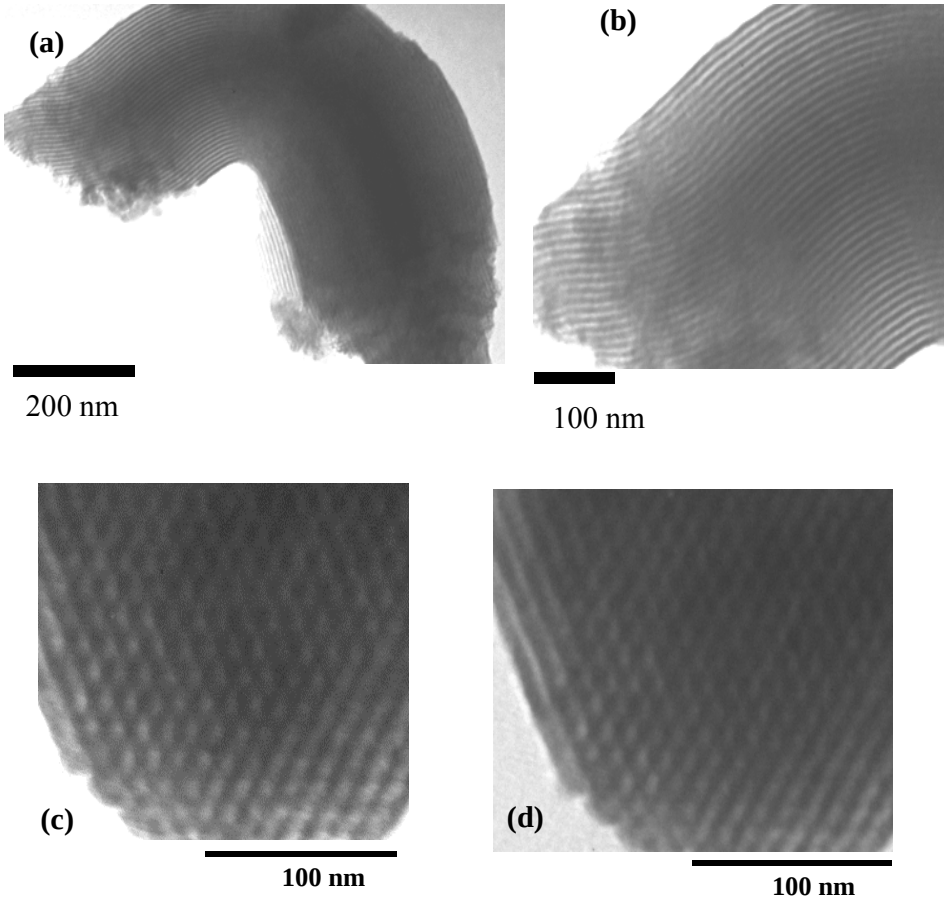

Fig. 2.11. TEM of SBA-15 ((a), (b) - mesoscopic range and (c) - microscopic range) and Ti-SBA-15 ((d) – microscopic range).

2.6. Organo-functionalized, Ordered Mesoporous Materials

Cycloaddition reaction investigated in the present study requires an acidic site and a basic site. SBA-15 being thermally more stable and having large pores is more appropriate for transformation of larger substrate molecules. In view of this the surface of SBA-15 was organo-functionalized with several amines of varying basicity. Ti and Al are incorporated in SBA-15 to form the acid centers. The synthesis of various organo-functionalized materials investigated is described below.

2.6.1. Synthesis

2.6.1.1. SBA-15-pr-NH_2 and Ti-SBA-15-pr-NH_2

In a typical organo-functionalization, SBA-15 and Ti-SBA-15 were activated under vacuum at 423 K for about 3 h. To it, 3-aminopropyltriethoxysilane (9 mmol per 3 g of SBA-15; Lancaster) in 100 ml of dry toluene was added and refluxed under nitrogen for 6 h. Soxhlet extraction with dichloromethane (12 h) and then with acetone (12 h) yielded NH_2-functionalized SBA-15 materials, SBA-15-*pr*-NH_2, Ti-SBA-15-*pr*-NH_2, respectively [27].

2.6.1.2. SBA-15-pr-Ade and Ti-SBA-15-pr-Ade

SBA-15 and Ti-SBA-15 were activated under vacuum at 423 K for about 3 h. To it, 3-chloropropyltriethoxysilane (9 mmol per 3 g of SBA-15; Lancaster) in 100 ml of dry toluene was added and refluxed under nitrogen for 6 h. Soxhlet extraction with first dichloromethane (12 h) and then with acetone (12 h) yielded Cl-functionalized SBA-15 materials, SBA-15-*pr*-Cl, Ti-SBA-15-*pr*-Cl, respectively.

Adenine (1.76 mmol, Aldrich Co.) was taken in 30 ml of dry DMF and stirred for 30 min under nitrogen environment at 393 K for complete dissolution. Then, 1.0 g of

SBA-15-pr-Cl or Ti-SBA-15-*pr*-Cl was added and stirring was continued for 12 h. The solid was filtered, Soxhlet extracted with DMF (10 h) initially and then with CH_3CN (12 h).

2.6.1.3. SBA-15-pr-Gua and Ti-SBA-15-pr-Gua

In a typical synthesis, guanine (1.76 mmol; Merck India) was taken in 30 ml of dry DMF and stirred for 30 min under nitrogen environment at 393 K for complete dissolution. Then, 1.0 g of SBA-15-pr-Cl or Ti-SBA-15-*pr*-Cl (prepared as above) was added and stirring was continued for 12 h. The solid product was filtered, Soxhlet extracted first with DMF (10 h) and then with CH_3CN (12 h).

2.6.1.4. SBA-15-pr-Im and Ti-SBA-15-pr-Im

In a typical organo-functionalization, imidazole (3.0 mmol; Merck. India) was taken in 30 ml of dry chloroform and stirred for 30 min under nitrogen environment at 373 K for complete dissolution. Then, 1.0 g of SBA-15-pr-Cl or Ti-SBA-15-*pr*-Cl was added and stirring was continued for 12 h. The solid was filtered, Soxhlet extracted first with $CHCl_3$ (for 10 h) and then with CH_3CN (for 12 h).

2.6.1.5. Al-SBA-15

Mesoporous silica Al-SBA-15 was synthesized according to the reported procedure [28]. In a typical synthesis, 4 g of amphiphilic triblock copolymer, poly (ethylene glycol)-block-poly (propylene glycol)-block-poly (ethylene glycol) with (average molecular weight 5800, Aldrich), was dissolved in 30 ml of water. After stirring for 4 h at 298 K a clear solution was obtained. To that, 1.75 g of HCl diluted in 70 ml of distilled water was added. The solution was stirred for 2 h at 313 K and then 9 g of TEOS and 1.26 g of aluminum isopropoxide (input Si/Al = 7; Aldrich Co.) were added to it and

the stirring was continued to another 20 h at 313 K. The gel was aged at 373 K for 48 h. The solid obtained was filtered, washed thoroughly with distilled water and then calcined at 823 K for 6 h to obtain Al-SBA-15 with final Si/Al composition of 22.

2.6.1.6. Al-SBA-15-pr-Ade

In a typical organo-functionalization, Al-SBA-15 was activated under vacuum at 423 K, for about 3 h. To it, 3-chloropropyltriethoxysilane (9 mmol per 3 g of Al-SBA-15; Lancaster) in 100 ml of dry toluene was added and refluxed under nitrogen for 6 h. Soxhlet extraction with dichloromethane (for 12 h) and then with acetone (for 12 h) yielded Cl-functionalized material, Al-SBA-15-*pr*-Cl. Adenine functionalization was done in a similar way as described above for the Ti-containing samples.

2.6.2. Characterization

2.6.2.1. XRD

Fig. 2.12 shows the XRD pattern of Ti-SBA-15 (Si/Ti = 40) and functionalized Ti-SBA-15. All the samples showed very similar XRD patterns. The samples showed three well-resolved diffraction peaks due to (100), (110) and (200) reflection in the 2θ range of 0.8 – 2°, that could be indexed according to a 2D hexagonal *p6mm* symmetry. The well-retained (110) and (200) peaks confirm the hexagonal pore arrangements in the functionalized SBA-15 materials. The low-angle peak corresponding to the (100) reflection broadened and reduced in intensity on encapsulation of organic bases due to pore filling (Fig. 2.12). The d-spacing (d_{100}), estimated from the position of the low-angle peak is in the range of 9.8 to 10.4 nm. The unit cell parameter calculated using the equation $a = 2d_{100}/\sqrt{3}$ (11.3 – 11.9 nm) (Table 2.3) is in good agreement with the values reported by others [29].

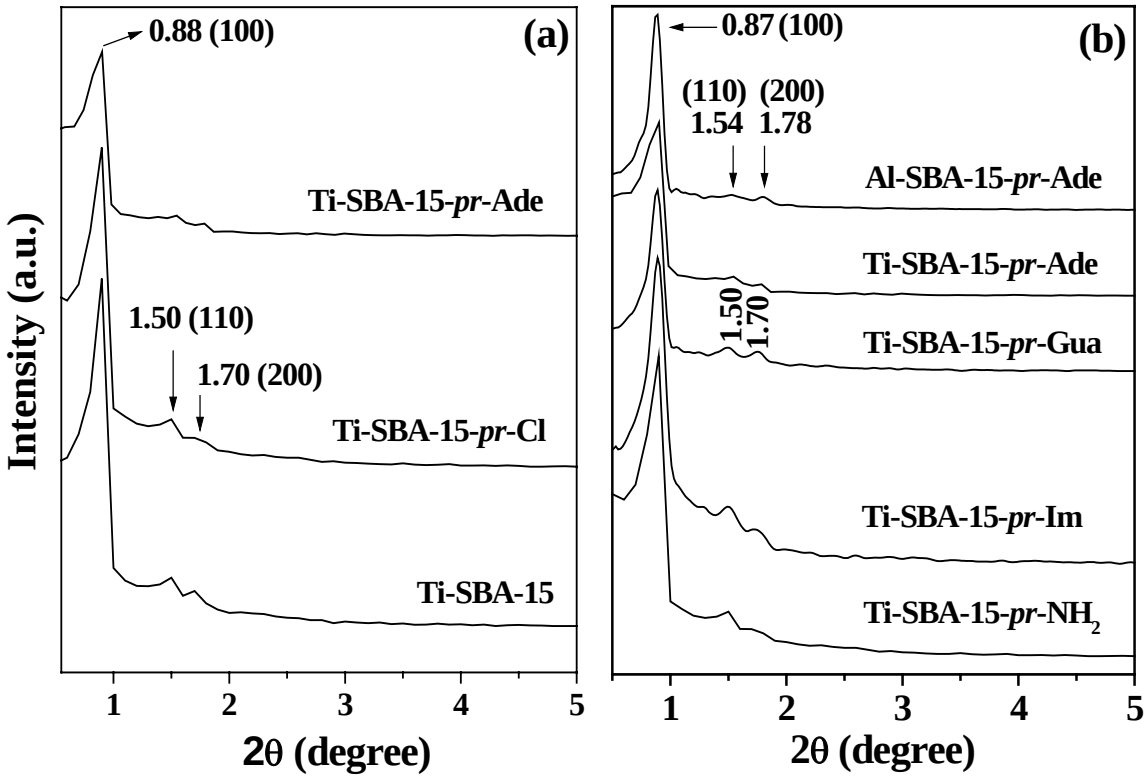

Fig. 2.12. XRD profiles of base-functionalized Ti-SBA-15 molecular sieves.

2.6.2.2. Chemical composition

The Si/Ti and Si/Al contents in metal ion-incorporated SBA-15 materials were determined by XRF and EDAX (Table 2.3). The organic composition (C, H and N) was estimated by elemental analysis. The amount of the functionalized base was estimated to be 0.8 - 2.5 mmol/g SBA-15 (Table 2.3). As expected, the amount functionalized varied with the size of the organic base. In the case of metal-incorporated materials, the amount of functionalized organic base is lower than that in the materials containing no Ti or Al ions.

2.6.2.3. TEM

Transmission electron micrograph (TEM) (Fig. 2.13) viewed through different orientations clearly reveal the 2D hexagonal pore arrangement and the long-range mesopore architecture. It may be noted that the long-range mesoporous-ordering characteristic of good-quality SBA-15 materials (see curved ordered features in TEM) is not disturbed due to metal incorporation and organic-functionalization (Figs. 2.13 (b) and (c)). The pore diameter estimated form the TEM measurement agrees well with that obtained from nitrogen adsorption (BJH) method for SBA-15 and Ti-SBA-15 (Table 2.3).

2.6.2.4. N_2 Adsorption

All the catalysts showed type IV nitrogen adsorption-desorption isotherms with H_1 hysterisis (Fig. 2.14). The textural properties of the materials are listed in Table 2.3. On introduction of the acid-base functionality a marked decrease in specific surface area (S_{BET}), pore volume and average pore diameter was observed. The adsorption branch of each isotherm showed a sharp inflection at a relative pressure value of about 0.68. This is characteristic of capillary condensation within uniform pores. The position of the inflection point corresponds to mesopore structure.

2.6.2.5. FT-IR

FT-IR spectroscopy provided clear evidence for metal incorporation and organo-functionalization (Fig. 2.15). SBA-15 showed a characteristic, broad band in the NIR region attributable to surface hydroxyl groups and H-bonded network –OH groups in the spectral range 3200 – 3700 cm^{-1}.

Table 2.3. Physicochemical properties of SBA-15 materials

Material	Si/M Output mol ratio (XRF/ EDAX)	Organic amine (mmol/g material)[a]	Elemental analysis (wt%)			XRD analysis		S_{BET} (m^2/g)	Pore volume (cm^3/g)			Pore diameter (nm)[b]	Wall thick-ness (nm)
			C	H	N	d_{100} (nm)	Unit cell parameter (nm)		Total	Meso pore	Micro pore		
SBA-15	-	-	0.5	1.5	0	9.8	11.3	871	1.55	1.44	0.11	7.2	4.1
Ti-SBA-15	40	-	0.6	1.7	0	10.3	11.8	662	1.07	0.99	0.08	6.5 (8.0)	5.3
Al-SBA-15	22	-	0.3	0.7	0	10.4	11.9	808	1.15	1.0	0.15	5.7 (7.9)	6.2
SBA-15-*pr*-NH_2	-	2. 5	10.2	1.9	3.4	10.0	11.5						
Ti-SBA-15-*pr*-NH_2	40	2.2	10.2	2.3	3.1	9.8	11.3	615	1.04	0.98	0.06	6.7	4.6
SBA-15-*pr*-Im	-	2.3	12.2	1.4	5.5	10.0	11.5						
Ti-SBA-15-*pr*-Im	40	1.9	11.9	1.2	5.4	9.9	11.4	432	0.65	-	-	6.1	5.3
SBA-15-*pr*-Gua	-	1.1	11.9	1.4	7.9	10.1	11.6						
Ti-SBA-15-*pr*-Gua	40	1.0	11.5	1.4	6.8	10.0	11.5						
SBA-15-*pr*-Ade	-	1.3	11.3	1.5	7.7	10.0	11.5						
Ti-SBA-15-*pr*-Ade	40	0.9	10.7	1.3	6.4	10.0	11.5	627	1.04	0.96	0.08	6.7 (7.6)	4.3
Al-SBA-15-*pr*-Ade	22	0.8	8.9	2.1	6.0	10.0	11.5	426	0.66	0.64	0.02	5.7 (7.5)	4.8

[a]Values estimated from C, H & N analysis.

[b]Values in parentheses are those estimated from TEM.

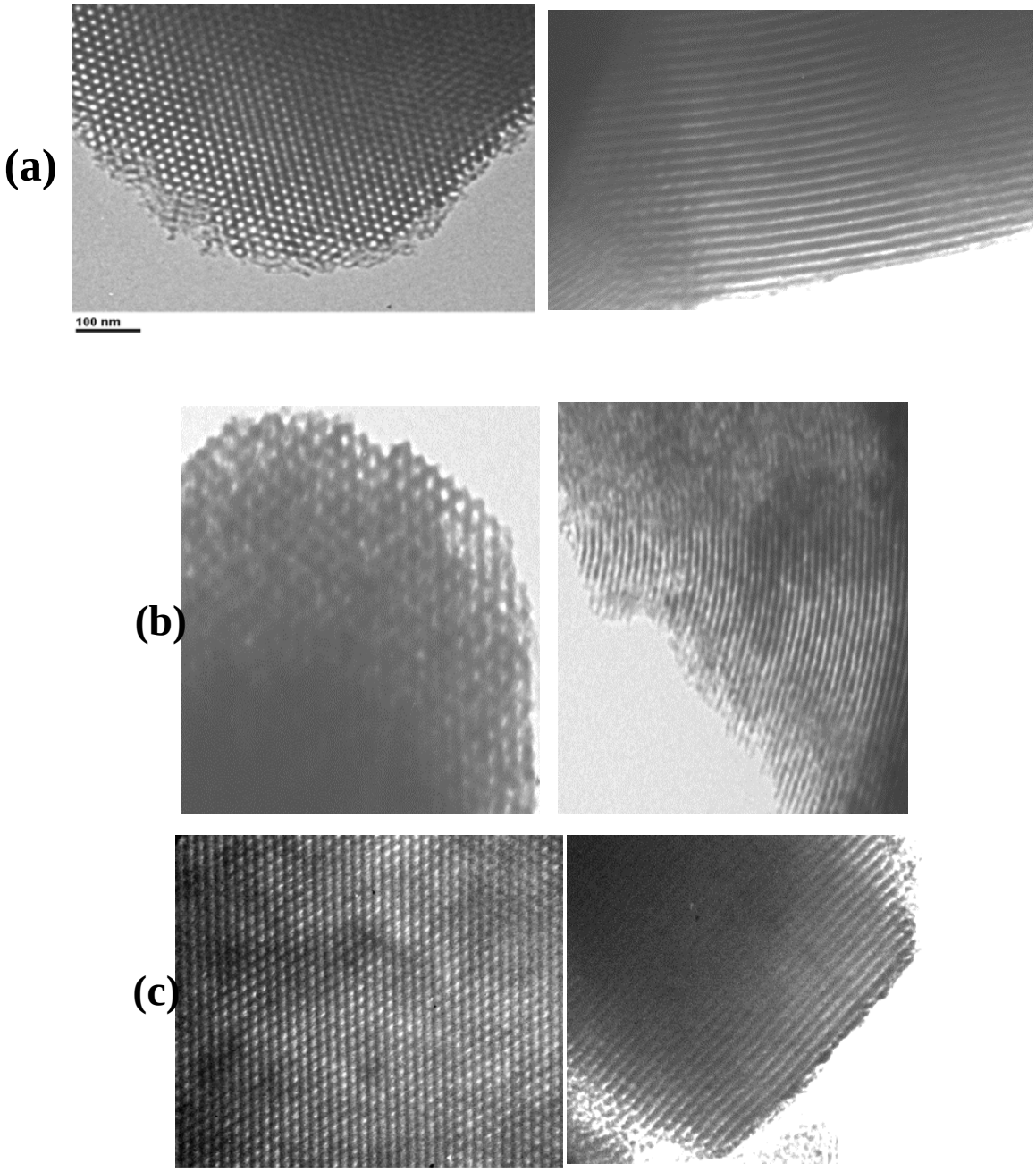

Fig. 2.13. TEM images (magnification 100 nm) of (a) Al-SBA-15 at microscopic range (left) and mesoscopic range (right), (b) Al-SBA-15-*pr*-Ade at microscopic range (left) and mesoscopic range (right) and (c) Ti-SBA-15-*pr*-Ade at microscopic range (left) and mesoscopic ranges (right).

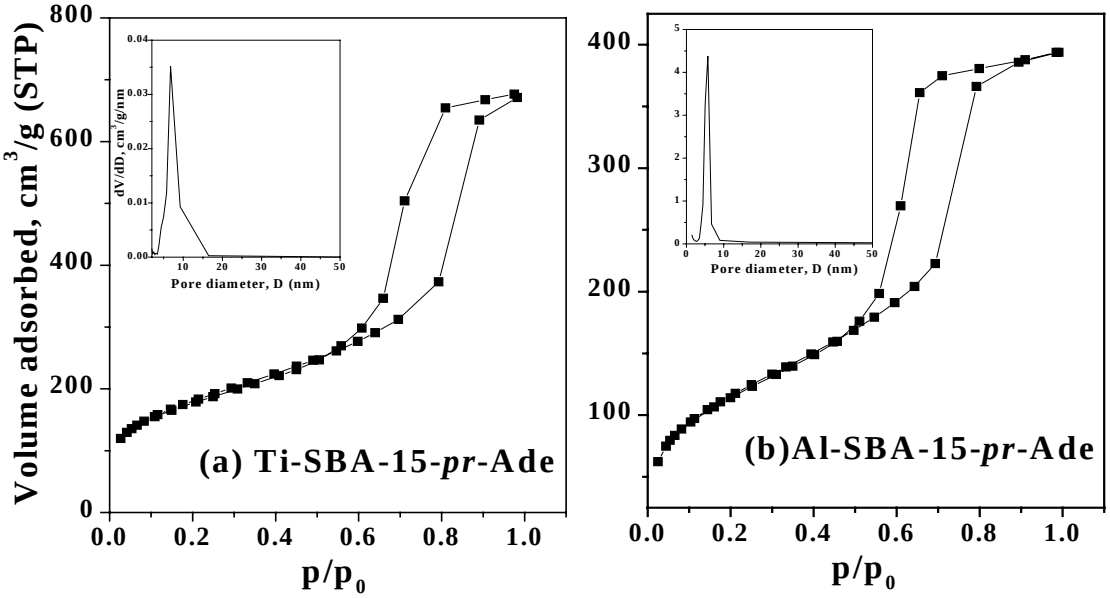

Fig. 2.14. Nitrogen adsorption/desorption isotherms of Ti-SBA-15-*pr*-Ade and Al-SBA-15-*pr*-Ade. Inset shows pore size distribution.

Upon metal incorporation and organic functionalization the intensity of this band decreased and became relatively sharper indicating that some of the surface –OH groups (involved in forming H-bonded networks) are utilized in functionalization. The IR peaks marked at 3325, 3300 and 3124 cm^{-1}, are due to N-H stretching modes of the functionalized-adenine and guanine. It may be noted that these peaks are absent in imidazole-functionalized materials. In the case of imidazole the hydrogen of secondary NH is used-up during anchoring covalently to the SBA-15 surface. Hence, the imidazole-functionalized materials contained no NH group that can be seen in the NIR spectrum. Characteristic peaks due to C-H stretching vibrations (of propyl spacer, Im, Gua and Ade) appeared at 2857 and 2930 cm^{-1}. Further, evidence for the presence of the organic bases was obtained from the sharp, characteristic peaks in the mid-IR region (Fig. 2.15). It should be noted that these peaks are absent in non-functionalized SBA materials. While

the bands at 1557 cm^{-1} (for Ti-SBA-15-*pr*-Gua) and 1600 cm^{-1} (for Ti-SBA-15-*pr*-Ade) correspond to azomethine (C=N) group, the band at 1700 cm^{-1} present only in the case of Ti-SBA-15-*pr*-Gua corresponds to the C=O group of guanine. The rest of the bands are due to ring and skeletal vibrations. Adenine and other bases could not be deposited directly by impregnation on the unsilynated SBA-15 surface as it leached out during Soxhlet extraction with DMF and CH_3CN. In this case, the IR spectrum of the solid after the extraction did not detect adsorbed adenine. In other words, in the absence of –Cl groups of the 3-chloropropyltriethoxysilane, the adenine and the other bases could not be anchored. The –NH group of adenine, guanine and imidazole reacts with the –Cl forming N-C bonds and eliminating HCl in the process.

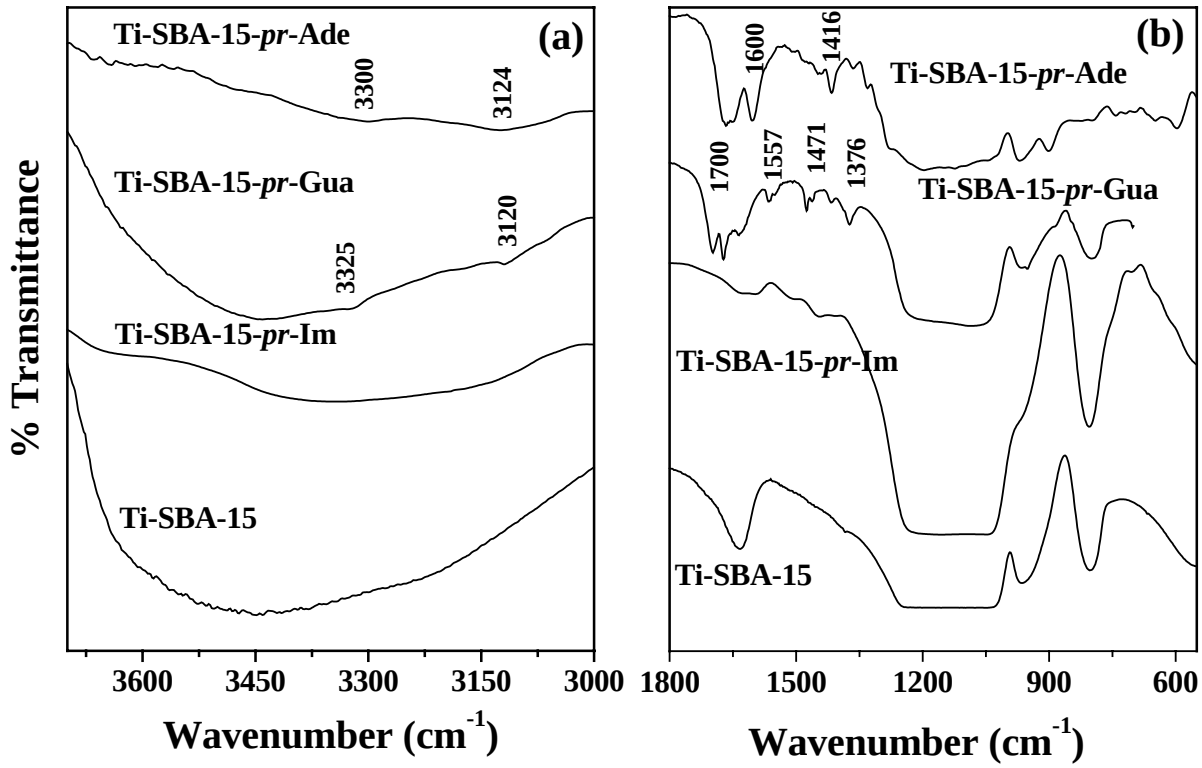

Fig. 2.15. (a) Near-IR (b) Mid-IR spectra of functionalized Ti-SBA-15 samples.

2.6.2.6. DRUV-Visible

Pure adenine showed two characteristic UV bands at 244 and 288 nm due to π-π^* and n-π^* transitions. Adenine in SBA-15-*pr*-Ade, Ti-SBA-15-*pr*-Ade and Al-SBA-15-*pr*-Ade showed only one electronic band at 265 nm (Fig. 2.16). Similarly, pure guanine showed UV bands at 247 and 294 nm. However, SBA-15-*pr*-Gua and Ti-SBA-15-*pr*-Gua, showed these bands at 250 and 302 nm. The charge transfer band at 211 nm corresponds, probably, to dispersed tetrahedral Ti and Al ions.

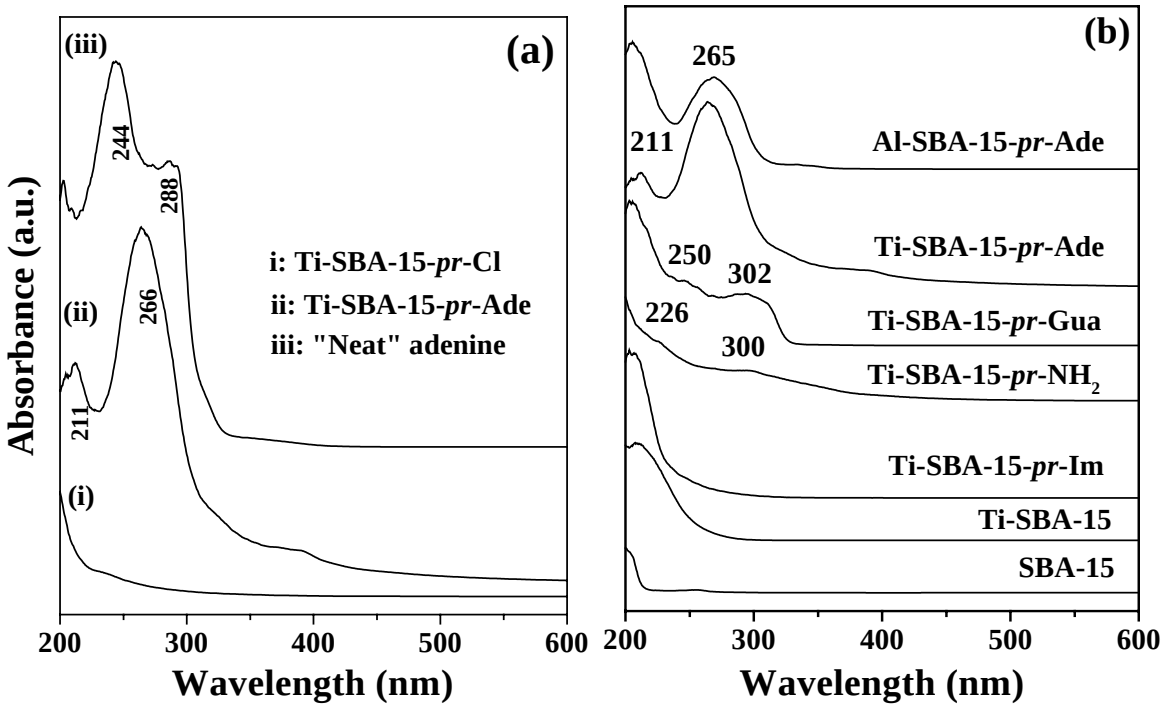

Fig. 2.16. DRUV-Visible spectra of "neat" adenine and functionalized SBA-materials.

2.6.2.7. Thermal Analysis

The thermal stability of functionalized SBA-15 materials was estimated using thermogravimetric and differential thermal analysis (TG-DTA) (Fig. 2.17). SBA-15 showed two stages of weight loss: Stage I (308 – 410 K, 6.8 wt%) is due to desorption of

adsorbed water. Stage II (410 – 535 K, 40.6 wt%) is due to decomposition of silanol groups (2Si-OH → Si-O-Si + H_2O). Pure adenine decomposed in the temperature range 483 – 618 K. Functionalized SBA-15 materials showed three stages of weight loss (Fig. 2.17 and Table 2.4). As in the case of unsilynated samples, stage I in the silynated samples is also due to desorption of adsorbed water. Stages II and III (in functionalized materials *ca.*, SBA-15-*pr*-NH_2, SBA-15-*pr*-Ade and Ti-SBA-15-*pr*-Ade) are attributed to decomposition of functionalized organic matter (base NH_2/Ade and propyl group, respectively). Stage II has contribution also from the silanol groups. In an independent analysis (by C, H & N), we have also estimated the amount of organic base (from C, H, and N content) (Table 2.4). From the total weight loss (TG-DTA) and base content (C, H & N), the decomposed silanol groups, contributing to stage II, were determined (Table 2.4). Interestingly, the weight loss due to silanols decomposition decreased, significantly, from 45.2 mmol/g (in SBA-15) to 3.8 – 7 mmol/g (in functionalized SBA-15). This is because during the process of silynation/functionalization of SBA-15 with 3-aminopropyltriethoxysilane and 3-chloropropyltriethoxysilane a significant part of the silanols are consumed. The functionalized organic base is thermally stable at least up to 473 K. Apart from the thermal stability this analysis also provided unequivocal evidence for silynation/organic-functionalization.

Table 2.4. Thermal and elemental analysis of functionalized SBA-15 materials

Material	Stage No.	Temperature region (K)	Weight loss (%)	Assignment for weight loss	N-content (mmol/g silica)	Concentration of H_2O/Si-OH Desorbed/decomposed (mmol/g silica)[b]
SBA-15	I	308 – 410	6.8	Desorption of physisorbed/chemisorbed water	-	3.8 (H_2O)
	II	410 - 535	40.6	Decomposition/condensation of silanol groups (2Si-OH → Si-O-Si + H_2O)	-	45.2 (Si-OH)
SBA-15-*pr*-NH_2	I	308 – 375	5.4	Desorption of physisorbed/chemisorbed water	-	3.0 (H_2O)
	II	375 – 530		Decomposition organic functional	2.5	3.8 (Si-OH)
	III	530 – 862	17.1[a]	group (propyl amine) and silanol groups		
"Neat" Adenine	I	483 - 618	100.0	Decomposition of Adenine	-	-
SBA-15-*pr*-Ade	I	308 – 463	5.7	Desorption of physisorbed/chemisorbed water	-	3.2 (H_2O)
	II	463 – 607		Decomposition organic functional	1.3	5.6 (Si-OH)
	III	607 – 848	25.0[a]	group (propyl adenine) and silanol groups		
Ti-SBA-15-*pr*-Ade (Si/Ti = 40)	I	308 – 415	5.2	Desorption of physisorbed/ chemisorbed water	-	2.9 (H_2O)
	II	415 – 586		Decomposition organic functional	0.91	7.0 (Si-OH)
	III	586 – 835	23.1[a]	group (propyl adenine) and silanol groups		

[a]Refers to total weight loss in stages II and III.
[b]Values are estimated from the total weight loss in thermal analysis and the functionalized organic base content estimated from C, H & N analysis.

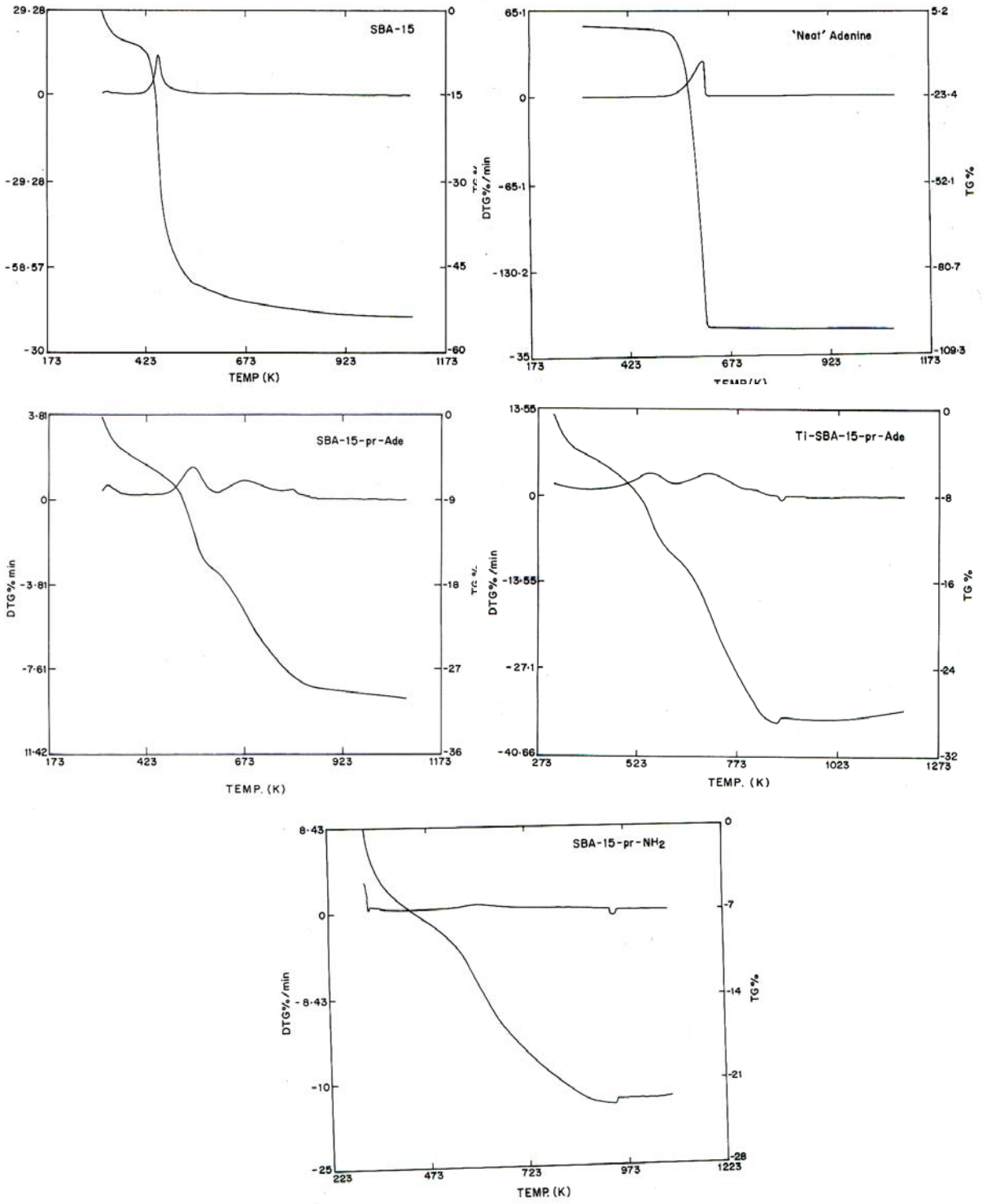

Fig. 2.17. TGA-DTA plots for SBA-15, "neat" Adenine, SBA-15-*pr*-Ade, Ti-SBA-15-*pr*-Ade and SBA-15-*pr*-NH_2.

2.7. Organic-Inorganic Hybrid Catalysts

Commercially quaternary ammonium halide salts are used as catalysts in the synthesis of cyclic carbonates. However, separation of them at the end of the reaction is an issue in those process. There are reports immobilizing the quaternary ammonium salts on resins and their use as heterogeneous catalysts in catalytic reactions. Most of the zeolites and mesoporous silica material are prepared using quaternary ammonium salts as structure directing agents. The as-synthesized forms of zeolite materials contain the salts in an encapsulated form. Hence, they can be used as heterogeneous catalysts. Further, encapsulation, dispersion and the nature of zeolite structure may influence the catalytic activity of the entrapped quaternary ammonium salts. Two systems of organic-inorganic hybrid catalysts viz., as-synthesized zeolite beta and MCM-41 are investigated in this section.

2.7.1. Synthesis and Characterization

2.7.1.1. Zeolite-Beta

Zeolite-beta was synthesized using following molar composition of the synthesis gel: $3Na_2O$: $5(TEA)_2O$: Al_2O_3: $60SiO_2$: 1500 H_2O [30]. In a typical synthesis, 2.46 g of NaOH was mixed with a slurry of 72 g of fumed SiO_2 in 440 g of double distilled water. To it, a mixture of 73.5 g of tetraethyl ammonium bromide (Aldrich Co.) and a solution of 4.65 g of sodium aluminate (Aldrich Co.) in 55.9 g of water was added with stirring. The synthesis was carried out at 423 K for 8 days. Then the solid was filtered and dried at 353 K.

Analysis: Si/Al = 50; nitrogen content in as synthesized zeolite beta = 2.09 wt %; S_{BET} (calcined zeolite beta) = 520 m^2/g; $S_{External}$ (calcined zeolite beta) = 85 m^2/g; pore

volume = 0.25 ml/g; average pore diameter = 0.59 nm; S_{BET} (as synthesized zeolite beta) = 46 m^2/g.

2.7.1.2. MCM-41

MCM-41 was synthesized from the gel of molar composition: TEOS:0.25 CTMABr:0.3 TMAOH::40 H_2O:5 CH_3OH [19]. In a typical synthesis, 10.9 g of tetramethylammonium hydroxide (25 wt.% TMAOH, 99% Aldrich) was taken in 72 g of distilled water. To that, 8.75 g of cetyltrimethylammonium bromide (CTMABr, S. D. Fine Chem. Ltd., India) was added. Then, 20.8 g of tetraethylorthosilicate (TEOS, Aldrich) in 16 g of methanol was added drop-wise over a period of 20 min. The resultant gel was stirred for further 4 h at 298 K and then transferred into a Teflon-lined stainless steel autoclave and heated to 373 K for 72 h. The solid product was filtered, washed with distilled water and dried at 353 K.

Analysis: Si/Al = ∝; nitrogen content in as synthesized MCM-41 = 2.58 wt %; S_{BET} (calcined MCM-41) = 1020 m^2/g; $S_{External}$ (calcined MCM-41) = 102 m^2/g; pore volume = 0.77 ml/g; average pore diameter = 2.8 nm; S_{BET} (as synthesized MCM-41) = 83 m^2/g.

2.8. Solid Double Metal Cyanide Catalysts of Fe and Zn

Double metal cyanides have been widely investigated from the point of view of their structure and electronic properties [31]. One of the members of this family studied extensively is Prussian blue. Only recently (in 2003), their catalytic properties have been reported in a commercially important organic transformation [32]. Fe- and Co-Zn double metal cyanides exhibited remarkable catalytic activity in polyethers synthesis by ring opening polymerization (ROP) of ethene and propene oxides [33]. Interestingly, this

catalyst is insoluble in almost all of the known solvents. It is insoluble even in strong acids and aqua-regia. Hence, it could be used as a solid, reusable catalyst. Zn coordinated to imine groups exhibited superior activity for CO_2 insertion in the epoxide ring to produce cyclic and polycarbonates [34]. A similar structural environment for Zn in Fe-Zn double metal cyanide catalysts was attributed the cause for its high catalytic activity in ROP [33]. In the present study, the activity of Fe-Zn catalysts in another important organic transformation (transesterification reaction) is evaluated, for the first time. Influence of synthesis method (presence of complexing and co-complexing agents) on the catalytic activity of Fe-Zn catalysts is examined. A detailed synthesis of different materials prepared under this category and their characterization is presented below.

2.8.1. Synthesis

2.8.1.1. Double Metal Cyanide Fe-Zn Catalyst Prepared in the Presence of Complexing and Co-complexing Agents (Fe-Zn-1)

$K_4[Fe(CN)_6]$ (0.01 mol; Merck India) was dissolved in 40 ml of double distilled water (solution-1). In a separate beaker, 0.1 mol of $ZnCl_2$ (Merck India) was dissolved in a solution of 100 ml of distilled water and 20 ml of tert.-butanol (Merck India) (solution-2). Tri-block copolymer, poly(ethylene glycol)-block-poly(propylene glycol)-block-poly(ethylene glycol) ($E0_{20}$-PO_{70}-EO_{20}; molecular weight of about 5800) (15 g) was separately dissolved in 2 ml of distilled water and 40 ml of tert.-butanol (solution-3). Solution-2 was added to solution-1 slowly over a period of 60 min at 323 K with vigorous stirring. White precipitation occurred during the addition. Then, solution-3 was added to the above reaction mixture (i.e., solution 1 + solution 2) over a period of 5 - 10 min and stirring was continued for further 1 h. The solid Fe-Zn catalyst (designated as

Fe-Zn-1) formed was filtered, washed thoroughly with distilled water (500 ml) and dried at 298 K for about 2 days. This material was used in catalytic reactions either as-prepared or after activation at a desired temperature (ca., 333 – 673 K) for 4 h. Tert.-butanol acts as complexing agent and tri-block copolymer acts as co-complexing agent [32].

2.8.1.2. Double Metal Cyanide Fe-Zn Catalyst Prepared in the Presence of Complexing Agent (Fe-Zn-2)

The complex was prepared in a similar manner as described above except that the co-complexing agent (tri-block co-polymer) is not used in the synthesis. In a typical preparation procedure, $K_4[Fe(CN)_6]$ (0.01 mol) was dissolved in 40 ml of double distilled water (solution-1). In a separate beaker, 0.1 mol of $ZnCl_2$ was dissolved in a solution of 100 ml of distilled water and 20 ml of complexing agent tert.-butanol (solution-2). Solution-2 was added to solution-1 slowly over a period of 60 min at 323 K with vigorous stirring. White precipitation occurred during the addition. Stirring was continued for further 1 h. The solid Fe-Zn catalyst (designated as Fe-Zn-2) formed was filtered, washed thoroughly with distilled water (500 ml) and dried at 298 K for about 2 days.

2.8.1.3. Double Metal Cyanide Fe-Zn Catalyst Prepared in the Absence of both Complexing and Co-complexing Agents (Fe-Zn-3)

The complex was prepared in the absence of both the complexing and co-complexing agents. In this method, $K_4[Fe(CN)_6]$ (0.01 mol) was dissolved in 40 ml of double distilled water (solution-1). In a separate beaker, 0.1 mol of $ZnCl_2$ was dissolved in 100 ml of distilled water (solution-2). Solution-2 was added to solution-1 slowly over a period of 60 min at 323 K with vigorous stirring. White precipitation occurred during the

addition. Stirring was continued for further 1 h. The solid Fe-Zn catalyst (designated as Fe-Zn-3) formed was filtered, washed thoroughly with distilled water (500 ml) and dried at 298 K for about 2 days.

2.8.2. Characterization

2.8.2.1. Chemical Composition

XRF studies revealed that Fe, Zn and Cl in **Fe-Zn-1** catalyst are in the ratio of 3.7: 6.2: 0.29. C, H and N contents (%, by elemental analysis) were found to be 23.25, 2.24 and 17.27, respectively. From the chemical composition the molecular formula of **Fe-Zn-1** catalyst was estimated as:

Fe-Zn-1 catalyst: $Fe_2Zn_3(CN)_{10}(H_2O)_5(C_4H_{10}OH).0.3\ ZnCl_2$.

Based on the molecular formula and the X-ray structural information available on some ferrocyanide complexes [32] a tentative structure for the complexes may be written as follows:

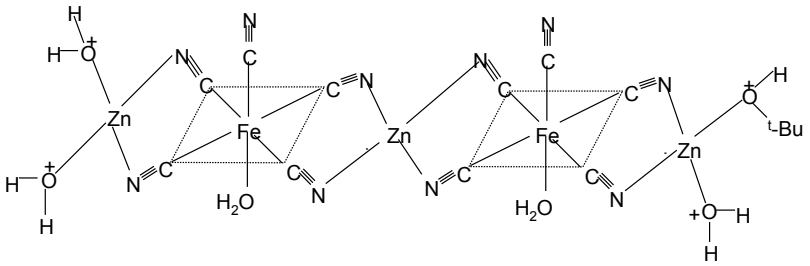

Further confirmation to this structural entity was obtained (see later on) from spectroscopic investigations.

The percentage C, H and N contents for Fe-Zn-2 catalyst were found to be 16.66, 1.23 and 18.5, respectively. Based on these results the following molecular formula is proposed:

Fe-Zn-2 catalyst: $Fe_2Zn_3(CN)_{10}(H_2O)_6.0.3\ ZnCl_2$.

The percentage C, H and N for Fe-Zn-3 catalyst were found to be 18.03, 1.4 and 18.87, respectively. The molecular formula of Fe-Zn-3 catalyst is as follows:

Fe-Zn-3 catalyst: $Fe_2Zn_3(CN)_{12}(H_2O)_4.0.3\ ZnCl_2$.

2.8.2.2. XRD

Fig. 2.18 shows the XRD pattern of Fe-Zn-1 catalyst and its precursor compounds $ZnCl_2$ and $K_4Fe(CN)_6$. The XRD profiles provide clear evidence that the catalyst is highly crystalline and contains no impurity of the starting compounds $ZnCl_2$ and $K_4Fe(CN)_6$. The X-ray pattern indicates that the catalyst system belongs to a cubic lattice with unit parameter of 0.904 nm. The peaks corresponding to various planes are indicated in Fig. 2.18. It may be noted that a Co analogue of this complex - $Zn_3[Co(CN)_6]_2.xZnCl_2.y(tert.\text{-}BuOH).z(H_2O)$ also forms a cubic crystalline structure [35].

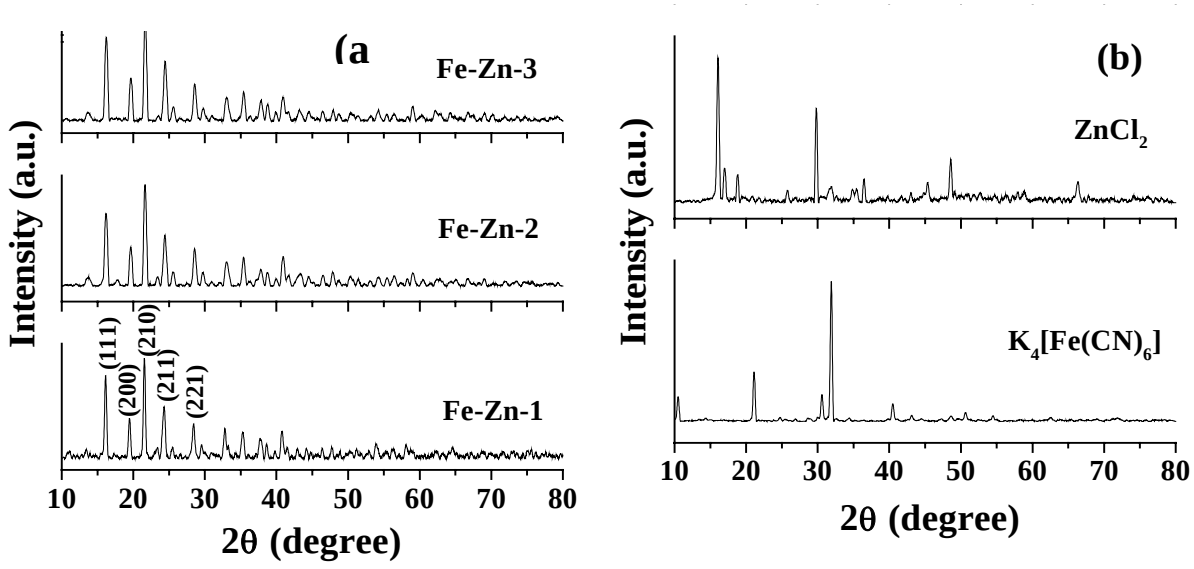

Fig. 2.18. XRD profiles of (a) Fe-Zn double metal cyanide catalysts and (b) their precursor compounds $ZnCl_2$, and $K_4Fe(CN)_6$.

With a view to check the structural stability, Fe-Zn-1 was activated at different temperatures for 4 h and the XRD patterns were recorded. The catalyst was found to be stable up to a minimum temperature of 473 K and then transforms into another compound (Fig. 2.19).

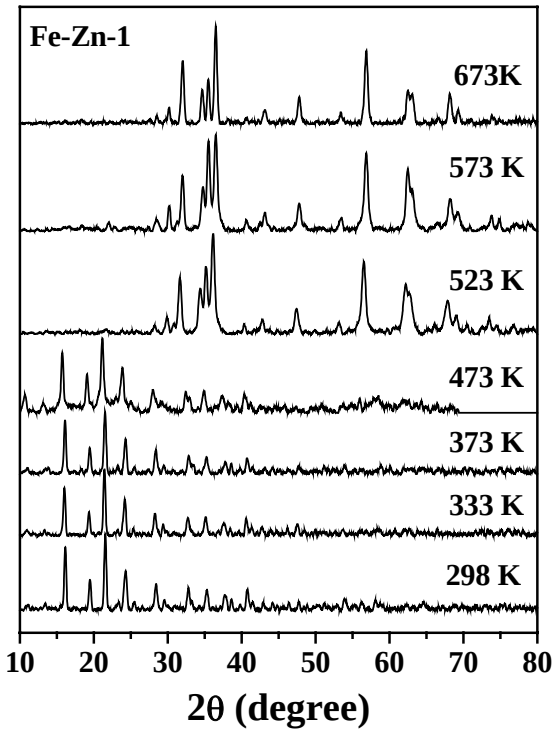

Fig. 2.19. XRD profiles of Fe-Zn-1 catalyst activated at different temperatures.

2.8.2.3. N_2 Adsorption

When the catalyst (Fe-Zn-1) was heated to different temperatures (for 4 h) and activated the specific surface area (S_{BET}) decreased with an increase in the activation temperature. This decrease is marginal below 473 K and more significant above this temperature (S_{BET} for Fe-Zn-1 catalyst: 51.6, 47.2, 41.6 and 19.0 for the catalyst activated at 298 K, 333 K, 473 K and 673 K, respectively).

2.8.2.4. FT-IR

As expected $ZnCl_2$ showed no IR bands. $K_4Fe(CN)_6$ showed an intense band characteristic of ν(C≡N) at 2039 cm^{-1}. In the case of Fe-Zn catalysts, this band shifted to higher wave number region (2096 cm^{-1}) (Fig. 2.20). Cyanide group in a free state shows characteristic ν(CN) band at 2080 cm^{-1} [36]. The shift of this band to higher frequency in the case of Fe-Zn catalysts indicates the coordination of cyanide group to both Zn^{2+} and Fe^{2+} ions. Electron donation tends to raise the ν(CN) since electrons are removed from the 5σ orbital, which is weakly antibonding, while π-back-bonding tends to decrease the ν(CN) because the electrons enter into the antibonding 2pπ* orbital. In general, CN^- is a good σ-donor and a poorer π-acceptor. Thus, ν(CN) for the complexes is generally higher than the value for free CN^-. These results demonstrate that the cyanide ligands are oriented linearly between the divalent Zn and Fe with the C atom coordinated to Fe. The divalent Zn ions are linked to the Fe ions by cyanide bridging. The presence of water molecules and tert.-butanol in the catalyst composition Fe-Zn-1 can be inferred from the additional bands at 3635, 3465, 1620, 1095, 604 and 500 cm^{-1} and several weak bands in the range 1100 – 800 cm^{-1} (Fig. 2.20 (a)). These bands are not present in the other two Fe-Zn catalysts (Fe-Zn-2 and Fe-Zn-3). When Fe-Zn-1 was heated/activated at higher temperatures the following spectral changes were noted (Fig. 2.20 (b)): (1) No major changes in IR spectral pattern was observed up to 473 K. (2) A marked decrease in intensity of the cyanide band (at 2096 cm^{-1}) was observed in samples activated at above 473 K and this band was almost absent in 673 K activated samples. (3) New, intense bands were observed at 1495 and 1380 cm^{-1} for the samples activated above 473 K. These observation in agreement with the X-ray results reveal that catalyst is stable up to

473 K and above that temperature it decomposes into metal nitrogen oxide compounds showing characteristic nitrate bands at 1495 and 1380 cm^{-1}.

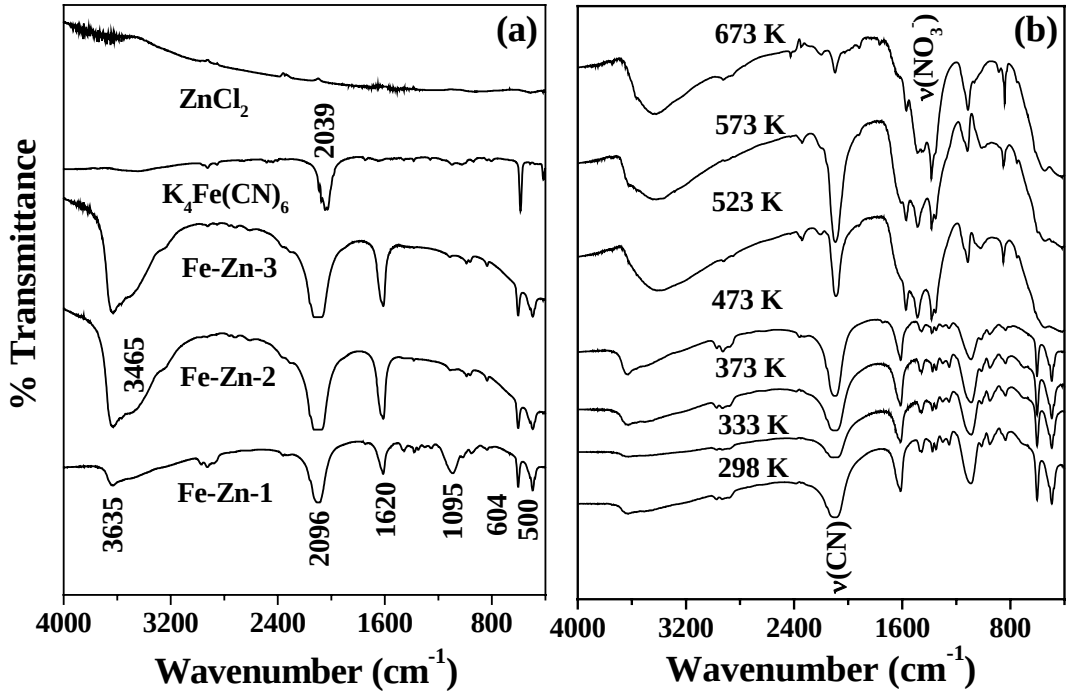

Fig. 2.20. DRIFT spectra of (a) $ZnCl_2$, $K_4Fe(CN)_6$, and Fe-Zn double metal cyanide catalysts (b) Fe-Zn-1 catalyst at various activation temperatures.

2.8.2.5. DRUV-Visible

As expected, $ZnCl_2$ did not show UV-visible bands. $K_4Fe(CN)_6$ showed an intense band at 236 nm and two medium intensity bands at 278 and 330 nm (Fig. 2.21(a)). While the latter two bands are attributed to LMCT transitions, the former one at 236 nm is attributed to π-π* charge transfer of CN ligand. All these bands are blue shifted in the case of Fe-Zn catalysts (Fig. 2.21(a)). Interestingly, while the intensities of the LMCT bands are not much affected, that of π-π* charge transfer transition decreased

considerably in Fe-Zn catalysts. A bridging coordination of CN group to Fe and Zn is the possible cause for this spectral difference.

Information about catalyst stability was deduced also from DRUV-visible spectroscopy (Fig. 2.21(b)). The spectrum was unaffected up to 473 K and beyond that a broad absorption was observed. The disappearance of characteristic charge transfer bands is a clear indication for the decomposition of cyanide ligands into nitrogen oxide groups when the samples are heated to temperatures above 473 K.

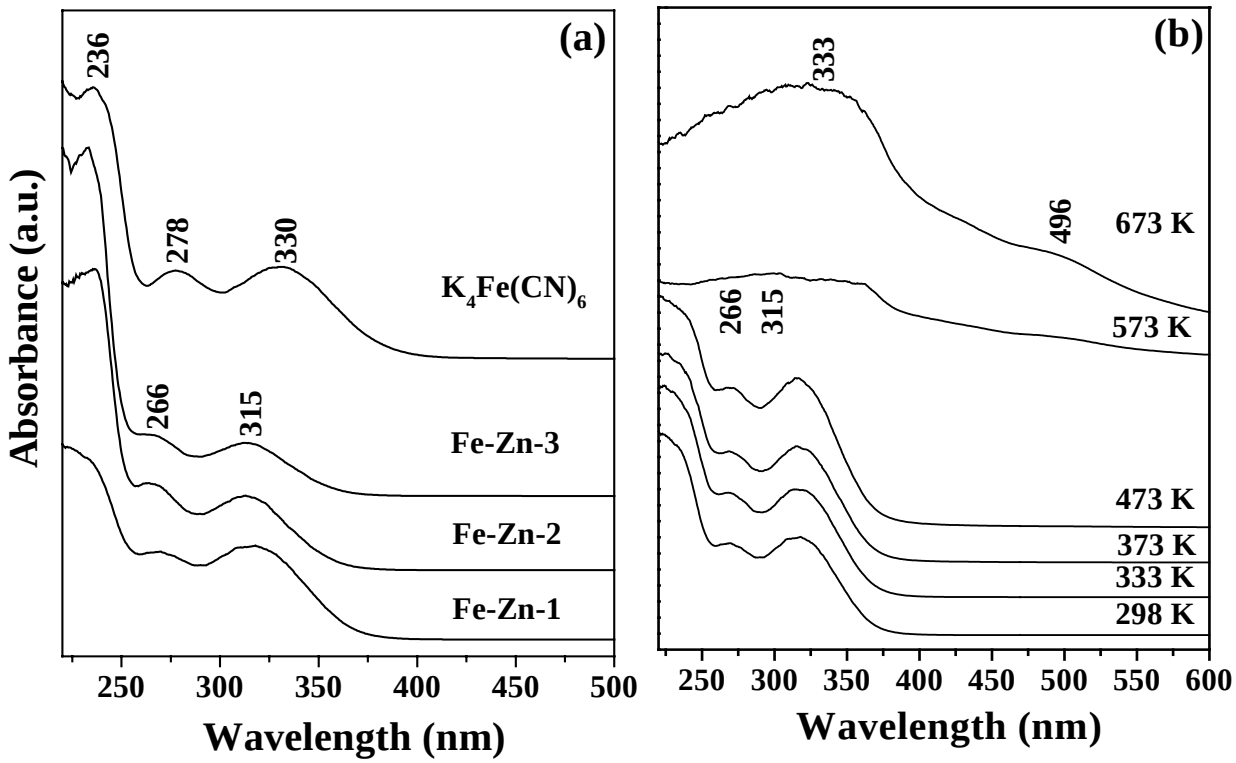

Fig. 2.21. DRUV-Visible spectra: (a) $K_4Fe(CN)_6$ and Fe-Zn double metal cyanide catalysts; (b) Spectra of Fe-Zn-1 catalyst at various activation temperatures.

2.8.2.6. SEM

Scanning electron microscopy (Fig. 2.22) reveals that the catalyst material is highly crystalline and has a spherical morphology. Particle size of the material is in the range 1 - 3 μm.

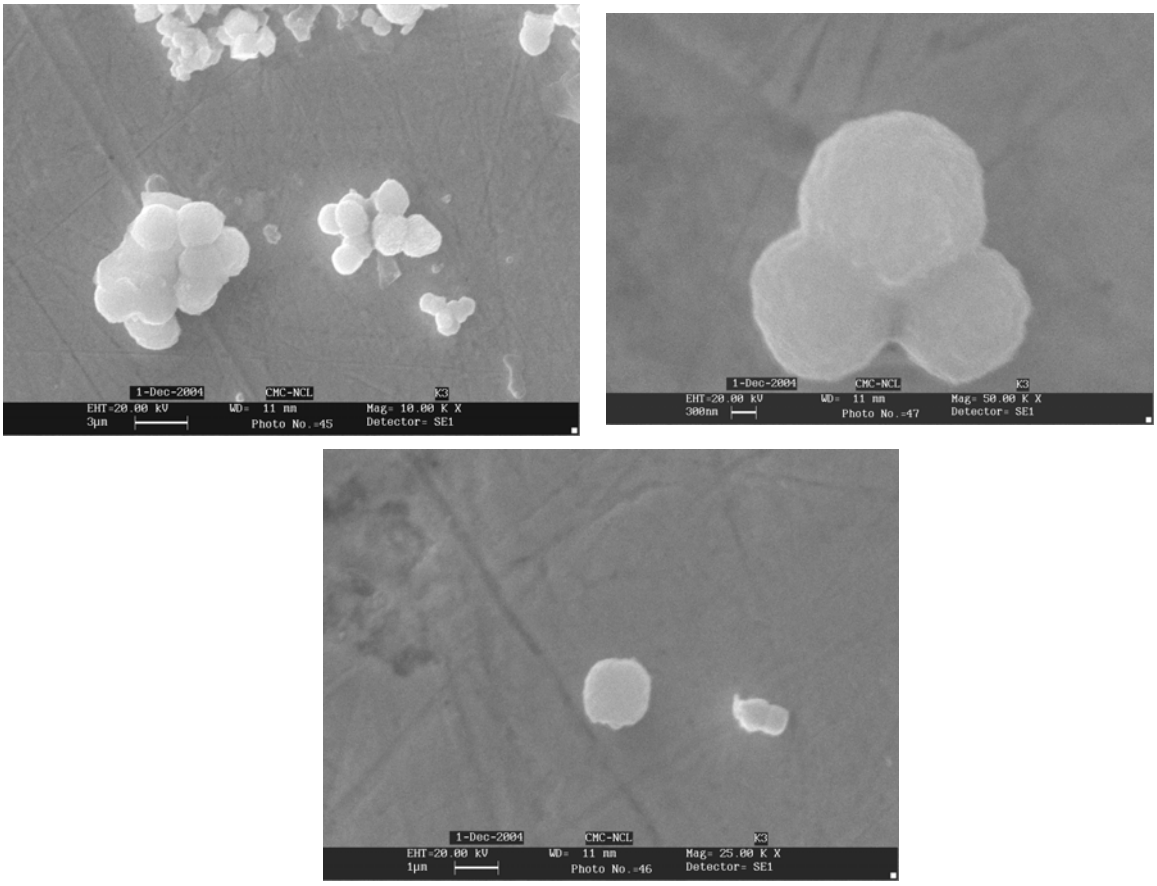

Fig. 2.22 SEM photographs of Fe-Zn-1 catalyst.

2.8.2.7. XPS

X-ray photoelectron spectra of Fe-Zn-1 activated at 473 and 673 K, are shown in Fig. 2.24. The peak arising from Zn(2p) core level in the catalyst appeared at 1021.2 eV. The corresponding peak for $ZnCl_2$ appeared at higher binding energy values (1023.7 eV). Similarly, the peak arising from Fe(2p) core level in the catalyst appeared at 707 eV. The

corresponding peak in $K_4Fe(CN)_6$ occurs at 708.0 eV. The lower energy shift of the peaks indicates the formation of Fe-Zn-1 catalyst and confirms the mutual influence of Fe and Zn ions on binding energy. The peak arising from N (1s) core level appeared at 397 eV. This peak in $K_4Fe(CN)_6$ occurred at 398 eV. The peak corresponding to O (1s) appeared at 531 eV. A weakly intense peak arising from Cl(2p) appeared at 198 eV. Its low intensity suggests that its concentration in the catalyst (present as $ZnCl_2$ adduct phase) is very low.

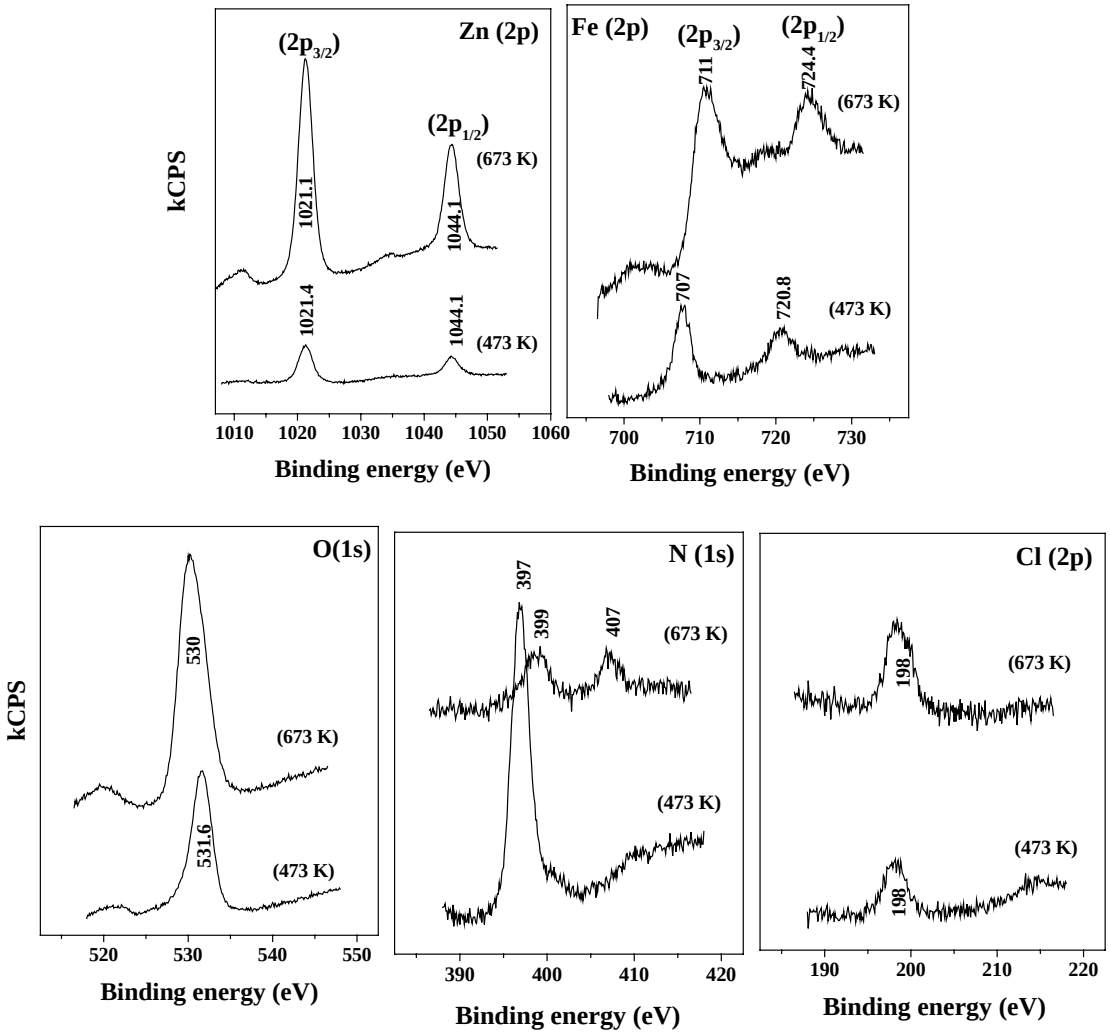

Fig. 2.23: XPS of Fe-Zn-1 catalyst.

Significant changes in XPS peak positions were observed when the samples were activated at 673 K (Fig. 2.24). The marked shift in peaks position indicates decomposition of the complex into metal oxides and nitrates [37]. In fact evidence for the presence of nitrate groups comes from N(1s) core level region by the peaks appearing at 399 and 407 eV [37]. The high intensity of the peaks corresponding to O(1s), Zn(2p) and Fe(2p) in samples activated at 673 K suggests increased accessibility of the elements due to formation of a different kind of material by decomposition process. The formation of Fe_2O_3 in high temperature activated samples can be discerned from the peak at 711 eV [38].

2.9. Pd-loaded Silicoaluminophosphates

A major limitation of palladium catalyzed coupling processes is the poor reactivity of aryl chloride. Aryl chlorides are more attractive substrates, as they are cheaper and easily available than the corresponding bromides, iodide and triflet. Traditional palladium/triarylphosphene catalysts are only effective for the coupling of certain activated aryl chloride such as heteroarylchloride and substrates that bear electron-withdrawing group but not for any aryl chloride in general [39]. Most of the homogeneous Pd complexes are notorious for air and moisture sensitivity, they deactivate fast and it is tedious and not an economical affair to recover and recycle the catalyst. Much attention has been paid to heterogeneous palladium catalysts due to their easy recovery and recycling. Aim of the present work is to explore heterogeneous, recyclable transition metal based catalysts for C-C bond forming reactions. Reports reveal that Pd supported on basic metal oxides (MgO) is less active than the Pd supported on Al_2O_3, SiO_2, mordanite and H-Y [40]. In the present study apart from Pd, cheaper metals such as

Cu and Ni are loaded on SAPOs of different structures (SAPO-11, SAPO-31 and SAPO-41) and their activation of olefins and aryl halide for C-C coupling Heck reactions is evaluated.

2.9.1. Synthesis

2.9.1.1 SAPO-11, SAPO-31 and SAPO-41

Silicoaluminophosphates SAPO-11, SAPO-31 and SAPO-41 were prepared hydrothermally using di-*N*-propylamine (DPA) and di-*N*-ethylamine (DEA) as organic templates. The starting materials were fumed silica (Aldric Co.), pseudoboehmite (Catapal B, Vista Co.), orthophosphoric acid (85%, S. D. Fine, India), di-*N*-propylamine (98% DPA, Aldrich, Co.) and di-*N*-ethylamine (98% DEA, Aldrich, Co.). Synthesis was carried out in a 300 ml stainless steel reactor lined with Teflon at autogeneous pressure without agitation. The molar composition of the synthesis mixtures and synthesis conditions for the preparation of the pure SAPOs are given in Table 2.5.

Table 2.5. Molar composition of the synthesis gels and crystallization conditions in the preparation of different SAPOs

Structure	Gel composition					Temp.	Time (h)
	Al_2O_3	P_2O_5	SiO_2	R	H_2O	(K)	
SAPO-11	1.0	1.0	0.3	1.16DPA	45	473	24
SAPO-31	1.0	1.0	0.3	1.16DPA	45	473	48
SAPO-41	1.0	1.0	0.3	1.16DEA	45	473	120

In a typical synthesis, 1:1 molar mixture of Al_2O_3 and P_2O_5 was prepared by slowly adding pseudoboehmite to dilute phosphoric acid, and the mixture was stirred well to form thick white paste. This paste was aged overnight for SAPO-31 and SAPO-41. After adding the remaining part of water, the template was added drop-wise to the mixture. Finally fumed silica was added. The active gel was stirred well for another half-an-hour. The gel was then charged into an autoclave and kept at required temperature for the specified duration. After crystallization the product was separated from the mother liquor, washed with distilled water and dried at 383 K for 12 h. The solid product obtained has the following molar composition: SAPO-11 (0.24 SiO_2: 1.02 Al_2O_3: 0.96 P_2O_5); SAPO-31 (0.28 SiO_2: 0.96 Al_2O_3: 0.90 P_2O_5); SAPO-41 (0.20 SiO_2: 1.02 Al_2O_3: 0.90 P_2O_5).

2.9.1.2. Metal-SAPOs

SAPOs with 3 wt.% of Pd were prepared by the ion exchange method using an aqueous solution (10 ml) of $(NH_3)_4PdCl_2.H_2O$ (74.46 mg). The suspension was stirred for 10 h at 363 K. The solid (Pd-SAPOs) were calcined at 823 K for 6 h and then reduced at 673 K under hydrogen flow (20 ml/min) for 6 h.

Ni-SAPOs and Cu-SAPOs were prepared in a similar manner using the $Ni(NO_3)_2.2H_2O$ and $Cu(NO_3)_2.2.5\ H_2O$, respectively.

2.9.2. Characterization

2.9.2.1 XRD

The X-ray powder diffraction patterns of calcined SAPO-11, SAPO-31 and SAPO-41 are shown in Fig. 2.24. The position and intensity of the XRD peaks agree with the earlier reports [41] and indicate that the samples are free of impurity phases. The high

intensity of XRD lines confirms high crystallinity of the samples. Metal incorporation did not alter the crystallinity and framework structure of SAPOs.

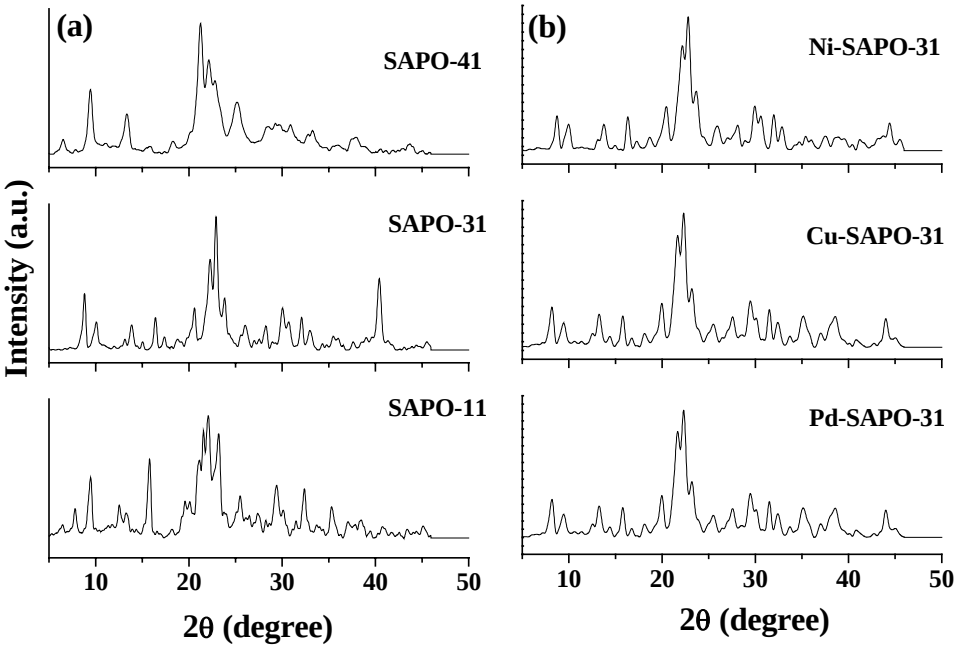

Fig. 2.24. XRD profiles of metal-free and metal-loaded SAPOs.

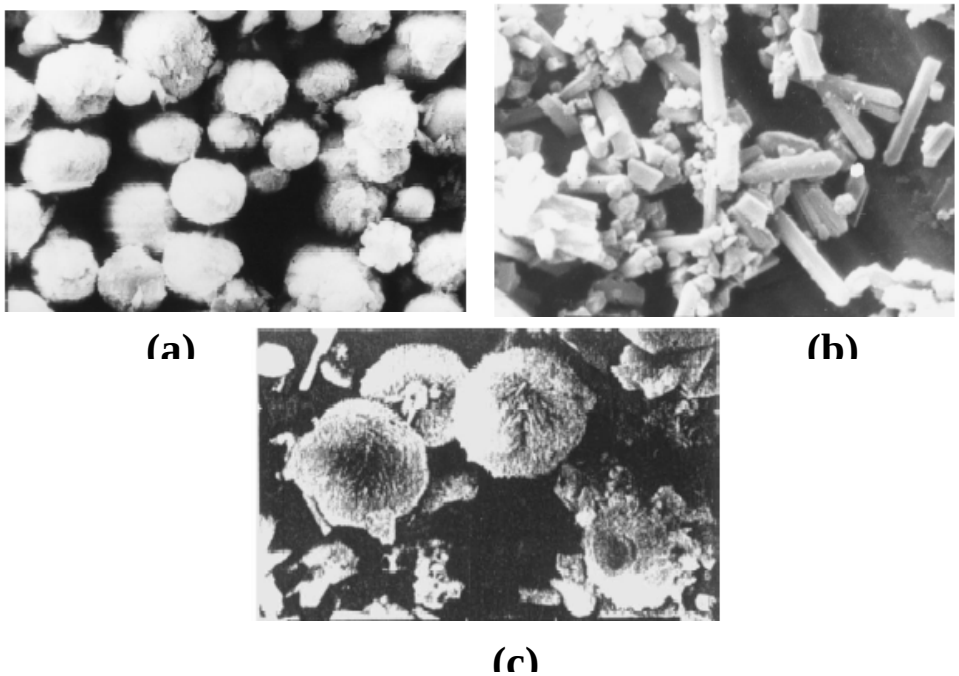

Fig. 2.25. SEM images of (a) SAPO-11, (b) SAPO-31 and (c) SAPO-41.

2.9.2.2. SEM

Scanning electron micrographs of the samples are shown in Fig. 2.25. A different morphology is observed for each SAPO. The crystal size distributions in the SAPO samples are not uniform and they differ from each other. SAPO-11 forms crystallites of spherical morphology. The sizes of this spherical particle is in the range of 3 - 4 μm. SAPO-31 forms rectangular rod-like crystal of sizes in the range of 1.0 x 0.5 μm to 3.0 x 0.5 μm. SAPO-41 forms crystals of very large spheres (8-12 μm).

2.9.2.3. DRUV-Visible

Cu-SAPO-31 (before reduction with hydrogen) exhibited a weak, broad band at 600–800 nm in the DRUV-visible spectrum (Fig. 2.26) that could be assigned to the $^2E_g(D) \rightarrow {}^2T_{2g}$ spin allowed, Laporte-forbidden transition of Cu^{2+} in an octahedral geometry [42]. An intense band due to a ligand-to-metal charge transfer (LMCT) transition was observed at 310 nm. Calcined Ni-SAPO-31 showed characteristic bands at 410 and 700 nm due to $^3A_{2g} \rightarrow {}^3T_{1g}(P)$ and $^3A_g \rightarrow {}^3T_{1g}(F)$ transitions, respectively [43]. Pd-SAPO-31 showed a LMCT band at 250–300 nm. This band disappeared and an increased absorbance in the visible region was observed when treated with hydrogen indicating that all the Pd^{2+} ions had been converted to metallic Pd [44].

2.9.2.4. EPR

EPR spectroscopy (Fig. 2.26) revealed that the metal ions are highly dispersed. The Cu^{2+} in Cu-SAPO (before hydrogen reduction) is characterized by signals with spin Hamiltonian parameters, $g_{II} = 2.388$, $g_{\perp} = 2.088$ and $A_{II}^{Cu} = 118.1$ G. Ni-SAPO-31 showed a perpendicular signal at g = 2.345 corresponding to a highly distorted octahedral

environment around the Ni^{2+} ions [45]. Pd-SAPO-31 reduced with hydrogen exhibited a broad signal at g = 2.12 characteristic of dispersed metallic Pd [46].

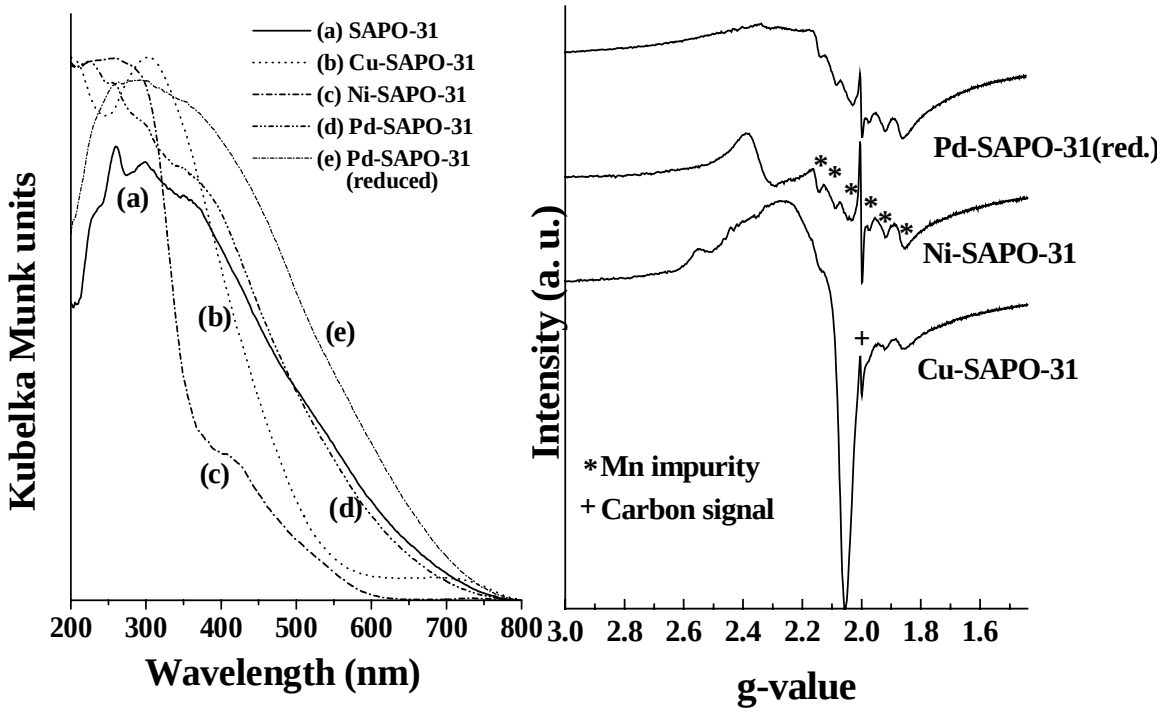

Fig. 2.26. DRUV-Visible (left) and EPR (right) spectra of Cu/Ni/Pd-SAPO-31. Asterisk indicates signal due to Mn impurities and + indicates signal due to unburned template.

2.10. Characterization Techniques

2.10.1. XRD

The XRD of the zeolite samples were recorded on a Rigaku, (Model D/MAX III VC, Japan) instrument with Ni-filtered, Cu-Kα radiation (λ = 1.5404 Å) and graphite crystal monochromator. All measurements were made at 298 K and the data were collected in the 2θ range of 5-50º at a scan rate of 2°/min (for zeolite–Y) and 1.5-10º at a scan rate of 1º/min (for MCM-41). X-ray diffractograms of SBA-15 materials were recorded on an X'Pert Pro (Philips) diffractometer using Cu Kα radiation and a

proportional counter as detector. A divergent slit of 1/32° on the primary optics and an anti-scatter slit of 1/16° on the secondary optics were employed to measure the data in the low-angle region.

2.10.2. N_2 Adsorption

A commercial adsorption unit (NOVA 1200 Quanta Chrome equipment) was used for measurements of nitrogen adsorption. Initially, the samples (approx. 300 - 400 mg) were activated at 473 K for 16 h in high vacuum (~10^{-5}mm). The samples were then cooled to 77 K using liquid nitrogen and nitrogen gas was allowed to adsorb on the catalyst surface. By measuring the amount of N_2 adsorbed at different equilibrium pressures, the BET surface area was calculated. The anhydrous weight of the sample was used in the surface area calculation. To obtain the surface area, the results were fitted to the equation: surface area = V_m x N x A_m, where, V_m is the monolayer volume, N is the Avagadro's number and A_m is the cross sectional area of adsorbent.

2.10.3. Chemical Analysis

C, H & N analysis of the catalysts was done on a Carlo Erba (Model EA 1108) elemental analyzer. Si and Al contents were estimated by wavelength dispersive XRF spectrometer (Rigaku 3670E). An atomic absorption spectrometer (AAS, Hitachi Model Z-8000) was used to estimate the metal content in the samples.

In a typical sample preparation for AAS, a known amount of the sample was digested in HF or H_2SO_4 or (3:1 HNO_3/HCl mixture) depending upon the solubility of the sample. Then the solution was made up to the mark of the volumetric flask with distilled water and was then analyzed for metal content by atomic absorption spectroscopy.

2.10.4. FT-IR

The Infrared spectra were recorded using a Shimadzu (Model 8201PC) spectrophotometer in a range 4000-400 cm^{-1}. The spectra were recorded as Nujol mulls or as KBr pellets (1wt%). Acidity measurements of the samples were performed by pyridine adsorption studies. Basicity measurements were carried out by adsorbing CO_2.

2.10.4.1. Pyridine-Adsorption FT-IR

IR spectral measurements were performed on a Shimadzu SSU 8000 DRIFT-IR spectrometer equipped with liquid nitrogen cooled MCT detector. Samples were activated at 698 K for 2 h under nitrogen flow. Then they were cooled to 323 K and pyridine (30 μl) was adsorbed. The sample temperature was raised to a desired value and held at that temperature for 30 min and then the spectrum was recorded. In some measurements, the samples were initially hydrated by keeping them overnight in a desiccator containing water. Then they were subjected to IR measurements by adsorbing pyridine at 298 K.

2.10.4.2. CO_2 adsorption FT-IR

The samples were made into a paste with dichloromethane and then exposed to CO_2 at different experimental conditions (temperature = 253 – 298 K; CO_2 pressure = 2 – 20 bar; time = 1 h). The spectra before and after CO_2 adsorption were recorded (Shimadzu 8201 PC spectrophotometer; region 400 - 4000 cm^{-1}). The difference spectrum was obtained by subtracting the spectrum of the unexposed SBA sample from that of the corresponding CO_2 adsorbed sample. The average number of scans was 100 and the spectral resolution was 4 cm^{-1}.

2.10.5. DRUV-Visible

The UV-Visible spectra of the samples were obtained in the wavelength range of 200-850 nm using a Shimadzu (Model UV-2550) PC spectrometer. The spectra were recorded in solid state (in diffuse reflectance mode) and in solution medium (in normal absorption mode). In the case of colored materials for examples, phthalocyanine, the samples were diluted with spectral grade barium sulfate.

2.10.6. EPR

EPR spectra of samples were recorded on a Bruker EMX spectrometer operating at X-band frequency and 100 kHz field modulation. The samples were taken in Suprasil quartz tubes of 4.5 mm o.d. Measurements at 77 K were carried out using a quartz insert dewar. Spectral manipulations and simulations were done using Bruker WINEPR and Simfonia software packages. Microwave frequency was calibrated using a frequency counter fitted in the microwave bridge (Bruker ER 041XGD) and the magnetic field was calibrated by a ER 035M NMR Gaussmeter.

2.10.7. Transmission Electron Microscopy

Transmission electron micrographs (TEM) were taken on a JEOL Model 1200 EX instrument. TEM provided information of mesoporous materials at near atomic resolution. A fine suspension of the sample was made in isopropanol with the help of ultrasonication and was mounted on a copper grid. Images were recorded using a camera.

2.10.8. Thermal Analysis

Thermo-gravimetric analysis were done by taking 30 mg of samples on a Seiko DTA-TG 320 instrument under nitrogen atmosphere (50 cm^3/min), at a ramp rate of 10 K/min, in the temperature range of 308 – 1078 K. A known weight of the samples was

taken in a platinum crucible with lid and heated at 393 K to get the dry weight of the sample. The sample was weighed after equilibration. The difference in weights gave the loss in weight on heating.

2.10.9. TPD

Acidity and basicity were estimated by NH_3-TPD and CO_2-TPD measurements, respectively.

2.10.9.1. NH_3-TPD

The acidity of the samples was estimated by NH_3-TPD technique. The measurements were performed on a Micromeritics Autochem 2910 instrument. The sample (500 mg) was initially activated at 773 K for 2 h in He flow (20 ml/min). It was then cooled to 353 K and 10% NH_3 in He was adsorbed for 30 min. The sample was flushed with He (30 ml/min) for 1 h at 373 K and the desorption was monitored by increasing temperature from 373 to 723 K at a ramp rate of 10 K/min.

2.10.9.2. CO_2-TPD

In CO_2-TPD experiments the catalyst was pretreated at 473 K for 1 h. CO_2 was adsorbed at 300 K for 1 h. The sample was then flushed for 1 h to remove physisorbed CO_2. The TPD was carried from 298 to 523 K at a heating rate of 10 K/min. The sample was kept at 523 K for 30 min.

2.11. Conclusions

The synthesis of various catalysts used in the present work for (1) CO_2 utilization, (2) transesterification and (3) C-C coupling Heck reactions is presented. These catalysts were characterized by elemental analysis (C, H & N; AAS), N_2 adsorption/desorption, XRD, FT-IR, DRUV-Visible, EPR, XPS, TEM and thermal analysis techniques. Acidity

of the catalysts was determined by NH_3-TPD and pyridine adsorption FT-IR techniques. Basicity of the catalysts was measured by CO_2-TPD and FT-IR of adsorbed CO_2.

2.12. References

1. W. L. F Armarego, D. D Perrin, Purification of Laboratory Chemicals 4th Edn. Butterworth-Heinemann Publishers, Oxford, 1996.
2. K. Srinivasan, P. Michaud, J. K. Kochi, J. Am. Chem. Soc. 108 (1986) 2309.
3. W. M. Coleman, R. K. Bogess, J. W. Taylor, Inorg. Chem. 20 (1981) 700.
4. K. J. Catalan, S. Jackson, J. D. Zubkowske, D. L. Perry, E. J. Valente, L. A. Feliu, A. Polanco, Polyhedron 14 (1995) 2165.
5. A. D. Adler, F. R. Longo, J. D. Finarelli, J. Goldmacher, J. Assour, L. Korsakoff; J. Org. Chem. 32 (1966) 476.
6. A. D. Adler, F. R. Long, F. Kampas, J. Kim, J. Inorg. Nucl. Chem. 32 (1970) 2443.
7. J. E. Richmann, T. J. Atkins, J. Am. Chem. Soc. 96 (1974) 2268.
8. J. E. Richmann, W. F. Orttle, Org. Synth. 58 (1978) 86.
9. H. Eckert, G. Fabry, Y. Kiesel, G. Raudaschl, C. Seidel, Angew. Chem. Int. Ed. Engl. 22 (1983) 881.
10. N. Herron, C. A. Tolman, G. D. Stucky, J. Chem. Soc. Chem. Commun. (1986) 1521.
11. R. Belal, b. Meunier, J. Mol. Catal. 44 (1988) 187.
12. K. J. Jr. Balkus, A. G.Gabrielov, J. Incl. Phenom. Mol. Recog. Chem. 21 (1995) 159.
13. K. J. Jr. Balkus, A. G. Gabrielov, S. L. Bell, F. Bedioui, L. Roue, J. Devynck, Inorg. Chem. 33 (1994) 67.
14. S. Seelan, A. K. Sinha, D. Srinivas, S. Sivasanker, J. Mol. Catal. A: Chem. 157 (2000) 163.
15. R. Raja, P. Ratnasamy. J. Catal 170 (1997) 244.
16. N. Kobayashi in " Phthalocyanine-Properties and Applications", C. C. Lenznoff, A. B. P. Lever (Eds.) VCH Publishers, Inc., New York, 2 (1997) 97.
17. W. Hoelderich, M. Hesse, F. Newman, Angew. Chemie. Int. Ed. Engl. 27 (1998)

226.

18. A. Thangaraj, R. Kumar, P. Ratnasamy, J. Catal. 130 (1991) 1.
19. R. Srivastava, D. Srinivas, P. Ratnasamy, Catal. Lett. 91 (2003) 131.
20. D. Zhao, J. Feng, Q. Huo, N. Melosh, G.H. Fredrickson, B.F. Chmelka, G.D. Stucky, Science 279 (1998) 548.
21. P. Wu, T. Tatsumi, T. Komatsu, T. Yashima, Chem. Mater. 14 (2002) 1657.
22. B. Notari, Adv. Catal. 41 (1996) 253.
23. Q. Yang, S. Wang, J. Lu, G. Xiong, Z. Feng, Q. Xin, C. Li, Appl. Catal. A: Gen. 194 (2000) 507.
24. P. Ratnasamy, D. Srinivas, H. Knozinger, Adv. Catal. 48 (2004) 1.
25. R. Bal, K. Chaudhari, D. Srinivas, S. Sivasankaer, P. Ratnasamy, J. Mol. Catal. A: Chem. 162 (2000) 199.
26. A. D. Janssen, P. V. D. Voort, A. J. Koster, K. P. de Jong, Chem. Commun. (2002) 1632.
27. (a) P. Sutra, D. Brunel, Chem. Commun. (1996) 2485. (b) X.-G. Zhou, X.-Q. Yu, J.-S. Huang, S.-G. Li, L.-S. Li, C.-M. Che, Chem. Commun. (1999) 1789.
28. A. Vinu, V. Murugesan, W. Böhlmannn, M. Hartmann, J. Phys. Chem. B 108 (2004) 11496.
29. P. Sutra, D. Brunel, Chem. Commun. (1996) 2485.
30. R. N. Bhatt, R. Kumar, J. Chem. Tech. Biotech. 48 (1990) 453.
31. (a) H. T. Takeyasu, T. Watabe, T. Doi, JP 2,265,921, 1990. (b) T. Watabe, H. Takeyasu, T. Doi, N. Kunii, Eur Pat Appl EP 383,333, 1990.
32. B. Le-Khac, US Patent 5,789,626, 1998.
33. I. Kim, J-T. Ahn, C. S. Ha, C. S. Yang, I. Park, Polymer 44 (2003) 3417.
34. K. Nakano, K. Nozaki, T. Hiyama, J. Am. Chem. Soc. 125 (2003) 5501.
35. (a) D. F. Mullica, G. W. Milligan, G. W. Beall, Acta Crystallogr. 34 (1978) 3558. (b) B. Le-Khac, EP O755716A1, 1997.
36. K. Nakamoto, Infrared and Raman spectra of inorganic and coordination compounds, 3rd ed. New York: Wiley; 1978. p. 266.
37. Handbook of X-ray photoelectron spectroscopy, G.E. Muilenberg (Ed.), Perkin-Elmer Co., Physical Electronic Division, Eden Prairie, Minnesota 55344 (1979).

38. T.J. Udovic, J.A. Dumesic, J. Catal. 89 (1984) 303.

39. A. F. Littke, G. C. Fu, Angew. Chem. Int. Ed. 41 (2002) 4176.

40. A. Biffis, M. Zecca, M. Basato, J. Mol. Catal. A: Chem. 173 (2001) 249.

41. P. Mériaudeau, Vu A. Tuan, Vu T. Nghiem, G. Sapaly, C. Naccache, J. Catal. 185 (1999) 435.

42. S. Velu, L. Wang, M. Okazaki, K. Suzuki, S. Tomura, Micropor. Mesopor. Mater. 54 (2002**)** 113.

43. A. Kukovecz, Z. Ko´nya, D. Mo¨ nter, W. Reschetilowski, L. Kiricsi, J. Mol. Struct. 563-564 (2001**)** 403.

44. B. M. Choudary, S. Madhi, N. S. Chowdari, M. L. Kantam, B. Sreedhar, J. Am. Chem. Soc. 124 (2002**)** 14127.

45. K. Velavan, T. M. Rajendiran, R. Venkatesan, P. Sambasiva Rao, Solid State Commun. 122 (2002) 15.

46. H. Choo, S. B. Hong, L. Kevan, J. Phys. Chem. B 105 (2001) 7730.

Chapter-3

Activation and Utilization of CO_2 in Cyclic Carbonates Synthesis

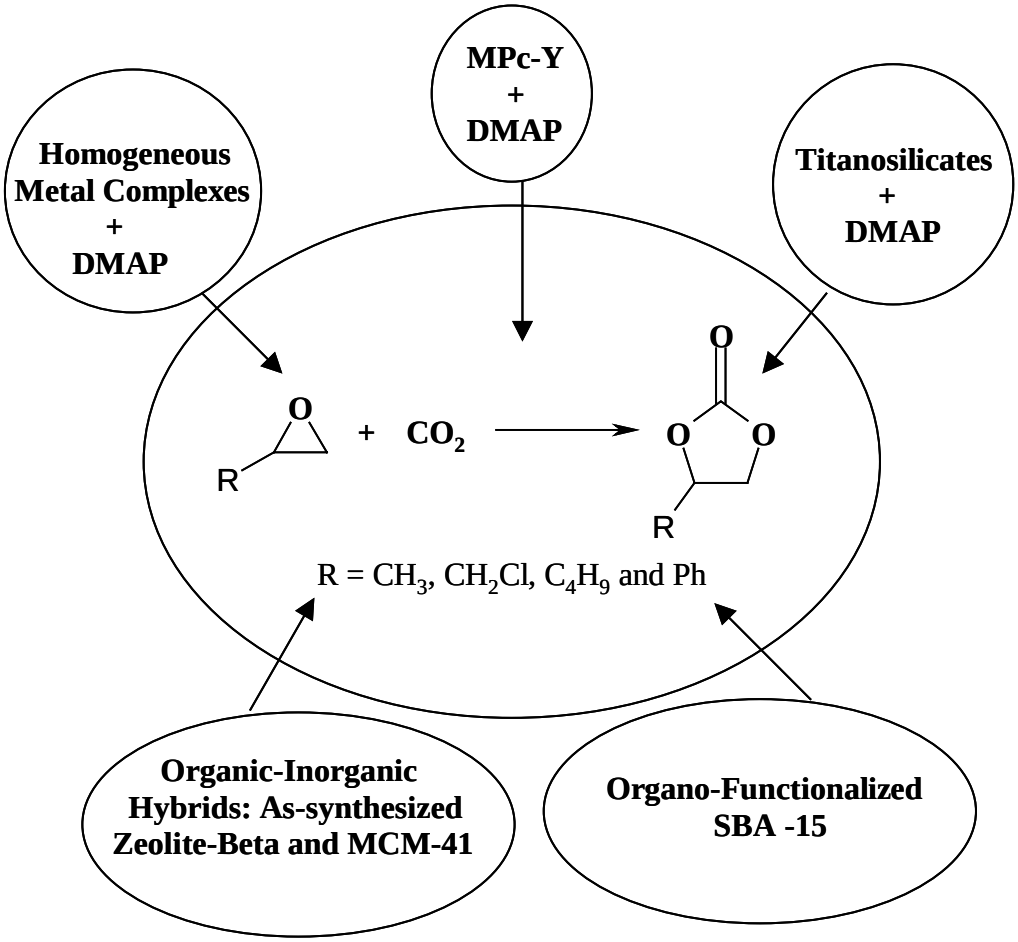

3.1. Introduction

Cyclic carbonates are valuable compounds that have application in a variety of chemical fields. They are important raw materials for engineering plastics like polycarbonates. Because of their high solubility, high boiling and flash points, low odor levels and evaporation rates, low toxicities and biodegradability, cyclic carbonates are utilized as aprotic polar solvents in degreasing, paint stripping and cleaning. They are also used as electrolytes in secondary batteries and in general, as intermediates in organic synthesis, pharmaceuticals and biomedical applications [1-3]. Biologically active molecules that contain a cyclic carbonate component have also been isolated from various kinds of natural sources. Their synthesis using phosgene is non-eco-friendly [4]. One of the most successful, popular and benign methods of their preparation is from CO_2 [5-7]. The alarmingly growing levels of CO_2 in the atmosphere necessitate chemical industry to develop alternative chemical processes that either do not generate CO_2 as a by-product or those processes that utilize CO_2 in chemical synthesis. Cyclic carbonates synthesis by cycloaddition of CO_2 to epoxides is an efficient way to CO_2 utilization.

A variety of homogeneous metal complexes have been reported to catalyze the cycloaddition reaction of CO_2 to epoxides [8-9]. Obviously, heterogeneous catalysts offer more advantages such as easy catalyst separation, reusability and engineering benefits. Several heterogeneous catalysts such as polystyrene bound onium salts [10], basic metal oxides [11], Mg-Al mixed oxides [12], Nb-catalysts [13], lanthanide oxychlorides [14], alkali metal loaded zeolites and alumina [15], poly(4-vinylpyridine)-supported zinc halide [16], silica supported guanidine [17] and Schiff base and phthalocyanine complexes covalently bonded to porous silica [18] have been reported. Commercial production of cyclic carbonates, by a non-phosgene route, with quaternary

ammonium salt-based catalysts, has been announced recently by BASF and Chimei-Asahi Co., Taiwan [19]. However, with most of the above-mentioned solid catalysts and with the commercial quaternary ammonium salt catalysts the reaction had to be carried out at high temperatures and pressures for high yields of carbonates. In some cases, a large amount of catalyst and solvent are also required. Hence, there is a need to develop more efficient, solid, reusable catalysts for this reaction. In view of this, in this chapter, five different types of catalyst systems have been evaluated for their catalytic activity in cycloaddition reaction of CO_2 to epoxides. The sites for CO_2 activation were probed by TPD, DRIFT and other spectroscopic techniques.

3.2. Experimental Section

3.2.1. Cyclic Carbonate Synthesis - Reaction Procedure

In a typical cycloaddition reaction, a known quantity of epoxide (epichlorohydrin (ECH), propene oxide (PO), n-butene oxide (BO) and styrene oxide (SO)) and catalyst were taken in a 300 ml stainless steel pressure reactor. In some reactions a co-catalyst (N- or P-based compound) and solvent were also taken in the reactor. The reactor was pressurized with CO_2 (1.6 – 10 bar), temperature was raised (333 - 433 K) and the reaction was conducted for a specified period of time (3 – 10 h). The reactor was then cooled to 298 K, unreacted CO_2 was released, and the products were analyzed by GC-Varian 3400; CP-SIL8CB column; 30 m long and 0.53 mm i.d. for all the cyclic carbonates except propene carbonate; injection temperature, = 553 K, detector temperature, 573 K, program: 313 K (5 min hold) – 5 K/min – 393 K (5 min hold) – 10 K/min – 513 K (10 min hold) for chloropropene carbonate and butene carbonate. 353 K (5 min hold) - 5 K/min – 393 K (5 min hold) – 10 K/min – 513 K (10 min hold) for styrene carbonate. Propene carbonate was analyzed with a GC-Shimadzu; CP-SII 8CB column; 60 m x 0.25 mm x 0.25 μm thick capillary column and

identified by GC-MS (Shimadzu QP-5000; 30 m x 0.25 mm x 0.25 μm thick capillary column DB-1), GC-IR (Perkin Elmer 2000; BP-1 column; with a 25 m long, and 0.32 mm i.d.), and FT-IR and ^{1}H NMR spectroscopies (Bruker AC 200). In some cases, cyclic carbonates, thus prepared utilizing CO_2, were isolated by column chromatography (silica gel 100 – 200 mesh, petroleum ether – ethyl acetate mixture (80: 20 volume)) and mass balances were confirmed.

Spectral characteristics of cyclic carbonate products

Chloropropene carbonate – IR (cm^{-1}): $\nu_{C=O}$, 1800, ν_{C-O}, 1133, 1080; ^{1}H NMR ($CDCl_3$), δ(ppm): 5.03 – 4.94 (1H, m), 4.61 – 4.52 (1H, q), 4.44 – 4.35 (1H, q), 3.84 – 3.74 (2H, m).

Propene carbonate – IR (cm^{-1}): $\nu_{C=O}$, 1793, ν_{C-O}, 1121, 1078; ^{1}H NMR ($CDCl_3$), δ(ppm): 4.88 – 4.77 (1H, m), 4.55 – 4.49 (1H, t), 4.01 – 3.96 (1H, t), 1.45 (3H, d).

Styrene carbonate – IR (cm^{-1}): 1812, 1163, 1062 ($\nu_{C=O}$); ^{1}H NMR ($CDCl_3$), δ(ppm): 7.47-7.3 (5H, m), 5.73-5.63 (1H, t), 4.83-4.75 (1H, t), 4.37-4.29 (1H, t).

3.3. Results and Discussion

3.3.1. Cyclic Carbonates Synthesis with Homogeneous Copper Complexes

The preparation and characterization of different homogeneous copper complexes of acyclic and cyclic ligands used in the study are presented in Chapter-2. The reaction of epoxide and CO_2 yielded the corresponding cyclic carbonate as the selective product; diols and ethers formed in the minor amounts. Table 3.1 shows the catalytic activity of various homogeneous Cu^{2+} complexes. Ligand structure markedly affected the catalytic activity. The catalytic activity of Cu coordinated to different ligands varied in the order: phthalocyanine (Pc) > tetraphenylporphyrine (TPP) > 1,10-phenanthroline (phen) > salpoh > salen > cyclen > 2,2'-bipyridine (bipy). Among the

cyclic systems the unsaturated ligand systems (Pc and TPP) are more efficient than the saturated ligand system (cyclen). The metal complexes of cyclic aza ligands exhibited higher activity than the acyclic systems (bipy and phen). Electron donating substituents (methyl) decreased the catalytic activity. On the other hand, an increase in catalytic activity was observed when Cu^{2+} replaced by Mn^{3+}. The difference in catalytic activity is due to a difference in the mode of CO_2 binding. The mode of CO_2 binding was investigated with the help of various spectroscopic techniques such as FT-IR, UV-visible and EPR technique.

The reaction of CO_2 with Cu-cyclen generated two new IR peaks, at 1716 and 1225 cm^{-1}, attributable to formation of an activated CO_2 complex. When both ECH and CO_2 were reacted (in CH_3CN) additional peaks (denoted by asterisk; Fig. 3.1) appeared at 1805, 1649, 1170 and 1074 cm^{-1}. These additional peaks compared well with the IR spectrum of a commercial cyclic carbonate sample. The peak due to CO_2-complex (at 1716 and 1225 cm^{-1}) could not be detected from the spectra of CO_2 + ECH reaction solutions due to overlap of a highly intense peak of cyclic carbonate. Based on this, it may be concluded that Cu-cyclen complexes (showing ν_3 and ν_1 IR band at 1716 and 1225 cm^{-1}, respectively) form a pentacoordianted structure and η^1-C type CO_2 coordination. Co-tetraza macrocycles [20] and Schiff bases [21] form similar η^1-CO_2 complexes and show IR peaks at around 1702 and 1217 cm^{-1}.

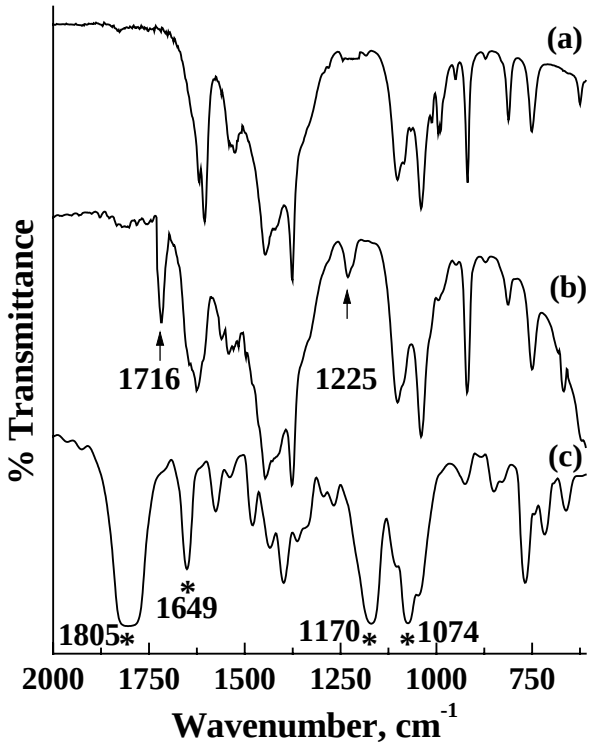

Fig. 3.1. FT-IR spectra in CH_3CN: (a) Cu(cyclen) + DMAP, (b) Cu(cyclen) + DMAP + CO_2, (c) Cu(cyclen) + DMAP + CO_2 + ECH. Asterisk indicates the characteristic IR bands for cyclic carbonate. DMAP = N,N-dimethyl aminopyridine.

Cu(cyclen)-DMAP-CH_3CN showed a weak d-d band at around 660 nm (Fig. 3.2). The CO_2 reacted-solution showed a new band at 415 nm consistent with the formation of an activated CO_2 complex. This band is attributed to metal–to-ligand charge transfer transition (Cu (d orbital) $\rightarrow CO_2$ (π^* orbitals)). When both ECH and CO_2 were reacted, the d-d band shifted to higher energy side and a new resolved feature appeared at 524 nm (Fig. 3.2 (I)). These spectral variations indicate a change in the molecular structure of the Cu complex due to formation of cyclic carbonate and adduct complexes. Similar conclusions are drawn also from the EPR spectra (vide infra). When the reactions were conducted over Cu(phen) and Cu(bipy) complexes, the

position of the charge transfer band of the activated CO_2 complex shifted from 415 nm (originally observed for Cu(cyclen) complexes) to 409 nm. This shift in the charge transfer band position can be corresponded to a change in the mode of CO_2 coordination and weaker Cu-CO_2 bond. A similar type of charge transfer band at around 400 nm is reported for Ag(CO_2) system [22].

Cu(cyclen) + DMAP in CH_3CN showed an axial EPR spectrum with spin Hamiltonian parameters being $g_{||}$ = 2.211, $g_{\perp}$ = 2.054 and $A_{||}^{Cu}$ = 169.4 G (Fig. 3.2 (II)). Upon reaction with CO_2, new signals (denoted as A in Fig. 3.2 (II); resolved mainly in the parallel region) appeared at $g_{||}$ = 2.252 and $A_{||}^{Cu}$ = 165.0 G in addition to the signals characteristic of Cu(cyclen)-DMAP complex. These new EPR signals, in agreement with the FT-IR and UV-visible results, could be attributed to the activated CO_2 complex. The higher g value ($g_{||}$ = 2.252) compared to that of Cu(cyclen)-DMAP complex indicates stronger pentacoordinated Cu^{2+} species [23]. The axial spectrum indicates a symmetric coordination of CO_2 to Cu. Upon reaction with CO_2 + ECH, significant changes in the spectral parameters were observed (Fig. 3.2 (II)). Two types of Cu^{2+} with the following spin Hamiltonian parameters were observed. Species A with $g_{||}$ = 2.258 and $A_{||}^{Cu}$ = 155.0 G is the activated CO_2-complex and species B with $g_{||}$ = 2.208, $g_{\perp}$ = 2.056 and $A_{||}^{Cu}$ = 173.5 G is the cyclic carbonate adduct. The origin of species B was confirmed by recording the spectra of Cu(cyclen)-DMAP + propene carbonate. The EPR studies suggest that CO_2 coordination is influenced by the geometry as well as ligand field strength at the site of Cu. The higher g-value ($g_{||}$ = 2.252) is consistent with a five-coordinated geometry of Cu. Lower Cu hyperfine constant ($A_{||}^{Cu}$ = 155 – 165 G) indicates more delocalization of the electron density onto the ligand/CO_2 orbitals. These results from EPR agree well with those of FT-IR and UV-visible studies discussed above. The spectral investigations have provided

evidence for the formation of Cu^{2+}-CO_2 complexes, an activated intermediate in the cyclic carbonates synthesis.

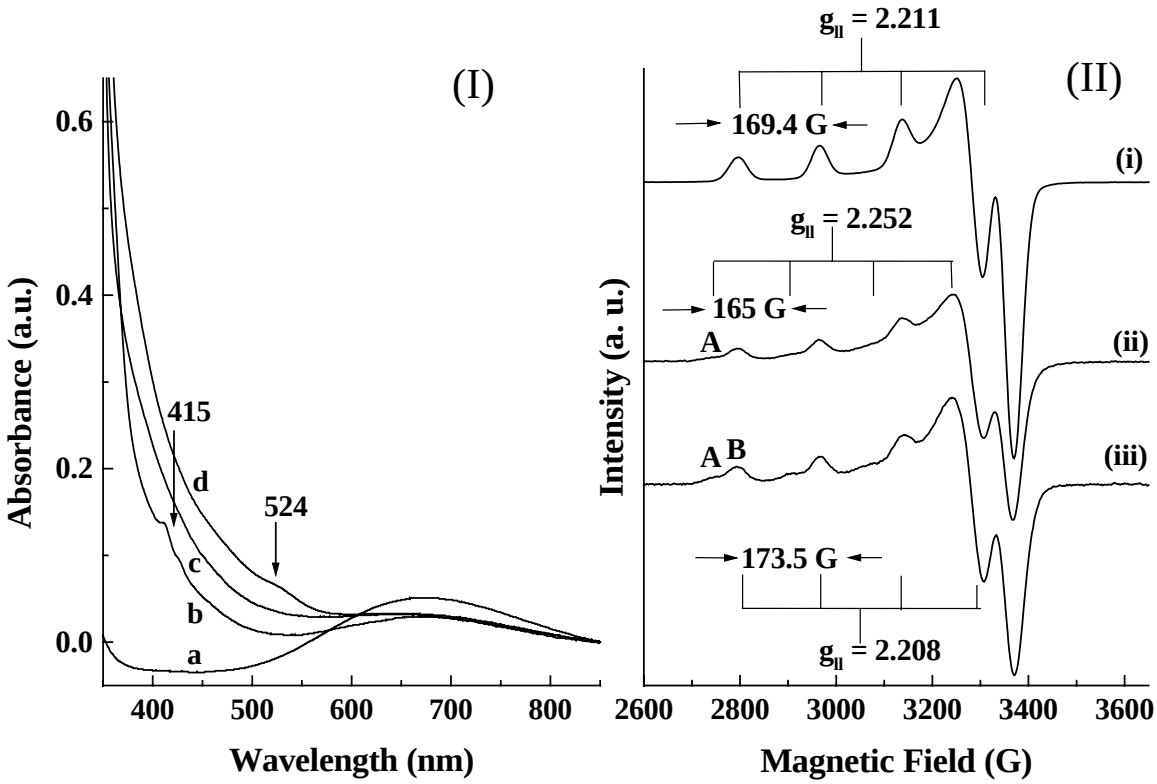

Fig.3.2. (I) UV-visible spectra in CH_3CN: (a) Cu(cyclen) + DMAP, (b) Cu(cycle) + DMAP + CO_2, (c) Cu(cyclen) + DMAP + ECH, (d) Cu(cyclen) + DMAP + CO_2 + ECH. (II) EPR spectra in CH_3CN at 100 K: (i) Cu(cyclen) + DMAP, (ii) Cu(cyclen) + DMAP + CO_2, (iii) Cu(cyclen) + DMAP + CO_2 + ECH.

The complexes under study are also known to activate and facilitate ring opening of epoxides [24]. Based on these experimental evidences a tentative mechanism is proposed in Fig. 3.3 which is similar to that reported for Cr(III) salen complexes [8]. Accordingly, the Cu complex activates the epoxides and the Cu-DMAP system activates CO_2. The activated CO_2 complex then attacks the activated epoxide at the less hindered carbon leading to formation of a dimeric intermediate species, which eventually yields the cyclic carbonate.

The differences in catalytic activity of Cu complexes (Table 3.1) can be explained based on the mode of CO_2 coordination. As discussed above, activation of reactants is the crucial step in CO_2 fixation. The metal-substrate bonding should be optimum. Metal complexes with unsaturated aza-ligands (Pc and TPP) provide optimum bonding and enable higher yields of cyclic carbonates. In contrast, the complexes with acyclic ligands (phen and bipy) form weaker metal-CO_2 bonds and result in lower catalytic activity. Methyl substitution on cyclen results in more stable metal-CO_2 complexes, which are less reactive giving lower yields of the product carbonate. In other words, the metal-CO_2/epoxide bonding should neither be too stronger nor too weak. By a suitable fine-tuning of the ligand system it is possible to develop a highly active catalyst. These homogeneous complexes are efficient only if a co-catalyst such as N,N-dimethyl aminopyridine (DMAP) and solvent such as dichloromethane are used in the reaction. Separation of these homogeneous catalysts is a major issue.

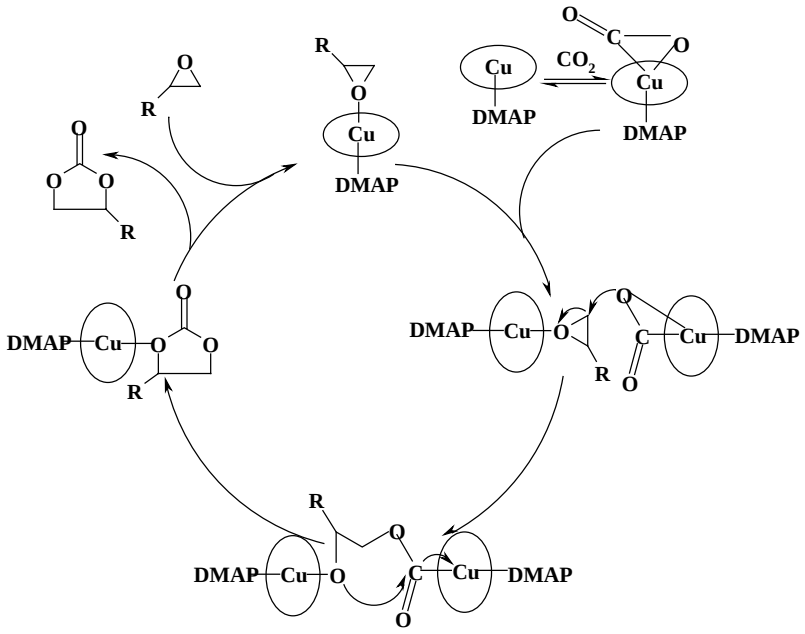

Fig. 3.3. Possible reaction mechanism for cyclic carbonate synthesis over homogeneous Cu complexes.

Table 3.1. Catalytic activity of Cu and Mn complexes for cyclic carbonate synthesis from CO_2 and epoxides

Catalyst (mmol)	Epoxide	Epoxide conversion (wt%)	TOF	Cyclic carbonate selectivity%
CuPc (0.0072)	ECH	80.3	502	97.2
CuTPP (0.0072)	ECH	78.2	489	96.4
$[Cu(cyclen)(NO_3)]ClO_4$ (0.0078)	ECH	71.4	412	95.2
Cu(saloph) (0.0072)	ECH	71.8	449	98.2
$Cu(phen)_2(NO_3)_2(H_2O)$ (0.0069)	ECH	69.6	454	97.2
Cu(salen) (0.0072)	ECH	66.1	413	95.8
$Cu(bipy)_2(NO_3)_2(H_2O)$ (0.0069)	ECH	61.4	400	96.7
$[Cu(Me_4cyclen)(CH_3CN)](ClO_4)_2$ (0.0066)	ECH	37.8	258	96.8
$[Mn(Me_4cyclen)(NO_3)](ClO_4)_2$ (0.0064)	ECH	63.8	449	97.2
$[Cu(cyclen)(NO_3)]ClO_4$ (0.0078)	PO	49.6	286	91.3
Cu(saloph) (0.0072)	PO	34.2	214	97.5
$Cu(phen)_2(NO_3)_2(H_2O)$ (0.0069)	PO	38.0	248	98.4
Cu(salen) (0.0072)	PO	30.6	191	100
$Cu(bipy)_2(NO_3)_2(H_2O)$ (0.0069)	PO	29.6	193	97.9
$[Mn(Me_4cyclen)(NO_3)](ClO_4)_2$ (0.0064)	PO	30.2	206	91.8

Reaction conditions: Epoxide (18 mmol), catalyst (0.0064 – 0.0078 mmol), DMAP (0.0072 mmol), CH_2Cl_2 (20 ml), CO_2 (6.9 bar), temperature (393 K), reaction time (4 h). Turnover frequency (TOF) = moles of epoxide converted per mole of metal per hour. ECH = Epichlorohydrin. PO = Propene carbonate.

3.3.2. Cyclic Carbonates Synthesis over Zeolite-Y-Encapsulated Metal Phthalocyanines

Metallophthalocyanines (MPcs) are attractive biomimetic catalysts for oxidation and epoxidation reactions. They are extensively used because of their simple preparation process, inexpensiveness and their chemical and thermal stability. However, it has been rarely reported that metal phthalocyanines could be used as catalysts for the insertion reaction of CO_2 with epoxides for the preparation of cyclic carbonates. In the previous section, CuPc was found to be the best among the various metal complexes studied for this cycloaddition reaction. It is known that in solutions, MPc complexes agglomerate and as a consequence, exhibit lower catalytic activity. Encapsulation of MPc complexes inside the cages of zeolites and zeolitic materials enhances their catalytic activity.

In the present section, binary catalysts comprising metal phthalocyanines encapsulated in zeolite-Y (MPc-Y) and a co-catalyst (such as quaternary ammonium and phosphonium salts or organic bases), are used to catalyze the formation of cyclic carbonates from CO_2 and epoxides. The catalytic property of various metal phthalocyanines in the presence of different co-catalysts and solvents are investigated. Plausible reaction mechanism is also presented. Unlike most of the known catalysts, these heterogeneous metal complex catalysts are not sensitive to air and moisture and could be subjected to utilization in several recycling experiments without much loss in activity.

The experimental investigation reveals that carbon dioxide reacts with epoxides to produce cyclic carbonates only in presence of MPc, while metal free phthalocyanine itself did not catalyze the reaction (Table 3.2). MPc, combined with a Lewis base or quaternary ammonium salt efficiently promoted the conversion of epoxide to cyclic

carbonate, although these bases themselves showed very low catalytic activity under employed conditions (Table 3.2). There was a synergistic increase in the rate of cycloaddition reaction when both the catalyst and co-catalyst were present together. AlPcCl was deposited on SiO_2 by impregnation and the resulting AlPcCl-SiO_2 was investigated as a catalyst for this reaction in combination with different co-catalysts. Among several co-catalysts, DMAP was found to be a highly efficient co-catalyst (Fig. 3.4).

Table 3.2. Influence of co-catalyst on cycloaddition reaction of epichlorohydrin and CO_2 over AlPcCl-SiO_2

Entry no.	Catalyst	Co-Catalyst	ECH conversion (mol %)	Cyclic carbonate selectivity (mol %)
1	H_2Pc	none	0	0
2	AlPcCl-SiO_2	none	4.7	100
3	None	Bu_4NBr	9.8	97.9
4	None	Ph_3P	6.3	100
5	None	Bu_4PBr	9.8	97.2
6	None	Pyridine	18.4	98.3
7.	None	DMAP	32.1	89.3
8.	AlPcCl-SiO_2	Ph_3P	64.3	76.0
9.	AlPcCl-SiO_2	Bu_4PBr	71.3	91.1
10.	AlPcCl-SiO_2	Bu_4NBr	76.7	85.0
11.	AlPcCl-SiO_2	Pyridine	80.4	77.3
12.	AlPcCl-SiO_2	DMAP	90.2	90.9

Reaction conditions: Epoxide, 18 mmol; AlPcCl-SiO_2, 83 mg; temperature, 393 K; CO_2 pressure, 6.9 bar; dichloromethane (DCM), 20 ml; run time, 4 h.

3.3.2.1. Influence of Catalyst to Co-catalyst Ratio

The amount of base co-catalyst affected the formation of cyclic carbonates from carbon dioxide and epichlorohydrin. It was found that when the molar ratio of

DMAP/AlPc-Y was below four the formation rate of cyclic carbonate increased with the amount of co-catalyst and above that the formation rate decreased with a further increase in DMAP concentration (Table 3.3).

Table 3.3. Effect of catalyst/cocatalyst molar ratio for cycloaddition reaction of epichlorohydrin and CO_2 over AlPc-Y and DMAP binary system

Entry no.	DMAP/AlPc-Y	ECH conversion (wt %)	Cyclic carbonate selectivity (wt %)
1	1	82.8	93.5
2	2	94.2	98.1
3	4	97.4	94.1
4	6	92.4	93.2
5	8	88.2	85.0
6.	10	84.3	87.0

Reaction conditions: Epoxide, 18 mmol; AlPc-Y, 83 mg; temperature, 393 K; CO_2 pressure, 6.9 bar; CH_2Cl_2, 20 ml; run time, 4 h.

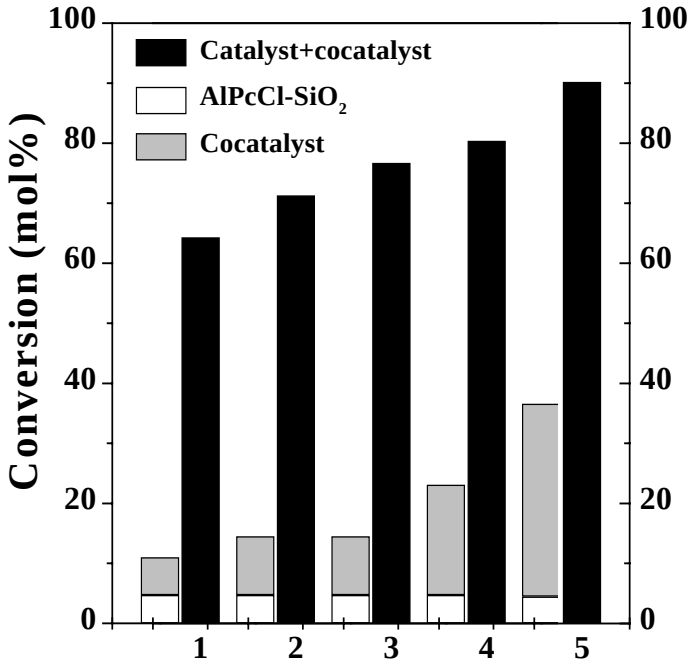

Fig. 3.4. Synergism of catalyst and cocatalyst in cyclic carbonate synthesis.

3.3.2.2. Influence of Temperature and Pressure

Both temperature and pressure showed marked effect on the yield of cyclic carbonates (Table 3.4). High temperatures favored depolymerization of polycarbonates and high yields of cyclic carbonates. The reaction proceeds even near atmospheric pressures (1.6 bar), but the cyclic carbonate yield was very low. The optimum conditions for the reaction were found to be 6.9 bar and 393 K. At pressures beyond 6.9 bar, there were no further increase in the yield of cyclic carbonates.

Table 3.4. Influence of temperature and pressure on cycloaddition reaction of CO_2 with epichlorohydrin over AlPc-Y and DMAP binary system

Entry no.	Temperature (K)	Pressure (bar)	ECH conversion (wt %)	Cyclic carbonate selectivity (wt %)
1	353	6.9	82.8	91.2
2	373	6.9	90.9	90.9
3	393	6.9	97.3	99.7
4	433	6.9	98.2	100
5	353	1.6	17.4	90.5
6	353	4.8	59.7	92.5
7.	353	13.8	83.5	94.3

Reaction conditions: Epoxide, 18 mmol; AlPc-Y, 83 mg; DMAP; 0.0072 mmol; dichloromethane, 20 ml; run time, 4 h.

3.3.2.3. Influence of Solvent

Solvent also has a marked influence on catalytic activity (Table 3.5). Non-polar solvents do not show much effect on the reaction. Polar solvents, on the contrary, showed a notable influence on cyclic carbonate formation. Among the polar solvents, alcoholic solvents markedly influenced the reaction. In the case of alcoholic solvents, epoxide conversion is less and side products formed in larger amounts. The weak activity in alcoholic solvents may be explained due to competition of alcohol and

reactant molecules for the active sites. Reactions proceeded very well even in absence of solvents but the product was brown in color.

In DMF, the reaction proceeds efficiently. CO_2 is highly soluble in DMF. Hence, there is enough amount of CO_2 available in the medium for the reaction and as a consequence higher conversions are observed. There are reports [25] that cyclic carbonate formation occurs in high yields in DMF solvent even in the absence of any catalyst but at supercritical conditions. At the reaction conditions discussed in this section, about 27% of ECH conversion was observed in DMF in the absence of a catalyst.

Table 3.5 Effect of solvent on cycloaddition reaction of epichlorohydrin and CO_2 over AlPc-Y and DMAP binary system

Entry no.	Solvent	ECH conversion (wt %)	Cyclic carbonate selectivity (wt %)
1	None	93.0	100
2	Toluene	92.6	97.8
3	Dichloromethane	95.6	98.6
4	Acetonitrile	97.3	99.7
5	Methanol	46.9	80.6
6.	N,N-Dimethyl formamide	98.2	97.6

Reaction conditions: Epoxide, 18 mmol; AlPc-Y, 83 mg; DMAP; 0.0072 mmol; Solvent, 20 ml; CO_2 pressure, 6.9 bar; Temperature, 393 K; run time, 4 h.

3.3.2.4. Influence of Metal and Zeolite Encapsulation

Zeolite-encapsulated metal phthalocyanine complexes (MPc-Y) exhibited high catalytic activity for cycloaddition of CO_2 to epichlorohydrin. The catalytic activity (TOF, h^{-1}) increased with the central metal ion (M) in the order: Cu (768)> Ni (543)>

Co (524) (Table 3.6). The zeolite-Y encapsulated complexes (MPc-Y) exhibited superior activity as compared to "neat" and silica-supported phthalocyanine complexes (TOF, h^{-1}: CuPc-Y (768) > CuPc-SiO_2 (506) > CuPc (502)) (Table 3.6). No leaching of MPc was observed in case of zeolite-Y encapsulated catalysts. The solid catalyst was recovered by simple filtration and reused in a minimum of three cycles; little loss in activity was observed.

EPR signals for "neat" CuPc complex were broad and copper hyperfine features were not resolved indicating intermolecular interactions and agglomeration of CuPc molecules (Chapter 2). CuPc-SiO_2 also did not show resolved Cu hyperfine features. Zeolite-encapsulated CuPc, in contrast, showed resolved, parallel hyperfine features characteristic of isolated molecules (Chapter 2). These findings reveal the isolation and confinement of the CuPc complexes in the cavities of zeolite-Y. The superior activity of MPc-Y catalyst, compared to both "neat" and silica-supported complexes is probably due to the isolation of MPc complexes in the cavities of zeolite-Y and the consequent electronic changes. When the reaction was conducted using propene oxide (PO), the conversion and cyclic carbonate selectivity were found to be lower than that observed with ECH. In presence of electron withdrawing substituents (like Cl), activation of the epoxide and subsequent CO_2 insertion to form cyclic carbonate were facilitated.

Fig. 3.5 represents proposed, possible mechanism. This reaction proceeds through acid-base properties of the catalyst. In the present case, metal center acts as the Lewis acid site and DMAP acts as basic site. The acid-base combination together enables opening of the epoxide ring and then the reaction with CO_2 to give the corresponding cyclic carbonate *via* a ring opening and ring cyclization process.

Table 3.6. Cyclic carbonate synthesis from CO_2 and epoxide over MPc complexes

Catalyst	Epoxide	Conv. (wt%)	Cylic carbonate selec. (wt%) (TOF h^{-1})
AlPcCl-"neat"	Epichlrohydrin	83.0	95.5
AlPcCl-"neat"	Propylene oxide	60.9	87.8
AlPcCl-SiO_2	Epichlrohydrin	90.2	90.9
AlPc-Y	Epichlrohydrin	97.3	99.7
AlPc-Y(**recycle-1**)	Epichlrohydrin	95.7	99.3
AlPc-Y(**recycle-2**)	Epichlrohydrin	93.8	96.7
AlPc-Y(**recycle-3**)	Epichlrohydrin	94.0	98.3
AlPc-Y	Propene oxide	84.7	85.3
CuPc-"neat"	Epichlrohydrin	80.3	97.2 (502)
CuPc-"neat"	Propylene oxide	46.2	89.2 (289)
CuPc-SiO_2	Epichlrohydrin	76.4	94.7 (506)
CuPc-Y	Epichlrohydrin	91.4	96.3 (768)
CuPC-Y	Propene oxide	71.7	90.3 (602)
CoPc-Y	Epichlrohydrin	90.9	95.5 (524)
CoPc-Y	Propene oxide	63.5	91.3 (366)
NiPc-Y	Epichlrohydrin	83.4	87.7 (543)
NiPc-Y	Propene oxide	75.9	84.6 (494)

Reaction conditions: Epoxide, 18 mmol; AlPc-Y, 83 mg; DMAP; 0.0072 mmol; dichloromethane, 20 ml; CO_2 pressure, 6.9 bar; temperature, 393 K; run time, 4 h.
TOF = mole of epoxide converted per mole of metal ion per hour.

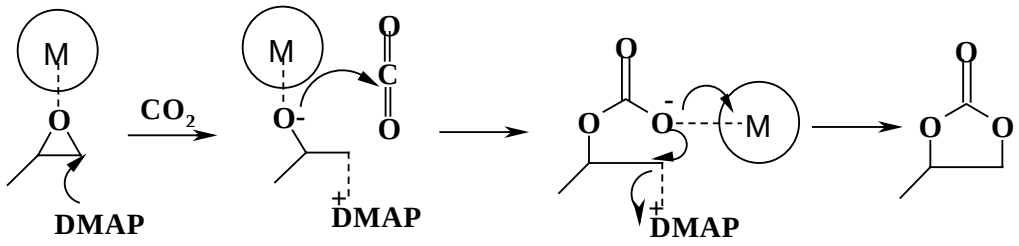

Fig. 3.5. Proposed reaction pathway for the cyclic carbonate synthesis.

3.3.3. Cyclic Carbonates Synthesis over Titanosilicate Molecular Sieves

Titanosilicate are attractive heterogeneous catalysts for oxidation and epoxidation reactions. Use of titanosilicates in Lewis acid catalyzed reactions is not explored much. The catalytic properties of various titanosilicates e.g., TS-1, Ti-MCM-41 and Ti-SBA-15, in the cycloaddition reaction are investigated, for the first time. These catalysts are also not air and moisture sensitive and could be reused in several recycles without much loss in activity.

3.3.3.1. Catalyst Co-catalyst Synergism

The reaction did not take place in the absence of catalyst and co-catalyst (Table 3.7). With TS-1 alone, an epoxide conversion of 18.2% with cyclic carbonate selectivity of 87.4% was obtained in the cycloaddition reaction of CO_2 and epichlorohydrin (ECH). On the other hand, with co-catalyst alone, an epoxide conversion of 6.2 to 32 mol% and a cyclic carbonate selectivity of 89 – 100 mol% was obtained. The activity (turnover frequency per hour; TOF) of cocatalysts (in the absence of titanosilicates) increased in the order: Ph_3P (39) < Bu_4PBr, Bu_4NBr (61) < pyridine (115) < DMAP (200). There was a synergistic increase in the rate of cycloaddition when both the catalyst and co-catalyst were present. The synergistic increase, i.e., the ratio of TOF for the reactions with (TS-1+ co-catalyst) to the sum of TOFs for the reaction with TS-1 and cocatalyst alone increase in the order: TS-1+Ph_3P

(1.85) < TS-1+DMAP (2.44) < TS-1+ pyridine (3.5) < TS-1+Bu_4PBr (5.36) <TS-1+Bu_4NBr (5.6) (Fig. 3.6). Apparently, the nucleophilicity of the nitrogen or phosphorous atom is augmented by the electrophilic interaction of Ti^{4+} ions with the epoxide (Fig. 3.7). The synergism is lower with Ph_3P, DMAP and pyridine because the active complex formed during the cycloaddition reaction is larger than the pore diameter of TS-1 (~ 5.6 Å) and hence the complex may not form inside the TS-1 pores. With these bulkier co-catalysts, the reaction probably takes place mainly at titanium sites on the external surface of the particles and hence, lower activities were observed. The synergistic effect was much lower when TiO_2 was used as the source of Ti instead of TS-1 (Fig. 3.8). In addition to the main cyclic carbonate, the side products in the case of epichlorohydrin included 3-chloro-1,2-propanediol and 3-chloropropanaldehyde.

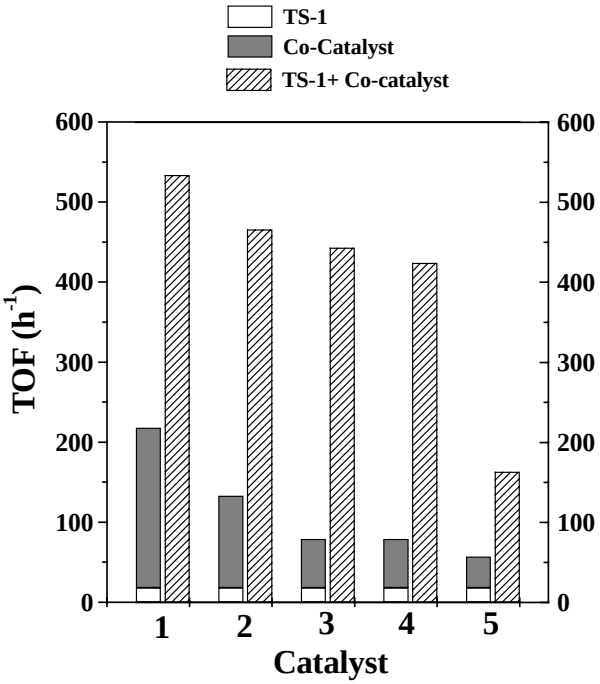

Fig. 3.6. Catalyst - cocatalyst synergism and influence of cocatalyst in the synthesis of cyclic carbonates from epichlorohydrin and CO_2. Reaction conditions: catalyst (TS-1; 100 mg; Si/Ti = 36), cocatalyst (0.0072 mmol), epichlorohydrin (18 mmol), CH_2Cl_2 (20 ml), CO_2 (6.9 bar), temperature = 393 K, run time = 4 h. Cocatalyst: 1 – DMAP, 2 – pyridine, 3 – Bu_4NBr, 4 – Bu_4PBr, 5 – Ph_3P.

Table 3.7. Synergism of catalyst (TS-1) and co-catalyst combination in the synthesis of cyclic carbonates from epichlorohydrin and CO_2

Catalyst	Cocatalyst	ECH Conv. (mol %)	Cyclic carbonate Selec. (%)	TOF (h^{-1})
None	None	<1	-	-
TS-1	None	18.2	87.4	18
None	DMAP	32.1	89.3	200
TS-1	DMAP	85.4	92.6	533
None	Pyridine	18.4	98.3	115
TS-1	Pyridine	74.5	91.0	466
None	Bu_4NBr	9.8	97.9	61
TS-1	Bu_4NBr	70.8	73.0	443
None	Bu_4PBr	9.8	97.2	61
TS-1	Bu_4NBr	67.8	98.4	424
none	Ph_3P	6.2	100	39
TS-1	Ph_3P	26.1	71.0	163

Reaction conditions: Epoxide, 18 mmol; TS-1, 100 mg; DMAP; 0.0072 mmol; dichloromethane, 20 ml; CO_2 pressure, 6.9 bar; temperature, 393 K; run time, 4 h.
TOF = mole of epoxide converted per mole of metal ion per hour.

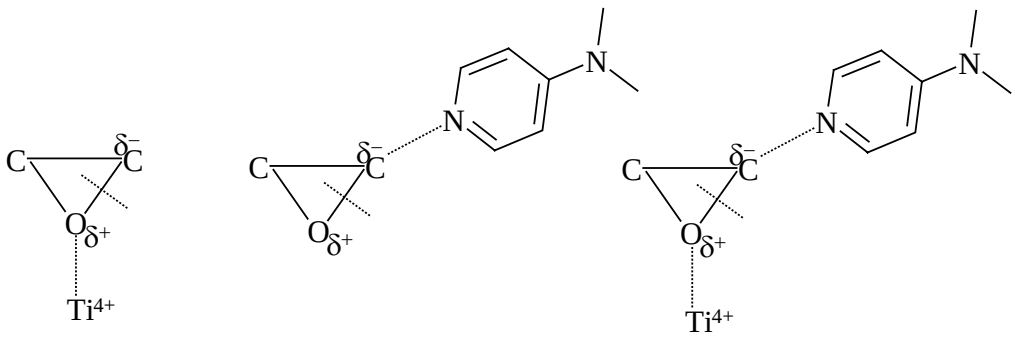

TS-1 alone DMAP alone TS-1+ DMAP

Fig. 3.7. Activation of epoxide by titanosilicates and DMAP co-catalyst.

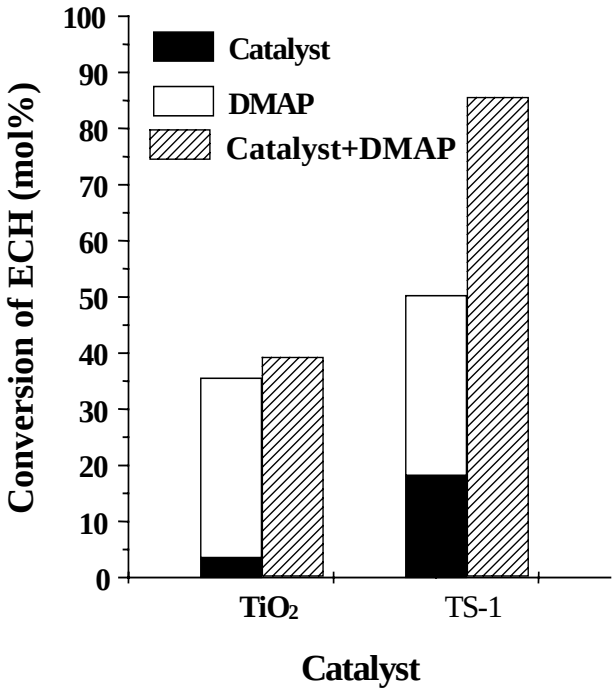

Fig. 3.8. Influence of Ti source on the catalyst-cocatalyst synergism in the synthesis of cyclic carbonates from epichlorohydrin and CO_2. Reaction conditions: catalyst (TS-1 = 100 mg; TiO_2 = 5.5 mg (equivalent of Ti content in TS-1)), cocatalyst (DMAP; 0.0072 mmol); epichlorohydrin (18 mmol), CH_2Cl_2 (20 ml), CO_2 (6.9 bar), temperature = 393 K, run time = 4 h.

3.3.3.2. Influence of Reaction Parameters

Reaction temperature and CO_2 pressure significantly influenced the catalytic activity. The yield of cyclic carbonates increased with an increase in reaction temperature. A complete conversion of epicholorohydrin was achieved at 413 – 433 K (Fig. 3.9 (a)). Cyclic carbonate formed in higher yields also with an increase in pressure up to 13.8 bar, and beyond that it decreased due to formation of significant quantities of side products (Fig. 3.9 (b)).

3.3.3.3. Influence of Pore Structure

Epoxides like propene oxide (PO), epichlorohydrin (ECH), butene oxide (BO) and styrene oxide (SO) were converted into their corresponding cyclic carbonates in

near quantitative yields (Table 3.8). All the titanosilicate chosen showed similar activity for epoxides of smaller dimensions (ECH and PO). However for styrene oxide, mesoporous titanosilicates (Ti-MCM-41 and Ti-SBA-15) were found to be the best catalysts. The active complex formed during the cycloaddition reaction is larger than the pore diameter of TS-1 (~ 5.6 Å) and hence, the reaction takes place only on the external surface of the particles in the case of TS-1 samples. In the case of Ti-MCM-41 and Ti-SBA-15 there is no pore size limitation and high activity was observed. The titanosilicate catalysts could be easily recovered and reused (at least in three recycles) with not much loss in activity. Although all the reactions were conducted in a solvent medium like dichloromethane, the reaction proceeds even in absence of a solvent to a similar extent (Table 3.8). However, the product was slightly colored in absence of solvent. At higher temperatures/pressures/reaction period (413 K, 24.1 bar, 24 h) HPLC analysis revealed the formation of the methanol insoluble, solid, aliphatic polycarbonates.

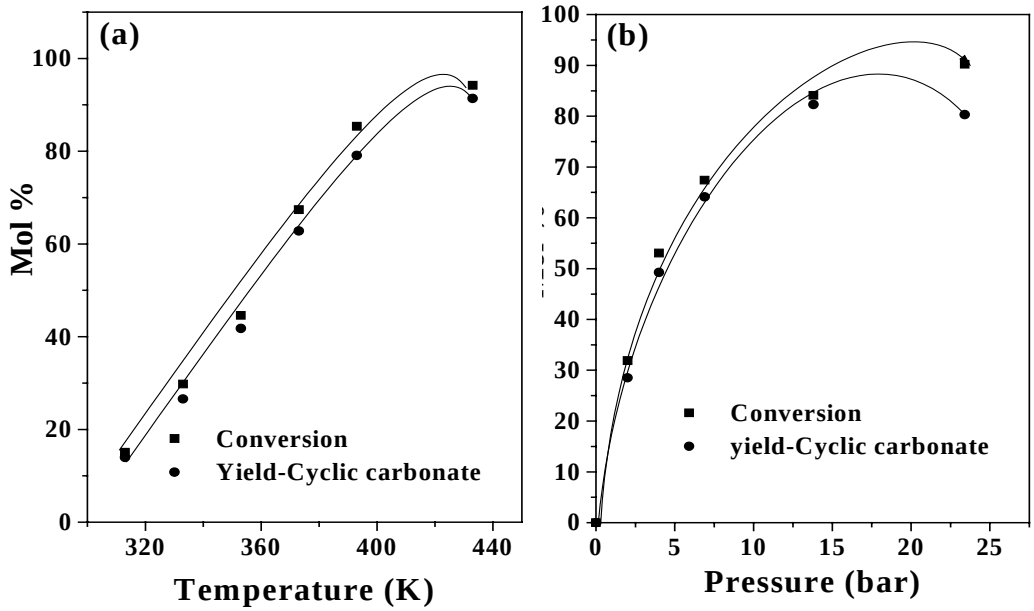

Fig. 3.9. Effect of (a) temperature (at 6.9 bar CO_2 pressure) and (b) CO_2 pressure (at 393 K) on cycloaddition of CO_2 to epichlorohydrin over TS-1. Epoxide, 18 mmol; TS-1, 100 mg; DMAP; 0.0072 mmol; DCM, 20 ml; run time, 4 h.

Table 3.8. Catalytic activity of titanosilicates in the synthesis of cyclic carbonates from epoxides and CO_2

Run No.	Catalyst	Co-catalyst	Temp. (K)	Run time (h)	Epoxide[b]	Conv. of epoxide (mol%)	TOF[f]	Sel. for cyclic carbonate (mol%)
1	TS-1	DMAP	393	4	EC	85.4	534	92.6
			433	4	EC	94.2	588	97.0
2	TS-1 (no solvent)	DMAP	393	4	EC	89.6	560	97.5
3	TS-1 (3^{rd} recycle)	DMAP	393	4	EC	77.0	489	90.4
4	TiMCM-41	DMAP	393	4	EC	78.8	492	84.0
5	Ti-SBA-15	DMAP	393	4	EC	92.9	580	89.7
6	TS-1	DMAP	393	6	PO	66.8	278	84.6
			433	6	PO	94.0	391	83.0
7	TS-1 (no solvent)	DMAP	393	6	PO	77.6	323	88.1
8	TiMCM-41	DMAP	393	6	PO	63.7	265	91.2
9	Ti-SBA-15	DMAP	393	6	PO	69.5	290	95.3
10	TS-1	DMAP	393	6	BO	76.6	319	70.9
11	TS-1	DMAP	413	8	SO	44.7	140	45.5
12	TiMCM-41	DMAP	413	10	SO	98.1	245	73.1
13	Ti-SBA-15	DMAP	413	8	SO	89.6	280	100
14	TiMCM-41(no solvent)	DMAP	413	10	SO	100	312	82.0

Reaction conditions: Catalyst (100 mg), co-catalyst (0.0072 mmol), epoxide (18 mmol), CH_2Cl_2 (20 ml), CO_2 (6.9 bar). DMAP = N,N-dimethylaminopyridine, EC = epichlorohydrin, PO = propene oxide, SO = styrene oxide, BO = α-butene oxide. TOF = turnover frequency (moles of epoxide converted per mole of Ti per hour)

3.3.3.4. Synthesis of Cyclic Carbonates from Olefins

Titanosilicate molecular sieves are known to be efficient catalysts for the oxidation of olefins to epoxides using H_2O_2 or TBHP as oxidant [26]. Hence, an attempt was made to achieve both the epoxidation and the subsequent cycloaddition reaction using the same titanosilicate catalyst, in the same reactor. A conversion of 54.6% and cyclic carbonate selectivity of 55.6% were obtained when allyl chloride was the olefin. Some amount of ring-hydrolyzed products is also detected.

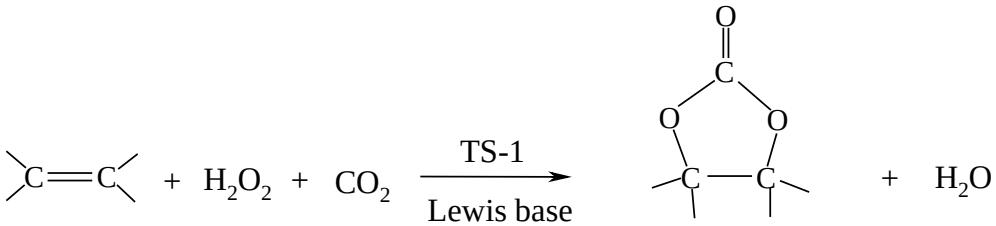

Cyclic carbonate

With styrene, a conversion of 50.4% and cyclic carbonate selectivity of 26% were obtained. When the reaction was conducted with Ti-MCM-41 as catalyst and TBHP as the oxidizing agent, the conversions of olefins to epoxides (stage 1) were lower (allyl chloride conv. = 13.3% and styrene conv. = 44%) but the further conversion of epoxide formed during the reaction to cyclic carbonate (stage 2) was almost 100% (Table 3.9). As expected, Ti-MCM-41, with its larger pore diameter was more active and selective than TS-1 for the cycloaddition of CO_2 to the epoxide (stage 2; rows 2 and 4, Table 3.9). When H_2O_2 was used as the oxidizing agent, water was also there in the reaction medium, so side product formation was more, but when TBHP in EDC was used the side product formation was not observed and enhancement in cyclic carbonates selectivity was observed. Aresta and Dibenedetto [27] reported the synthesis of styrene carbonate from styrene in the presence of O_2 (5 atm) and CO_2 (45

atm) at 408 K and 12 h reaction time. A styrene carbonate yield of 1.9% over Nb_2O_5 and 11% over Nb_2O_5 + $NbCl_5$ was reported.

Table 3.9. One-pot synthesis of cyclic carbonates from olefins: Epoxidation (Stage 1)-cum-cycloaddition (Stage 2)

Catalyst (weight in mg)	Olefin	Oxidizing agent	Stage 1 Olefin to epoxide		Stage 2 Epoxide to cyclic carbonate	
			Olefin conv. to epoxide (%)	Epoxide sel. (%)	Epoxide conv. (%)	Cyclic carbonate sel. (%)
TS-1 (400)[a]	Allyl chloride	H_2O_2	54.6	100.0	92.5	55.6
TS-1 (400)[a]	Styrene	H_2O_2	50.4	89.0	49.2	26.0
TiMCM-41 (100)[b]	Allyl chloride	TBHP	13.3	100	100	100
TiMCM-41 (100)[b]	Styrene	TBHP	44.0	93.1	97.2	83.4

[a]Runs with TS-1 (400 mg) were carried out with 26.2 mmol olefin, 0.0072 mmol DMAP, 14.7 mmol 50% H_2O_2 and CO_2 (6.9 bar) in acetone (20 ml).
[b]Runs with TiMCM-41 (100 mg) were carried out with 8 mmol olefin, 0.0036 mmol DMAP, 8 mmol 40% tert-butyl hydroperoxide (TBHP) in CH_2Cl_2 and CO_2 (6.9 bar) in acetonitrile (6.4 g).

3.3.4. Cyclic Carbonate Synthesis over Organo-functionalized, Ordered Mesoporous Materials

With zeolite-encapsulated MPc and titanosilicates an additional homogeneous co-catalyst (DMAP) was also required in cyclic carbonate synthesis. Hence, in the true sense, those systems are not completely heterogeneous. It is, therefore, highly desirable to develop an efficient, reusable heterogeneous catalyst for this reaction. The catalyst should consist an acidic site (to activate epoxides) as well as a basic site (to activate CO_2). SBA-15 is more appropriate for the transformation of larger substrate molecules. In view of this, the surface of SBA-15 was organo-functionalized with several amines of varying basicity. Ti and Al are incorporated in SBA-15 to form acid centers.

Samples of Ti/Al-SBA-15 (Si/Ti = 40 – 119 and Si/Al = 22) were prepared by the post-synthesis method (Chapter 2). They were then organofunctionalized with 3-chloropropyltriethoxysilane to get Ti/Al-SBA-15-*pr*-Cl. Further reaction with bases such as imidazole, guanine and adenine (under water-free, inert conditions) yielded Ti-SBA-15-*pr*-Im, Ti-SBA-15-*pr*-Gua and Ti-SBA-15-*pr*-Ade, respectively (Fig. 3.10). For comparative studies Ti-SBA-15-*pr*-NH_2 samples were also prepared by reacting Ti-SBA-15 with 3-aminopropyltriethoxysilane (Chapter 2). These catalysts were characterized by various physicochemical techniques (Chapter-2, Table 2.3). On introduction of metal ions and base molecules the following changes were noted: (a) surface area (S_{BET}) decreased from 871 to 627 m^2/g, (b) total pore volume decreased from 1.55 to 1.04 cc/g, and (c) average pore diameter decreased from 7.2 to 6.5 nm. The pore diameter estimated from TEM measurements (~ 8 nm) agree well with that obtained (7.2 nm) from nitrogen adsorption (BJH) method. FT-IR and diffuse reflectance UV-visible spectroscopies provided evidence for strong interaction of the N-H bond in various bases anchored onto the Ti-SBA-15 surface. The band at 211 nm in the UV-visible spectrum of Ti-SBA-15-*pr*-Ade corresponds to dispersed tetrahedral Ti ions. Bases could not be supported directly on the unmodified SBA-15 surface. This observation and the differences in the spectral features (FT-IR and UV-visible) (Chapter-2) suggest that bases are covalently linked through the N-H bond to the modified SBA-15 surface.

3.3.4.1. Surface Acidity

The acidic properties of functionalized SBA-15 materials were investigated by TPD (Fig. 3.11) and DRIFT spectroscopy (Figs. 3.12 and 3.13). Surface acidity was estimated using NH_3 and pyridine as probe molecules. SBA-15 showed two desorption maxima (T_{max}) at 360 and 515 K in NH_3-TPD measurements (Fig. 3.11). In the case of

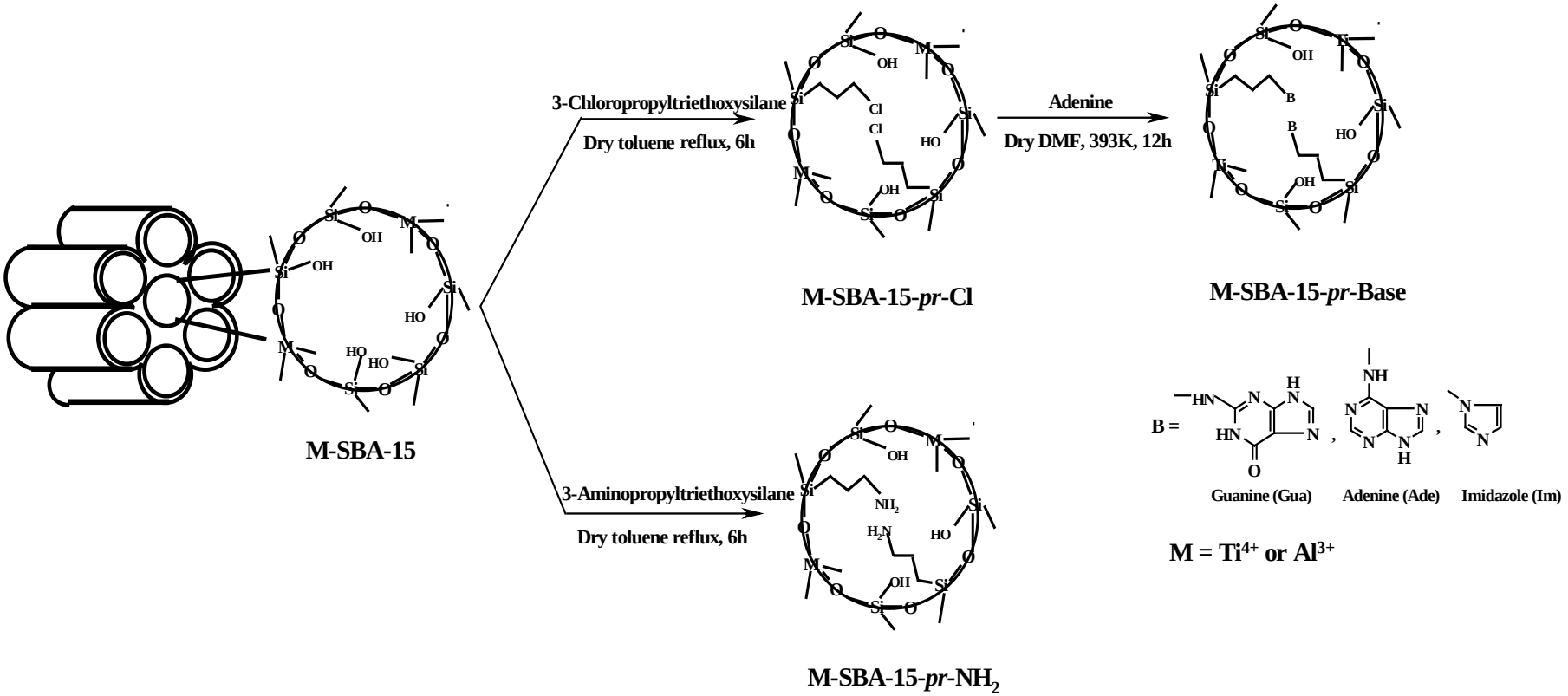

Fig. 3.10. Synthesis of base functionalized Ti- and Al-SBA-15 materials.

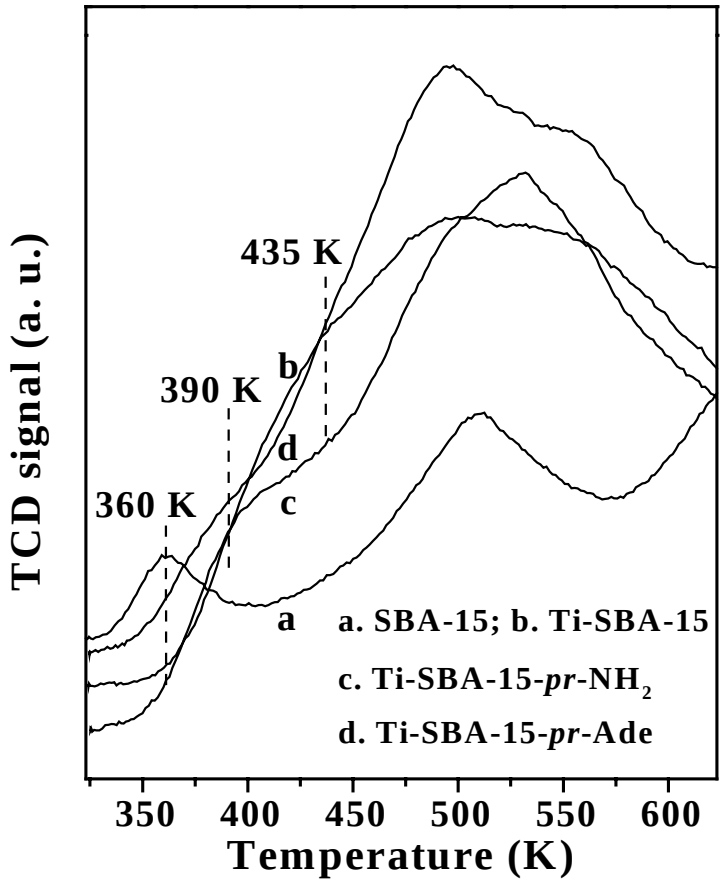

Fig. 3.11. NH_3-TPD profiles of SBA-15 materials.

titanated materials, the desorption peak at 360 K disappeared and instead, two additional desorption maxima appeared at 390 and 435 K indicating higher acidity of Ti-SBA-15. There is also an increase in the amount of NH_3 desorbed on going from SBA-15 to Ti-SBA-15 (0.34 to 0.9 mmol/g).

The spectra of pyridine adsorbed on these samples clearly reveal the absence of Brönsted (1546 and 1639 cm^{-1}) and strong Lewis (1623 and 1455 cm^{-1}) acid sites (Fig. 3.12 (a)).

In Al-containing samples (Al-SBA-15, for example), the IR peaks corresponding to Lewis acid sites shifted marginally to 1580 and 1487 cm^{-1} (Fig. 3.12 (b)), indicating that the Al-containing samples are more acidic than Ti-containing samples. Figs. 3.12 (b) and 3.12 (c) illustrate the expected decrease in the intensity of

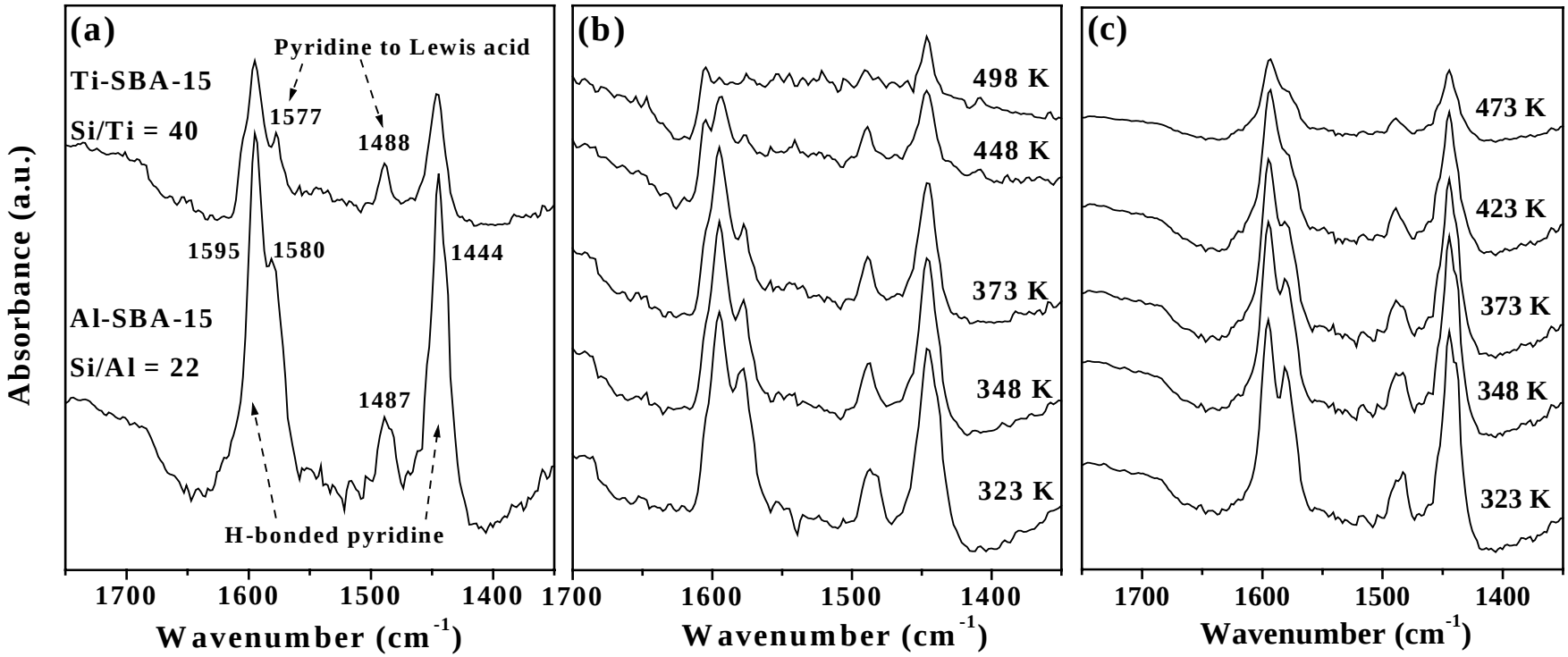

Fig. 3.12. DRIFT spectra of adsorbed pyridine on (a) Ti-SBA-15 and Al-SBA-15 at 373 K and normalized spectral intensity, (b) Ti-SBA-15 at different temperatures, and (c) Al-SBA-15 at different temperatures.

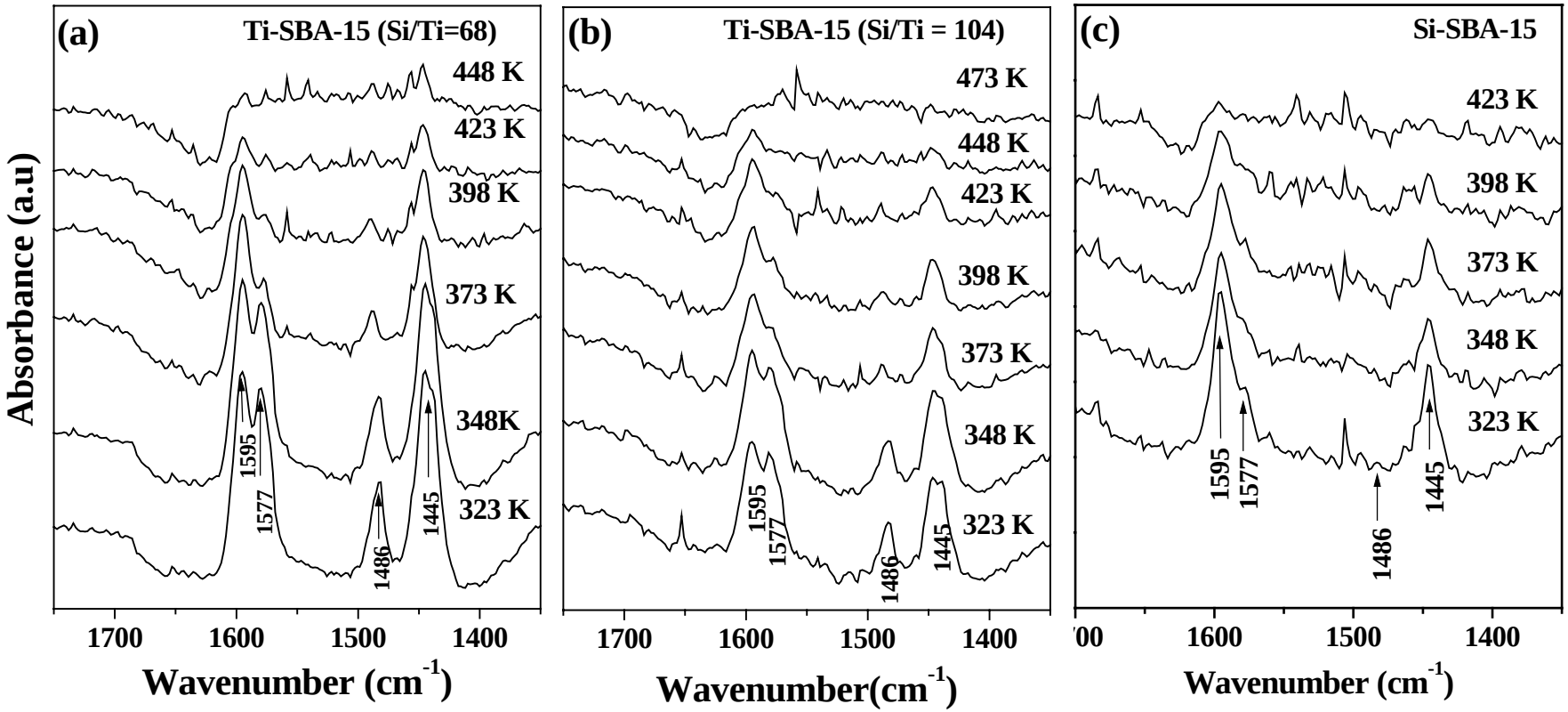

Fig. 3.13. DRIFT spectra of adsorbed pyridine at different temperature on (a) Ti-SBA-15 (Si/Ti = 68) (b) Ti-SBA-15 (Si/Ti = 104) and (c) Si-SBA-15.

adsorbed pyridine at higher temperatures. While the pyridine peaks associated with Lewis acid sites had almost disappeared at around 473 K in the case of Ti-SBA-15, they were present, in significant intensity, in Al-SBA-15 (Fig. 3.12 (c)). The intensity of the pyridine peaks was, in general, more in Al- than Ti-containing samples. This is in agreement with the metal ion content (Si/Al = 22 and Si/Ti = 40) as well as stronger acidity of Al than Ti. Activity of the materials varied proportionately with the Ti content (Fig. 3.13). "Bare" SBA-15 did not possess any Brönsted or Lewis acid sites, while the Ti- and Al-samples contained only weak Lewis acid sites. In NH_3-TPD studies of Ti- containing samples, the peak at 390 K (Fig. 3.11) is attributed to NH_3 bound to Lewis acid sites and the one at 435 K to NH_3 associated with the surface –OH groups through H-bonding interactions. Both TPD and DRIFT studies reveal that organo-functionalization doesn't influence the Lewis acidity of Ti and Al sites.

3.3.4.2. Surface Basicity

Surface basicity was studied by adsorption of CO_2, an "acidic" molecule (Fig. 3.14). "Bare" SBA-15 and Ti-SBA-15 showed a desorption peak at 348 K in CO_2-TPD. In SBA-15-*pr*-NH_2 the intensity of the desorption peak at 348 K decreased and an additional peak appeared at 475 K. The latter is, possibly, due to CO_2 chemisorbed on the amine function (-NH_2). In adenine-functionalized materials, CO_2 desorption occurred at 435 K and 360 K. These desorptions are attributed to CO_2 chemisorbed at the secondary (NH) and tertiary amine functions in adenine, respectively. The shift in T_{max} to higher temperatures compared to that in SBA-15 and Ti-SBA-15 clearly indicates that amine-functionalization, as expected, enhanced the surface basicity. CO_2 uptake was similar (around 2.9 mmol/g of catalyst) for both SBA-15 and Ti-SBA-15. When the amine functions were grafted on the surface, the amount of CO_2 adsorbed increased to 3.8 (for SBA-15-*pr*-NH_2 and Ti-SBA-15-*pr*-NH_2), 4.3 (for SBA-15-*pr*-

Ade) or 5.3 mmol of CO_2/g of catalyst (for Ti-SBA-15-*pr*-Ade), respectively. In terms of mmoles of CO_2 adsorbed *per mole of grafted amine molecule*, the values for the above four catalysts were 0.9, 1.0, 1.4 and 2.4, respectively. The TPD data indicate that the binding energy of CO_2 to different amines decreases in the order: primary amine > secondary amine > tertiary amine.

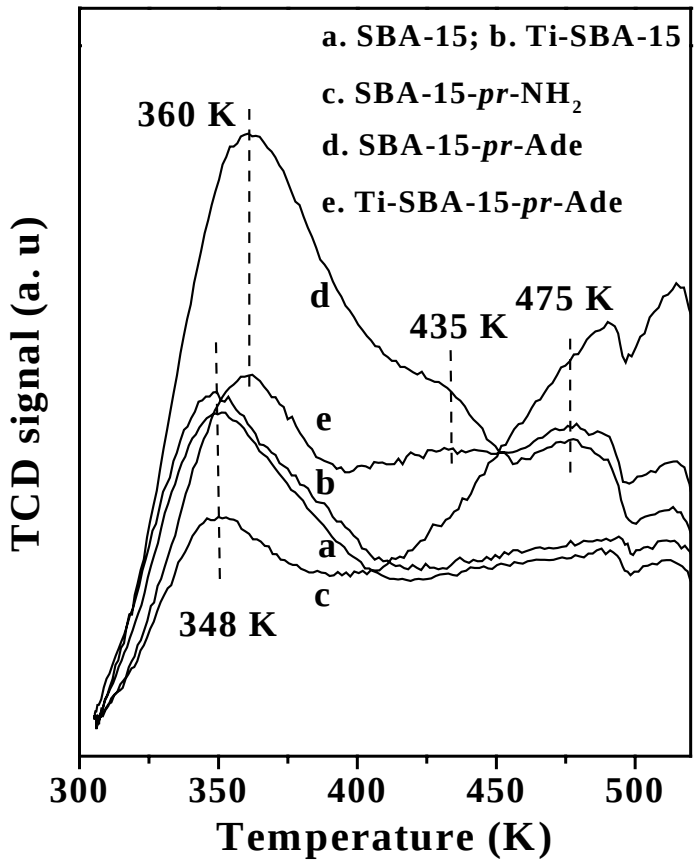

Fig. 3.14. CO_2 -TPD profiles of SBA-15 materials.

The acid-base properties of these modified materials can be exploited for the cycloaddition reaction of CO_2 to epoxide. These materials can activate CO_2 efficiently. The activation of CO_2 and its mode of coordination to the functionalized SBA-15 surface are studied by DRIFT spectroscopy.

3.3.4.3. Active Sites for CO_2 Activation

CO_2 activation is a key prerequisite step for its utilization in chemical synthesis. FT-IR spectroscopy differentiates the different mode of CO_2 coordination. In the present study, the active sites for CO_2 activation have been characterized using *in situ* DRIFT spectroscopy. The solid samples were heated to 373 K and exposed to CO_2 at 253 - 298 K for 1 h. DRIFT spectra of the samples were recorded before and after CO_2 exposure. The difference spectrum yielded spectral features due to adsorbed CO_2. No new IR peaks were detected in the difference IR spectrum of "bare" SBA-15, Ti-SBA-15 and Al-SBA-15. There was no significant activation of CO_2 on these samples. The organo-functionalized SBA-15 materials showed new IR peaks due to CO_2 activated at the basic sites (-NH_2, Im, Gua and Ade). The assignments of these peaks are listed in Table 3.10. Various activated CO_2 species (carbonates, bicarbonates, carbamates and formates) are formed on reaction of activated CO_2 with water, hydroxyls and amine/bases present on the surface. CO_2 can also react with the amine (N-H) functionality in SBA-15-*pr*-Ade and Ti-SBA-15-*pr*-Ade to form carbamates [28-30]. Representative DRIFT spectra of activated CO_2 on Ti- and Al-containing materials are shown in Fig. 3.15.

Metal complexes, metal oxides and zeolites are known to activate CO_2 and form a variety of activated CO_2 complexes (terminal and bridged) [28-31]. CO_2 exhibits different coordination modes - η^1(O), η^1(C) and η^2(C, O). CO_2 molecules can be activated at the carbon atom if the active site (M) is electron-rich or through the oxygen atom if M is electron-deficient. IR spectroscopy can differentiate these coordination modes of CO_2. The DRIFT spectra (Fig. 3.15) reveal that CO_2 is activated through η^1(C)-type coordination on organo-functionalized SBA-15 materials. Several new peaks were observed in the range 1250 – 1700 cm^{-1}. Amines upon reaction with CO_2 form carbamate

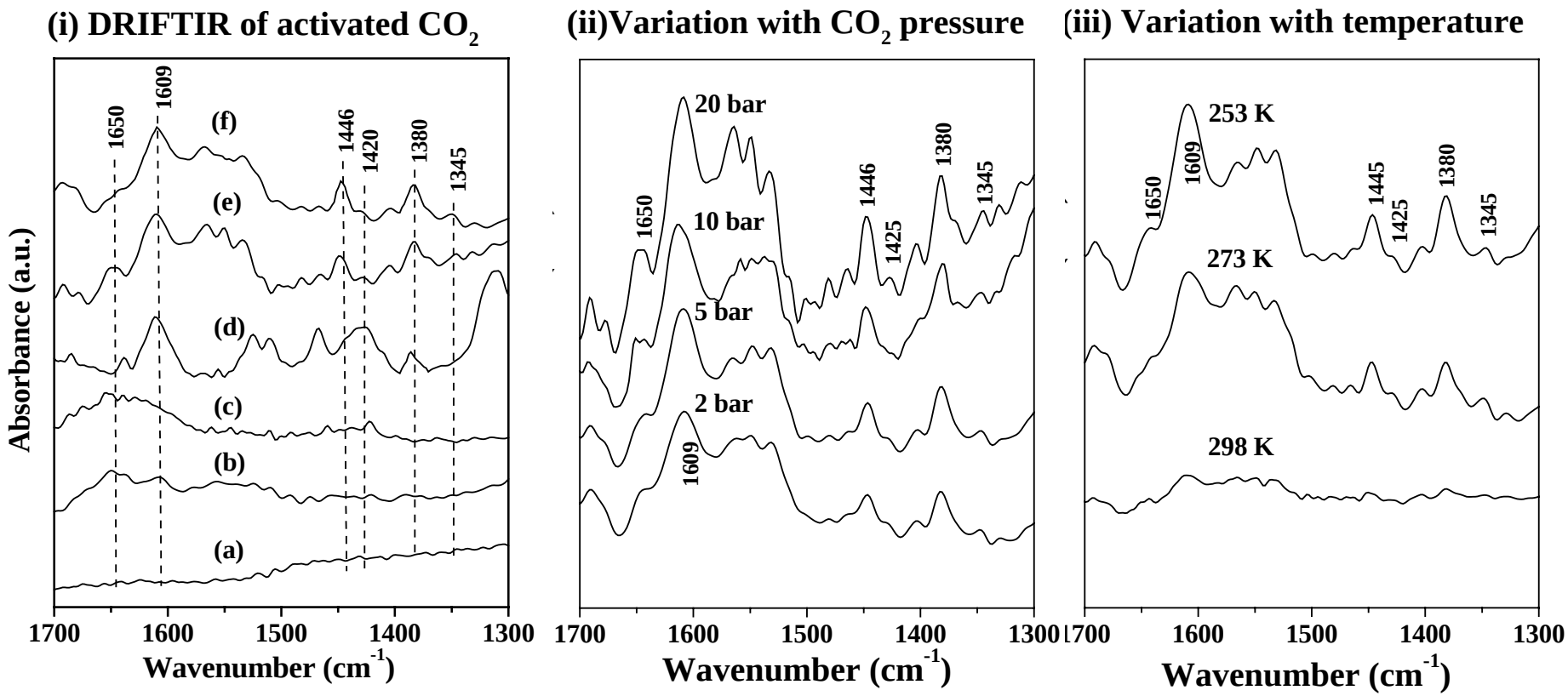

Fig. 3.15. (i) DRIFT spectra of activated CO_2: (a) Ti-SBA-15, (b) Ti-SBA-15-*pr*-NH_2, (c) Ti-SBA-15-*pr*-Im, (d) Ti-SBA-15-*pr*-Gua, (e) Ti-SBA-15-*pr*-Ade, and (f) Al-SBA-15-*pr*-Ade (ii) Influence of CO_2 pressure – catalyst = Ti-SBA-15-*pr*-Ade, temperature = 253 K. (iii) Influence of adsorption temperature – catalyst = Ti-SBA-15-*pr*-Ade, CO_2 pressure = 5 bar.

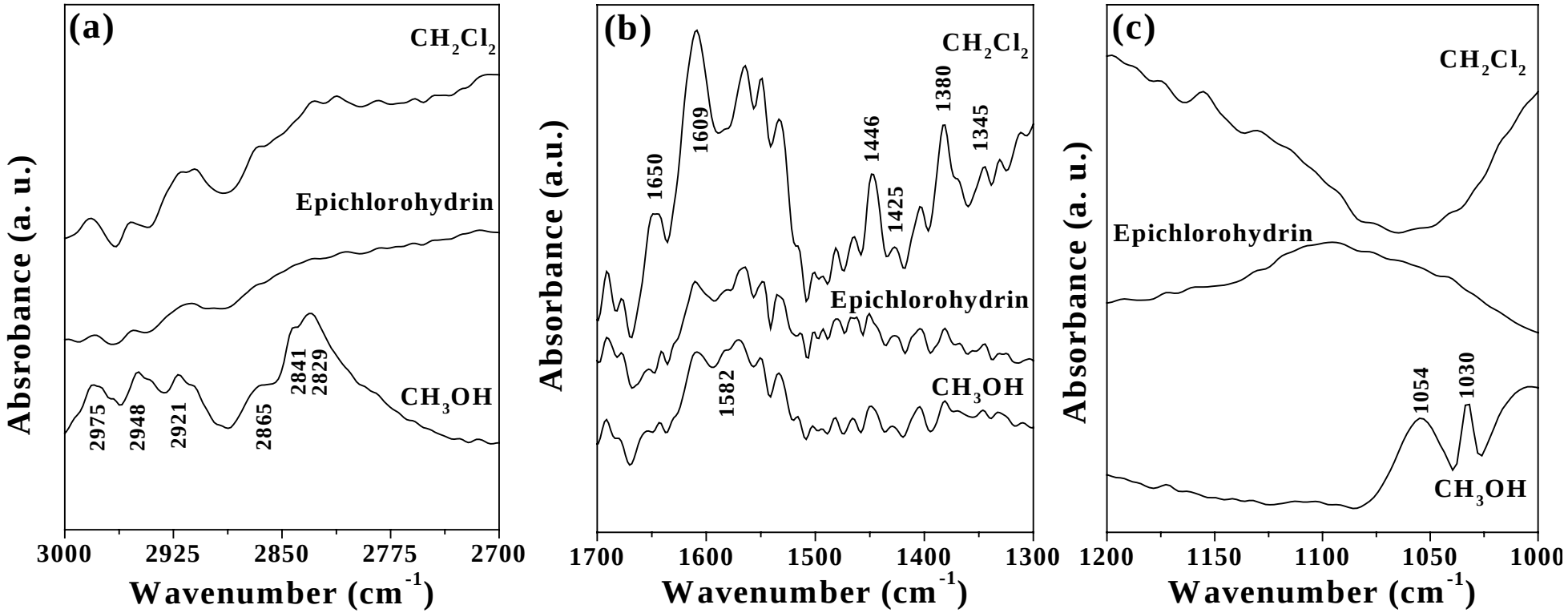

Fig. 3.16. Difference FT-IR spectra of Ti-SBA-15-*pr*-Ade after exposure to CO_2 in the presence of CH_2Cl_2, epichlorohydrin or CH_3OH. Pressure = 20 bar, temperature = 253 K, reaction time = 1 h.

Table 3.10. FT-IR spectral assignments of activated CO_2 species

IR peak position (cm^{-1})	Assignment	Species	IR peak position (cm^{-1})	Assignment	Species
1345	C-O stretching of monodentate carbonate	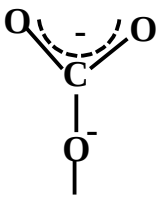	1609 and 1446	Antisymmetric and symmetric C-O stretching vibrations of carbamate anion	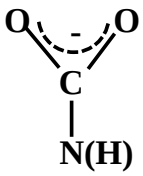
			1622 and 1446	C-O stretching vibrations of carbamate anion (in "neat" adenine)	
1380	C-O stretching vibration of bidentate carbonate	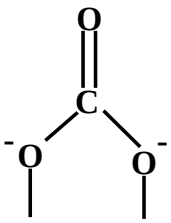	2948 and 2841	C-H stretching vibrations of molecularly adsorbed methanol	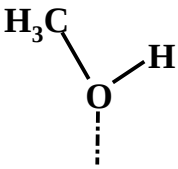
1420	C-O stretching vibration of monodentate bicarbonate	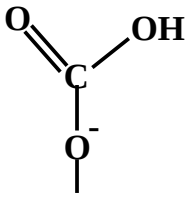	2921 and 2829 1054 and 1030	C-H stretching vibration of methoxides C-H bending modes of methoxide	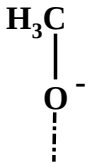
1582	Stretching vibration of methyl carbonate	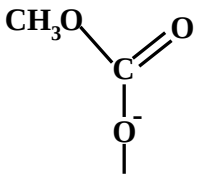	2975 and 2865	C-H stretching vibrations of the bidentate formate species	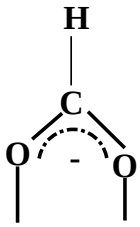
1650	C-O stretching vibration of bidentate bicarbonate	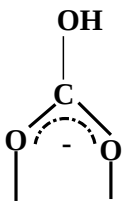			

species [30]. The latter are in equilibrium with the carbamic acid species (Fig. 3.16). DRIFT peaks at 1609 and 1446 cm^{-1} (Fig. 3.15) are due to these surface carbamate species. These carbamate species react with adsorbed water or surface hydroxyl groups forming product carbonates, bicarbonates or formats. Formation of all these forms of CO_2 species on SBA-15 surfaces is apparent from the DRIFT spectra (Fig. 3.15). The peak at 1345 cm^{-1} arises due to monodentate carbonates and that at 1380 cm^{-1} is due to the bidentate carbonate species. The peaks at 1420 and 1650 cm^{-1} are due to monodentate and bidentate bicarbonate species, respectively [31]. The following conclusions are drawn from the DRIFT spectra shown in Fig. 3.15.

1. "Bare" SBA-15, Ti-SBA-15 and Al-SBA-15 activate CO_2 only weakly.
2. Amine-functionalization significantly enhances CO_2 activation (Fig. 3.15(i)). In the IR spectra of adenine- and guanine-functionalized SBA-15, the peaks at 1609 and 1446 cm^{-1} (due to the activated CO_2 species – carbamate) are more pronounced and sharper than those due to carbonates, bicarbonates and formates. These peaks are less intense for propyl amine-functionalized SBA-15 and are barely seen for the Im-functionalized materials. It may be recalled from CO_2-TPD results that the T_{max} for CO_2 desorption from primary amine-functionalized SBA-15 is higher (475 K) than those for secondary (T_{max} = 435 K) and tertiary (T_{max} = 360 K) amines. However, the stability of surface carbamates formed on the different amines follows the reverse trend: tertiary < secondary < primary. This is because the primary and secondary amines can form carbamate anions, which exist in equilibrium with the corresponding carbamic acid species (Fig. 3.17). Such an equilibrium is not possible for carbamate anions formed on tertiary amines since there is no H-atom attached to

(a) CO_2 activation at primary amines:

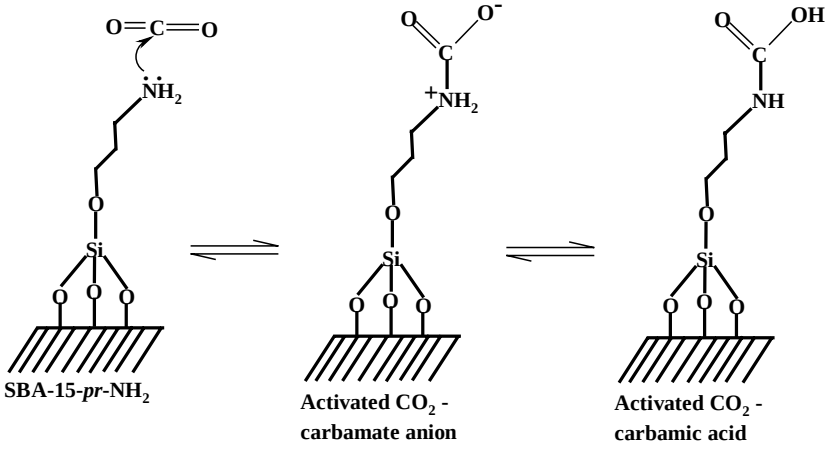

(b) CO_2 activation at secondary amines:

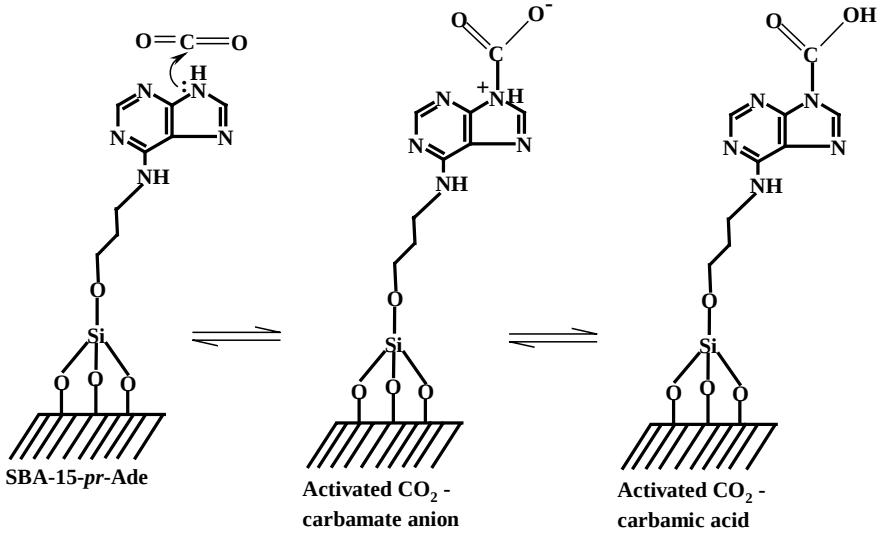

(c) CO_2 activation at tertiary amines:

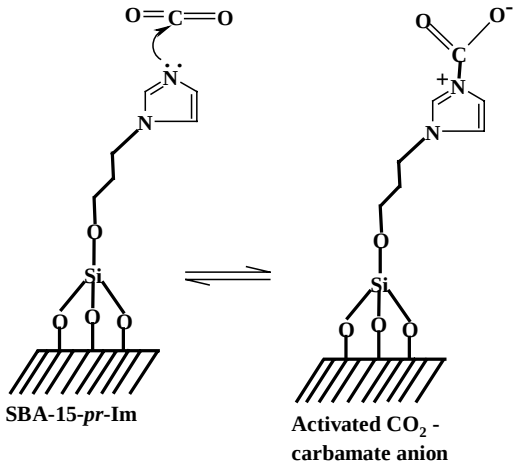

Fig. 3.17. CO_2 activation at primary, secondary and tertiary amines.

the tertiary N atom. Hence, the lifetime of a carbamate species formed on tertiary amines is relatively shorter. As a consequence, their IR peaks are not detected (see for example the IR spectrum of Im-functionalized materials) (Fig. 3.15 (i)).

3. The intensity of IR peaks due to various activated CO_2 species increased with CO_2 pressure (2 – 20 bar), As noted later (Fig. 3.15 (ii)) the catalytic activity also increased at a higher partial pressures of CO_2.
4. The IR peaks are more intense at lower temperatures due to the higher concentration of the adsorbed CO_2 and increased stability of the corresponding carbamate species at lower temperatures (Fig. 3.15 (iii)).
5. Solvents have a marked effect. The intensity of the IR peaks is higher in CH_2Cl_2 than in CH_3OH (Fig. 3.16). Distinct peaks are noticed in the spectrum of CO_2 adsorbed on Ti-SBA-15-pr-Ade in the presence of CH_3OH (Fig. 3.16 (a)). The peaks at 2948 and 2841 cm^{-1} are associated with molecularly adsorbed CH_3OH [31]. Those at 2921 and 2829 cm^{-1} are due to C-H stretching vibrations of the monodentate and bidentate methoxide groups. The peaks at 2975 and 2865 cm^{-1} (present also in CH_2Cl_2 and ECH pre-adsorbed samples) are due to C-H stretching vibrations of the bidentate formate species (Fig. 3.16 (b)). In the case of CH_3OH, new peaks are also observed at 1030 and 1054 cm^{-1} (Fig. 3.16 (c)) corresponding to the bending modes of the methoxide groups [31].
6. The intensity of the surface carbamate peaks (1609 and 1446 cm^{-1}, respectively) decreased on addition of epoxide (Fig. 3.18) due to formation of cyclic carbonates.

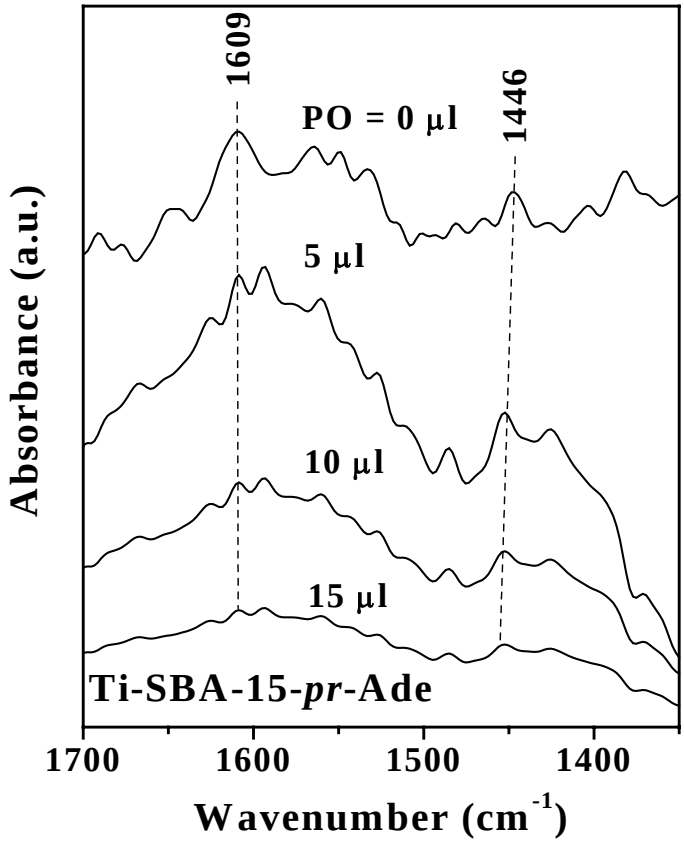

Fig 3.18. DRIFT spectra showing the spectral changes of activated CO_2 on Ti-SBA-15-*pr*-Ade upon contacting with propene oxide (PO).

3.3.4.4. Catalytic Activity

Cycloaddition of CO_2 to epoxides yielded cyclic carbonates as the main product, with the diol and ethers as minor products. Organo-functionalization of SBA-15 with propyl-adenine significantly enhanced the catalytic activity of SBA-15 (Table 3.11). Bare SBA-15, which was weakly active (ECH conversion = 1.5 mol%; in CH_3CN solvent) showed an ECH conversion of 62.3 mol% after adenine functionalization. The cyclic carbonate selectivity increased from 9 to 83.8 mol% (Table 3.11). The adenine-modified SBA-15 showed superior activity compared to other base (-NH_2, -Im and -Gua) modified materials. These results parallel the IR intensities of adsorbed CO_2 on these samples (Fig. 3.15).

An increase in the activity (ECH conversion increases from 1.5 to 16.8 mol%) and selectivity (from 9 to 87.5%) was observed also when SBA-15 was titanated (Table 3.11). The activity and selectivity was much higher when both Ti and adenine were present (Table 3.11). The catalytic activity increased with an increase in Ti content up to a Si/Ti value of 40 (Tables 3.11 and 3.12). Independent adsorption experiments (5% of ECH in CH_2Cl_2; at 298 K for 1 h) indicated that the adsorption of epoxide (ECH) on the catalyst surface increased upon titanation (ECH adsorption = 3.4 wt.% on SBA-15 and 13.4 wt.% on Ti-SBA-15). Hence, the role of Lewis acidic Ti^{4+} ions is to increase the surface concentration of epoxide molecules thereby enhancing the catalytic activity. Cyclic carbonate selectivity was much lower on "bare" SBA-15. Ti-SBA-15-*pr*-Ade was active for cycloaddition of CO_2 with a variety of epoxides of different sizes and structures (Table 3.11 and 3.12). Styrene oxide, for example, could be converted into styrene carbonate in high yields over these catalysts (epoxide conversion = 94% and cyclic carbonate selectivity = 94.6%; Table 3.12, entry no.22). The catalysts were reused (after filtration and drying at 353 K) in several recycling experiments (vide infra). No leaching of Ti or adenine into the reaction medium was observed.

In contrast to all the earlier catalysts including the commercial processes wherein a significant amount of solvent (dichloromethane) is used in the synthesis of cyclic carbonates, the present catalysts are highly active and selective even in the absence of any solvent and cocatalysts/promoters (Table 3.12).

The Mg/Al oxide-based catalyst system reported earlier, for example, required a high catalyst loading (1.8 g per g of substrate), substantial amounts of solvent (85% v/v DMF) and longer reaction times (24 h). Silica-supported guanidine catalysts required longer reaction times (70 h) and high CO_2 pressures (50 bar). In contrast, the adenine-functionalized Ti-SBA-15 system reported in the present study requires only 0.06 g of

Table 3.11. Cyclic carbonate synthesis over adenine-modified Ti-SBA-15 in CH_3CN solvent

Entry No.	Catalyst (Si/Ti)	Epoxide	Run time (h)	Epoxide conversion (%)	Cyclic carbonate selectivity (%)
1	SBA-15	Epichlorohydrin	4	1.5	9.0
2	SBA-15-*pr*-NH_2	Epichlorohydrin	4	36.7	89.7
3	SBA-15-*pr*-Ade	Epichlorohydrin	4	62.3	83.8
4	Ti-SBA-15 (40)	Epichlorohydrin	4	16.8	87.5
5	Ti-SBA-15-*pr*-NH_2 (40)	Epichlorohydrin	4	51.5	93.5
6	Ti-SBA-15-*pr*-Ade (40)	Epichlorohydrin	4	84.8	97.7
7	Ti-SBA-15-*pr*-Ade (68)	Epichlorohydrin	4	79.0	90.2
8	Ti-SBA-15-*pr*-Ade (104)	Epichlorohydrin	4	66.0	86.7
9	Ti-SBA-15-*pr*-Ade (40)	Propylene oxide	6	95.3	100.0
10	Ti-SBA-15-*pr*-Ade (40)	Styrene oxide	8	79.8	87.0

Reaction conditions: Catalyst, 100 mg in all the SBA-15 catalysts except in entry nos. 2 and 5 where 200 mg was used; epoxide, 18 mmol; solvent (CH_3CN), 10 cm^3; CO_2, 6.9 bar; temperature, 393 K.

Amine content: SBA-15-pr-NH_2 = 2.45 mmol/g catalyst; Ti-SBA-15-pr-NH_2 (40) = 2.2 mmol/g catalyst. Adenine content: SBA-15-pr-Ade = 1.29 mmol/g catalyst; Ti-SBA-15-pr-Ade (40) = 0.91 mmol/g catalyst; Ti-SBA-15-pr-Ade (68) = 0.95 mmol/g catalyst; Ti-SBA-15-pr-Ade (104) = 0.96 mmol/g catalyst.

Table 3.12. Cyclic carbonate synthesis over adenine-modified SBA-15 materials: Reactions with no solvent

Entry No.	Catalyst (Si/Ti or Al)	Epoxide	Run time (h)	Epoxide conversion (%)	Cyclic carbonate selectivity (%)
1	SBA-15	Epichlorohydrin	4	15.8	59.0
2	SBA-15-*pr*-NH_2	Epichlorohydrin	4	35.8	87.7
3	SBA-15-*pr*-Im	Epichlorohydrin	4	23.2	80.6
4	SBA-15-*pr*-Gua	Epichlorohydrin	4	69.0	85.8
5	SBA-15-*pr*-Ade	Epichlorohydrin	4	80.5	75.0
6	Ti-SBA-15 (40)	Epichlorohydrin	4	20.1	86.3
7	Ti-SBA-15 (68)	Epichlorohydrin	4	18.7	80.5
8	Ti-SBA-15 (104)	Epichlorohydrin	4	16.0	68.1
9	Al-SBA-15 (22)	Epichlorohydrin	4	22.1	92.2
10	Ti-SBA-15-*pr*-Cl (40)	Epichlorohydrin	4	19.1	96.4
11	Ti-SBA-15-*pr*-NH_2 (40)	Epichlorohydrin	4	50.5	88.7
12	Ti-SBA-15-*pr*-Im (40)	Epichlorohydrin	4	31.7	93.9
13	Ti-SBA-15-*pr*-Gua (40)	Epichlorohydrin	4	81.3	93.5
14	Ti-SBA-15-*pr*-Ade (40)	Epichlorohydrin	4	93.9	89.1
15	Al-SBA-15-*pr*-Ade (22)	Epichlorohydrin	4	98.1	89.1
16	Ti-SBA-15-*pr*-Ade (40)	Propylene oxide	6	89.2	91.7
17	SBA-15-*pr*-Im	Styrene oxide	8	18.7	95.5
18	SBA-15-*pr*-Gua	Styrene oxide	8	82.4	97.5
19	SBA-15-*pr*-Ade	Styrene oxide	8	86.4	97.2
20	Ti-SBA-15-*pr*-Im (40)	Styrene oxide	8	28.2	97.9
21	Ti-SBA-15-*pr*-Gua (40)	Styrene oxide	8	97.9	97.1
22	Ti-SBA-15-*pr*-Ade (40)	Styrene oxide	8	94.0	94.6
23	Al-SBA-15-*pr*-Ade (22)	Styrene oxide	8	98.4	97.9

Reaction conditions: catalyst, 100 mg in all the SBA-15 catalysts except in entry nos. 2 and 11 where 200 mg was used; epoxide, 18 mmol; solvent, nil; CO_2, 6.9 bar; temperature, 393 K. Amine content: SBA-15-pr-NH_2 = 2.45 mmol/g catalyst; Ti-SBA-15-pr-NH_2 (40) = 2.2 mmol/g catalyst. Adenine content: SBA-15-pr-Ade = 1.29 mmol/g catalyst; Ti-SBA-15-pr-Ade (40) = 0.91 mmol/g catalyst; Ti-SBA-15-pr-Ade (68) = 0.95 mmol/g catalyst; Ti-SBA-15-pr-Ade (104) = 0.96 mmol/g catalyst; Al-SBA-15-pr-Ade = 0.86 mmol/g catalyst. Guanine content: SBA-15-pr-Gua = 1.13 mmol/g catalyst; Ti-SBA-15-pr-Gua = 0. 97 mmol/g catalyst. Imidazole content: SBA-15-pr-Im = 2.30 mmol/g catalyst; Ti-SBA-15-pr-Im = 1.92 mmol/g catalyst.

catalyst per g of substrate; high cyclic carbonate yields are obtained in shorter contact times (4 h) and at mild reaction conditions (6.9 bar, 393 K). The intensity of the IR peak for activated CO_2 species (at 1609 cm^{-1}, carbamate anion) correlates with the cyclic carbonate yield (Fig. 3.19).

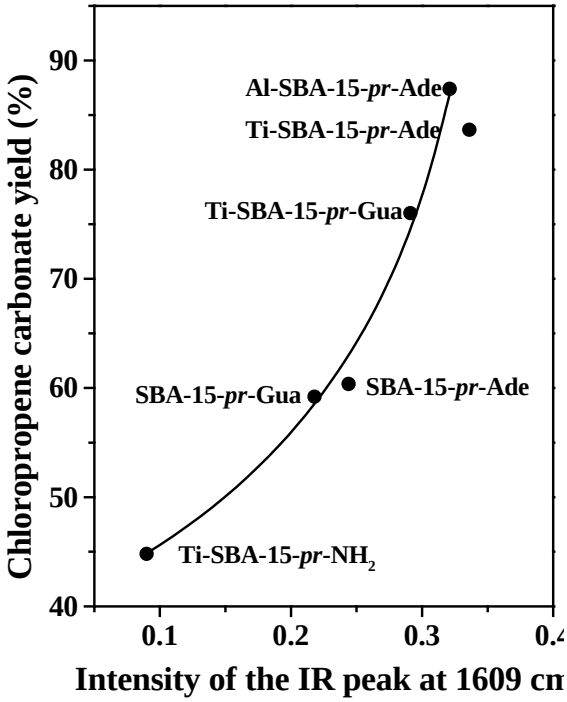

Fig. 3.19. Correlation between chloropropene carbonate yield (mol%) and intensity of IR peak at 1609 cm^{-1} due to activated CO_2.

Interestingly, a plot of CO_2 desorption temperature (T_{max}) versus chloropropene carbonate yield (mol%) shows a "volcanic plot" variation (Fig. 3.20). The plot reveals that SBA-15 samples containing tertiary and primary amines are less active than secondary amines in cyclic carbonates synthesis. There is hence, an optimal value in the binding of CO_2 to the active sites. Basic sites wherein CO_2 is held either weakly (tertiary N atoms) or too strongly (primary amines) are less active than those with an intermediate strength of binding of CO_2 (secondary amines).

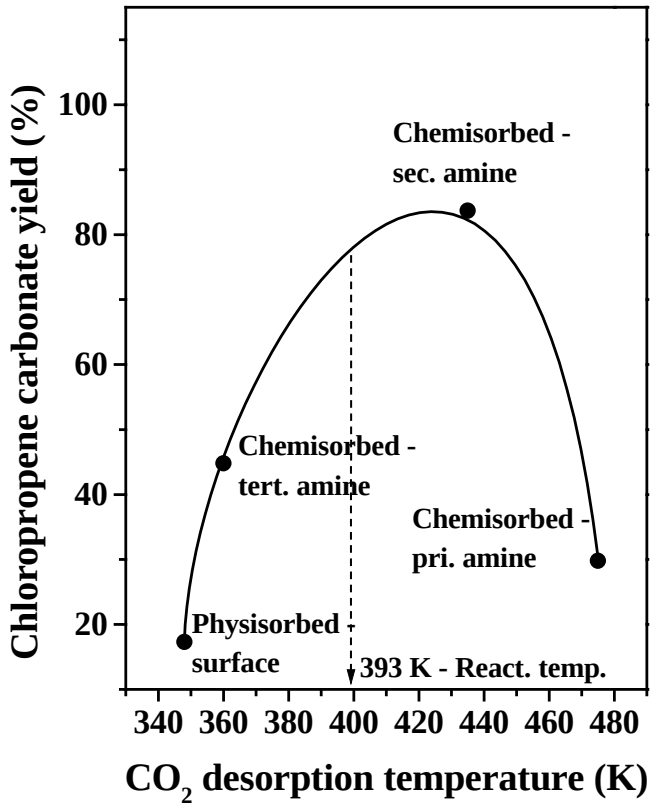

Fig.3.20. Correlation between chloropropene carbonate yield (mol%) and CO_2 desorption peak maximum (T_{max}) of SBA-15 samples functionalized with different amines.

When the reaction was carried out at 353 K, a very less conversion of ECH was observed. A sudden jump in the ECH conversion from 21% to 72% was observed when the temperature was increased from 373 K to 383 K. Optimum temperature for the reaction was found to be 393 K (Table 3.13). Similarly, reaction was greatly influenced by CO_2 pressure. An ECH conversion of 59% was observed when the reaction was conducted at low CO_2 pressures (1.6 bar). The optimum pressure for the reaction was found to be 6.9 – 10 bar (Table 3.13). Both epoxide conversion and carbonate yield

were higher at higher pressure (Fig. 3.21). Epoxide conversion correlated with the intensity of the IR peak at 1609 cm^{-1} (Figs. 3.19 and 3.21).

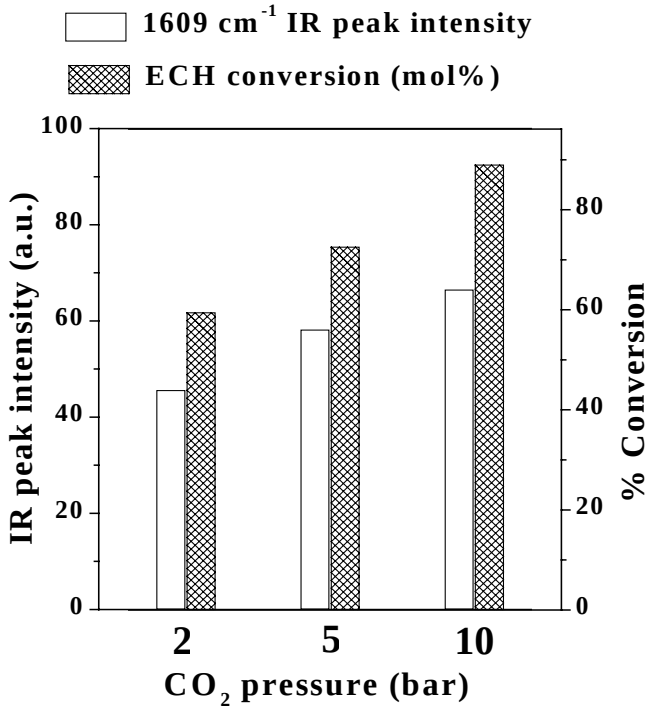

Fig.3.21. Correlation between IR peak (1609 cm^{-1}) intensity and epichlorohydrin (ECH) conversion over Ti-SBA-15-*pr*-Ade (Si/Ti = 40) at different CO_2 pressures.

Table 3.13. Influence of temperature and pressure on chloropropene carbonate synthesis

Temperature (K)	Pressure (psig)	Conversion (mol %)	Selectivity Cyclic carbonate (mol %)	Others
353	100	2.0	100.0	0
363	100	4.6	100.0	0
373	100	21.6	96.3	3.4
383	100	72.0	96.1	3.9
393	100	84.8	97.7	2.3
413	100	98.4	97.5	2.5
393	25	59.9	92.2	7.8
393	50	65.8	92.1	7.9
393	75	72.6	95.5	4.5
393	150	89.0	95.8	4.2
393	200	87.3	94.4	5.6
393	300	85.9	93.2	6.8

Reaction conditions: Epichlorohydrin, 18 mmol; Ti-SBA-15-*pr*-Ade, 100 mg; solvent, 10 ml; Run time, 4 h.

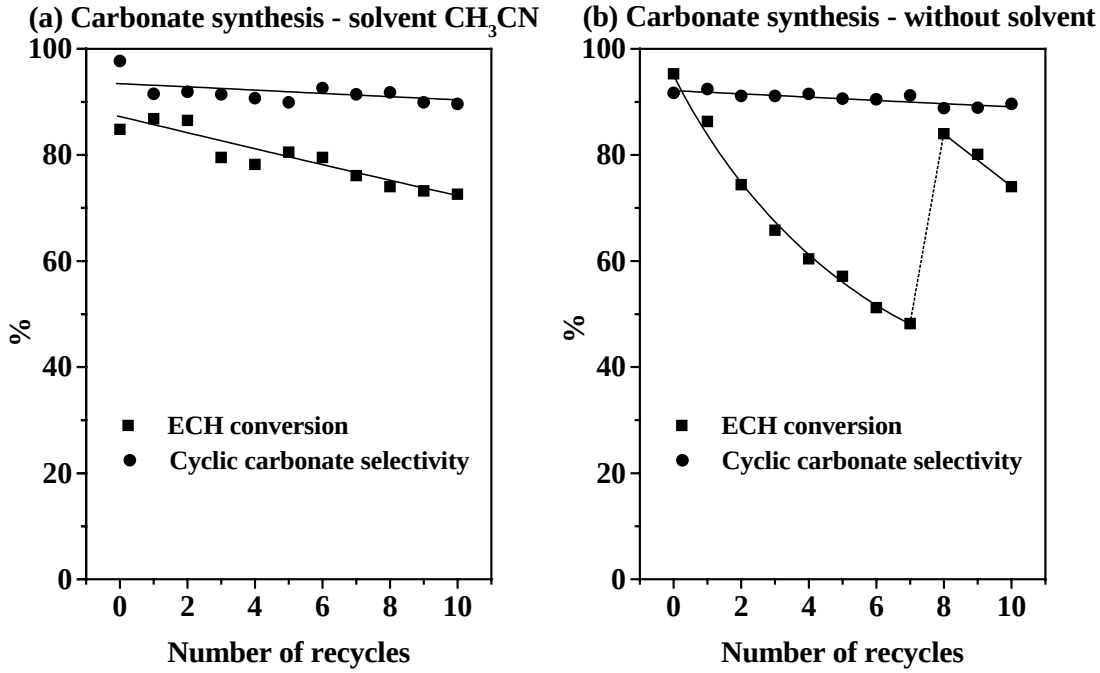

Fig. 3.22. Recycling study of Ti-SBA-15-pr-Ade in chloropropene carbonates synthesis

3.3.4.5. Catalyst Reusability

Even though the cycloaddition could be carried out in the absence of solvents over these catalysts with high conversions and selectivities (Table 3.12), the use of solvents prolonged the catalyst life significantly. When the cycloaddition was carried out in the presence of solvents, the catalysts could be reused (after filtration and drying at 353 K) in several recycling experiments without any significant loss in activity or selectivity (Fig. 3.22). However, when the same reactions were conducted in the absence of any solvent, a progressive decrease in catalytic activity (but not selectivity) was observed in successive runs as shown in Fig. 3.22. To explore the cause for this deactivation, the catalyst, after the 7th recycle experiment (conversion = 48.2 %) was washed first with acetonitrile and then with acetone and dried at 383 K for 1 h. The color of the catalyst, which was dark brown before this solvent extraction was almost

restored to its original off-white color. The dark brown extract contained some heavy products. In the subsequent cycloaddition (8^{th} recycle, Fig. 3.22), the conversion increased to 84.0%. One of the main roles of the solvents is, hence, to suppress the deposition of carbonaceous deposits on the catalyst surface. After the 10^{th} recycle experiment, the catalyst was analyzed for Ti and amine content. There was no change in the Ti content. However, there was a decrease in the amine content (about 11%, from 0.09 to 0.08 mmol of adenine/g of catalyst) compared to the fresh catalyst. These results indicate that the major cause of catalyst deactivation is not the leaching of Ti. The active site pore blocking by the residual carbonaceous matter is probably the reason.

3.3.5. Cyclic Carbonates Synthesis over Organic-Inorganic Hybrid Catalysts

As-synthesized zeolite-beta and MCM-41 are used as heterogeneous catalysts for the cycloaddition reaction of various epoxide to CO_2. Complete conversion of epoxides was achieved in 3 h. Propene oxide (PO), styrene oxide (SO) and n-butene-oxide (BO) required longer hours (5-8 h). The reaction could be conducted even in the absence of solvent but the cyclic carbonate selectivity was lower (85.3% for ECH, 97.5% for PO, and 92.8% for SO) (Table 3.14). Carbonate selectivity can be improved if the reaction was conducted in presence of solvent like DMF, CH_3CN and CH_2Cl_2. CH_3OH suppressed the selectivity of cyclic carbonate. When the organic template was removed by calcination, both the catalytic activity and selectivity for cyclic carbonates were drastically decreased (conversion = 13.6 mol%; selectivity = 68.7 % for zeolite-beta and conversion = 15.3 mol%; selectivity = 73.2 mol% for MCM-41). Adsorption of ECH was higher on as-synthesized form of zeolite-beta than on the calcined form. Also, CO_2 was activated in higher amounts (DRIFT spectroscopic study) on as-

synthesized catalysts than on the calcined catalysts. The more availability of activated reactant molecules could be the possible reason for superior activity of the as-synthesized form of zeolite-beta compared to the calcined zeolite-beta.

3.3.5.1. Catalyst Recyclability

The catalyst was recycled several times. After the reaction, the catalyst was separated by centrifugation, air-dried and reused without any further treatment. Zeolte-beta was recycled eight times with little loss in activity and carbonate yield (Fig 3.23). A comparison of the XRD profiles and FT-IR spectra of fresh and recycled catalysts (Figs. 3.24 and 3.25, respectively) reveals that the crystalline structure of zeolite beta is stable even after the 8th recycle. With as-synthesized MCM-41, the mesoporous structure collapsed after the 5th recycled (Fig 3.24).

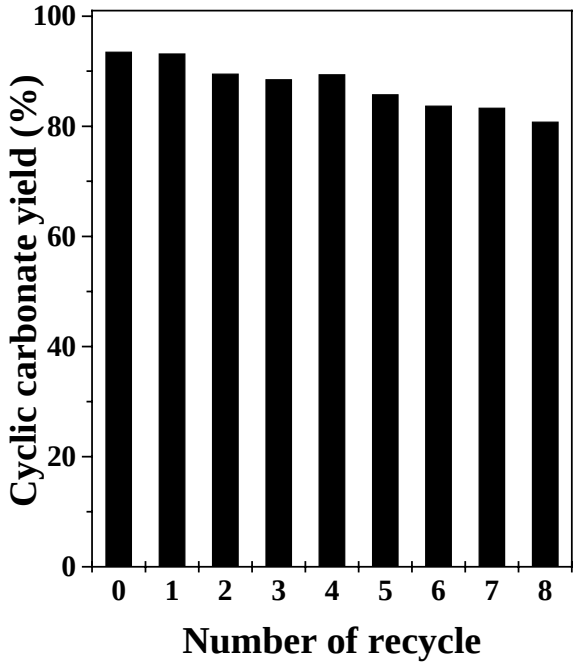

Fig. 3.23. Recyclaibility of zeolite-beta in chloropropene carbonate synthesis.

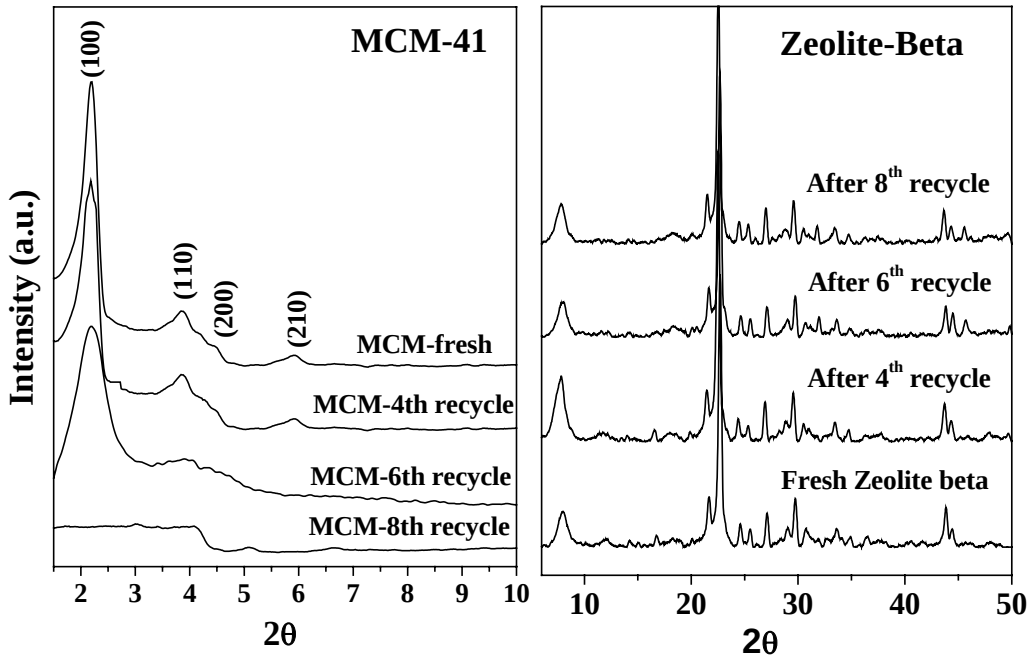

Fig. 3.24. XRD profiles of fresh and used MCM-41 and zeolite-beta catalysts.

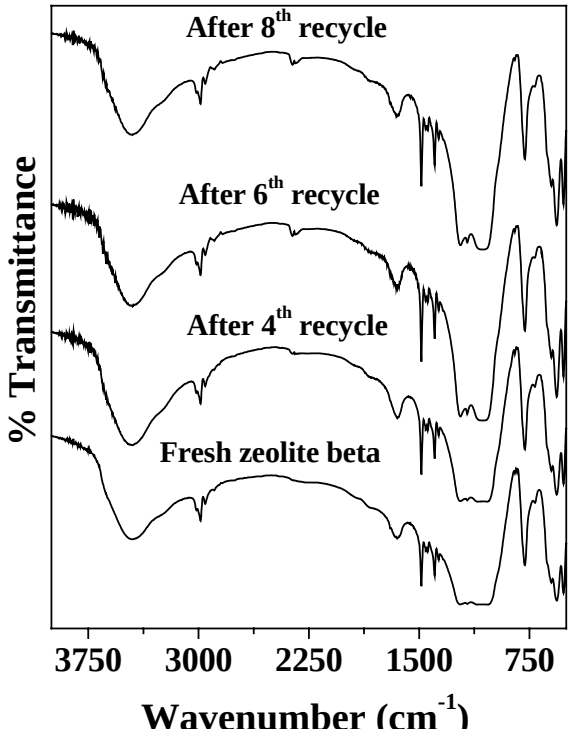

Fig. 3.25. FT-IR spectra of fresh and used zeolite-beta catalyst.

Table 3.15. Cycloaddition reaction of CO_2 with epoxides over zeolite-beta and MCM-41

Entry no	Epoxide	Solvent	Run time (h)	Zeolite beta			MCM-41		
				Epoxide Conv. (%)	Cyclic carboante Selc. (%)	TOF (h^{-1})	Epoxide Conv. (%)	Cyclic carboante Selc. (%)	TOF (h^{-1})
1	ECH	Nil	3	100	85.3	27	99.0	80.0	64
2	ECH	CH_3CN	3	99.6	93.9	27	98.6	89	64
3	ECH	CH_2Cl_2	3	99.4	89.7	27	99.6	83.2	64
4	ECH	CH_3OH	3	96.6	75.7	26	99.8	62.7	64
5	ECH	DMF	3	99.0	98.6	27	100	100	64
6	PO	Nil	5	88.5	97.5	14	91.9	93.7	36
7	PO	CH_3CN	5	100	100	16	90.1	100	35
8	SO	Nil	8	98.0	92.8	10	93.7	95.2	23
9	SO	CH_3CN	8	96.3	100	10	88.4	98.8	22
10	BO	CH_3CN	5	86.7	80.7	14	94.0	81.8	37

Reaction conditions: epichlohydrin (ECH, 18 mmol); catalyst, (150 mg for zeolite-beta and 50 mg for MCM-41); CH_3CN, 10 ml; CO_2 pressure, 6.9 bar; temperature, 393 K.

3.3.5.2. Reactions using Homogeneous Quaternary Ammonium Halide Catalysts

Quaternary ammonium halides are used as catalysts in the commercial synthetic process for cyclic carbonates [19]. Here, a comparative study of the homogeneous catalysts with the heterogeneous, as-synthesized zeolite beta and MCM-41 catalysts is made. Table 3.15 shows that the alkyl group and the counter anion of the quaternary ammonium salt markedly influence the catalytic activity. For different alkyl groups, catalytic activity increases in the following order: $Me_4N^+ < Et_4N^+ < Pr_4N^+ < Bu_4N^+ <$ cetyltrimethylammonium ion. With different halide ions, the activity varied in the order: $Bu_4NBr < Bu_4NI$. These salts are soluble in the reaction mixture and hence, special methods have to be adopted for their separation.

Table 3.16. Catalytic activity of quaternary ammonium salts in cycloaddition reactions

Catalyst	Conversion	Selectivity		TOF (h^{-1})
		Carbonate	Others	
Me_4NBr	19.8	97.8	2.2	12
Et_4NBr	47.8	99.1	0.9	29
Et_4NBr	40.5	95.5	4.5	25
Pr_4NBr	68.7	98.8	1.2	43
Bu_4NBr	74.1	100	0	46
Bu_4NI	91.5	99.1	0.9	57
Cetyltrimethyl ammonium bromide	84.5	99.1	0.9	52

Reaction conditions: epichlohydrin (ECH, 18 mmol); catalyst, 0.072 mmol; CH_3CN, 10 ml; CO_2 pressure, 6.9 bar; temperature, 393 K; runtime, 4 h.

In the case of as-synthesized zeolite beta, the catalyst could be separated by simple filtration. The as-synthesized zeolite beta contained Et_4N^+ ion as the template while the solid catalyst and the homogeneous quaternary ammonium salt are almost comparable. However, it may be noted that in the case of as-synthesized molecular sieve catalysts the reaction occurs only at the external surface, which is about 8-9% of the total surface area. The sites in the interior part of the zeolite-beta and MCM-41 are not assessable for the reaction. Thus the actual TOF for the solid catalysts is higher than the apparent value. The study reveals that the solid catalysts exhibit higher activity in addition to possessing the advantageous feature of catalyst reusability.

3.4. Conclusions

Cyclic carbonates have been prepared by the cycloaddition of CO_2 to epoxides. This method of carbonates synthesis is eco-friendly. In this study, the toxic phosgene usually used for the synthesis of carbonates is replaced by non-toxic CO_2. Catalytic activity of five different types of catalysts was evaluated. Both acid and base catalysts catalyze this reaction. The reaction is initiated by activation of epoxides at the acidic sites. CO_2 is activated at the basic sites. When both acidic and basic sites are available in the catalyst system, yields of cyclic carbonate were higher. Zeolite-encapsulated metal complexes (MPc-Y) showed enhanced activity compared to the corresponding "neat" complexes. This is because of the better dispersion of active sites and influence of zeolitic environment on the electronic structure of the encapsulated-metal complexes. While homogeneous complexes, zeolite-encapsulated metal complexes and titanosilicates required additional co-catalyst, DMAP, the reaction could be conducted with high efficiency over organo-fuctionalized Ti-/Al-SBA-15 and as-synthesized zeolite-beta and MCM-41 catalysts without using any additional co-catalyst. The latter are highly active even in the absence of solvents. The organo-functionalized SBA-15

catalysts used in this study are reusable and found to be the best among the heterogeneous catalysts reported so far for the cyclic carbonate synthesis. Activation of CO_2 was monitored by spectroscopy and TPD techniques. Ligand structure (in the case of metal complexes) and type of functionalized amine (primary, secondary and tertiary; in the case of organo-functionalized SBA-15) influence the mode of stability of CO_2 coordination. The study points out that a proper fine-tuning of acid-base properties enables highly efficient reusable catalysts. ^{1}H NMR spectra of representative cyclic carbonates isolated in this study are shown in Appendix-3.A.

3.5. References

1. A. Behr, Angew. Chem. Int. Ed. Engl. 27 (1988) 661.
2. B. Elvers, S. Hawkins, G. Schulz (Eds.), Ulmann's Encyclopedia of Industrial Chemistry A, vol. 21, fifth ed., VCH, Weinheim, Germany, 1992, p. 207.
3. E.J. Beckman, Science 283 (1999) 946.
4. Encyclopedia of Chemical Processing and Design, Executive Ed. J. J. McKetta and Associate Ed. W. A. Cunningham, Marcel Decker Inc., New York (1984), Vol. 20, p.177.
5. (a) S. Inoue, H. Koinuma, T. Tsuruta, Polymer Lett. 7 (1969) 287. (b) S. Inoue, CHEMTECH (1976) 588.
6. D. J. Darensbourg, M. W. Holtcamp, Coord. Chem. Rev. 153 (1996) 155.
7. A.-A. G. Shaikh, S. Sivaram, Chem. Rev. 96 (1996) 951.
8. R. L. Paddock, S. T. Nguyen, J. Am. Chem. Soc. 123 (2001) 11498.
9. T. Aida, M. Ishikawa, S. Inoue, Macromolecules 19 (1986) 8.
10. T. Nishikubo, A. Kameyama, J. Yamashita, M. Tomoi, W. Fukuda, J. Polym. Sci. Part A: Polym. Chem. 31 (1993) 939.
11. (a) T. Yano, H. Matsui, T. Koike, H. Ishiguro, H. Fujihara, M. Yoshihara, T. Maeshima, Chem. Commun. (1997) 1129. (b) B.M. Bhanage, S.-i. Fujita, Y. Ikushima, M. Arai, Appl. Catal. A: Gen. 219 (2001) 259.
12. K. Yamaguchi, K. Ebitani, T. Yoshida, H. Yoshida, K. Kaneda, J. Am. Chem. Soc. 121 (1999) 4526.
13. M. Aresta, A. Dibenedetto, L. Gianfrate, C. Pastore, Appl. Catal. A: Gen. 255

(2003) 5.

14. H. Yasuda, L.-N. He, T. Sakakura, J. Catal. 209 (2002) 547.
15. (a) M. Tu, R.J. Davis, J. Catal. 199 (2001) 85. (b) E.J. Doskocil, S.V. Bordawekar, B.G. Kaye, R.J. Davis, J. Phys. Chem.B 103 (1999) 6277.
16. H.S. Kim, J.J. Kim, H.N. Kwon, M.J. Chung, B.G. Lee, H.G. Jang, J. Catal. 205 (2002) 226.
17. A. Barbarini, R. Maggi, A. Mazzacani, G. Mori, G. Sartori, R. Sartorio, Tetrahedron Lett. 44 (2003) 2931.
18. (a) X.-B. Lu, Y.-J. Zhang, K. Jin, L.-M. Luo, H.Wang, J. Catal. 227 (2004) (b) X.-B. Lu, H. Wang, R. He, J. Mol. Catal. 186 (2002) 33.
19. S. Fukuoka, M. Kawamura, K. Komiya, M. Tojo, H. Hachiya, K. Hasegawa, M. Aminaka, H. Okamoto, I. Fukawa, S. Konno, Green Chem. 5 (2003) 497.
20. E. Fujita, C. Creutz, N. Sutin, B.S. Brunschwig, Inorg. Chem. 32 1993) 2657.
21. S. Gambarotta, F. Arena, C. Floriani, P.F. Zanazzi, J. Am. Chem. Soc. 104 (1982) 5082.
22. G.A. Ozin, H. Huber, D. McIntosh, Inorg. Chem. 17 (1978) 1472.
23. B.J. Hathaway, in: G. Wilkinson, R.D. Gillard, J.A. McCleverty (Eds.), Comprehensive Coordination Chemistry, 5, Pergamon press, Oxford, 1987, p. 558, Chapter 53.
24. K.B. Hansen, J.L. Leighton, E.N. Jacobsen, J. Am. Chem. Soc. 118 (1996) 10924.
25. H. Kawanami, A. Sasaki, K. Matsui, Y. Ikushima, Chem. Commun. (2003) 896.
26. B. Notari, Adv. Catal. 41 (1996) 253.
27. M. Aresta and A. Dibenedetto, J. Mol. Catal. A: Chem. 182-183 (2002) 399.
28. F. Solymosi, H. Knözinger, J. Catal. 122 (1990) 166.
29. K. Tomishige, Y. Ikeda, T. Sakaihori, K. Fujimoto, J. Catal. 192 (2000) 355.
30. A.C.C. Chang, S.S.C. Chuang, M.Gray, Y. Soong, Engery & Fuels 17 (2003) 468.
31. K.T. Jung, A.T. Bell, J. Catal. 204 (2001) 339.

Appendix-3.A

^{1}H NMR spectra (Bruker Avance 200 MHz, in $CDCl_3$) of chloropropene carbonate (top), propene carbonate (middle) and styrene carbonate (bottom) synthesized using CO_2.

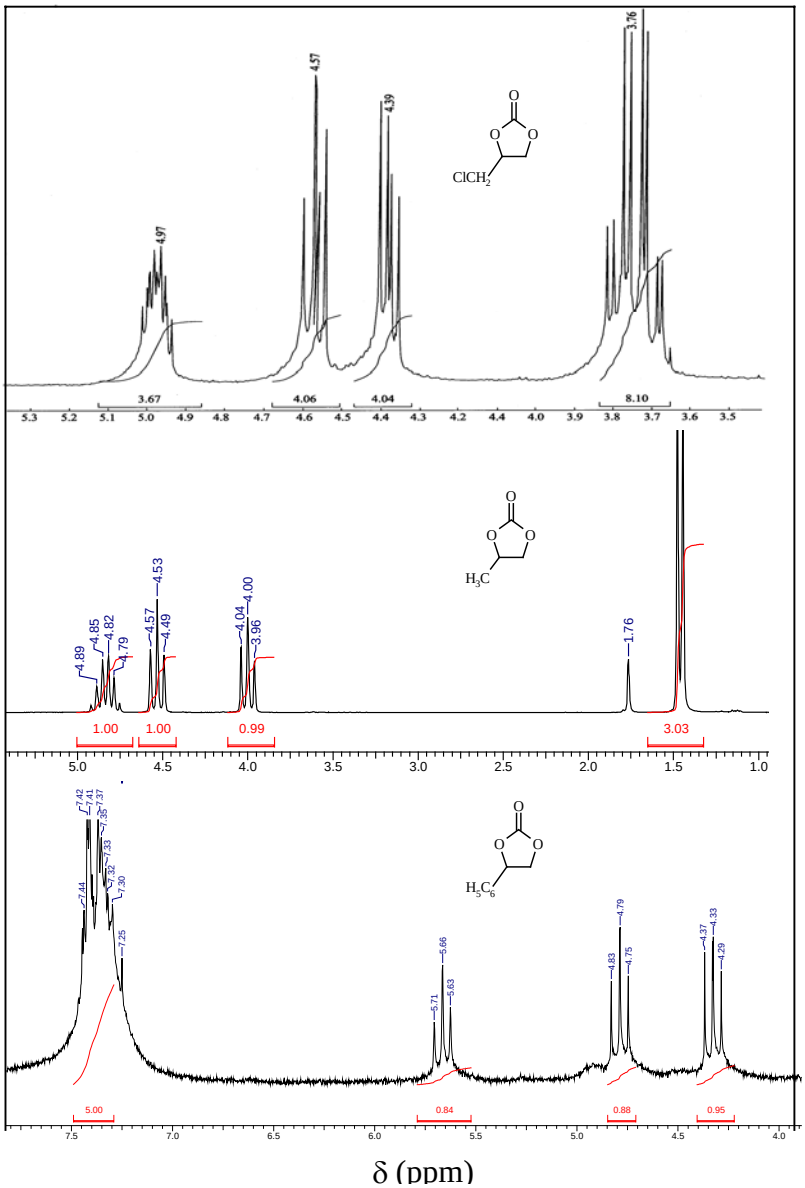

Chapter-4

Activation and Utilization of CO_2 in Alkyl and Aryl Carbamates Synthesis

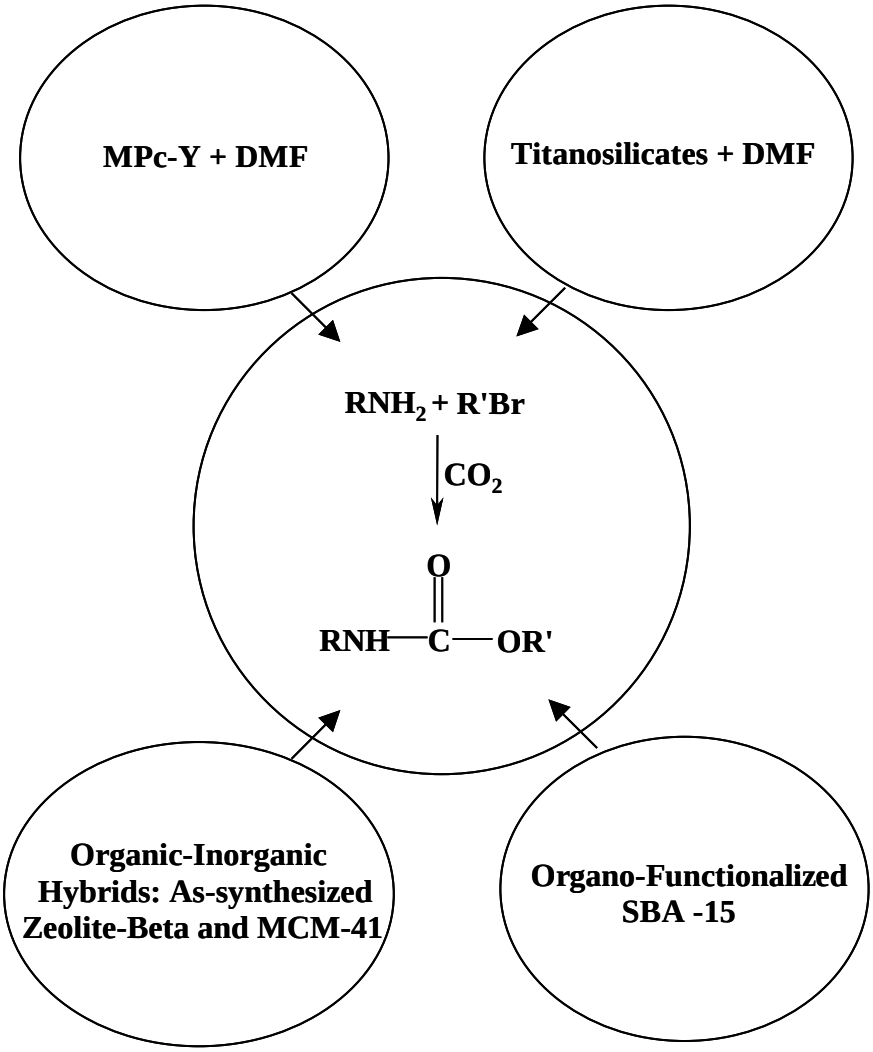

4.1. Introduction

Organic carbamates represent an important class of compounds, largely employed in pharmacology (medical drugs) [1], agriculture (pesticides, fungicides, herbicides) [2], polymer industry (in the synthesis of polyurethanes) [3], and chemical industry. Their use as protective groups for the amine function of amino acids in peptide chemistry is also well known [4]. Several methods have been developed to replace the classical synthesis, which involves the direct reaction of alcohols with phosgene or its derivative isocyanates, with new, non-toxic and less hazardous methodologies. Most of the alternative, non-phosgene routes to carbamates synthesis like reductive carbonylation (with expensive platinum group metal catalysts) [5], oxidative carbonylation [6], and methoxycarbonylation of amines [7] (involves separation of methanol-DMC azeotrope, an expensive operation) all have significant disadvantages. The coupling reaction of primary amines, CO_2, and alkyl halides is a benign route to carbamates synthesis.

The direct incorporation of carbon dioxide into amines, which leads to ionic carbamates, can be mediated by both metal and non-metal species. These compounds behave as bidentate ions and in the presence of alkylating agents, reaction of O-alkylation (formation of carbamic esters) and N-alkylation are both theoretically possible. A variety of catalysts such as onium salts, basic catalysts, sterically hindered organic bases, crown ethers and solid cesium carbonates [8-10] have been known to form selective carbamate products. However, due to their low activity, very large quantity of such catalysts have to be used at long reaction times (24 h). Hence, there still exists a need for efficient, solid catalysts for the phosgene-free synthesis of carbamates.

In this chapter four types of solid catalysts: (1) titanosilicates (2) zeolite-Y-encapsulated metal phthalocyanines (3) organo-functionalized, ordered mesoporous materials and (4) organic-inorganic hybrids have been investigated for their activity in the synthesis of a variety of alkyl and aryl carbamates. The carbamates are synthesized in high yields under mild reaction conditions (273 – 353 K; 1 – 3.4 bar) using these catalyst systems.

4.2. Experimental Section

4.2.1. Carbamates Synthesis – Reaction Procedure

In a typical reaction, an amine (2 mmol), alkyl halide (n-butyl bromide or chloride; 1–6 mmol), solvent (CH_3OH, CH_3CN, N,N-dimethyl formamide (DMF), N,N-dimethyl acetamide (DMA) or N-methyl-2-pyrolidone (NMP); 10 g) and catalyst were charged into a 300 ml stainless steel Parr reactor. In some cases, reactions were conducted in the absence of solvent. The reactor was then pressurized with CO_2 (1 - 10 bar). Temperature was raised to a desired value (323–353 K) and reactions were conducted for a specified period of time. The reactor was then cooled to 298 K and unutilized CO_2 was vented out. The catalyst was recovered from the reaction mixture by filtration.

When reaction was conducted in a solvent like DMF, DMA and NMP, the filtrate was poured into water (30 ml) and extracted with ethyl acetate (30 ml, 3 times). The organic layer was washed with water (30 ml, 2 times) and brine (30 ml) and dried over anhydrous sodium sulfate. The solvent was evaporated.

The products were analyzed by thin layer chromatography (TLC) and gas chromatography (Shimadzu 14B GC; SE-52 packed column (6-feet long · 1.25-mm i.d.)). They were characterized and identified by GC-MS (Shimadzu QP-5000 (30-m long 0.25-mm i.d.)), FT-IR (Shimadzu 8201 PC spectrophotometer) and ^1H NMR

(Bruker AC 200) spectroscopies. In some cases, the products were isolated by column chromatography (silica gel 60–120 mesh; 98:2 petroleum ether: ethyl acetate mixture as eluent) and yields were estimated.

Experiments were also performed without any solvent. A range of carbamates were synthesized and characterized in a similar manner as described above.

Spectral Characteristics of Products

Butyl N-phenyl carbamate – IR (cm^{-1}): $\nu_{N-H,}$ 3392, $\nu_{C=O}$, 1728, 1242, ν_{Bu-O}, 1040; ^1H NMR ($CDCl_3$), δ(ppm): 7.3 (2H, m), 6.3 (3H, m) 3.5 (2H, t), 1.75 (2H, m), 1.5 (2H, m); 0.9 (3H, t).

N,N-dibutyl aniline – IR (cm^{-1}): $\nu_{(Bu)C-N-C(Bu),}$ 921 and 652 bending/deformation; ^1H NMR ($CDCl_3$), δ(ppm): 6.7 (2H, m), 6.3 (3H, m) 2.7 (4H, t), 1.3 (4H, m), 0.9 (4H, m); 0.6 (6H, t).

4.3. Results and Discussion

4.3.1. Carbamates synthesis over Titanosilicate Molecular Sieves

The coupling reaction of aniline, CO_2 and n-butyl halide yielded two products, butyl-N-phenyl carbamate as the major product and N,N-dibutylaniline (N-alkylation) as the minor product . Butyl-N-phenyl carbamate was confirmed by FT-IR peaks at 3053 and 3392 cm^{-1} due to N–H stretching vibration, 1728 and 1242 cm^{-1} due to anti-symmetric and symmetric O=C-O vibrations and 1040 cm^{-1} due to Bu–O stretching vibration, respectively. N,N-dibutylaniline was characterized by peaks at 921 and 652 cm^{-1} due to (Bu)C-N-C(Bu) bending/deformations. ^1H NMR further confirmed the structure.

Even though the reaction proceeds in the absence of a catalyst, aniline conversion is lower (26.2% in DMF, 5.9% in CH_3OH and 3.9% in CH_3CN; higher conversion in DMF is probably due to higher solubility of CO_2 in this solvent.) (Tables

4.1 and 4.2). With aniline as substrate, no marked difference in catalytic activity was observed over different titanosilicate catalysts (Table 4.1; Run nos. 2–5). Solvents influence, significantly, the catalytic activity and product selectivity (Table 4.2); aniline conversion over TS-1 catalyst increases in the order: CH_3CN (44.6%) < CH_3OH (45.5%) < DMF (95.8 wt%). Carbamate selectivity is, however, lower in DMF (59.4%) than in CH_3CN and CH_3OH (~90%). The reaction occurs even in the absence of any solvent but N,N-dibutylaniline (N-alkylated product) is formed in higher amounts (64%) than the carbamate (36%). While conversion increased with temperature, selectivity to the carbamate decreased (88–59.4%) (Table 4.2). Carbamate selectivity decreased also at high alkyl halide concentrations (Table 4.3). High carbamate yields are obtained at low alkyl halide concentration (n-BuBr/aniline = 0.5 mol/mol), in the DMF solvent and at temperatures in the range 343–353 K.

Table 4.1. Synthesis of butyl-N-phenyl carbamates over titanosilicate molecular sieves

Run no.	Catalyst	Si/Ti	Aniline conversion (mol %)	Product selectivity (mol %)		TOF (h^{-1})
				Butyl-N-phenyl carbamate	N,N-dibutyl-aniline	
1	Nil	-	26.2	96.8	3.2	-
2	TS-1	36	81.6	82.9	17.1	12
3	Ti-MCM-41	46	63.1	85.6	14.1	12
4	Ti-SBA-15	40	78.1	82.5	17.5	10
5	Amorph. TiO_2-SiO_2	37	74.4	82.4	17.6	11

Reaction conditions: Aniline, 2 mmol; n-BuBr, 2 mmol; CO_2, 3.4 bar; DMF, 10 g; atalyst, 100 mg; temperature, 353 K; run time, 3 h.

Table 4.2. Influence of temperature and solvent on the synthesis of butyl-N-phenyl carbamates over TS-1

Run no.	Temp. (K)	Solvent	Aniline conversion (mol %)	Product selectivity (mol %)		TOF (h^{-1})
				Butyl-N-phenyl carbamates	N,N–dibutyl-aniline	
1	353	CH_3CN	44.6	89.2	10.8	6
2[a]	353	CH_3CN	3.9	100	0	-
3	353	CH_3OH	45.5	89.7	10.3	6
4[a]	353	CH_3OH	5.9	96.0	4.0	-
5	353	DMF	95.8	59.4	40.6	14
6[a]	353	DMF	26.2	96.8	3.2	-
7	343	DMF	80.6	76.9	23.1	12
8	333	DMF	70.1	88.0	12.0	10
9	323	DMF	47.0	88.0	12.0	7
10	353	No solvent	89.4	36.0	64.0	13

Reaction conditions: Aniline, 2 mmol; n-BuBr, 2 mmol; CO_2, 3.4 bar; DMF, 10 g; TS-1, 100 mg; temperature, 353 K; run time, 3 h.

[a]runs 2,4 and 6 were performed with no catalyst.

A broad range of amines could be converted to carbamates by this method (Table 4.4). Carbamate yields decreased in the order: n-dodecylamine (89.5%) > aniline (89.3%) > hexylamine (86.4%) > benzylamine (63.4%) > cyclohexylamine (58.5%) > 2,4,6-trimethylaniline (54.7%) > cyclododecylamine (8.1%). In the case of bulky substrates like 2,4,6-trimethylaniline and cyclododecylamine, the mesoporous Ti-SBA-15 was more active than the medium-pore TS-1 (Table 4.4). Ti in titanosilicate molecular sieves is Lewis acid in nature. The amines molecules get activated by the Ti

and react further with CO_2 to form carbamate anions. This carbamate anion readily reacts with alkyl halides yielding the corresponding carbamates.

Table 4.3. Influence of alkyl halide concentration on catalytic activity

Run no.	Concentration of n-BuBr (mmol)	Aniline conversion (mol %)	Product selectivity (mol %)		TOF (h^{-1})
			Butyl-N-phenyl carbamate	N,N-dibutyl-aniline	
1	1.0	46.5	96.0	4.0	7
2	1.5	53.0	92.3	7.7	8
3	2.0	81.6	82.9	17.1	12
4	3.0	82.4	78.2	21.8	12
5	4.0	91.4	77.7	22.3	13
6	6.0	95.8	59.4	40.6	14

Reaction conditions: Aniline, 2 mmol; CO_2, 3.4 bar; DMF, 10 g; TS-1, 100 mg; temperature, 353 K; run time, 3 h.

4.3.2. Carbamate Synthesis over MPc-Y

The catalytic activity of "neat" CuPc and zeolite-Y encapsulated MPc-Y (Fig. 4.1) were investigated for butyl-N-phenyl carbamates synthesis from aniline, n-BuBr and CO_2. The intrinsic activity (TOF) decreased in the order: CuPc-Y (107) > NiPc-Y (96) > ''neat'' CuPc (85) > CoPc-Y (65). The MPc-Y catalysts could be easily separated and recycled with negligible loss in activity (Table 4.5). The superior activity of the CuPc-Y compared to the ''neat'' CuPc complex is attributed to the geometric distortion of the isolated MPc molecules in the supercages of zeolite-Y and consequent electronic change (Fig. 4.1) [11].

Table 4.4. Carbamate synthesis-Influence of substrate

Amine	Titanosilicate	Alkyl halide	Amine conversion (mol%)	Product selectivity (mol %)		Carbamate yield %	TOF (h^{-1})
				Carbamate	N-alkylated product		
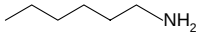	TS-1	n-BuBr	91.4	94.5	5.5	86.4	13
	TS-1	n-BuCl	83.0	96.4	3.6	80.0	12
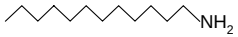	TS-1	n-BuBr	92.8	96.5	3.5	89.5	13
	TS-1	n-BuCl	78.4	95.2	4.8	74.6	11
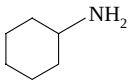	TS-1	n-BuBr	63.2	92.5	7.5	58.5	9
	TS-1	n-BuCl	53.8	96.4	3.6	51.9	8
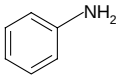	TS-1	n-BuBr	93.0 (94.2)[a]	96.0 (96.1)[a]	4.0 (3.9)[a]	89.3 (90.5)[a]	13 (13)[a]
	TS-1	n-BuCl	81.4	96.7	3.3	78.7	12
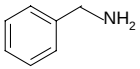	TS-1	n-BuBr	66.6	95.2	4.8	63.4	10
	TS-1	n-BuCl	60.4	87.6	12.4	52.9	9
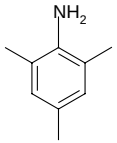	TS-1	n-BuBr	56.0	97.8	2.2	54.7	8
	Ti-SBA-15	n-BuCl	76.0	97.1	2.9	73.8	9
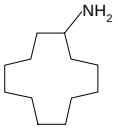	TS-1	n-BuBr	8.6	93.8	6.2	8.1	1
	Ti-SBA-15	n-BuCl	27.4	88.4	11.6	24.2	3

Reaction conditions: Amine, 2 mmol; n-BuX, 1 mmol; catalyst, 100 mg; DMF, 10 g; CO_2, 3.4 bar; temperature, 353 K; run time, 3 h.

[a] Value in parenthesis are those obtained on 3rd recycle of the catalyst.

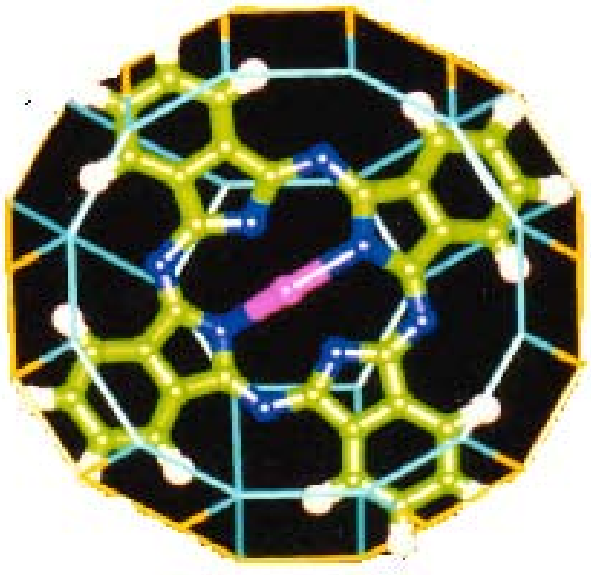

Fig. 4.1. MPc-Y encapsulated in zeolite-Y.

Table 4.5. Synthesis of butyl-N-phenyl carbamate over MPc-Y catalysts

Run no.	MPc-Y	Aniline conversion (mol %)	Product selectivity (mol %)		TOF (h^{-1})
			Butyl-N-phenyl carbamates	N,N-dibutyl-aniline	
1	CuPc-Y	86.1	79.6	20.4	107
2	CuPc-Y[a]	59.4	92.6	7.4	74
3	NiPc-Y	83.3	78.7	21.3	96
4	CoPc-Y	89.2	74.8	25.2	65
5	CoPc-Y-I[b]	91.5	70.2	29.8	67
6	CoPc-Y-II[c]	92.9	69.8	30.2	68
7.	CuPc-"neat"	93.1	71.0	29.0	85

Reaction conditions: Aniline, 2 mmol; n-BuBr, 6 mmol; CO_2, 3.4 bar; DMF, 10 g; catalyst, 83 mg and 0.0072 mol for CuPc-"neat"; temperature, 353 K; run time, 3 h.
[a] n-BuBr 2 mmol instead of 6 mmol was used. [b] Ist recycle, [c] 2nd recycle.

High carbamate selectivity (92%) could be achieved when lower amounts of alkyl halides are used (Table 4.5). The carbamate yields in different solvents over CuPc-Y decreased in the order: N-methyl-2-pyrolidone (NMP) > N,N-dimethylacetamide (DMA) > N,N-dimethylformamide (DMF) > CH_3OH > CH_3CN

(Table 4.6). A tentative reaction mechanism for carbamate synthesis over MPc catalysts is shown in Scheme 4.1.

Table 4.6. Influence of solvent on the synthesis of butyl-N-phenyl carbamate over CuPc-Y catalyst

Run no.	MPc-Y	Aniline conversion (mol %)	Product selectivity (mol %)	
			Butyl-N-phenyl carbamates	N,N-dibutylaniline
1	No solvent	99.1	41.4	58.6
2	CH_3CN	46.0	92.4	7.6
3	CH_3OH	61.6	85.4	14.6
4	DMF	93.6	80.0	20.0
6	NMP	98.2	64.0	36.0
7.	DMA	94.4	64.1	35.9

Reaction conditions: Aniline, 2 mmol; n-BuBr, 6 mmol; CO_2, 3.4 bar; DMF, 10 g; CuPc-Y, 83 mg; temperature, 353 K; run time, 3 h.

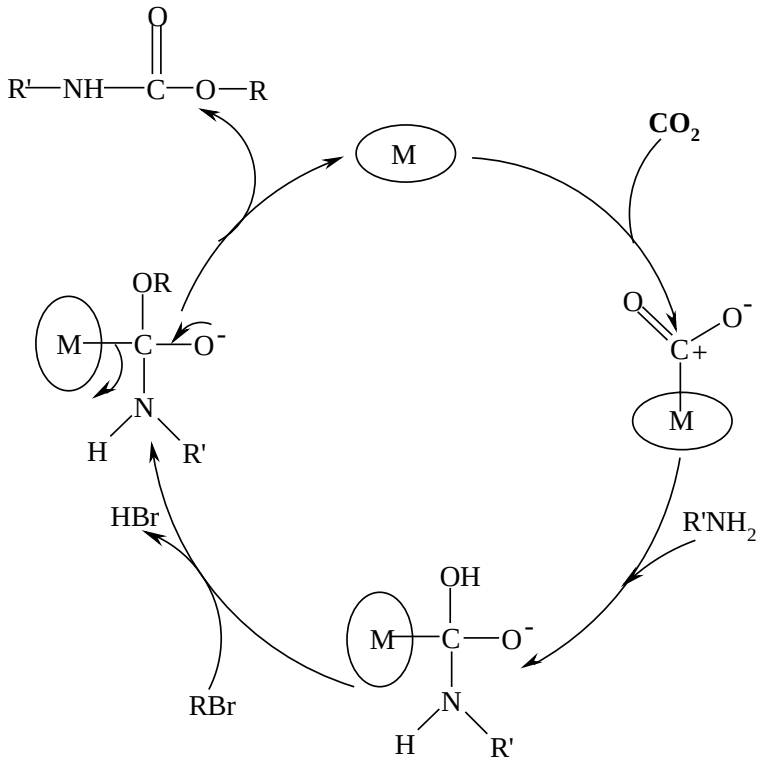

Scheme 4.1. Carbamate synthesis over MPc-Y catalysts.

4.3.3. Carbamates synthesis over Organo-Functionalized, Ordered Mesoporous Materials

In case of zeolite-encapsulated metal phthalocyanines and titanosilicates use of a basic solvent is essential for high carbamate yields. DMF enables the availability of CO_2 in the liquid phase and even, perhaps, keeps CO_2 in its activated state. The metal ions activate amine molecules. Carbamates synthesis would be more efficient when both the acidic and basic active functionalities are present in the catalyst system. This hypothesis is investigated in this section using organo-functionalized Ti-SBA-15 catalysts. Using these, novel, hybrid catalysts the reaction can be conducted even in the absence of solvent. Various alkyl and aryl carbamates were synthesized, under mild conditions, by a reaction of amines, CO_2, and n-butyl bromide (Table 4.7).

Butyl-N-phenyl carbamate is the major product and N,N-dibutylamine (N-alkylation) is the minor product. Both aliphatic and aromatic amines could be converted into their corresponding carbamates. Aliphatic amines could be more easily converted. The carbamate yields decreased in the order octylamine > hexylamine > cyclohexylamine > benzylamine > aniline > 2,4,6 trimethylaniline (Table 4.7). With most of the hitherto known catalyst systems, the reaction occurs in the presence of a solvent like DMF. In the absence of solvents, the N-alkylated compound was the main product. Interestingly, over Ti-SBA-15-*pr*-Ade, carbamate product could be obtained in high selectivity (84–95%), even without any solvent (Table 4.7). SBA-15 alone is only weakly active (Table 4.7, entry no. 1). The catalytic activity enhanced upon titanation (see entry nos. 5–7). A slight enhancement in activity was observed upon adenine functionalization (see entry no. 3). When both Ti and adenine were present, the catalytic activity was much higher, and complete conversion of amine (aniline) was observed (see entry no. 10). Similar conversions could be achieved even on SBA-15-

pr-Ade but at longer hours (10 h instead of 4 h) (compare entry nos. 3 and 4). When both Ti and adenine were present (Ti-SBA-15-*pr*-Ade), there was a synergistic effect that significantly enhanced the conversion (see entry nos. 3, 5, and 10, 13). Substrate (aniline) conversion increases with a decrease in Si/Ti ratio up to a value of 40. The adenine-modified Ti-SBA-15 showed superior activity compared to the propyl amine and propyl chloride catalysts (compare entry nos. 8–10).

Fig. 4.2 shows the efficiency of the Ti-SBA-15-*pr*-Ade catalyst system for carbamate synthesis from aniline, CO_2, and n-butyl bromide in three recycling experiments. Deposition of carbonaceous matter is also likely the cause for catalyst deactivation.

As revealed by Table 4.7, both the titanium ions (weak Lewis acid sites) and the amine moieties (the basic sites) are necessary for maximum catalytic activity and selectivity. Attempt to quantify the relationship between the concentration of these sites and conversion by calculating turnover frequency (TOF) values were made. Even though the calculation of TOF values is not unambiguous in this case, where the "active sites" comprise two structurally different surface species (acidic Ti ions and basic amine moieties) and the rate-determining step is not known with certainty, such values can be of use in determining the relative importance of the two sites and, thereby, lead to the design of superior catalysts. Table 4.8 presents TOF values per acid site (moles of substrate converted per mole of NH_3 desorbed per hour) or per basic site (moles of substrate converted per mole of CO_2 desorbed per hour). Samples that contain the more basic adenine molecule and those that contain both Ti and adenine molecule have higher intrinsic catalytic activity. It should be born in mind that the TOFs in Table 4.8 are the *minimum* values, since many of the sites, from which CO_2 or NH_3 desorb, may not participate in the catalytic reaction. Aniline adsorption studies on different catalyst

Table 4.7. Carbamate synthesis over adenine-modified SBA-15 in the absence of solvent

Entry No.	Catalyst (Si/Ti)	Amines	Run time (h)	Amine conversion (%)	Product selectivity (%)	
					Carbamate	N,N-Dialkylation
1	SBA-15	Aniline	4	16.5	81.1	18.9
2	SBA-15-*pr*-NH_2	Aniline	4	20.0	94.8	5.2
3	SBA-15-*pr*-Ade	Aniline	4	44.2	87.3	12.7
4	SBA-15-*pr*-Ade	Aniline	10	99.4	77.9	22.1
5	Ti-SBA-15 (40)	Aniline	4	48.1	79.1	20.9
6	Ti-SBA-15 (68)	Aniline	4	32.9	78.2	21.8
7	Ti-SBA-15 (104)	Aniline	4	26.5	79.3	20.7
8	Ti-SBA-15-*pr*-Cl (40)	Aniline	4	51.2	83.2	16.8
9	Ti-SBA-15-*pr*-NH_2 (40)	Aniline	4	61.6	69.1	30.9
10	Ti-SBA-15-*pr*-Ade (40)	Aniline	4	100	89.0	11.0
11	Ti-SBA-15 (40)	2,4,6-trimethylaniline	4	21.8	87.4	12.6
12	SBA-15-*pr*-Ade	2,4,6-trimethylaniline	4	32.5	93.5	6.5
13	Ti-SBA-15-*pr*-Ade (40)	2,4,6-trimethylaniline	4	74.5	87.8	12.4
14	SBA-15-*pr*-Ade	Benzylamine	4	62.0	98.0	2.0
15	Ti-SBA-15-*pr*-Ade (40)	Benzylamine	4	88.6	92.8	7.2
16	SBA-15-*pr*-Ade	Cyclohexylamine	4	91.0	83.5	16.5
17	SBA-15-*pr*-Ade	Hexylamine	4	96.5	88.0	12.0
18	SBA-15-*pr*-Ade	Octylamine	4	98.8	93.5	6.5

Reaction conditions: catalyst, 100 mg; amine, 10 mmol; n-butyl bromide, 12 mmol; CO_2, 3.4 bar; solvent, nil; temperature, 353 K.
Amine content: SBA-15-*pr*-NH_2 = 2.45 mmol/g catalyst; Ti-SBA-15-*pr*-NH_2 (40) = 2.2 mmol/g catalyst. Adenine content: SBA-15-*pr*-Ade = 1.29 mmol/g catalyst; Ti-SBA-15-*pr*-Ade (40) = 0.91 mmol/g catalyst; Ti-SBA-15-*pr*-Ade (68) = 0.95 mmol/g catalyst; Ti-SBA-15-*pr*-Ade (104) = 0.96 mmol/g catalyst.

supports have also been studied. The study reveals that aniline adsorption is higher when Ti (Lewis acid) is present in the catalyst. The carbamate yield increases with an increase in the amount of available adsorbed aniline. It may be recalled that DRIFT spectroscopy of adsorbed CO_2 on various catalysts (Chapter 3, Fig. 3. 15) had indicated that CO_2 activation (based on the intensity of the carbamate peak at 1609 cm^{-1}) takes place only in the case of propylamine- and adenine-functionalized SBA-15 and Ti-SBA-15 supports. Pure SBA-15 or Ti-SBA-15 could not activate CO_2. Furthermore, the amounts of activated CO_2 were higher in the case of adenine-functionalized supports than in the case of propylamine-functionalized supports. In other words, while the Ti ions adsorb the epoxides or the alkyl or aryl amines, the adenine functionality activates CO_2. Accordingly, the carbamate yields correlate with the availability of the adsorbed aniline and activated CO_2 (Fig. 4.3).

Table 4.8. Turnover frequencies (TOF) for n-butyl-N-phenyl carbamate synthesis over Ti-SBA-15 catalyst systems

Catalyst	CO_2 desorbed (mmol/g. catalyst)	NH_3 desorbed (mmol/g. catalyst)	TOF(h^{-1})[a]	
			Based on CO_2 desorbed[b]	Based on NH_3 desorbed[c]
Ti-SBA-15 (Si/Ti = 40)	2.9	0.9	-	13.8
SBA-15-*pr*-NH_2	3.8	-	1.4	-
Ti-SBA-15-*pr*-NH_2 (Si/Ti = 40)	3.9	0.9	3.9	15.9
SBA-15-*pr*-Ade	4.3	-	2.5	-
Ti-SBA-15-*pr*-Ade (Si/Ti = 40)	5.3	1.0	4.7	23.2

[a] TOF values are calculated from the conversions reported in Table 4.7
[b]TOF = moles of aniline converted per mole of CO_2 desorbed per hour.
[c]TOF = moles of aniline converted per mole of NH_3 desorbed per hour.

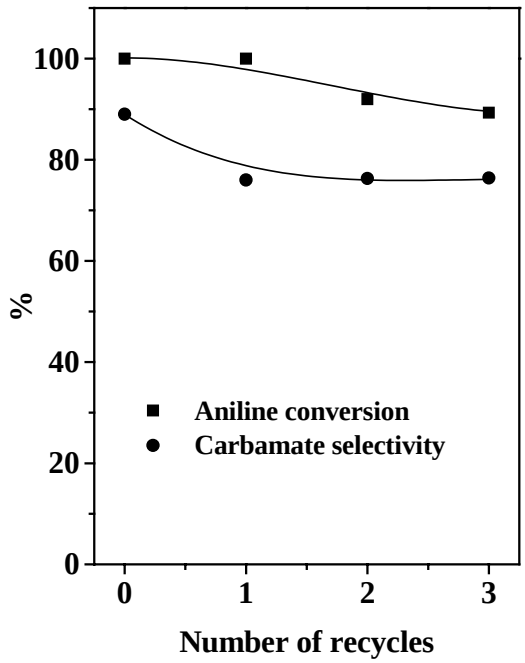

Fig. 4.2. Reusability of Ti-SBA-15-*pr*-Ade in butyl-N-phenyl carbamate synthesis.

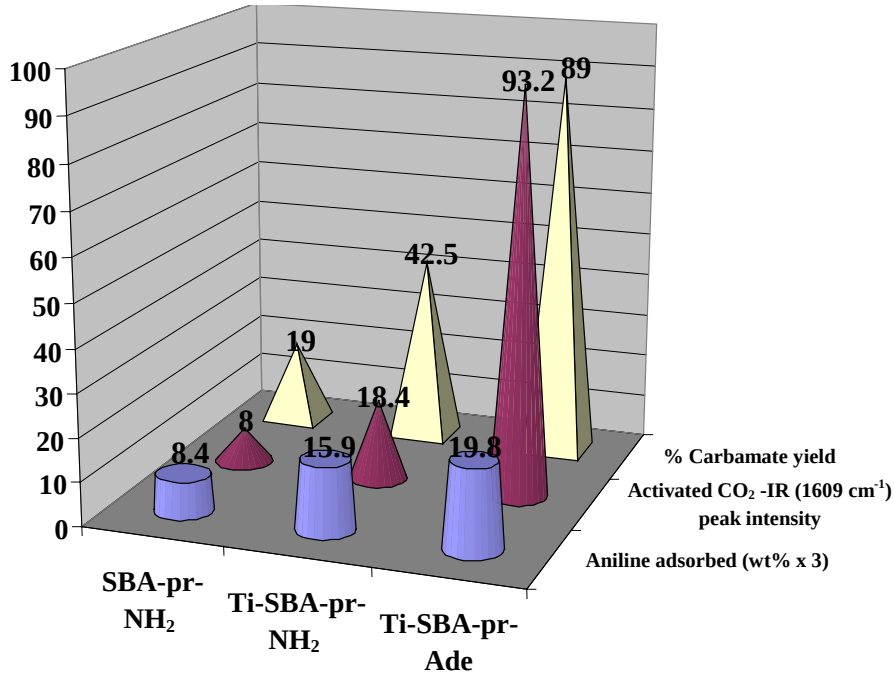

Fig. 4.3. Correlation of n-butyl-N-phenyl carbamate yield with the amount of aniline adsorbed (×3, wt%) and carbamate IR peak intensity (1609 cm^{-1}) over different solid catalysts.

4.3.4. Carbamate Synthesis over Organo-Inorganic Hybrid Catalysts

It is known that carbamates can be synthesized using homogeneous onium salts [12]. Since as-synthesized zeolite-beta and MCM-41 contain onium ions in their cavities/pores, it is believed that they can be used as heterogeneous catalysts for cyclic carbonates synthesis. This section presents catalytic activity studies on these catalyst systems.

Various alkyl and aryl carbamates were synthesized under mild conditions from the corresponding amines, CO_2 and n-butyl bromide (n-BuBr) over zeolite-beta and MCM-41 catalysts. The reaction of CO_2 with a primary amine readily forms the carbamic acid ammonium salt (Eq. (1)). In the presence of quaternary ammonium ion catalysts (template), ion-exchange takes place, carbamate anion is stabilized, and equilibrium shifts to the right side (Eq. (2)). Further reaction of this carbamate anion with n-BuBr yields the corresponding alkyl carbamate (Eq. (3)). However, in the absence of an efficient catalyst, carbamic acid ammonium salt (in Eq. (1)) is unstable and the amine formed by the reverse reaction reacts with n-BuBr yielding predominantly the nitrogen-derived products (Eq. (4)). The inorganic–organic hybrid catalysts favor the formation of carbamate rather than that of the nitrogen-derived products (N-alkylated products).

$$2\,RNH_2 + CO_2 \rightleftharpoons [RNHCOO^-][RNH_3^+] \quad (1)$$

$$[RNHCOO^-][RNH_3^+] + Et_4N^+X^- \rightleftharpoons [RNHCOO^-][Et_4N^+] + [RNH_3^+X^-] \quad (2)$$

$$[RNHCOO^-][Et_4N^+] + [RNH_3^+X^-] + n\text{-}BuBr \longrightarrow RNHCOO(n\text{-}Bu) + RNH_2 + Et_4N^+X^- + HBr \quad (3)$$

$$RNH_2 + n\text{-}BuBr \longrightarrow RNH(n\text{-}Bu) + HBr \quad (4)$$

Both aliphatic and aromatic amines could be converted into their carbamates using zeolite-beta and MCM-41. With different amines, the carbamate yields varied in the order: octylamine > cyclohexylamine > hexylamine > benzylamine > aniline > 2,4,6

trimethyl aniline (Table 4.8). Aliphatic amines can be more easily converted to their corresponding carbamates as compared to aromatic amines. With all the known catalyst systems, the reaction had to be conducted in a solvent medium (DMF); in the absence of solvent, the *N*-alkylated compound formed as the main product. Interestingly, when as-synthesized zeolite-beta catalysts were used, carbamate product formed with high selectivity (84 – 95%) without any solvent.

Influence of pressure on the synthesis of butyl-N-phenyl carbamates by reacting aniline, CO_2 and n-BuBr was studied over MCM-41. It was found that aniline conversion increased by increasing pressure from 1 to 3.4 bar, but any further increase in pressure led to only a marginal increase in aniline conversion (Fig. 4.4 (a)). The catalysts were found stable in at least five recycling experiments (Fig. 4.4 (b)).

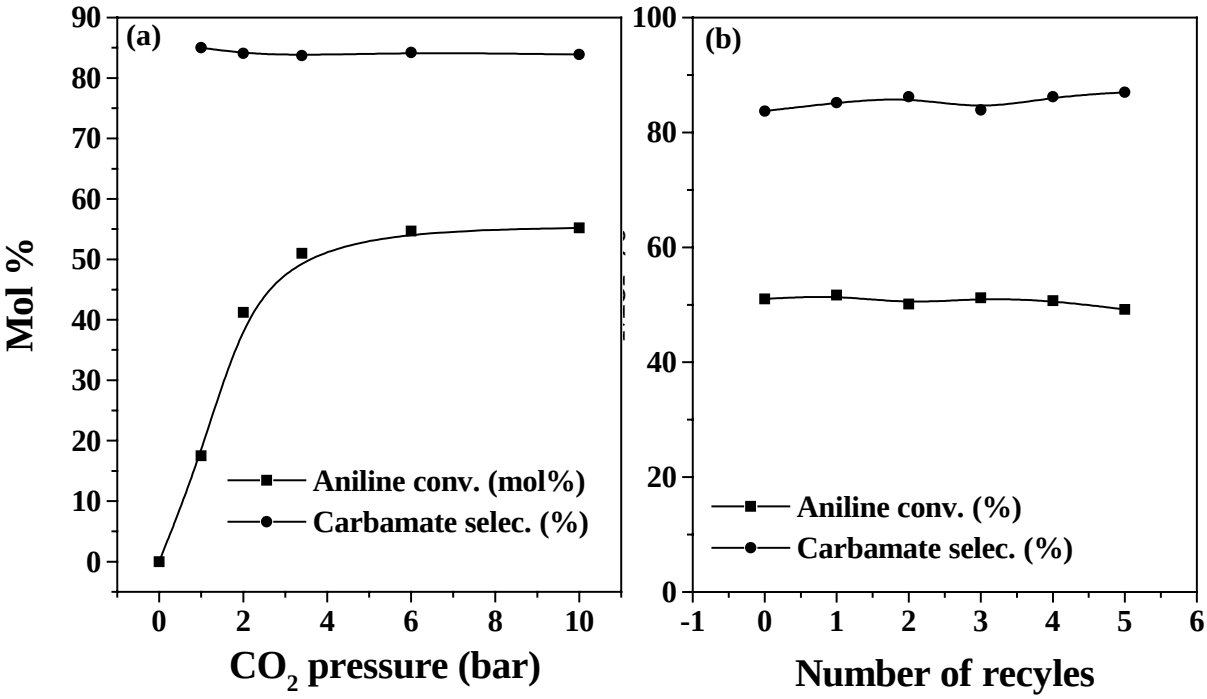

Fig. 4.4. (a) Influence of CO_2 pressure on the synthesis of butyl-N-phenyl carbamate (b) Catalytic activity of MCM-41 in recycling experiments.

Table 4.8. Synthesis of carbamates over zeolite-beta and MCM-41 in the absence of solvent

Entry no	Amines	Zeolite-beta			MCM-41		
		Amine Conv. (mol %)	carbamate Selc. (%)	TOF (h^{-1})	Amine conv. (mol%)	Carbamate Selec. (%)	TOF (h^{-1})
1	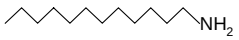	100	91.7	11.2	100	90.1	36.2
2	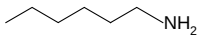	93.8	84.2	10.5	90.4	94.5	32.7
3	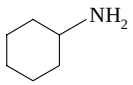	96.5	88.6	10.8	94.0	80.6	34.0
4	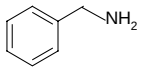	76.2	90.0	8.5	76.0	91.0	27.5
5	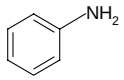	52.8	86.9	5.9	51.0	83.7	18.5
6	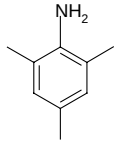	21.1	95.2	2.4	30.0	94.8	10.9

Reaction conditions: Amines, 10 mmol; n-butyl bromide, 10 mmol; catalyst, 150 mg; CO_2 pressure, 3.4 bar; run time, 3 h; temperature, 353 K.

[a] Turnover frequency (TOF) = moles of amine converted per mole of quaternary ammonium ion (template) in as-synthesized zeolite-beta or MCM-41 per hour.

4.4. Conclusions

Alkyl and aryl carbamates were synthesized at mild reaction conditions (353 K and 3.4 bar) from amines, alkyl halides and CO_2. The catalytic activities of four different solid catalyst systems have been evaluated. When titanosilicates and zeolite encapsulated metal phthalocyanine complexes were used as catalysts the reactions had to be conducted in solvents like DMF to obtain high yields of carbamtes. However, with as-synthesized zeolite-beta and MCM-41 as well as with organo-functionalized Ti-SBA-15 catalysts the reactions occur even in the absence of solvents. The latter type catalysts are reusable in several recycling experiments. Adsorption experiments reveal while the amines are activated at Ti sites, CO_2 is activated at basic sites (adenine). There exists synergism when both the acidic (Ti) and basic (adenine) sites are present in the catalyst system. This method of carbamate synthesis utilizing CO_2 is a benign process. The catalysts investigated in the present study especially adenine-functionalized Ti-SBA-15 are more efficient than the known heterogeneous catalysts. FT-IR and ^{1}H NMR spectra of the isolated product from the reaction of aniline, CO_2 and n-butyl bromide are presented in Appendices 4.A and 4.B, respectively.

4.5. References

1. (a) K. Okato, J. Appl. 217 (1984) 97. (b) P. Adams, F. A. Baron, Chem. Rev. 65 (1965) 567.
2. (a) A. Mateen, S. Chapalamadugu, B. Kashar, A. R. Batthi, G. R. Chaudry, Biol. Degrad. Biorem. Toxic. Chem. (1984) 198. (b) The Agrochemical Handbook 2nd Ed, Royel Society of Chemistry, 1987.
3. G. Oertel, Polyurethane handbook, Hanser Publishers, Munich, 1985.
4. (a) L. A. Caroino, Acc. Chem. Res. 6 (1973) 191. (b) T. W. Green, P. G. M. Wuts, Protective Group in Organic Synthesis 2nd Ed., Wiley, New York, 1991 pp 315.
5. (a) E. Alessio, G. Mestroni, J. Organomet. Chem. 291 (1985) 117. (b) A.

Bassoli, R. Rindone, S. Tollari, J. Mol. Catal. 61 (1990) L15. (c) F. Ragini, S. Cenini, J. Mol. Catal. A: Chem. 161 (2000) 31.

6. (a) F. Shi, Y. Deng, T. Sima, H. Yang, J. Catal. 203 (2001) 525. (b) B. Chen, S.S.C. Chuang, J. Mol. Catal. A: Chem. 195 (2003) 37. (C) S. Fukuoka, M. Chono, M. Kohno, J. Org. Chem. 49 (1984) 1458.
7. (a) D. P. N Satchell, R. S. Satchell, Chem. Soc. Rev. 4 (1975) 231. (b) S. Raucher, D. S. Jones, Synth. Commun. 15 (1985) 1025.
8. (a) W. McGhee, D. Riley, K. Christ, Y. Pan, B. Parnas, J. Org. Chem. 60 (1995) 2820. (b) F. Shi, J. Peng, Y. Deng, J. Catal. 219 (2003) 372.
9. (a) M. Yoshida, N. Hara, S. Okuyama, J. Chem. Soc., Chem. Commu. (2000) 151. (b) A. Inesi, V. Mucciante, L. Rossi, J. Org. Chem. 63 (1998) 1337. (c) M. Aresta, E. Quaranta, Tetrahedron 48 (1992) 1515.
10. (a) I. Vauthey, F. Valot, C. Gozzi, F. Fache, M. Lamaire, Tetrahedron Lett. 41 (2000) 6347. (b) F. Shi, Y. Deng, J. Catal. 211 (2002) 548. (c) A. Wolf, F. Schuth, Appl. Catal. A 226 (2002) 1.
11. (a) R. Raja, P. Ratnasamy, J. Catal. 170 (1997) 244. (b) S. Seelan, A.K. Sinha, D. Srinivas, S. Sivasankar, J. Mol. Catal., A: Chem. 157 (2000) 163.
12. (a) W. McGhee, D. Riley, K. Christ, Y. Pan, B. Parnas, J. Org. Chem. 60 (1995) 2820. (b) T. Sima, S. Guo, F. Shi, Y. Deng, Tetrahedron Lett. 43 (2002) 8145.

Chapter-5

Transesterification Reactions: Synthesis of Dialkyl Carbonates and Bio-fuel

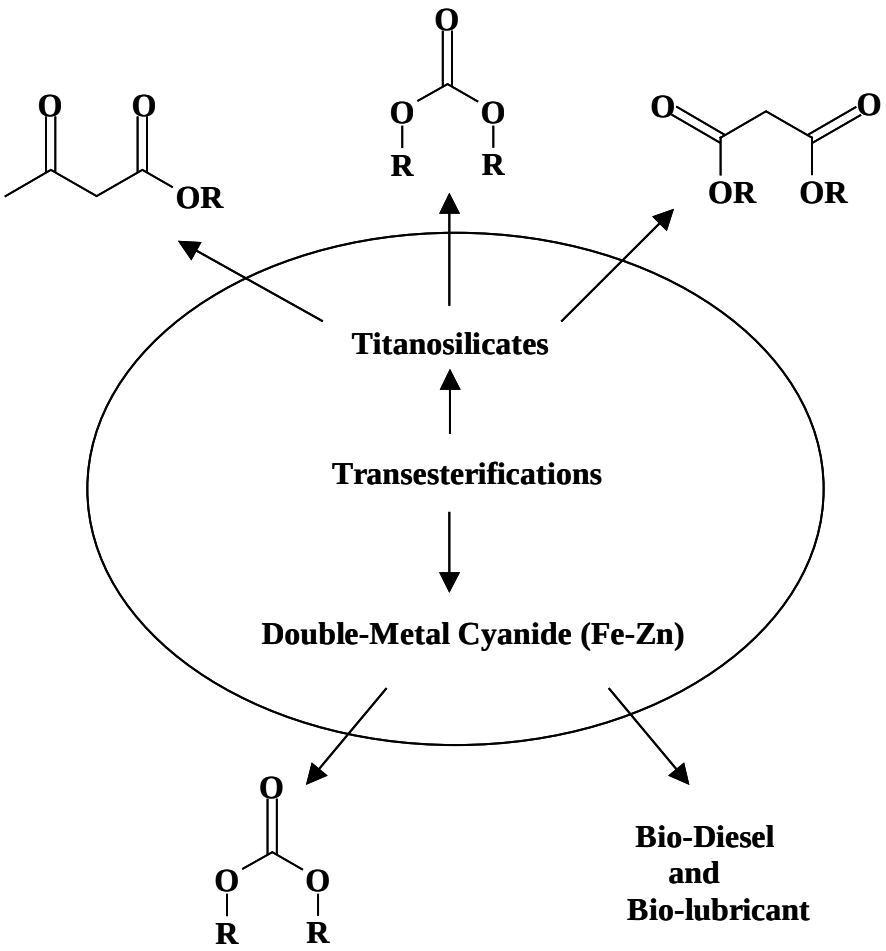

5.1. Introduction

Transesterification is a process where an ester is transformed into another through interchange of the alkoxy moiety. It is an equilibrium process and finds importance in several industrial manufacturing processes (Chapter 1; Section 1.5). Several homogeneous catalysts such as distannoxanes [1], $InCl_3$ [2], $LiClO_4$ [3], Ti(IV) alkoxides [4], and sulphated-SnO_2 [5] catalyze these reactions. A few heterogeneous catalysts like envirocat EPZG [6, 7], amberlyst-15 [8], polymer supported lipase [9], zeolites [10] and hydrotalcites [11] have also been employed recently. Dialkyl carbonates are useful chemical intermediates in organic synthesis and bis-phenol-A-polycarbonate manufacturing. They are conventionally synthesized using toxic phosgene chemicals or by hazardous oxidative carbonylation route [12]. Their synthesis by transesterification of cyclic carbonates with alcohols is an attractive, eco-friendly process. Tatsumi *et al* [13] reported the use of K-TS-1 for the synthesis of dimethyl carbonate (DMC) from ethylene carbonate and methanol. Ethene carbonate conversion of 68% and DMC yield of 51% were obtained. Hydrotalcite [14] and CaO/C [15] gave the DMC yields 58 and 42%, respectively. DMC can be synthesized directly by the reaction of epoxides, CO_2 and methanol. However the DMC yield in direct one-pot synthesis utilizing CO_2 was poor [16].

In recent years, there has been a growing interest in alternative fuels from vegetable and animal sources. Again, transesterification plays an important role in these bio-fuels manufacturing. A variety of homogeneous catalysts [17] and alkali loaded heterogeneous catalysts [18] were reported for the production of fatty acid methyl esters (bio-diesel). This chapter describes the catalytic activity of titanosilicate molecular sieves and double metal cyanide Fe-Zn catalysts for several transesterification reactions.

Titanosilicates have been widely investigated, for more than two decades, as selective oxidation catalysts [19]. Acid properties of titanosilicates are not much exploited**.** Here, the application of TS-1, Ti-MCM-41 and amorphous TiO_2–SiO_2 in transesterification of a cyclic ester — propene carbonate (PC) with several alcohols is studied.

Double metal cyanides were originally discovered by General Tire Inc. in 1960 [20]. They were revisited starting in the middle of 1980s, with improvements made by some companies like ARCO [21], Shell [22] and Asahi glass [23]. These improvements made double metal cyanide catalysts much more attractive for commercial production of polyether polyols [24]. Compared with the conventional KOH catalyst, this catalyst gave high quality PPG products that have low level of unsaturation, narrow molecular weight distribution and low viscosity. Kim et al. [25] recently reported the use of double metal cyanide catalyst for ring opening polymerization of propene oxide. This opened up the possibility to apply this for the transesterification reaction of cyclic carbonates with alcohols forming dialkyl carbonates. The acid properties of the catalysts were investigated using DRIFT spectroscopy of adsorbed pyridine and NH_3-TPD.

5.2. Experimental Section

Synthesis and physicochemical characterization of the titanosilicates and double metal cyanide Fe-Zn catalysts are described in Chapter-2.

5.2.1. Reaction Procedures

5.2.1.1. Transesterification of Propene Carbonate with Alcohols

10 mmol of propene carbonate, 100 mmol of alcohol and catalyst (50 - 250 mg) were taken in a rotating hydrothermal reactor (Hero Co., Japan; rotation speed = 50 rpm). The reaction was conducted at 373 - 443 K for 8 h. After the reaction, the reactor

was cooled to room temperature and sample was analyzed by gas chromatography (Varian 3800; CP-8907 column; 15 m x 0.25 mm x 0.25μm). The products were identified by GC-MS (Shimadzu QP-5000; 30 m-long, 0.25 mm-i.d., and 0.25 μm-thick capillary column DB-1), GC-IR (Perkin Elmer 2000; BP-1 column; 25 m-long, and 0.32 mm-i.d.) and ^{1}H NMR (Bruker AC 200). The product was purified by column chromatography (100-200 mesh silica gel) with dichloromethane as eluent; polarity of the eluent was increased with methanol.

5.2.1.2. Transesterification of Ethylacetoacetate (EAA) and Diethylmalonate (DEM)

In a typical reaction, a known quantity of reactants (ester and alcohol) and catalyst were taken and the reaction was conducted at a desired temperature (298 – 423 K) for a specific period. At the end of the reaction the catalyst was separated and the liquid portion was analyzed by gas chromatography (Varian 3400; CP-SIL8CB column; 30 m-long, and 0.53 mm-i.d.). The products were identified by GC-MS, GC-IR and ^{1}H NMR. In some cases the product was isolated by column chromatography (silica gel (60 – 120 mesh); petroleum ether : ethylacetate = 80 : 20 v/v eluent).

5.2.1.3. Bio-diesel/ lubricant Production

In a typical reaction, vegetable oil (5 g), alcohol (oil : alcohol = 1:6 mole ratio), catalyst (1 wt %; 50 mg) were charged into a 100 ml hydrothermal reactor. The reaction was carried out at 443 K for 4 h. The contents were allowed to cool to room temperature. Catalyst was separated by filtration from the reaction mixture. Then, the alcohol was removed by distillation. Now the reaction mixture contains unreacted oil, transesterified product (fatty acid alkyl ester) and glycerol. To this, petroleum ether (60 ml) and methanol (20 ml) were added. The methanol and petroleum ether layers were separated using a separating funnel. Again, 20 ml of methanol was added to the separated petroleum ether layer and two layers were separated. The methanol fractions

containing glycerol were combined and treated with 60 ml of petroleum ether. Any trace amounts of unreacted oil and fatty acid esters present in the methanol layer along with glycerol were, thus, separated out. Later, methanol was distilled out and the by-product glycerol obtained was collected and its weight was noted for estimating the conversion of vegetable oil. The ether portion was evaporated to obtain the fatty acid esters and unconverted vegetable oil. The products were analyzed by gas chromatography (Shimadzu-14B; SE-52 packed column (6-feet long x 8 inch i.d.)) (Program: start at 425 K (2 min), ramp at 2.5 K/min to 477 K (0 min hold), ramp at 10 K/min to 513 K (20 min). 100 mg of ester was dissolved in 1 g of dichloromethane and used for analysis. The products were identified by GC-MS.

5.3. Results and Discussion

5.3.1. Acidic Properties

5.3.1.1. Titanosilicates

DRIFT Spectroscopy of Adsorbed Pyridine. The acidic properties of titanosilicates (TS-1, Ti-MCM-41 and amorphous TiO_2-SiO_2) were investigated by pyridine adsorption-IR (Fig. 5.1). It is known that upon hydration Ti ions in titanosilicates expand their coordination number from 4 to 5 or 6 [19]. Studies were also performed on titanium-free silicalites (Si-MCM-41, for example). Peaks around 1595 and 1445 cm^{-1} due to hydrogen-bonded pyridine and 1580 and 1485 cm^{-1} due to pyridine-coordinated to weak Lewis acid sites are observed. Absence of peaks at 1623 and 1455 cm^{-1} indicates the absence of strong Lewis acid sites. Brönsted acid sites (peaks at 1639 and 1546 cm^{-1}) are also absent in all the titanosilicate samples. The IR bands are relatively more intense for Ti-MCM-41 and amorphous TiO_2-SiO_2 than for TS-1 consistent with the easy accessibility of the Ti sites in the former two titanosilicalites than in the latter. Ti-free silicalite samples (Si-MCM-41) showed IR

peaks (Fig. 5.1(d)) due to hydrogen-bonded pyridine only. Absence of infrared bands at 1580 and 1485 cm^{-1} in Si-MCM-41 confirms that these bands in titanosilicate samples arise from pyridine attached to Lewis Ti sites.

The IR peaks due to pyridine disappeared completely above 398 K on TS-1 and 523 K on Ti-MCM-41 and amorphous TiO_2-SiO_2 suggesting that the strength of Lewis acid sites on the latter type catalysts is higher than the former. The easy accessibility of Ti sites in Ti-MCM-41 with open tetrahedral $Ti(OH)(OSi)_3$ structure form stabler Ti-pyridine complexes than the Ti in TS-1 possessing closed tetrahedral $Ti(OSi)_4$ structure.

NH_3-TPD. These studies showed a desorption peak at 448 K (Fig. 5.2 (a)). This band in Ti-MCM-41 and amorphous TiO_2-SiO_2 is more intense and asymmetric indicating that the strength of the Lewis acid sites on different titanosilicates increases in the order: TS-1 (NH_3 desorbed = 0.118 mmol/g) < Ti-MCM-41 (0.160 mmol/g) ≤ amorphous TiO_2- SiO_2 (0.175 mmol/g) in agreement with the IR spectra for adsorbed pyridine. NH_3-TPD measurements were also performed on TS-1 samples (Si/Ti = 33) calcined at different temperatures (723 – 923 K) (Fig. 5.2 (b)). The amount of NH_3 desorbed increased up to 823 K and then decreased (calcination temperature, ammonia desorbed: (723 K, 0.097 mmol/g); (773 K, 0.105 mmol/g); (823 K, 0.118 mmol/g); (923 K, 0.109 mmol/g)).

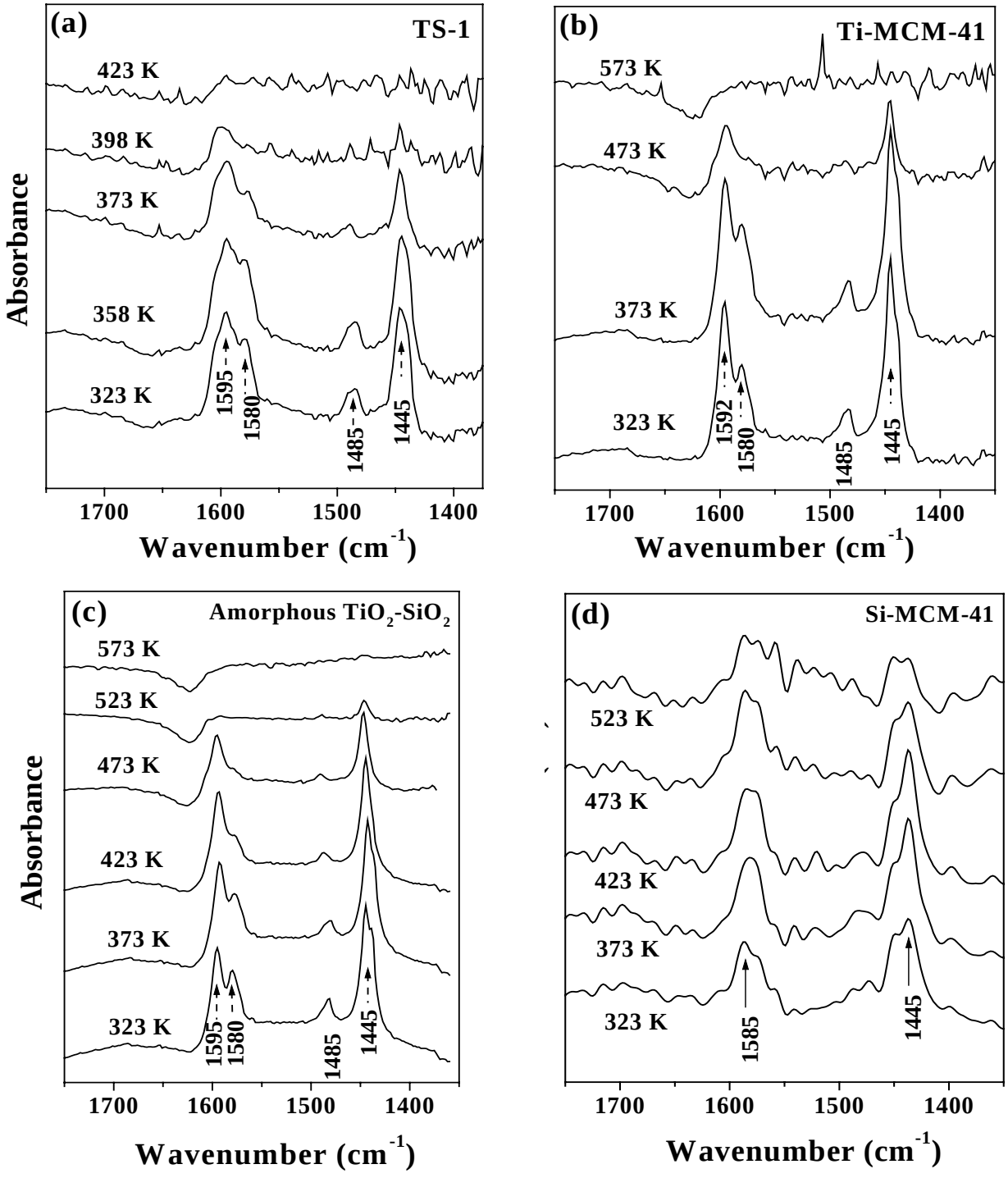

Fig. 5.1. DRIFT of adsorbed pyridine on (a) TS-1, (b) Ti-MCM-41, (c) amorphous TiO_2-SiO_2 and (d) Si-MCM-41.

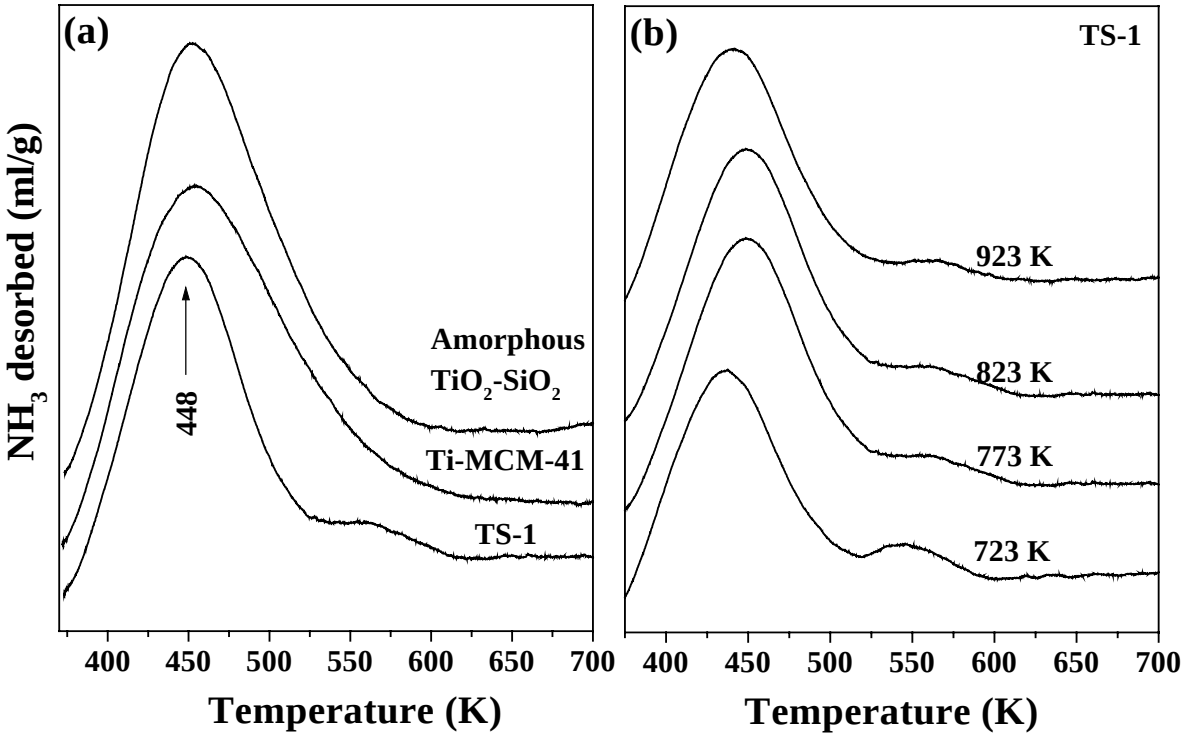

Fig. 5.2. NH_3-TPD of (a) TS-1, Ti-MCM-41 and amorphous TiO_2–SiO_2, (b) TS-1 calcined at various temperatures.

5.3.1.2. Fe-Zn Double Metal Cyanide Catalysts

DRIFT Spectroscopy of Adsorbed Pyridine. Fig. 5.3 depicts the difference FT-IR spectra (DRIFT mode) of adsorbed pyridine on double metal cyanide Fe-Zn catalysts prepared by different methods. After adsorption of pyridine, the temperature of the samples was raised to a desired value and the spectrum was recorded. Absence of peaks at 1639 and 1546 cm^{-1} in the difference FT-IR spectra (Fig. 5.3) confirm that the samples do not contain Brönsted acid sites. The peaks at 1608 and 1450 cm^{-1} reveal the presence of strong Lewis acid sites and the peak at 1490 cm^{-1} is due to pyridine coordinated to weak Lewis acid sites. Except for some marginal changes in peak positions, the difference FT-IR spectra of Fe-Zn catalysts prepared by different methods (Fe-Zn-1, Fe-Zn-2, Fe-Zn-3) were almost identical. The types of the acid sites

are the same in all the Fe-Zn catalysts investigated. As expected, with an increase in temperature (from 323 to 473 K) the intensity of the pyridine IR peaks decreased. However, they have not disappeared even at 473 K indicating that the samples are not weakly acidic.

A comparison of the pyridine adsorption-IR studies of titanosilicate samples (Fig. 5.1) and Fe-Zn double metal cyanide catalysts (Fig. 5.3) point out that the former type catalysts contained only weak Lewis acid sites while the latter contained both weak and strong Lewis acid sites. In the case of titanosilicate catalysts hydrogen-bonded pyridine is more in amount than pyridine coordinated to weak Lewis acid sites. Further, the number of acid sites is more in the case of Fe-Zn than in titanosilicate catalysts. Pyridine desorbed completely at 373 – 423 K from titanosilicates while a significant amount of pyridine was present even at 473 K on Fe-Zn catalysts indicating that the latter are more strongly acidic than the former.

NH_3-TPD. The samples were activated at 473 K, NH_3 was adsorbed at 323 K and the desorption of NH_3 was monitored in the temperature range 323 – 473 K. The double metal cyanide Fe-Zn samples showed a broad asymmetric desorption feature which could be deconvoluted into three desorption peaks with peak maxima at 357 K, 382 K and 417 K, respectively (Fig. 5.4). While the desorption peak at 357 K could be attributed to physisorbed NH_3, the peaks at 382 K and 417 K could be corresponded to weak and strong Lewis acid sites, respectively. The total amount of NH_3 desorbed from Fe-Zn-1, Fe-Zn-2 and Fe-Zn-3 samples is 1.96, 1.87 and 1.77 mmol/g, respectively. The amount of NH_3 desorbed from the deconvoluted peak with maximum at 417 K is 0.57 for Fe-Zn-1 and 0.29 mmol/g for Fe-Zn-2.

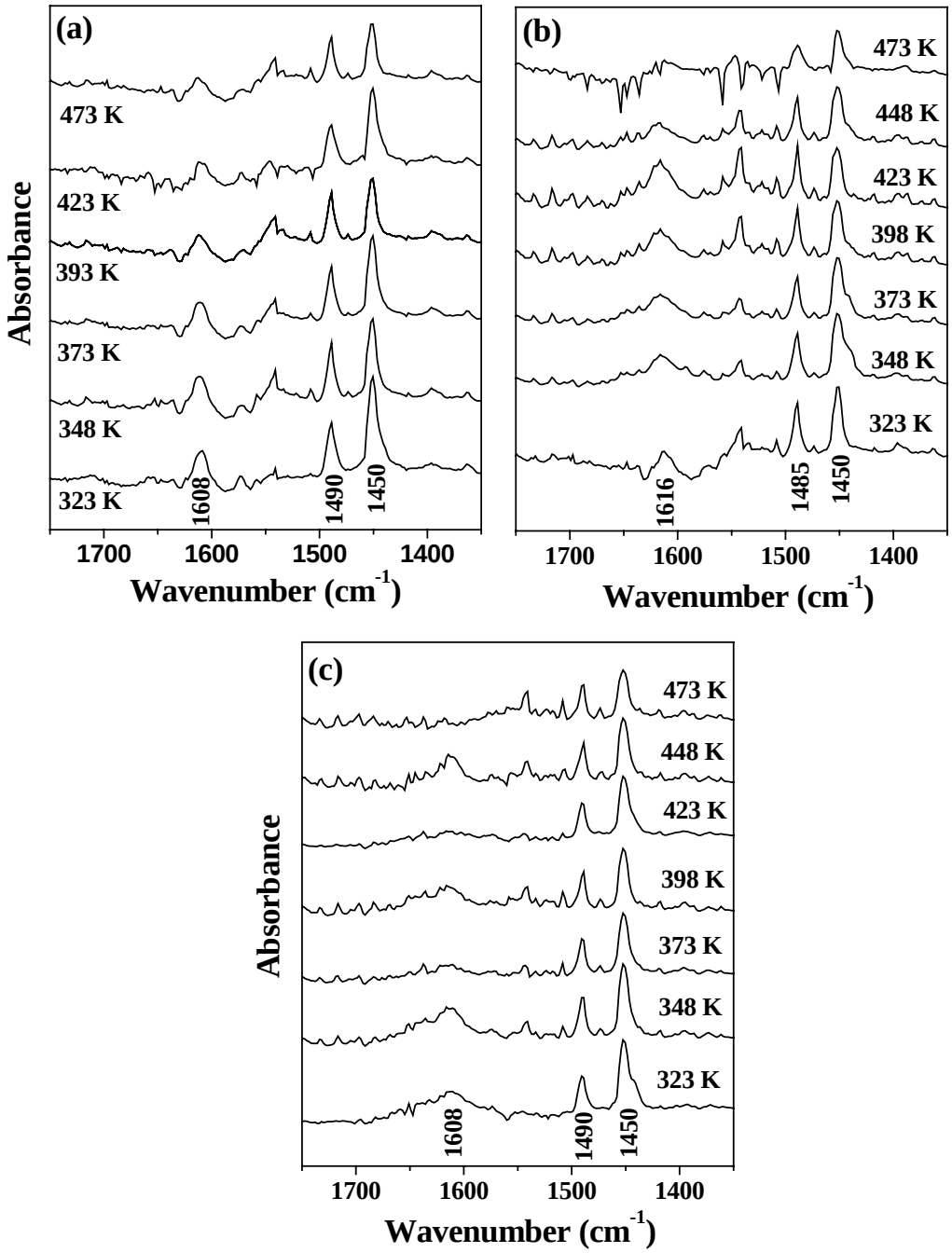

Fig. 5.3. DRIFT spectra of pyridine adsorbed on (a) Fe-Zn-1, (b) Fe-Zn-2 and (c) Fe-Zn-3 as the temperature is raised from 333 – 473 K.

NH_3 desorbed from the deconvoluted peak with maximum at 382 K is 0.85 for Fe-Zn-1 and 0.83 mmol/g for Fe-Zn-2 catalyst, respectively. The study thus reveals that the amount of strong acid sites is more on Fe-Zn-1 than on the other two catalysts while

the weak Lewis acid sites are in similar quantity. This result is in agreement with the acidity study by pyridine-IR technique.

The acidity measurement, thus, reveal that the method of preparation has a marked effect on acidity. Further, Fe-Zn double metal cyanide catalysts are more strongly acidic than titanosilicate catalysts. These differences in acidity affect the catalytic properties of the materials.

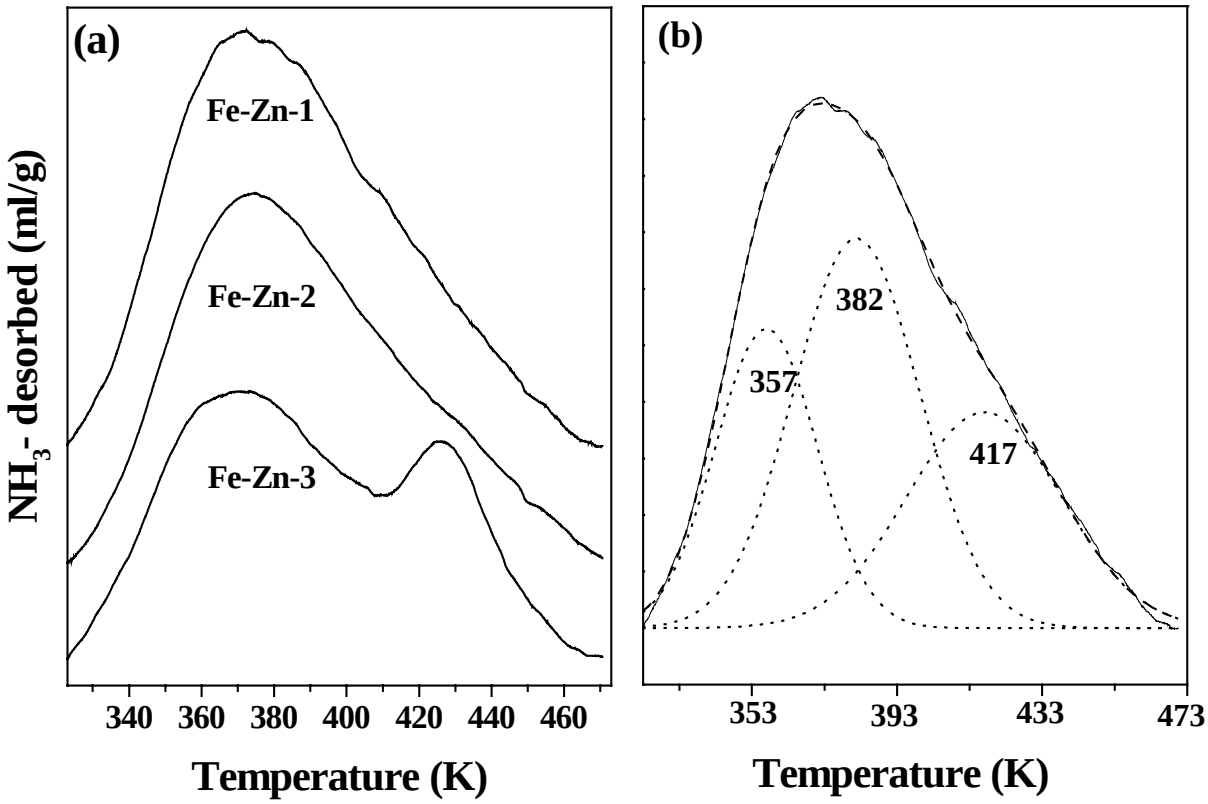

Fig. 5.4. NH_3-TPD of (a) Fe-Zn-1, Fe-Zn-2 and Fe-Zn-3. (b) Deconvoluted plot of Fe-Zn-1.

5.3.2. Synthesis of Dialkyl Carbonates over Titanosilicates

Transesterification of cyclic carbonates with methanol is important because the transester, dimethyl carbonate (DMC) is a value-added chemical for applications as an efficient methylating agent and precursor for polycarbonates. In addition to acidity, the pore structure of titanosilicates is found to play an important role in transesterification

of cyclic esters like propene carbonate (Scheme 5.1). TS-1 showed no activity for cyclic esters (Table 5.1). Amorphous TiO_2-SiO_2 exhibited the highest activity (Table 5.1).

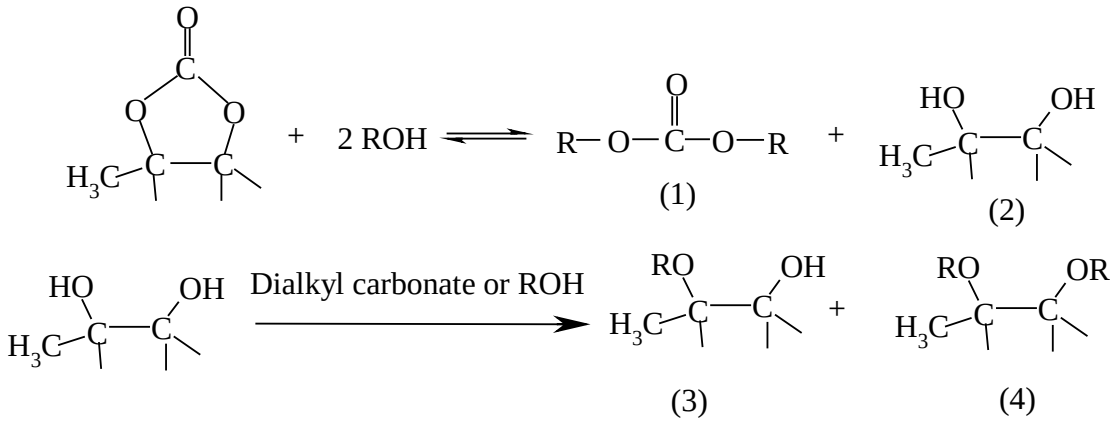

Scheme 5.1. Transesterification of propene carbonate (PC) with alcohols.

Table 5.1. Transesterification of cyclic propene carbonate (PC) with different alcohols and phenol (ROH) over titanosilicates[a, b]

Titanosilicate	ROH	Reaction time (h)	Conversion of PC, mol%	Selectivity of transester product, mol%[b]
TS-1	Methanol	2	Nil	-
TiMCM-41	Methanol	2	5.1	
	Phenol	8	58.9	24.4
Amorphous TiO_2-SiO_2	Methanol	4	71.4	48.2
		8	86.0	51.2
	Ethanol	8	73.0	61.8
	Propanol	12	86.3	69.4
	n-Butanol	12	85.0	73.4
	n-Hexanol	12	49.0	61.5

[a]*Reaction conditions:* Catalyst (TS-1 or TiMCM-41), 400 mg; propylene carbonate, 1.36 g, ROH (methanol, 3.2 g; phenol, 4.7 g); temperature, 393 K.

[b]Reaction conditions: Catalyst (amorphous titanosilicate), 400 mg; propylene carbonate, 1.02 g (0.01 mol); ROH, 0.1 mol; temperature, 423 K.

[c]Balance is the corresponding ether

Propene carbonate could be transesterified with various alcohols over amorphous TiO_2-SiO_2. However, with lower chain alcohols the selectivity for the transester product was low. The transester (dialkyl carbonate) possibly participates in subsequent O-alkylation reaction of the diol (Scheme 5.1). This was confirmed later by performing separate experiments of O-alkylation reactions of ethylene glycol with methanol and dimethyl carbonate. No alkylation occurred in the absence of Ti catalyst. With amorphous TiO_2-SiO_2, 30.1% of ethylene glycol was methylated when methanol was the alkylating agent. Complete conversion of ethylene glycol to dimethylated glycol occurred when dimethyl carbonate was the alkylating agent. The alkylating ability of dipropyl and dibutyl carbonates is lower than that of dimethyl or diethyl carbonates. Hence, the selectivity of dimethyl carbonate is lower that the other carbonates due to its participation in consequent alkylation reactions (Table 5.1).

5.3.3. Synthesis of Dialkyl Carbonates over Fe-Zn Double Metal Cyanides

To overcome the issue of low selectivity for dialkyl carbonates in transesterification reactions, new solid Fe-Zn-based double metal cyanide catalysts were developed. Transesterification of propene carbonate with different alcohols yielded dialkyl carbonates; 1,2-propene glycol formed as by-product in equivalent amounts (Scheme 5.1). The reaction occurred only in the presence of a catalyst. The influence of various reaction parameters (temperature, alcohol/propene carbonate ratio and catalyst amount) on the dialkylcarbonate yield was studied.

The influence of temperature on the yield of dimethyl carbonate (DMC) from propene carbonate (PC) and methanol over Fe-Zn-1 catalysts is shown in Fig. 5.5 (a). The reaction did not occur up to 353 K. At 373 K, a very low yield of DMC (6.6 %) was obtained. Catalytic activity increased with increasing reaction temperature. A maximum yield of DMC was obtained at 443 K.

Fig. 5.5(b) shows the effect of methanol to PC molar ratio on DMC yield. In these experiments while keeping the PC concentration constant, the amount of methanol in reaction mixture was increased and DMC (isolated) yield was monitored. DMC yield increased with increasing methanol content. As transesterification is an equilibrium reaction, increasing methanol content favored the forward reaction (Scheme 5.1) in agreement with the Le Chatelier's principle. A methanol to PC ratio of 8 – 10 (mol/mol) is optimum for the highest yield of DMC.

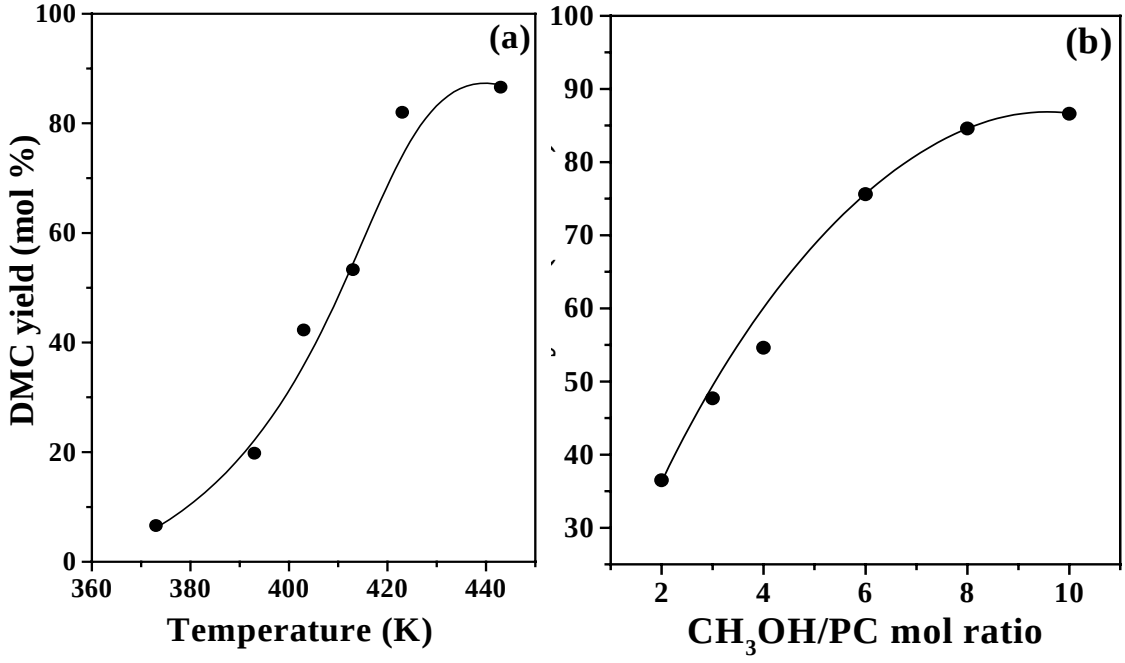

Fig. 5.5. Influence of (a) temperature and (b) alcohol to cyclic carbonate ratio on transesterification of propene carbonate (PC) with methanol over Fe-Zn-1 catalyst.

The amount of the catalyst has a significant effect on DMC yield (Fig. 5.6). The yield of DMC increased with an increase in catalyst amount and reached a maximum when the catalyst amount was 0.25 g. The catalysts formed a heterogeneous phase and at the end of the reaction it could be separated by centrifugation/filtration from the reaction mixture. Filtered catalyst was washed initially with methanol and then with acetone and air-drying at room temperature, the catalyst could be reused. No significant loss in activity was observed in at least 5 recycling experiments (Table 5.2; Run Nos. 6 - 11).

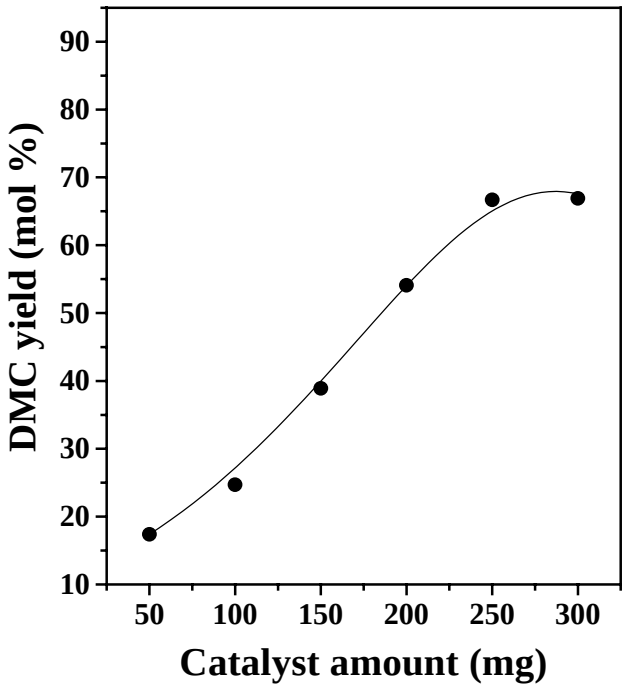

Fig. 5.6. Influence of catalyst amount on the transesterification of Pc with MeOH over Fe-Zn-1 catalyst.

Propene carbonate could be transesterified with various alcohols. A variety of dialkyl carbonates could be prepared over Fe-Zn-1 catalyst (Table 5.2). Chain length of the alcohol has a marked effect on catalytic activity. The yield of dialkyl carbonate decreased with increasing chain length. Transesterification of propene carbonate with

phenol yielded diphenyl carboanate (DPC) over Fe-Zn-1 catalyst but in very small amounts (~ 2%).

Table 5.2. Reaction of propene carbonate with various alcohols over Fe-Zn-1 catalyst

Run no.	Alcohol	Dialkyl carbonate yield (mol %)	TON
1	Benzyl alcohol	77.8	95
2	Hexanol	62.5	77
3	Butanol	69.3	85
4	Propanol	77.5	95
5	Ethanol	79.4	97
6	Methanol	86.6	106
7	Methanol (**recycle-1**)	83.2	102
8	Methanol (**recycle-2**)	83.5	102
9	Methanol (**recycle-3**)	84.9	104
10	Methanol (**recycle-4**)	83.2	102
11	Methanol (**recycle-5**)	82.6	101

Reaction conditions: Propene carbonate = 10 mmol; alcohol = 100 mmol; catalyst = 250 mg; reaction temperature = 443 K; reaction time = 8 h
TON = moles of propene carbonate converted per mole of catalyst.

5.3.4. Transesterification of Propene Carbonate with Alcohols Mixture over Fe-Zn-1 Catalyst

When propene carbonate was reacted with methanol, dimethyl carbonate (DMC) was the product along with an equivalent amount of by-product 1,2-propene glycol. When the reaction was carried out with ethanol instead of methanol, diethyl carbonate (DEC) was the product. The rate of the transeterification is lower in ethanol

than in methanol. When the reaction was conducted with an equimolar mixture of methanol and ethanol, methyl ethyl carbonate (MEC) formed in addition to DMC and DEC (Scheme 5.2). Asymmetric carbonates like MEC find important application as intermediates in chemicals synthesis. Organic carbonates like MEC could be synthesized with high selectivity by fine-tuning the reaction conditions.

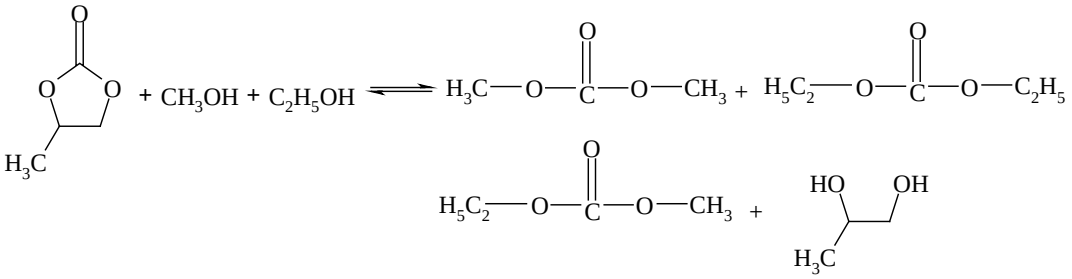

Scheme 5.2

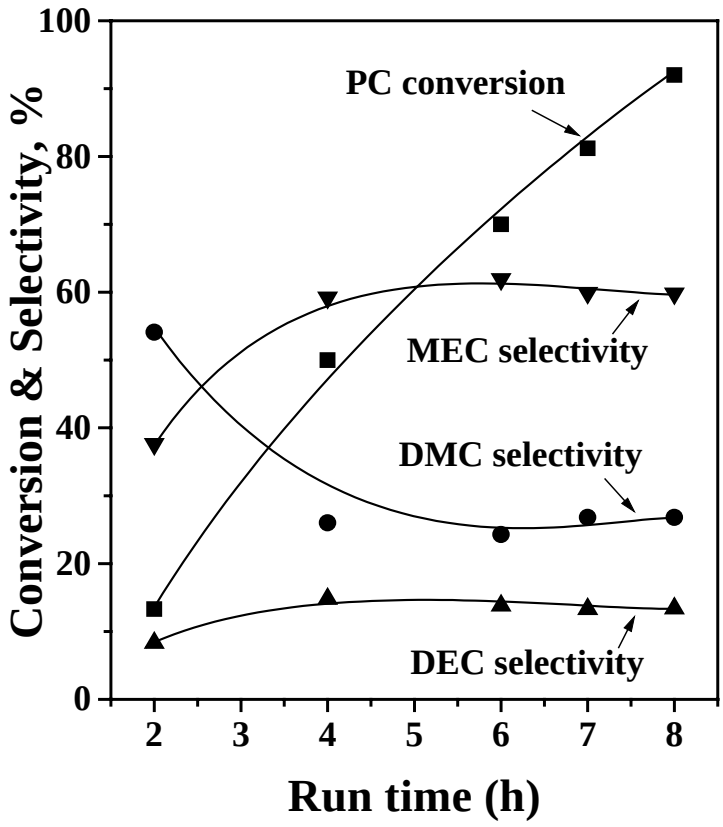

Fig. 5.7. Influence of reaction time on DMC, MEC and DEC selectivity.

Fig. 5.7 shows the catalytic activity and product distribution as a function of run time in reaction of propene carbonate with an equimolar mixture of methanol and ethanol. Initially, DMC was the main product and DEC formed in smaller quantities. When the reaction was conducted beyond 2 h, the concentration of MEC increased significantly at the expense of DMC. There was only a marginal increase in the concentration of DEC. The composition of the product mixture did not change beyond 4 h due to attainment of equilibrium.

5.3.5. Transesterification of Dimethyl Carbonate with Various Alcohols

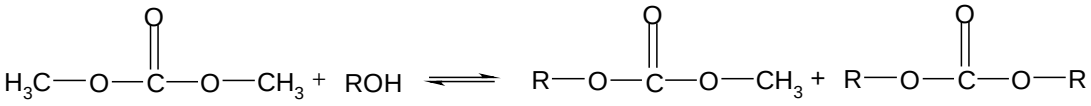

Scheme 5.3. Transesterification of DMC with alcohols

Having understood that asymmetric organic carbonates like MEC can be synthesized by transesterification of propene carbonate with a mixture of methanol and ethanol, detailed kinetics studies were undertaken to transesterify DMC with various alcohols to produce different organic carbonates (Scheme 5.3). Transesterification of DMC was found more facile than propene carbonate. As observed in the previous section, catalytic activity in transesterification decreased with an increase in the chain length of the alcohol (Table 5.3). This is more obvious in the product pattern. Symmetric alkyl carbonates were formed in higher amounts when smaller chain length alcohols were used. However, with longer chain length alcohols asymmetric carbonates formed with high selectivity.

Table 5.3. Reaction of dimethyl carbonate with various alcohols

Run no.	Alcohol	DMC conversion (mol %)	Dialkyl carbonate selectivity (%)	Methyl alkyl carbonate selectivity (%)	TON
1	Benzyl alcohol	96.0	63.4	36.6	117
2	Hexanol	92.8	26.1	73.9	113
3	Butanol	94.6	30.2	69.8	115
4	Propanol	93.4	34.9	65.1	114
5	Ethanol	97.4	60.9	39.1	118

Reaction conditions: Dimethyl carbonate (DMC) = 10 mmol; alcohol = 100 mmol; catalyst = 250 mg; reaction temperature = 443 K; reaction time = 8 h

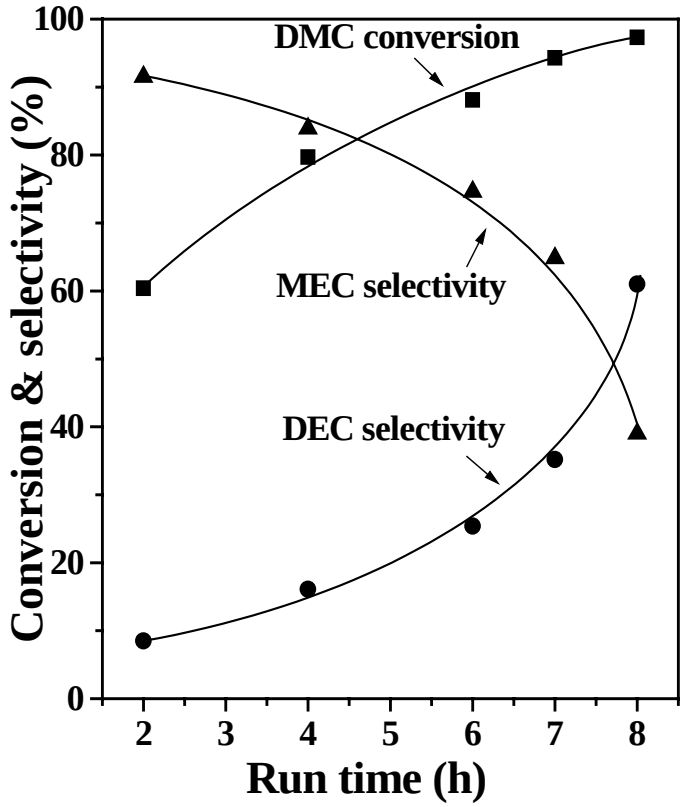

Fig. 5.8. Influence of reaction time on the transesterification of DMC with ethanol.

Fig. 5.8 shows the catalytic activity and product distribution as a function of time for transesterification of DMC with ethanol. About 60% conversion of DMC was observed in the first 2 hrs. The reaction had to be conducted for 8 hrs for complete conversion of DMC. MEC is the major product in the first 2 hrs while DEC formed as minor product. With time the selectivity of DEC increased from 8.5% (at 2 h) to 61% at 8 h. The slowed down DMC conversion beyond 2 h is due to competing transesterification reactions of DMC and MEC with ethanol.

5.3.5.1. Influence of Activation Temperature

The catalyst was activated at different temperature (333 – 673 K) and the activity was investigated for transesterification of DMC with ethanol (Table 5.4). No notable changes in catalytic activity and product selectivity were observed when the catalyst activation temperature was increased from 333 to 473 K. Above that temperature the activity of the catalyst decreased. DMC conversion decreased from 97% (activation temperature = 473 K) to 37.8 (activation temperature = 673 K). Interestingly, symmetric diethyl carbonate (DEC) selectivity increased from 61% to 81.5% when the catalyst activation temperature was raised from 473 K to 673 K. It may be recalled from Chapter 2 (Section 2.8) that the Fe-Zn catalyst decomposes beyond 473 K forming a different kind of mixed oxidic material. The mixed oxide formed from Fe-Zn-1 catalyst is therefore less active but more selective for symmetric dialkyl carbonates synthesis.

5.3.5.2. Influence of the Method of Catalyst Preparation

In the preparation of Fe-Zn-1 catalyst, tert-butanol and a tri-block copolymer $EO_{20}PO_{70}EO_{20}$ were used as complexing and co-complexing agents, respectively. In order to examine the influence of these chemicals on the catalyst formed, synthesis of

Table 5.4. Influence of Fe-Zn-1 activation temperature on the reaction of DMC with ethanol

Run no.	Catalyst activation temperature (K)	DMC conversion (mol %)	Dialkyl carbonate selectivity (%)	Methyl alkyl carbonate selectivity (%)	TON
1	298	95.5	58.6	41.4	116
2	333	94.8	59.5	40.5	116
3	373	95.0	58.2	41.8	116
4	473	93.4	65.1	34.9	114
5.	523	54.0	80.5	19.5	-
5	573	47.6	81.5	18.5	-
6	673	37.8	80.0	20.0	-

Reaction conditions: Dimethyl carbonate (DMC) = 10 mmol; alcohol = 100 mmol; catalyst = 250 mg; reaction temperature = 443 K; reaction time = 8 h

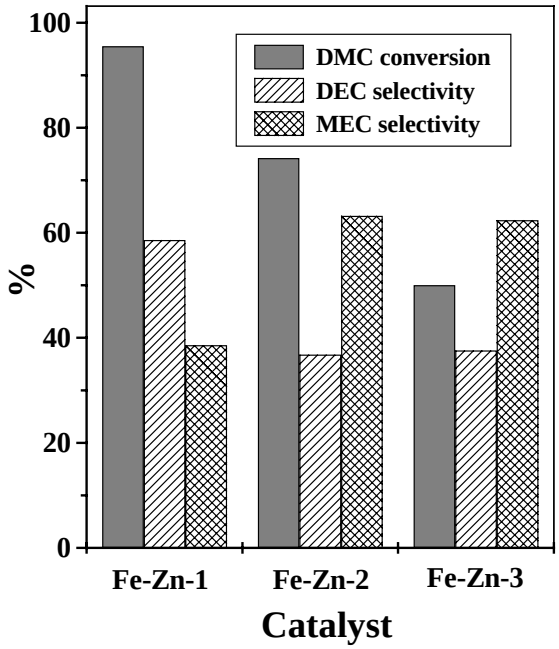

Fig. 5.9. Influence of method of catalyst preparation on the transesterification of DMC with ethanol.

Fe-Zn catalysts was performed with the complexing agent alone and with no complexing and co-complexing agents. The catalyst prepared with the former condition is designated as Fe-Zn-2 and the catalyst prepared with the latter conditions is designated as Fe-Zn-3.

Fe-Zn-1 catalyst prepared in the presence of both complexing and co-complexing agents showed the highest activity (Fig. 5.9). Fe-Zn-3 catalyst prepared in the absence of both the complexing and co-complexing agents showed the lowest catalytic activity (Fig. 5.9). DEC selectivity was the highest over Fe-Zn-1 catalyst while asymmetric organic carbonate (MEC) selectivity was more over Fe-Zn-2 and Fe-Zn-3 than over Fe- Zn-1 catalyst. The characterization studies (Chapter-2) revealed no spectral differences for the above three catalysts. Surface area of all the three catalysts was similar. X-ray diffraction patterns of these catalysts were also the same, suggesting that they are different polymorphic forms. Chemical composition and FT-IR spectroscopy reveal that Fe-Zn-1 catalysts contain a coordinated tert.-butanol (complexing agent) in the catalyst structure which is not present in the other two catalysts. The coordinated tert.-butanol is possibly replaced by water molecule in Fe-Zn-2 and Fe-Zn-3 catalysts. The coordinated tert-butanol in Fe-Zn-1 is possibly more labile than the coordinated water molecules in Fe-Zn-2 and Fe-Zn-3 leading to a more active Fe-Zn-1 catalyst. Although co-complexing agent is not present in the catalyst composition, it facilitated coordination of tert-butanol to the zinc moiety, which is the active Lewis acid site in the transesterification reaction. It may be gratifying to note the coordinated tert-butanol plays an important role also in ring opening polymerization of epoxides [25]. A similar enhancement in activity in the presence of coordinated tert.-butanol is observed even in the present case.

5.3.5.3. Kinetic Study

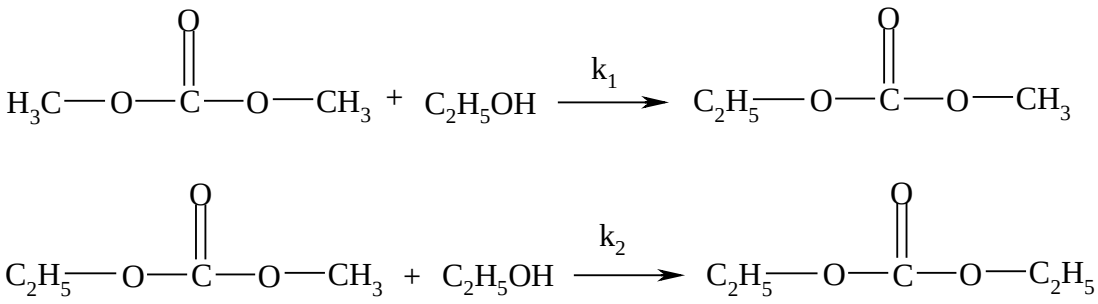

Scheme 5.4

The transesterification of DMC with ethanol (EtOH) involves two consecutive equilibrium steps: (1) formation of methyl ethyl carbonate (MEC) from dimethyl carbonate (DMC) and (2) formation of diethyl carbonate (DEC) from MEC (Scheme 5.4). In this experiment alcohol was taken in excess. This reaction can be treated as a psuedo-first-order series reaction with MEC as intermediate product. The rate constants were determined using the following equations:

$$C_A/C_{A0} = e^{-k_1 t}$$

$$C_R/C_{A0} = k_1(e^{-k_1 t} - e^{-k_2 t})/(k_2 - k_1)$$

where C_{A0} and C_A are the concentrations of DMC at t = 0 and at time t, respectively, C_R is the concentration of the intermediate product MEC at time t, and k_1 and k_2 are the rate constants for the first- and second-steps, respectively. The concentration profiles of DMC, MEC and DEC at two temperatures (413 and 423 K) and two EtOH/DMC concentration ratios (4 and 6 mol/mol) in the transesterification reaction of DMC with ethanol are presented in Fig. 5.10. The profiles are those expected for typical first-order consecutive reactions. The nature of the profile, especially that for MEC, depends on the relative values of k_1 and k_2. Energy of activation and rate constants (k_1 and k_2) are

listed in Table 5.5. Reaction temperature and EtOH/DMC ratio affected the concentration of MEC (Fig. 5.10).

Table 5.5. Kinetics parameters for transesterification of DMC with ethanol

DMC/EtOH (molar ratio)	Temperture (K)	Rate constant h^{-1} (10^{-3})		E_a (kJ/mole)
		k_1	k_2	
1:4	413	20	19	2.06
1:4	423	29	28	
1:6	413	22	21	1.87
1:6	423	29	28	

5.3.6. Comparative Study of the Transesterification of Propene Carbonate over Fe-Zn-1 and TS-1 catalysts

In this chapter propene carbonate was transesterfied with different alcohols over two types of catalysts *viz.*, titanosilicates (TS-1, Ti-MCM-41 and amorphous TiO_2-SiO_2) and double metal cyanide complexes (Fe-Zn-1) and the results are presented in Tables 5.1 and 5.2, respectively. As evident from Table 5.1, the reaction did not proceed over microporous TS-1 catalysts. A little conversion was observed over mesoporous Ti-MCM-41. Amorphous TiO_2-SiO_2 having the highest acidity (NH_3 desorbed = 0.175 mmol/g catalyst) compared to TS-1 (NH_3 desorbed = 0.118 mmol/g catalyst) and Ti-MCM-41 (NH_3 desorbed = 0.160 mmol/g catalyst) showed the highest

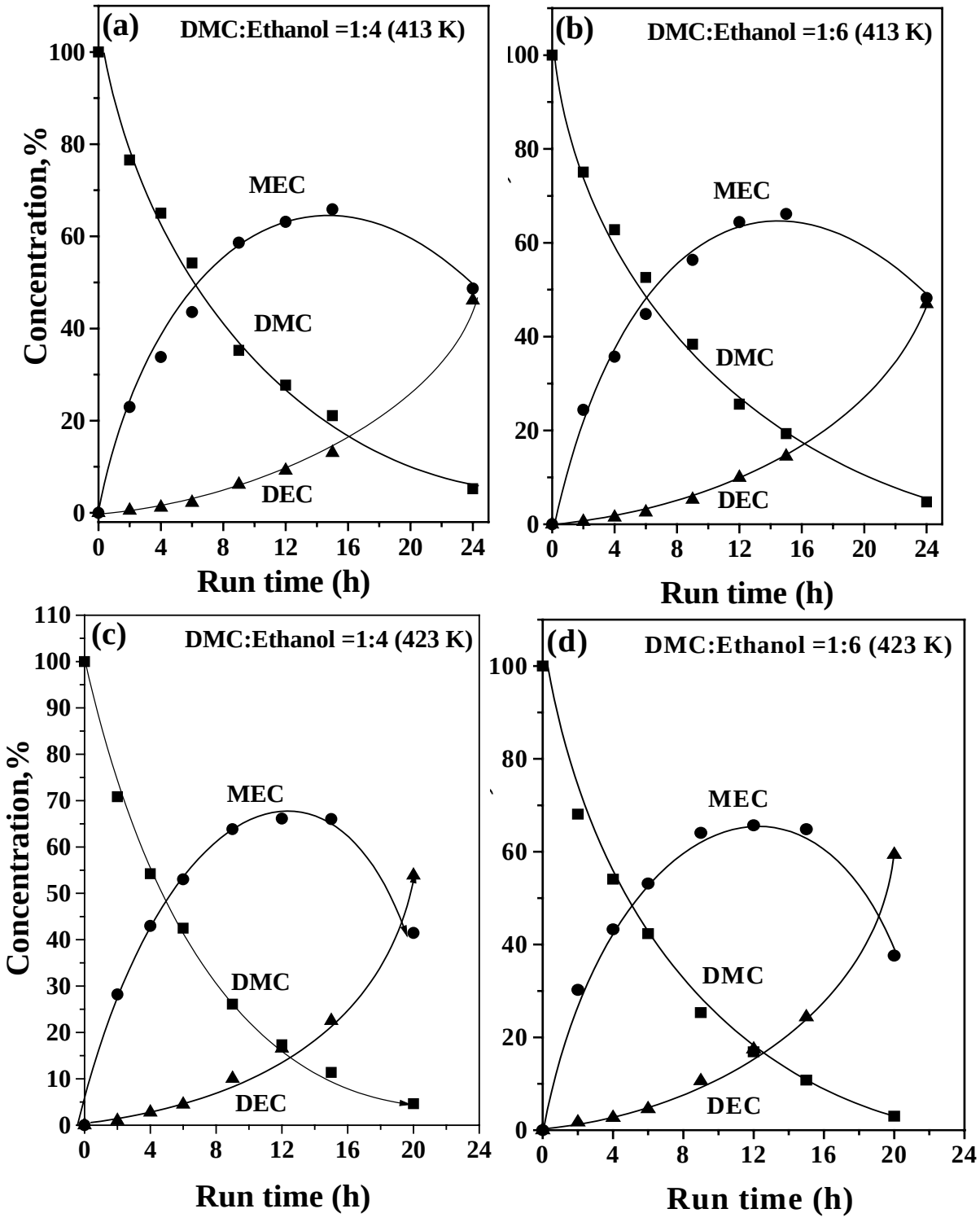

Fig. 5.10. Kinetics plots for the reaction of DMC with EtOH: (a) DMC: EtOH = 1:4 at 413 K, (b) DMC: EtOH = 1:6 at 413 K, (c) DMC: EtOH = 1:4 at 423 K and (d) DMC: EtOH = 1:6 at 423 K.

catalytic activity (propene carbonate conversion: nil over TS-1 (in 2 h), 5.1% over Ti-MCM-41 (in 2 h) and 71.4% over amorphous TiO_2-SiO_2 (in 4 h)). Conversions are higher over Fe-Zn-1 catalyst than on titanosilicate catalysts. Acidity (NH_3 desorbed = 1.97 mmol/g catalyst) of Fe-Zn-1 catalysts is higher than that of titanosilicates. The stronger Lewis acid sites present only on the former type of catalysts are possibly the cause for their superior activity in transesterification reactions. There have been several reports on the direct synthesis of DMC from epoxides, CO_2 and methanol in a one-pot reaction [16]. However, the yield of DMC in those studies was very poor. DMC synthesis by transesterification of cyclic carbonates with methanol, seems to be a more efficient way of its synthesis.

Having found that titanomolecular sieves and double metal cyanides catalyze transesterification of organic carbonates, the study is extended further to various other important transesterification reactions.

5.3.7. Transesterification of Monoester –Ethylacetoacetate (EAA) over TS-1

Acetoacetylated materials are of interest as chemical intermediates in the pharmaceutical, agrochemical, chemical and polymer industries. The reaction did not take place (at this experimental conditions) in the absence of TS-1 or with Ti-free silicalite samples indicating that the acid sites associated with substituted Ti are the active sites in the reactions. Fig. 5.11 shows the catalytic activity of TS-1 in the transesterification of EAA with n-butanol (Scheme 5.5) at room (298 K) and elevated (383 K) temperatures. TS-1 exhibits high activity in the transesterification reaction. About 70% EAA conversion, with 94% transester selectivity was achieved in the initial 1 h itself. Complete conversion of EAA was obtained at the end of 4 h. However, the transester selectivity decreased to about 84%. Mechanistic studies [26] suggested that this reaction proceeds via the intermediacy of acetylketene. During the initial hours,

transester is the major product. As the reaction continued further, the EAA conversion increased but the formation of side product, cyclic lactone also increased.

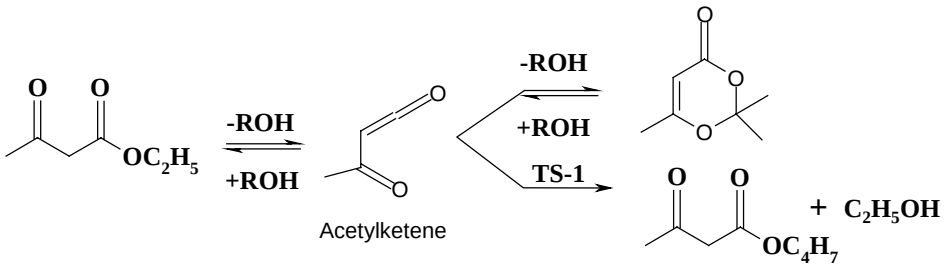

Scheme 5.5. Transesterfication of ethylacetoacetate (EAA) with alcohol.

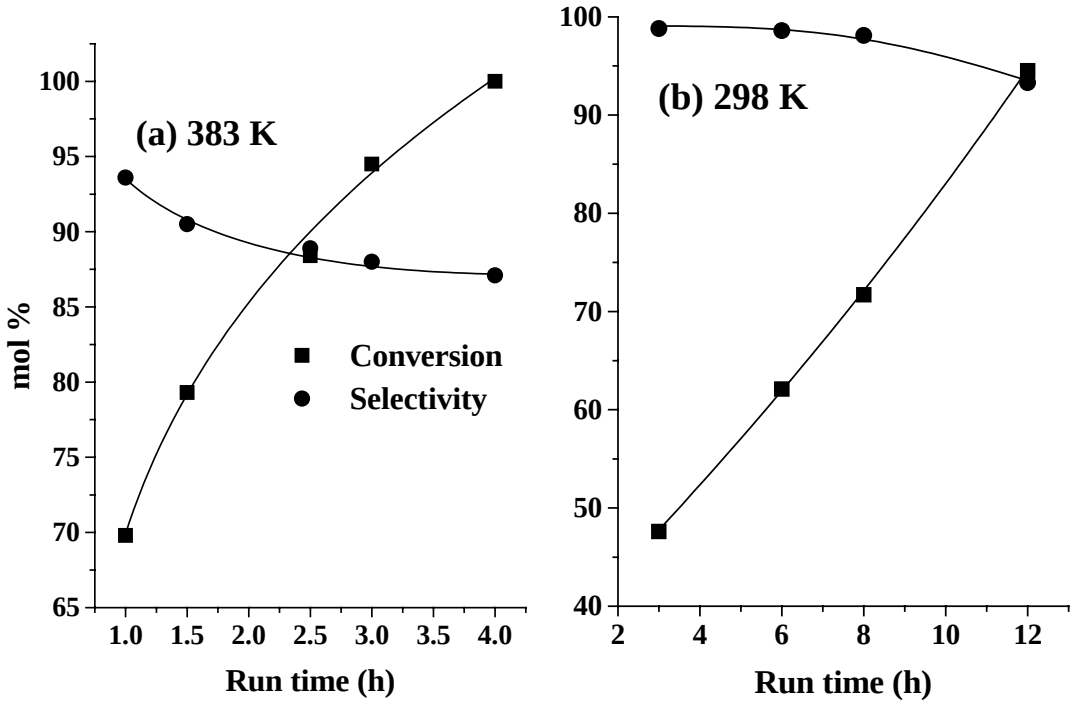

Fig. 5.11. Catalytic activities of TS-1 in transesterification of ethylacetoacetate (EAA) with n-butanol at (a) 383K and (b) 298 K. Reaction conditions: EAA, 5 mmol; n-butanol, 15 mmol; TS-1, 130 mg, reaction time = 4 h.

Upon fine-tuning the reaction conditions the side product can be eliminated. If the reaction was performed at 298 K (EAA conversion = 47% and transester selectivity = 100% at 1 h) no cyclic lactone was observed in the initial hours. Complete EAA

conversions were obtained at longer hours (~ 12 h) at 298 K instead of 4 h at 383 K. Table 5.6 shows that the transesterification of EAA can be performed with various alcohols with high efficiency over TS-1. Allylic acetoacetates are difficult to prepare because of facile decarboxylated rearrangement (Carrol rearrangement) [26]. TS-1 shows good activity for this reaction also (Table 5.6; entry 8).

Table 5.6. Reaction of ethylacetoacetate (EAA) with alcohols (ROH) over TS-1[a]

Entry	ROH	Transester product	Conv., (EAA mol%)	Product yield %
1	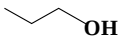	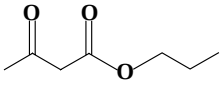	95.6	92.9
2	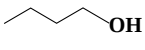	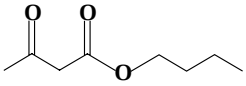	100	87.1
3	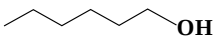	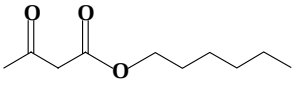	97.6	90.7
4	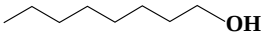	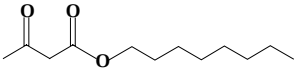	99.2	85.0
5		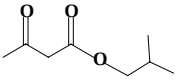	96.2	84.3
6	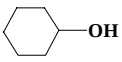	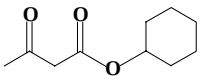	96.4	95.3
7	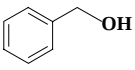	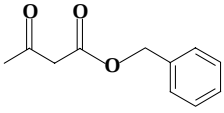	86.4	69.5
8	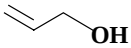	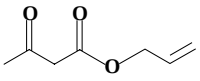	83.1	66.9
9	$CH_3(CH_2)_7CH=CH(CH_2)_7CH_2OH$	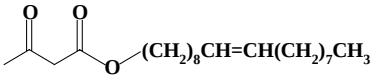		87.6[b]

[a]*Reaction conditions:* Catalyst (TS-1; Si/Ti = 33), 130 mg; EAA, 5 mmol; ROH, 15 mmol; temperature = 383 K, run time = 4 h.

[b] Isolated yield.

5.3.8. Transesterification of Diester – Diethylmalonate (DEM) over TS-1

TS-1 exhibits high activity in the reaction of DEM with various alcohols (Scheme 5.6). With DEM and n-butanol, about 85% DEM conversion could be achieved in the initial 3 h over TS-1; mono to diester selectivity was 70:30.

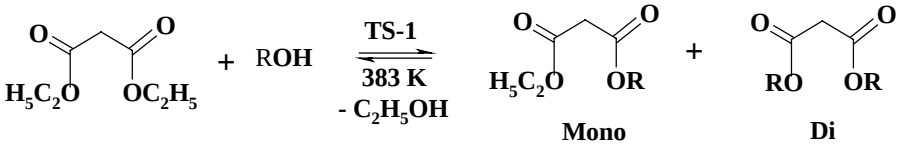

Scheme 5.6. Transesterification of diethylmalonate (DEM) with alcohols.

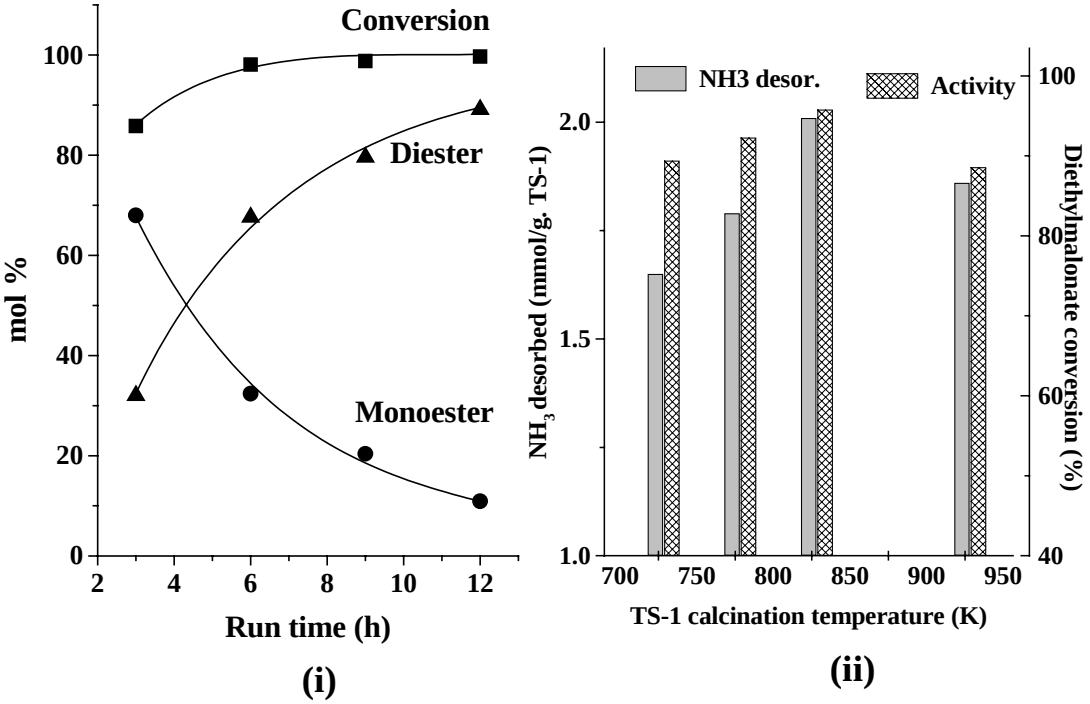

Fig. 5.12. (i) Transesterification of diethylmalonate (DEM) with n-butanol at 383 K. Reaction conditions: DEM, 5 mmol; n-butanol, 15 mmol; TS-1, 130 mg, temperature = 383 K, reaction time = 12 h. (ii) Total NH_3 desorbed in TPD and catalytic activity (DEM conversion) in the transesterification of DEM with n-butanol (at 383 K) over TS-1 catalysts calcined at different temperatures. Reaction conditions: same as in (i) except that the temperature = 353 K.

When the reaction was continued for 12 h, complete conversion of DEM and diester selectivity of 90% were achieved (Fig. 5.12 (i)). Entries 4 and 5 in Table 5.7 shows that the catalyst can be reused. No loss in activity and product selectivity was observed. Transesterifications were performed with various alcohols. Complete conversion of DEM was achieved in 12 h but the product selectivity (monoester/diester) depended on the alcohol group. The conversion was lower (84%) with benzyl alcohol (Table 5.7, entry 10), probably due to diffusional limitations in micropores of TS-1. On TS-1 samples calcined at different temperatures (723 – 923 K) activity (DEM conversion) varied with the acidity of the catalysts (Fig. 5.12 (ii)).

Table 5.7. Transesterification of diethyl malonate (DEM) with various alcohols (ROH) over TS-1[a]

ROH	DEM conversion, mol%	Total transester selectivity, %	Products distribution, %	
			Mono	Di
n-propanol	97.5	98.4	26.6	73.4
n-butanol	99.3	97.0	16.0	84.0
n-butanol[b]	95.8	100	46.4	53.6
n-butanol (**recycle I**)[b]	95.0	100	45.9	54.1
n-butanol (**recycle II**)[b]	94.4	100	46.6	53.4
n-hexanol	99.7	100	10.9	89.1
n-octanol	100	100	82.6	17.4
Iso-butanol	95.6	96.3	58.0	42.0
Cyclohexanol	100	100	34.4	65.6
Benzyl alcohol	84.2	88.8	39.0	61.0

[a]*Reaction conditions:* Catalyst (TS-1; Si/Ti = 33), 130 mg; DEM, 5 mmol (0.8 g); ROH, 15 mmol; temperature = 383 K, run time = 12 h. [b]Reaction conditions: Same as in "a" except the temperature = 353 K.

5.3.9. Comparative Activity of Titanosilicates in Transesterification Reactions

DRIFT spectroscopy of adsorbed pyridine and NH_3-TPD study reveals that the amorphous TiO_2-SiO_2 has more acidity as compared to TS-1 and Ti-MCM-41 (Figs. 5.1 and 5.2). Table 5.8 demonstrates the influence of catalyst structure/acidity on transesterification of (a) EAA with benzyl alcohol and allyl alcohol and (b) DEM with n-butanol. The efficiency and transester yield increase with acidity and catalyst structure in the order: TS-1 < Ti-MCM-41 < amorphous TiO_2-SiO_2.

Table 5.8. Comparative activity of TS-1, Ti-MCM-41 and amorphous TiO_2-SiO_2 in transesterification of (a) ethylacetoacetate with benzyl alcohol and allylalcohol and (b) diethylmalonate with n-butanol[a]

(a) Ester – Ethylacetoacetate (Run time = 4 h)				
Catalyst	Benzyl alcohol		Allylalcohol	
	Ester conversion, mol %	Transester yield, %	Ester conversion, mol %	Transester yield, %
TS-1	86.4	69.5	83.1	69.8
Ti-MCM-41	93.7	90.2	85.2	84.5
Amorphous TiO_2-SiO_2	95.2	91.9	87.3	86.1

(b) Ester – Diethylmalonate (Run time = 12 h); Alcohol – n-butanol				
Catalyst	Ester conversion, mol %	Transester yield, %	Monotransester selectivity %	Ditransester selectivity %
TS-1	58.2	57.4	59.0	41.0
Ti-MCM-41	66.5	65.6	87.2	12.8
Amorphous TiO_2-SiO_2	68.6	66.7	89.2	10.8

[a]*Reaction conditions:* Ester, 5 mmol; alcohol, 15 mmol; catalyst, 130 mg; temperature, 383 K.

5.3.10. Transesterification of Vegetable Oils over Fe-Zn-based Double Metal Cyanide Catalysts

The diminishing natural oil resources and environmental advantages of biofuels over the conventional petroleum-based fuels have led to intense research worldwide on the production of bio-fuels. Alkaline metal alkoxides (CH_3ONa) are the most active catalyst for this reaction; high yields (>98%) of transester are obtained in short contact times (30 min) [27]. The operation however, requires absence of water, which makes it inappropriate for typical industrial processes. Alkali hydroxides (NaOH and KOH) are cheaper than metal alkoxides but more amount of catalyst is needed (1 – 2 mol%) [28, 29]. NaOH is more superior to KOH; latter and other alkali hydroxides yield more soponified products than bio-diesel. In the commercial process fat or oil is reacted with an alcohol like methanol (methanolysis), in the presence of an alkali catalyst to produce glycerol and methyl esters or bio-diesel. Methanol is charged in excess to assist a quick conversion. The unreacted alcohol is recovered and reused. At the end of the reaction the base catalyst is neutralized with mineral acid and separated by washing the products with water. During this process saponified products are formed and complicate the bio-diesel recovery. Cost is the major factor slowing the commercialization of bio-diesel. Replacement of homogeneous catalyst by a solid, base catalyst eliminates the processing costs associated with the homogeneous catalysts. At the end of the reaction the solid catalyst can be recovered by simple filtration from the product mixture and reused. There have been some reports on the use of zeolites [30], immobilized enzymes [31] and metal oxides [32] as heterogeneous catalysts for this reaction.

In the present section, the activity of double metal cyanide catalysts (Fe-Zn-1) for transesterification of triglycerides of vegetable oils into fatty acid esters for bio-

diesel and lubricant applications is investigated (Scheme 5.7). Vegetable oils such as coconut oil, sunflower oil, soyabean oil and margarine oil were transesterified with C1 to C8-alcohols.

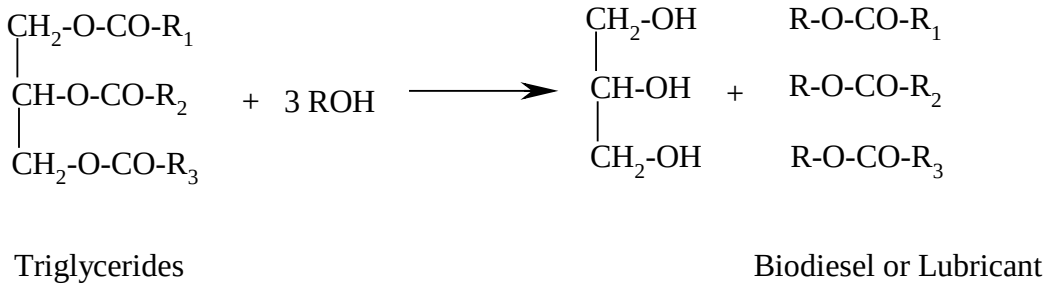

Scheme 5.7. Synthesis of bio-diesel from vegitable oils

5.3.10.1. Synthesis of bio-diesel

To start with oil-methanol mixture is cloudy and during reaction it converted into a transparent liquid. Methyl esters were less viscous than the original unesterified oil. A description of the physical state of reaction mixture of different oils is given in Table 5.9. Isolated yield of glycerol was used for estimating the vegetable oil conversion. Glycerol forms about 10 wt% of the unesterified oil. The catalyst shows extremely high activity for the transesterification reaction. Conversion of oil based on isolated glycerol is above 90% (Table 5.10). There could be some amount of diglyceride and monoglyceride components in the products mixture, which could not be estimated. These products could be identified only by HPLC technique. However, their concentrations in the present case are believed to be very low as the isolated glycerol itself is more than 90%. The fatty acid alkyl esters selectivity is as per the expected value.

Table 5.9. Physical state of reaction mixture (oil + methanol) before and after the reaction

Oil	Reaction mixture at ambient condition	At hot condition	After reaction at room temperature	Isolated ester product	Viscous nature
Sunflower oil	Liquid, cloudy	Cloudy /transparent	Transparent	Liquid, transparent	Less viscous than oil
Coconut oil	Liquid, cloudy	Cloudy /transparent	Transparent	Liquid containing solid portion transparent	Less viscous than oil
Margarine oil	Liquid, cloudy	Cloudy transparent	Transparent	Liquid transparent	Less viscous than oil

Sunflower oil is a triglyceride of C16 (palmitic) and C18 (stearic, oleic and linoleic) acids. Coconut oil is a triglyceride of C9 (caprilic), C10 (capric), C12 (lauric), C14 (myristic), C16 (palmitic) and C18 (stearic, oleic and linoleic) acids. Margarine oil is a triglyceride of C16 (palmitic) and C18 (stearic, oleic and linoleic) acids. The solid catalyst could be reused with no loss in activity (Table 5.10). Used oils contain free fatty acids in addition to the fatty acid triglyceride. Commercially, transesterification of cooked oils is done in two-states. In stage-1, the used oil is first esterified with an acid catalyst. This mixture is then used in stage-2 for transesterification using a base catalyst

(alkali salt or alkali methoxide, for example). However, it has been observed that over Fe-Zn-1 catalyst the reaction can be performed in a single-stage. Used oil could be transesterified forming high amounts of fatty acid alkyl esters. The catalyst exhibited almost similar activity for both the used and unused oils and in recycling experiments (Table 5.10).

5.3.10.2. Synthesis of Bio-lubricants

Fatty acid alkyl esters having 22 to 26 carbon atoms come under the category of lubricants. Transesterification of vegetable oils with C6 – C8 alcohols yields fatty acid esters applicable for lubricants purpose. Apart from their use in automobile industry, biolubricants find applications also in the manufacture of cosmetics, feedstuffs, soaps etc. Recently, there have been efforts to develop bio-based lubricants that are more stable toward oxidation and cold temperature. Biolubricants are renewable, biodegradable, less environmentally hazardous and safer to human contact unlike the petroleum-based lubricants and oils. The catalysts are highly active even in this transesterification reaction and triglyceride ester conversion of more than 90% was obtained (Table 5.11). The physical properties of fatty acid octyl esters obtained by transesterification of sunflower oil with octanol over Fe-Zn-1 catalyst are listed in Table 5.12. The studies reveal that the fatty acid octyl esters possess the desired properties for lubricants application.

Table 5.10. Biodiesel production: catalytic activity of Fe-Zn-1

Entry No.	Oil	Alcohol	Oil conversion based on isolated glycerol yield (mol%)	Alkyl esters selectivity (mol%)
1	Coconut oil	Methanol	92.5	Methyl caprilic ester (8.7%)+ Methyl capric ester (5.8) + Methyl lauric ester (45.6) + methyl myristic ester (18.4) + Methyl Palmitic ester (7.9%) + Methyl (oleate + stereate+linoleate) esters (13.7)
2	Sunflower oil	Methanol	92.3	Methyl Palmitic ester (6.8%) + Methyl (oleate + stereate+linoleate) esters (92.0)
3	Soybean oil	Methanol	92.0	Methyl esters (99%)
4	Margarine	Methanol	93.0	Methyl palmitate (10.1%) + Methyl (oleate + stereate+linoleate) esters (88.2)
5	Used/Cooked margarine	Methanol	92.8	Methyl palmitate (10%) + Methyl (oleate + stereate + linoleate) esters (88.0)
6	Coconut oil	Butanol	92.0	Butyl caprilic ester (9.5%)+ Butyl capric ester (8.0) + Butyl lauric ester (45.1) + Butyl myristic ester (19.6) + Butyl palmitic ester (9.2%) + Bytyl (oleate + stereate+linoleate) esters (8.3)
7	Sunflower oil	Butanol	91.0	Butyl palmitic ester (8.7%) + Butyl (oleate + stereate+linoleate) esters (91.1)
8	Margarine	Propanol	93.7	Propyl palmitate (12.7%) + Propyl (oleate + stereate+linoleate) esters (86.5)
9	Margarine	Butanol	92.1	Butyl palmitate (13.5%) + Butyl (oleate + stereate+linoleate) esters (86.0)

Table 5.11. Lubricants preparation: catalytic activity data

Entry No.	Oil	Alcohol	Conversion of triglycerides into glycerol (mol%)	Alkyl esters selectivity (mol%)
2	Coconut oil	Octanol	92.5	Octyl laurate (40.5%) Octyl myristate (22%) Octyl palmitate (11%) Octyl oleate + Octyl stereate + Octyl linoleate (13.6%)
3	Sunflower oil	Octanol	91.0	Octyl palmitate (7.9%) Octyl oleate + Octyl stereate + Octyl linoleate (92.1%)
4	Soybean oil	Octanol	92.0	Octyl esters (99%)
5	Margarine	Octanol	91.0	Octyl palmitate (13.8%) Octyl oleate + Octyl stereate + Octyl linoleate (86.2%)
6	Margarine	Hexanol	91.0	Octyl palmitate (12.7%) Octyl oleate + Octyl stereate + Octyl linoleate (84.2%)
7	Margarine-used/cooked oil	Octanol	92.0	Octyl palmitate (13.8%) Octyl oleate + Octyl stereate + Octyl linoleate (86.2%)
8	Margarine	Octanol	96.0	Octyl palmitate (13.8%) Octyl oleate + Octyl stereate + Octyl linoleate (86.2%)

Table 5.12. Physical properties of fatty acid octyl esters prepared from sunflower oil

S.No.	Test	Method	Result
1	Kinematic Viscosity, at 313 K, cst	IS:1448[P:25]	7.93
2	Kinematic Viscosity, at 373 K, cst	IS:1448[P:25]	2.74
3	Viscosity Index	IS:1448[P:56]	226
4	Density at 288 K	ASTM D 4052	0.8813
5	Pour Point, °C	IS:1448[P:10]	(-)3
6	Copper strip corrosion, at 373 K for 3 hours	IS:1448[P:15]	No.1
7	Total Acid number, mg KOH/g	IS:1448[P:1]	0.76
8	Rotary Bomb Oxidation test (RoBOT), Induction period, in minutes, at 373 K	ASTM D 4742	23
9	Lubricity on HFRR, Friction coefficient, Load 2N, 333 K	ISO 12156	280 μ
10	Lubricity on HFRR, wear scar dia, Load 2N, 333 K	ISO 12156	180 micro
11	Lubricity on HFRR, contact potential, Load 2N, 333 K	ISO 12156	44-48 mV

5.4. Conclusions

Catalytic activities of titanosilicates (microporous TS-1, mesoporous Ti-MCM-41 and amorphous TiO_2-SiO_2) and double metal cyanide Fe-Zn complexes for the synthesis of organic dialkyl carbonates by transesterification reaction was reported. The activity of these catalysts was investigated also for the transesterification of ethylacetoacetate (a monoester), diethylmalonate (a diester) and vegetable oils (a triester). While the titanosilicates showed efficient activity for the transesterification of ethylacetoacetate and diethylmalonate, Fe-Zn catalysts (having stronger acid sites) were found superior in reactions of organic carbonates and vegetable oils. The studies revealed that transesterification is an efficient pathway for the synthesis of dialkyl carbonates (DMC, for examples) as compared to the one-pot synthesis involving the

reaction of epoxides, CO_2 and alcohols. The catalysts are efficient in recycling experiments. The structure of the catalyst, amount and type of acidity and the method of preparation influenced the catalytic activity. Reusability and good activity at mild conditions makes these solid catalysts efficient for transesterification reactions and for the eco-friendly synthesis of organic carbonates. The GC charts of the product esters obtained from different oils and the ^{1}H NMR spectra of different isolated dialkyl carbonates are shown in Appendices-5.A and 5.B, respectively.

5.5. References

1. J. Otera, N. Dan-Oh, J. Nozaki, J. Org. Chem. 56 (1991) 5307.
2. B.C. Ranu, P. Dutta, A. Sarkar, J. Org. Chem. 63 (1998) 6027.
3. B.P. Bandgar, V.S. Sadavarte, L.S. Uppalla, Synlett (2001)1338.
4. G. Shapiro, M. Marzi, J. Org. Chem. 62 (1997) 7096.
5. P.S. Chavan, P.K. Zubaidha, S.W. Dantale, A. keshavaraja, A.V. Ramaswamy, T. Ravindranathan, Tetrahedron Lett. 37 (1996) 233.
6. B.P. Bandgar, L.S. Uppalla, V.S. Sadavarte, Green Chem. 3 (2001) 39.
7. B.P. Bandgar, N.B. Gaikwad, Monatsh. Chem. 129 (1998) 719.
8. S.P. Chavan, Y.T. Subbarao, R. Sivappa, Synth. Commun. 31 (2001) 289.
9. A. Cordova, K.D. Janda, J. Org. Chem. 66 (2001) 1906.
10. M. Sasidharan, R. Kumar, J. Mol. Catal. A: Chem 210 (2004) 93.
11. B. M. Choudary, M. L. Kantam, C. V. Reddy, S. Aranganathan, P. L. Santhi, F. Figueras, J. Mol. Catal. A: Chem 159 (2000) 411.
12. (a) D.M. Fenton, P.J. Steinwand, J. Org. Chem. 39 (1974) 701. (b) M. Graziani, P. Uguagliati, G. Carturan, J. Organometallic Chem. 27 (1971) 275.
13. T. Tatsumi, Y. Watanabe, K. A. Koyano, Chem. Commun. (1996) 2281.
14. T. Wei, M. Wang, W. Wei, Y. Sun, B. Zhong, Green Chem. 5 (2003) 343.
15. Y. Watanabe, T. Tatsumi, Micro. Mesop. Mater. 22 (1998) 399.
16. B.M. Bhanage, S.-I. Fuzita, Y. Ikushima, K. Torii, M. Arai, Green Chem. 5 (2003) 71.
17. (a) G. Vicente, M. Martinez, J. Aracil, Bioresource Tech. 92 (2004) 297. (b) F. R. Abreu, M. B. Alves, C. C. S Macedo, L. F. Zara, P. A. Z. Suarez, J. Mol. Catal. A: Chem. 227 (2005) 263. (c) F. R. Abreu, D. G. Lima, E. H. Hamu, C. Wolf, P.

A. Z. Suaraz, J. Mol. Catal. A: Chem. 209 (2004) 29.

18. (a) H-J Kim, B-S Kang, M-J Kim, Y. M. Park, D-K Kim, J-S Lee, K-Y Lee, Catal. Today 93-95 (2004) 315. (b) S. Furuta, H. Matsuhashi, K. Arata, Catal. Commun. 5 (2004) 721.
19. P. Ratnasamy, D. Srinivas, H. Knözinger, Adv. Catal. 48 (2004) 1.
20. (a) R. J. Herold, US Patent 3,278,459, 1966 (b) J. Milgrom, US Patent 3,404,109, 1968.
21. (a) S. D. Harper EP 283148, 1988 (b) H. R. Hinney, D. S. Wardius, US Patent 5,158,922, 1992 (c) B. Le-Khac, US Patent 5,470,813, 1995.
22. H. van der Hulst, G. A, Pogany, J. Kuyper, US Patent 4,477,589, 1984.
23. (a) H. T. Takeyasu, T. Watabe, T. Doi, JP 2,265,921, 1990. (b) T. Watabe, H. Takeyasu, T. Doi, N. Kunii, Eur Pat Appl EP 383,333, 1990.
24. B. Le-Khac, US Patent 5,789,626, 1998.
25. Il Kim, J-T. Ahn, C. S. Ha, C. S. Yang, I. Park, Polymer 44 (2003) 3417.
26. J.S. Witzeman, W.D. Nottingham, J. Org. Chem. 56 (1991) 1713.
27. B. Freedom, E. H. Pryde, T. L. Mounts, J. Am. Oil. Chem. Soc. 61 (1984) 1638.
28. J. Cvengros, F. Povazanec, Bioresour. Technol. 55 (1996) 145.
29. G. Antolin, F. V. Tinaut, Y. Briceno, V. Castano, C. Perez, A. I. Ramirez, Bioresour. Technol. 83 (2002) 111.
30. Y. Shimada, Y. Watanabe, A. Sugihara, Y. Tominaga, J. Mol. Catal. B: Enzymatic 17 (2002) 133.
31. G. J. Suppes, M. A. Dasari, E. J. Doskocil, P. J. Mankidy, M. J. Goff, Appl. Catal. A: Gen. 257 (2004) 213.
32. E.Leclercq, A. Finiels, C. Moreau, J. Am. Oil. Chem. Soc. 78 (2001) 1161.

Appendix-5.A

GC Charts: Fatty acid methyl esters (top), fatty acid butyl esters (middle) and fatty acid octyl esters (bottom) prepared from coconut oil by transesterification reaction

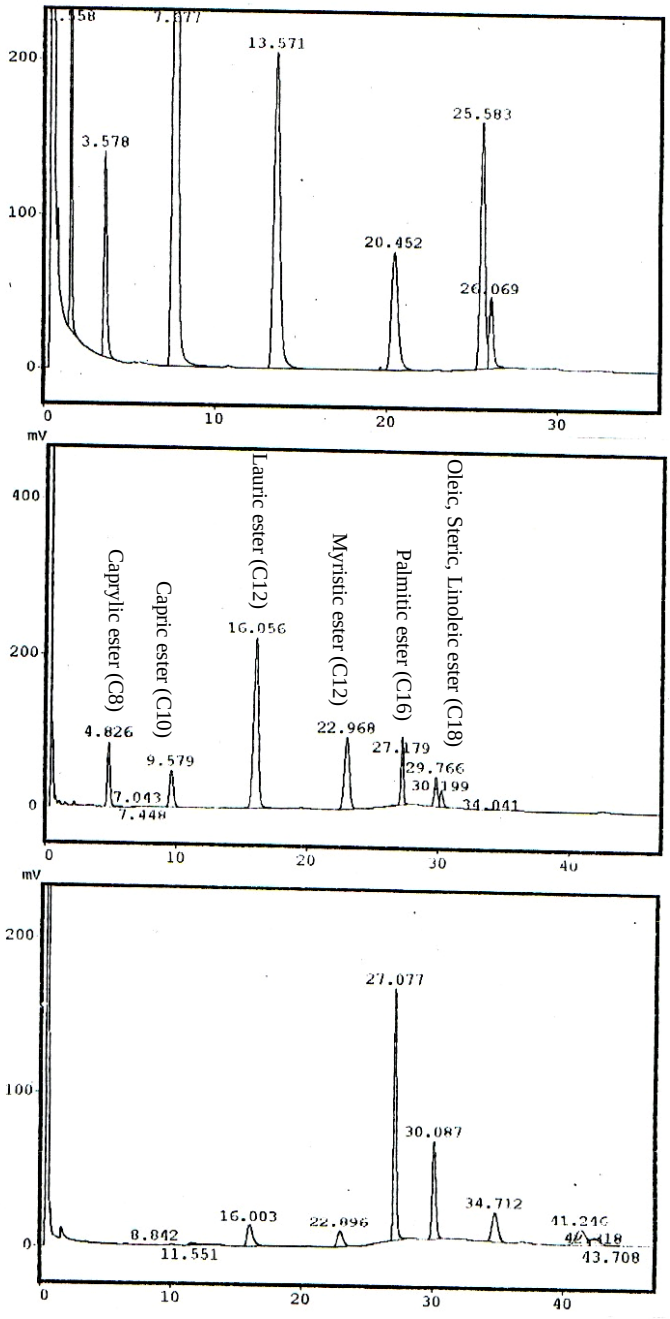

Appendix-5.A (contd.)

GC-Chart: Fatty acid methyl esters (top), Fatty acid butyl esters (middle), fatty acid octyl esters (borrom) prepared from sunflower oil

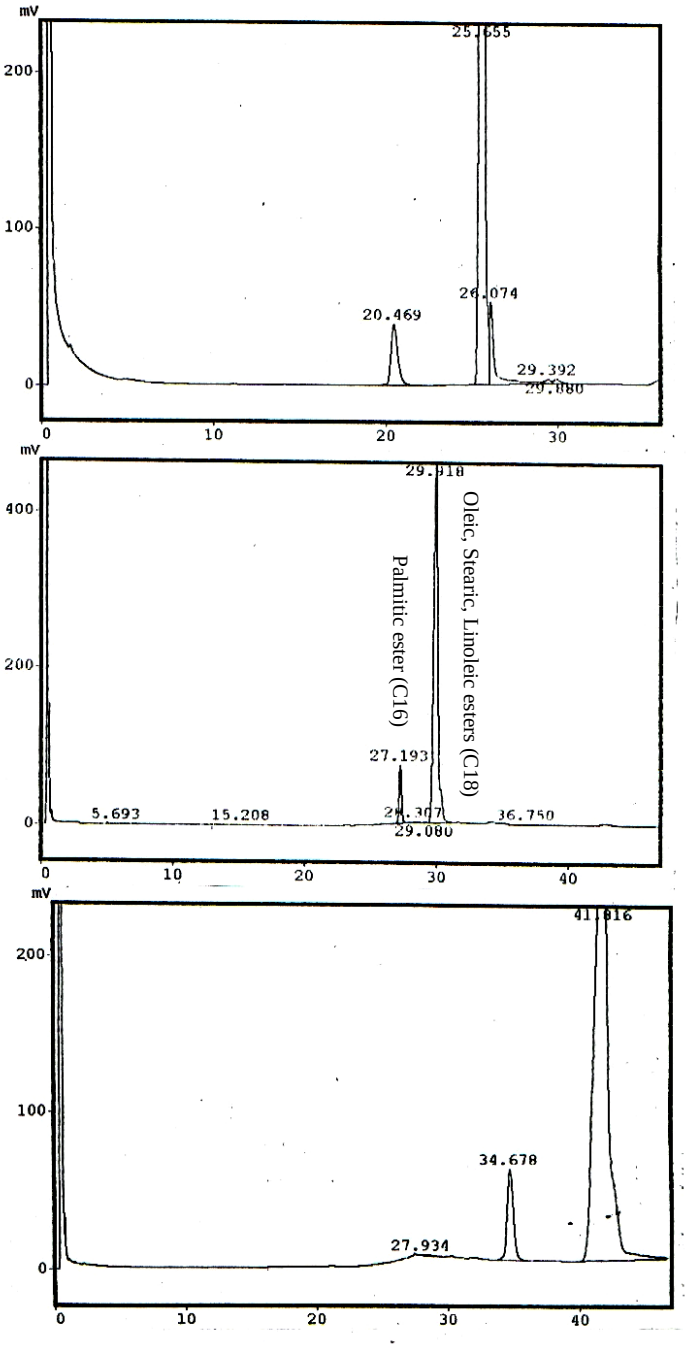

Appendix-5.A (contd.)

GC-Chart: Fatty acid methyl esters (top), fatty acid butyl esters (middle), fatty acid octyl esters (bottom) prepared from margarine oil

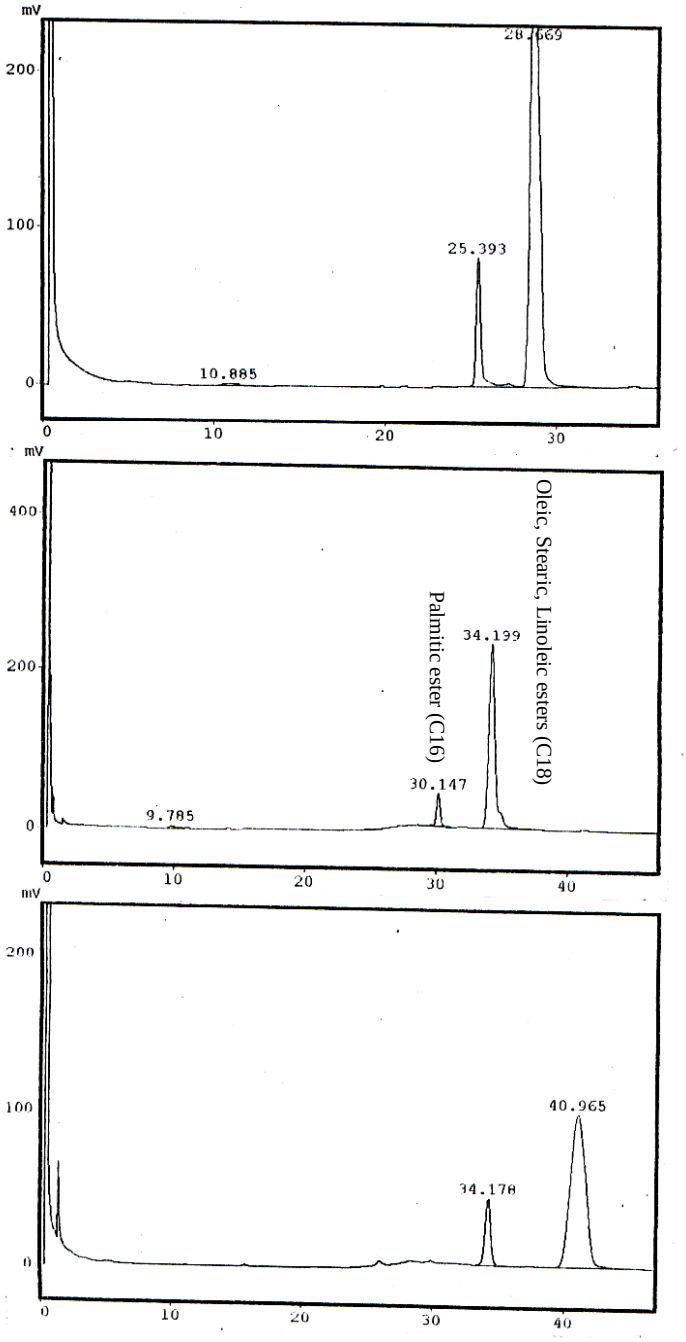

Appendix-5.B

^{1}H NMR spectra (Bruker Avance 200 MHz, in $CDCl_3$) of: dimethyl carbonate (top), diethyl carbonate (middle) and dipropyl carbonate (bottom) prepared by transesterification reactions

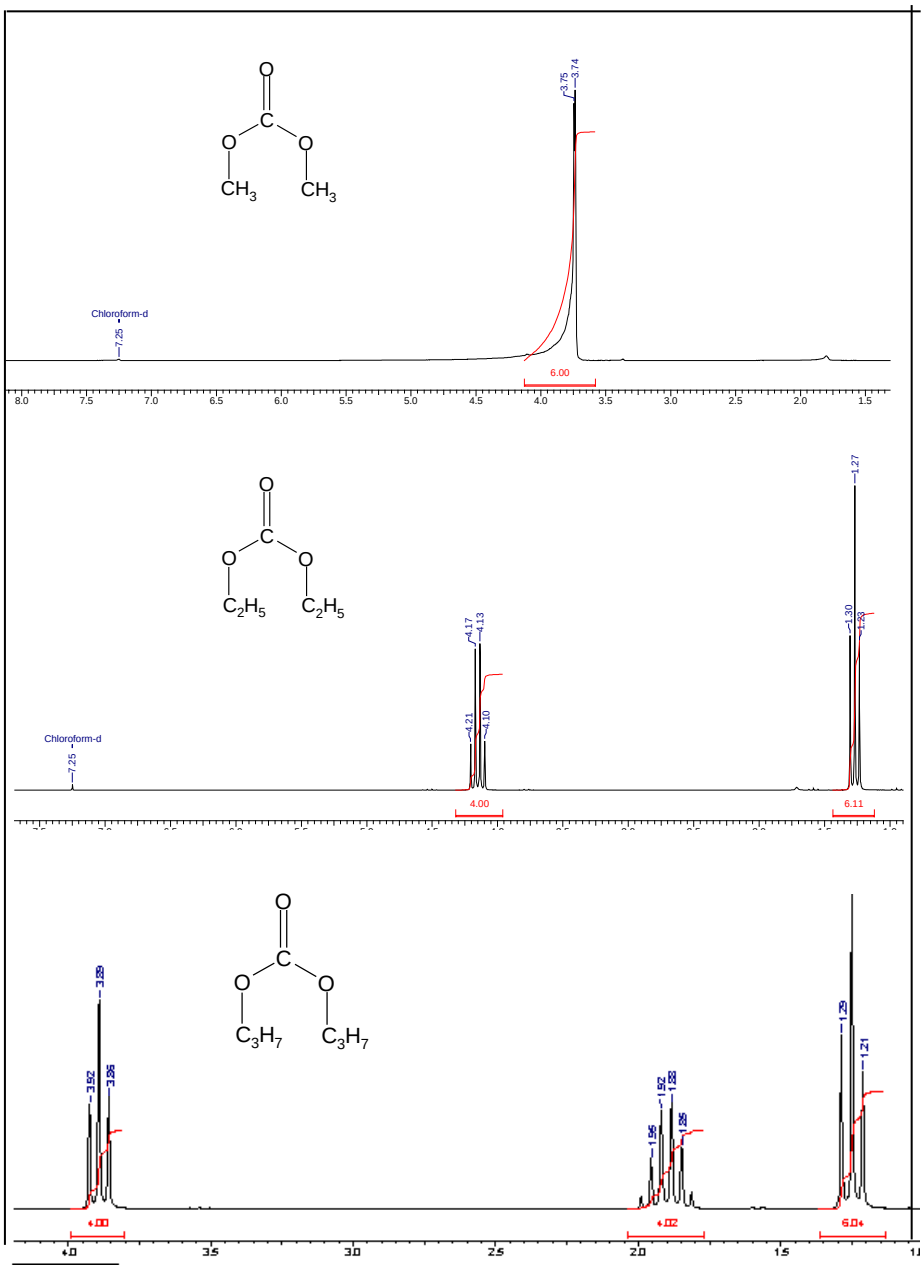

Appendix-5.B (contd.)

^{1}H NMR spectra (Bruker Avance 200 MHz, in $CDCl_3$) of: dibutylcarbonate (top) and dihexyl carbonate (bottom) prepared by transesterification reaction

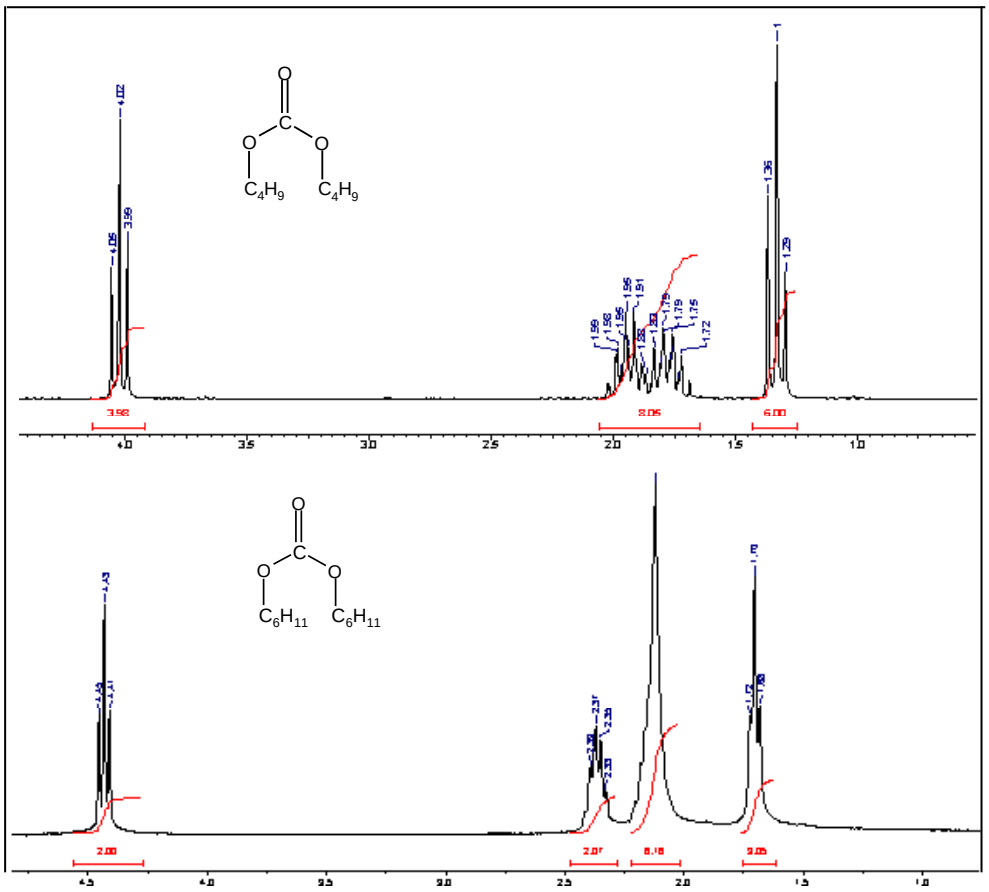

Chapter-6

Activation of Aryl Halides for C-C Coupling Heck Reaction

6.1. Introduction

Transition metal catalyzed carbon-carbon (C-C) coupling is one of the most important reactions in synthetic organic chemistry [1]. Palladium catalyzed C-C bond forming Heck reaction is one of them [2]. The recent applications of Heck reactions include the manufacture of Novartis' Prosulfuron^{TM}- an agrochemical, octyl-p-methoxycinnamte - a sunscreen agent, Albemarle's naproxen - an antibiotic and Singulair - an antiasthma drug [3]. The loss of the catalyst, which usually cannot be recovered and the need of aryl iodides or bromides as starting materials are the major bottlenecks that have prevented a more extensive exploitation of this reaction so far. A major limitation of palladium catalyzed coupling process has been the poor reactivity of aryl chloride. Aryl chlorides are more attractive substrates because they are cheaper and easily available than the corresponding bromides, iodides and triflets. Traditional palladium/triarylphosphene catalysts are only effective for the coupling of certain activated aryl chlorides such as hetero-arylchloride and substrate that bear electron-withdrawing group but not for aryl chloride, in general [4]. Most of the homogeneous Pd complexes are notorious for air and moisture sensitivity, they deactivate fast and it is tedious and not an economical affair to recover and recycle the catalyst. Much attention has been paid to heterogeneous palladium catalysts due to their easy recovery and recycling. Efforts have been made to support Pd on metal oxides, polymers, clay, MCM-41 etc. [5-8]. Cheap transition metals such as Ni and Cu containing materials have also been studied for this reaction [9].

The palladium catalyzed Heck reaction of aryl halide and olefins is generally catalyzed by Pd(0) or Pd(II) complexes (Scheme 6.1) [10]. The objective of the present study is to (1) replace palladium with less expensive transition metal-based catalysts, (2) replace aryl bromide and iodide with cheaper chlorides, (3) eliminate the use of

costly and non-recyclable catalyst system, and (4) utilize heterogeneous, reusable catalyst in place of present homogeneous systems. A new, efficient heterogeneous catalyst is reported here, for the first time, for C-C bond forming reactions.

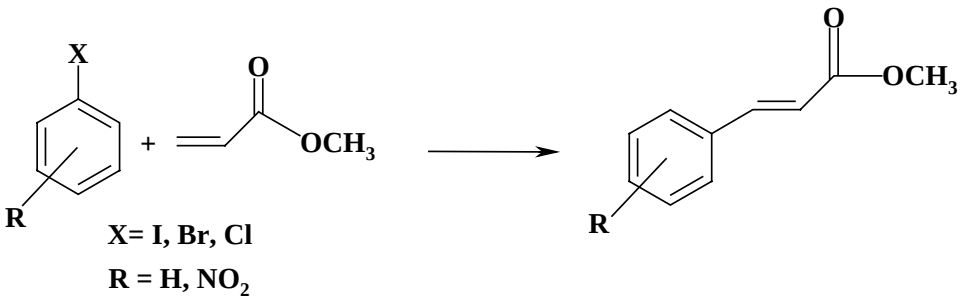

Scheme 6.1. C-C coupling Heck reaction

Literature reveals that Pd supported on basic metal oxide (MgO) is less active than Pd supported on Al_2O_3, SiO_2, mordanite and H-Y [11] due to low metal dispersion and low surface area in case of the former. Pd supported catalyst can be made by ion exchanging zeolites and MCM-41 followed by reduction with hydrogen. Mordenite and H-zeolite are active with high palladium loading. Acidic nature of catalyst makes metal surface less oxidizable than the required one, hence high metal loading is required. It was also found that, MCM-41 (high surface area, silica material) is not suitable for Heck reaction due to less stability [11]. In the present study, Cu, Ni and Pd containing silicoaluminophosphates, SAPO-11, SAPO-31 and SAPO-41 have been prepared. The catalysts were used for the activation of aryl halides and olefins for C-C coupling Heck reaction.

6.2. Silicoaluminophosphate as a Catalyst

SAPO-11 has non-intersecting, 10 member-ring channel with elliptical pore aperture of 0.63 × 0.39 nm. The topology consists of sheets of six-ring-six-ring-four-ring (S6R-S6R-S4R) units (Scheme 6.2). SAPO-31 has uni-dimensional, non-intersecting, 12 member ring channels with circular pore opening of 0.54 × 0.54 nm in

diameter and non-planner layer of alternating S4R and S6R building units. SAPO-41, a medium pore zeolite, has a uni-dimensional elliptical 10-membered ring pore of 0.43 × 0.70 nm in diameter (Scheme 6.2). In fact, the 10-membered ring in SAPO-41 is not strictly elliptical and further more is slightly larger in size than the elliptical 10-membered ring in SAPO-11. IR and TPD studies reveal that the distribution of weak and strong acid sites depends on the mode of Si substitution, the formation of Si-O-Si domain leads to reduced acidity. The acidity varies in the order: SAPO-41 > SAPO-11 > SAPO-31 [12]. SAPOs were found to be most suitable for obtaining high yield of isomerization of long chain alkanes [13]. SAPOs are well documented for alkylation reaction due to its acidic properties [14]. Pt-SAPOs were found to be efficient catalysts for *n*-octane hydroisomersiation [15].

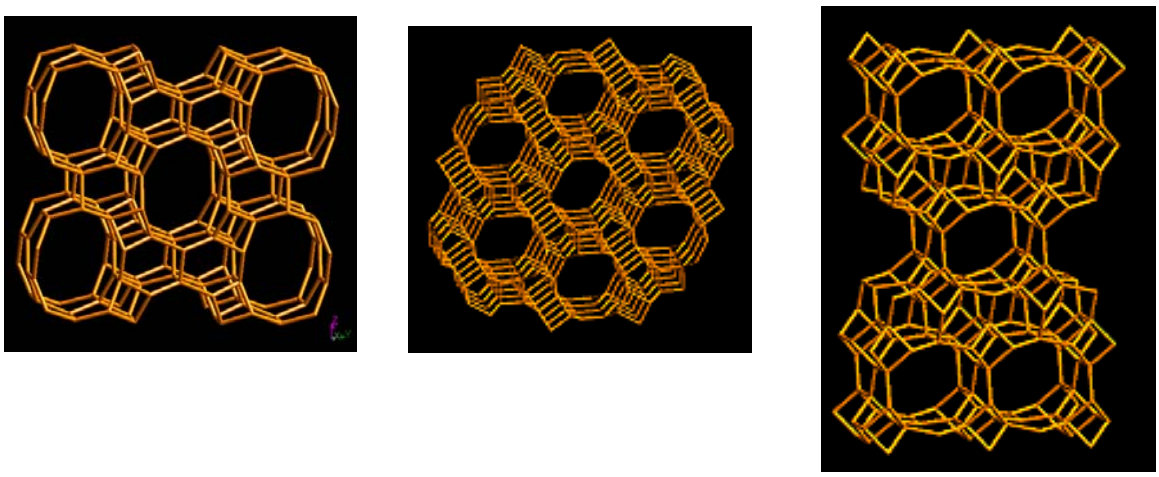

SAPO-11 **SAPO-31** **SAPO-41**

Scheme 6.2. Structural topology of SAPOs.

6.3. Experimental Section

6.3.1. Reaction Procedure

The Heck reactions were carried out in a glass, round bottom flask (25 ml) fitted with a water-cooled condenser. In a typical reaction, halo benzene (1 mmol), methyl acrylate (2 mmol), base (1.5 mmol) and catalyst (4 wt% with respect to halo benzene)

were taken in 5 g of solvent. The reaction was conducted at 333 – 393 K under a nitrogen atmosphere. The progress and completion of the reaction was monitored by gas chromatography. The products were identified by GC-MS, GC-IR and ^{1}H NMR. After the completion of the reaction, the catalyst was filtered, washed with acetonitrile and acetone and dried at 573 K. Water (25 ml) was added to filtrate and the product was extracted with ethyl acetate (30 ml; two times). The organic layer was given dil HCl, water and brine wash and was dried over sodium sulfate. The product obtained after evaporation of the solvent was purified by column chromatography.

Analysis: (E)-Methyl – 3 methyl propenoate

^{1}H NMR ($CDCl_3$) δ ppm: 3.8 (s, 3H), 6.47 (d, 1H J = 16 Hz), 7.39 (m, 3H), 7.5 (m, 2H), 7.65 (d, 1H, J = 14Hz). IR (Neat) cm^{-1}: 2920, 2850, 1725, 1635, 1445, 1310, 1165, 975,760.

(E)- Methyl – 3 methyl-(4-methoxyphenyl)-propenoate

^{1}H NMR ($CDCl_3$) δ ppm: 3.8 (s, 3H), : 3.84 (s, 3H), 6.26 (d, 1H J = 8 Hz), 6.89 (d, 1H J = 8 Hz), 7.39 (m, 3H), 7.46 (d, 2H, J = 8Hz), 7.62 (d, 1H, J = 8Hz). IR (Neat) cm^{-1}: 2948, 1710, 1637, 1602, 1562, 1454, 1290, 1170, 1025, 980, 765.

6.3.2. Recyclability Test

Iodo benzene (1 mmol), methyl acrylate (2 mmol), base (1.5 mmol) and catalyst (4 wt% with respect to halobenzene) were taken in 5 g of solvent. The reaction was conducted at 393 K for 2 h under nitrogen atmosphere. After the reaction, catalyst was separated by filtration, washed with acetonitrile and then with acetone. Then the catalyst was activated at 573 K before using for further recycling. The used catalyst was examined with TEM and XPS.

6.4. Results and Discussion

The silicoaluminophosphates, SAPO-11 and SAPO-31, were prepared hydrothermally using di-*N*-propylamine as the organic template. SAPO-41 was prepared using di-*N*-ethylamine. Pd-SAPOs was prepared by the ion exchanging the SAPOs with aqueous $(NH_3)_4PdCl_2.H_2O$ solution (Chapter-2). The solid Pd-SAPOs were calcined at 823 K for 6 h and then reduced at 673 K under hydrogen flow for 6 h. $Cu(NO_3)_2.2.5H_2O$ and $Ni(NO_3).2H_2O$ were used for preparing Cu-SAPOs and Ni-SAPOs, respectively. The metal contents were estimated by AAS. The metal contents in different catalysts are listed in the Table 6.1.

Table 6.1. Metal content and surface area of SAPOs

Catalyst	Metal (M) content (wt %)	Surface Area (m^2/g)
Pd-SAPO-11	2.91	175
Pd-SAPO-31	3.0	201
Pd-SAPO-41	2.72	195
Cu-SAPO-11	3.12	-
Cu-SAPO-31	3.19	196
Cu-SAPO-41	2.97	-
Ni-SAPO-11	2.98	-
Ni-SAPO-31	3.02	189
Ni-SAPO-41	2.87	-

The Cu and Ni loaded catalysts showed lower acitivity than Pd loaded catalysts (Table 6.2). Complete conversion of iodobenzene was observed in just 1.5 h using Pd-SAPO-31, DMF solvent and K_2CO_3 as base. However, complete conversion for Ni- and Cu-SAPO-31 was achieved in 24 h. Ni- and Cu-SAPO-31 catalysts were not efficient

with less activated bromobenzene; on the contrary, Pd-SAPO-31 efficiently activated bromobenzene (Table 6.2).

Table 6.2. Catalytic activity for the Heck reaction over various M-SAPO-31 catalysts

Catalyst	ArX	Run Time (h)	ArX Conv. (mol %)	C-C product Sel. (mol%)
Ni-SAPO-31	Bromobenzene	24	9.9	99.7
Cu-SAPO-31	Bromobenzene	24	9.8	97.0
Pd-SAPO-31	Bromobenzene	24	68.4	91.6
Ni-SAPO-31	Iodobenzene	10	99.7	97.3
Cu-SAPO-31	Iodobenzene	12	98.2	91.7
Pd-SAPO-31	Iodobenzene	1.5	100	98.8

Reaction conditions: Halobenzene, 1 mmol; methyl acrylate, 2 mmol; K_2CO_3, 1.5 mmol; DMF, 5 g; reaction temperature, 393 K.

Effect of temperature on coupling reaction of iodobenzene and methylacrylate over Pd-SAPO-31 using K_2CO_3 as base and DMF as solvent was investigated (Fig. 6.1). The reaction that takes ~ 74 h (100 % conv. of iodobenzene) at 333 K was completed in ~ 1.5 h when it was conducted at 393 K. Only the Pd catalyst was active for the reactions of chlorobenzene and its derivatives (Table 6.3). The reaction is more facile in the presence of electron-withdrawing substituents, such as a nitro group (compare runs 4 – 6). The catalysts can be used effectively for the arylation of a variety of olefins. In the reaction of iodobenzene and methyl acrylate, the *trans*-product was predominant with selectivity greater than 96%. However, with styrene, α-methylstyrene and ethyl cinnamate both *cis*- and *trans*-products were detected (Table 6.3; runs 13–15). Among the bases, potassium and cesium carbonates were more effective affording complete conversion of iodobenzene in 1.5 h with 98% selectivity

for the C-C product. Among the various solvents, *N*,*N*-dimethylacetamide (DMA) yielded higher amounts of the C-C product. Solvent played an important role for this reaction, solvent makes soluble complex with Pd(0) species that activates aryl halides.

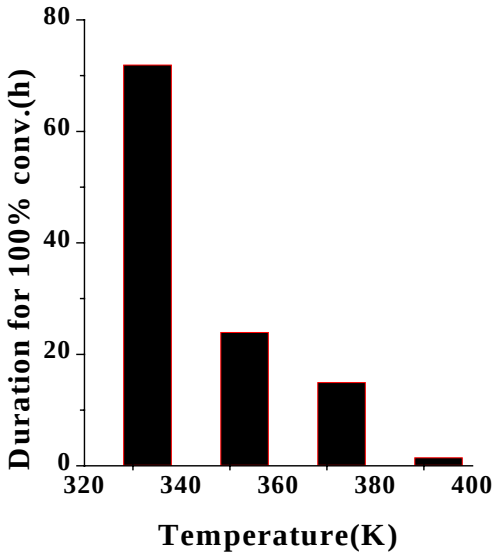

Fig. 6.1. Effect of temperature on C-C bond formation reaction over Pd-SAPO-31.

A comparative study reveals that Pd-SAPO-31 is more active and efficient than other heterogeneous catalysts. The reaction takes place in about 1.5 h as compared to 4 – 14 h with Pd supported on carbon [16], graphite [17], MgO [18] and Al_2O_3 [19] (for carbon–iodobenzene/methyl acrylate/Na_2CO_3; 423 K; 4 h - yield = 70%; for MgO – iodobenzene/acrylonitrile/Et_3N; 413 K; 14 h - yield = 78%; for Al_2O_3 – iodobenzene/acrylonitrile/Et_3N; 413 K; 14 h – yield = 72% and for graphite = 37 wt%; iodobenzene/styrene/K_2CO_3; 373 K; 95 h - yield = 82%). The amount of supported Pd is also lower in SAPO-31 catalysts (3 wt%) as compared to carbon, MgO and Al_2O_3 (5 wt%) and graphite (37 wt%). Further, the reaction for non-activated aryl halides takes place at relatively lower temperatures (333- 393 K) with Pd-SAPO-31 than with the other solid catalyst systems (373 – 423 K).

Table 6.3. Heck reaction of aryl halides and methyl acrylate over Pd-SAPO-31 at 393 K

Run No.[a]	Aryl halide	Base	Solvent	Run time (h)	Aryl halide conversion, mol%	C-C product selectivity, mol %
1	Chlorobenzene	NEt_3	DMF	24	29.5	79.9
2	Chlorobenzene	NEt_3	NMP	24	32.6	98.6
3	Chlorobenzene	NEt_3	NMP	70	50.3	94.6
4	Chlorobenzene	NEt_3	DMA	70	70.1	96.7
5	*o*-Nitro-chlorobenzene	NEt_3	DMA	70	77.5	96.2
6	*p*-Nitro-chlorobenzene	NEt_3	DMA	70	87.9	97.3
7	Iodobenzene	Na_2CO_3	DMF	6	99.8	97.9
8	Iodobenzene	K_2CO_3	DMF	1.5	100	98.8
9	Iodobenzene	Cs_2CO_3	DMF	1.5	99.8	98.3
10	Iodobenzene	NEt_3	DMF	2	100	96.8
10a	Iodobenzene	NEt_3	DMF	2	100	96.3
10b	Iodobenzene	NEt_3	DMF	2	98.9	97.2
10c	Iodobenzene	NEt_3	DMF	2	98.3	96.8
11	Iodobenzene	NPr_3	DMF	3	98.9	84.0
12	Iodobenzene	NBu_3	DMF	3	99.5	76.8
13[b]	Iodobenzene	K_2CO_3	DMF	2	99.2	93.7 (14/86)[e]
14[c]	Iodobenzene	K_2CO_3	DMF	12	96.7	80.0 (36/64)[e]
15[d]	Iodobenzene	K_2CO_3	DMF	8	99.4	78.1 (29/71)[e]

[a]Run Nos. 10a – 10 c are the 1st, 2nd and 3rd recycles of Run No. 10. [b]Styrene was used in place of methyl acrylate. [c]α-Methyl styrene was used in place of methyl acrylate. [d]Ethyl cinnamate was used in place of methyl acrylate. [e]Values in parentheses are distributions of *cis*-/*trans*-isomers.
DMF = *N*,*N*-dimethylformamide, NMP = *N*-methyl-2-pyrrolidinone, DMA = *N*,*N*-dimethylacetamide.

It has been found that SAPO-31 is showing better catalytic activity than other catalysts of the same family. Catalytic activity decreased in order: SAPO-31 > SAPO-11 > SAPO-41. The catalytic activity of different SAPOs for reactions with iodobenzene are compared (Table 6.4).

Table 6.4. Catalytic activity in the Heck reaction using various Pd-SAPO as catalysts

Run No.	Catalyst	Olefine	Run time (h)	Aryl halide conversion, mol%	C-C product selectivity, mol %
1	SAPO-31	Methylacrylate	2.0	100	96.8
2	SAPO-11	Methylacrylate	3.5	84.0	100.0
3	SAPO-41	Methylacrylate	3.5	70.2	98.4
4.	SAPO-31	Styrene	2.0	99.2	93.7 (14/86)
5.	SAPO-11	Styrene	4.0	100	96.2 (12/88)
6.	SAPO-41	Styrene	4.0	81.4	96.5 (18/82)

Reaction conditions: Iodobenzene, 1mmol; methyl acrylate, 2 mmol; K_2CO_3, 1.5 mmol; DMF, 5 g; reaction temperature, 393 K.

6.5. Catalyst Stability-Leaching Tests

Metal leaching from the supported catalysts under working conditions is a major issue with most of the known catalysts. It is, for instance, the major cause of deactivation of Pd/C catalysts employed for industrial hydrogenation of nitro compounds [20]. The following questions generally arise. If there is any palladium leaching, are the released species catalytically active? In this case, which is the minimum level of Pd leaching for appreciable catalytic activity in solution?

Table 6.5. Comparative activity of various heterogeneous catalysts in the C-C coupling Heck reaction

Catalyst % Pd (w/w)	Ar-X	Alkene	Base	Solvent	Temperature (K)	Time (h)	Yield(%)
Pd/C (5)	Ph-I	Methylacrylate	Na_2CO_3	Methanol	423	4	70
Pd/C (5)	Ph-Br	Styrene	NaOAc	DMA	413	20	84
Pd/C_{Gr} (33)	Ph-I	Ethylacrylate	NBu_3	None	373	6	87
Pd/C_{Gr} (37)	Ph-I	Styrene	K_2CO_3	DMF	373	95	82
Pd/MgO (5)	Ph-I	Acrylonitrile	NBu_3	CAN	413	14	78
Pd/MgO (4.9)	Ph-Br	Styrene	NaOAc	DMA	413	20	36.5
Pd/Al_2O_3 (5)	Ph-I	Acrylonitrile	NBu_3	CAN	413	14	72
Pd/SiO_2 (5)	Ph-Br	Styrene	NaOAc	DMF	413	20	8.2
Pd-Nb-MCM-41	Ph-Br	Butylacrylate	NEt_3	DMA	443	48	32
Pd-Nb-MCM-41	Ph-Cl	Butylacrylate	NEt_3	DMA	443	32	6.8
Pd/Na-Mor (7)	Ph-Br	Styrene	NaOAc	DMA	413	20	32
Pd/H-Mor(7)	F-Ph-Br	Styrene	NaOAc	DMA	413	20	92
Pd/Na-Mor (7)	F-Ph-Br	Styrene	NaOAc	DMA	413	20	92
Pd-SAPO-31 (3)	Ph-I	Methyl acrylate	K_2CO_3	DMF	393	1.5	100
Pd-SAPO-31 (3)	Ph-Cl	Methyl acrylate	NEt_3	NMP	393	24	32.6
Pd-SAPO-31 (3)	Ph-Cl	Methyl acrylate	NEt_3	NMP	393	70	50.3
Pd-SAPO-31 (3)	Ph-Br	Methyl acrylate	K_2CO_3	DMF	393	24	68.4

All these aspects are extremely important for both fundamental understanding of this reaction and its technological applications. Arai and co-workers [21] investigated the leaching process and reported very interesting results. It has been observed that some palladium catalysts, including 10% Pd/C and 1% Pd/SiO_2, underwent extensive leaching during the Heck reaction of iodobenzene and methylacrylate, in the presence of NEt_3 in *N*-methylpyrrolidinone. It was also found that the maximum apparent reaction rate was attained at a maximum palladium concentration in solution, which was monitored during the reaction course. At the end of reaction, finally, palladium re-precipitated onto the support. Palladium leaching at the end of the reaction (413 K) amounted to 4% for Pd/C (either Na_2CO_3 or NEt_3) and to 51% (NEt_3) or 76% (Na_2CO_3) for Pd/SiO_2, but it was limited to 2% (Pd/C) and 9% (Pd/SiO_2) with the mixed bases. Carbon showed the highest affinity to palladium and turned out to be the most effective support for palladium re-precipitation.

In the present study also a similar phenomenon is observed. During the reaction, metal ions leached out of the support (Pd was estimated by atomic absorption spectroscopy). However, when the reaction was complete (6 h for iodobenzene) the metal ions could not be detected in the liquid phase indicating that all the leached Pd was apparently redeposited onto the SAPO-31 support (Fig. 6.2). As a consequence of this redeposition phenomenon, the Pd-SAPO-31 catalyst could be recovered from the reaction mixture by filtration and recycled without significant loss in activity or selectivity for a minimum of three cycles (Table 6.3; Run Nos. 10a – 10c). Fig. 6.3 shows the TEM pictures of Pd metal on SAPOs before and after the reaction (Fig. 6.3).

X-ray photoelectron spectra of fresh and used samples are shown in Fig. 6.4. It is clear from XPS analysis that all the palladium is present as Pd(0). The binding energies are comparable with the binding energies for Pd(0), 335.3 eV and 340.5 eV

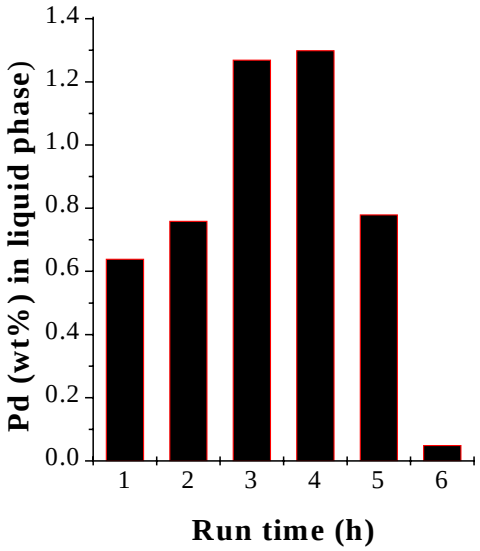

Fig. 6.2. Pd leached into the solution at different reaction times.

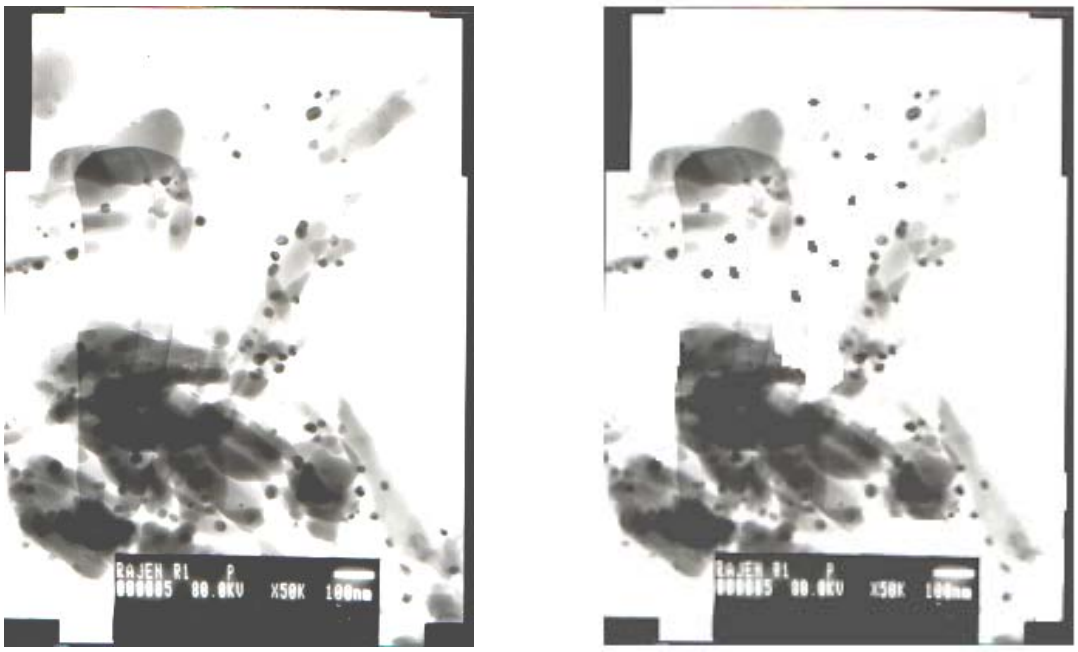

Before reaction After reaction

Fig. 6.3. TEM photographs of fresh and used Pd-SAPO-31 catalysts.

for $3d_{5/2}$ and $3d_{3/2}$, respectively. Pd (II) has binding energy in the range of 337-339 eV The binding energy for $3d_{5/2}$ level of Pd in $Pd(NH_3)_4Cl_2$, $PdCl_2$ and PdO are 338.2, 337.5 and 336.2 eV, respectively [22]. The binding energies for $3d_{3/2}$ level for $PdCl_2$ and PdO are 342.8 and 341.8 eV, respectively [22]. The Pd metal has binding energies of 335.4 and 340.2 for $3d_{5/2}$ and $3d_{3/2}$, respectively [22]. Pd is present in zero-valent state in both the used and in fresh catalysts.

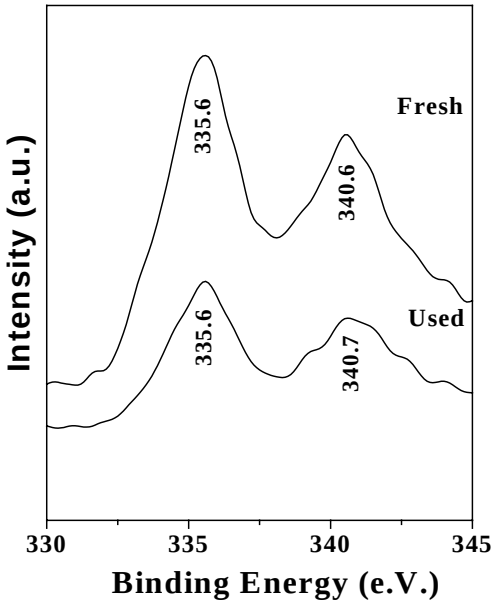

Fig. 6.4. XPS spectra of fresh and used Pd-SAPO-31 catalysts.

6.6. Mechanism

The possible mechanism of Heck olefination of iodobenzene over supported palladium catalysts is shown in Scheme 6.3. In the first step, soluble catalytically active Pd complexes $[Pd(solvent)_m(Base)_n]$ are formed by the coordination of polar solvents and base. Oxidative addition of iodobenzene, for example, to this species forms $[Ph\text{-}Pd(solvent)_m(Base)_nI]$. Then followed by syn-insertion of olefins an intermediate species is formed. Syn elimination of $[H\text{-}Pd(solvent)_m(Base)_nI]$ from the intermediate species forms the desired trans-product followed by reductive elimination of base.HI.

The active soluble Pd species is generated back. When iodobenzene is completely consumed, the soluble species [Pd(solvent)$_m$(Base)$_n$] which is short lived, dissociates and Pd is redeposited onto the SAPO surface.

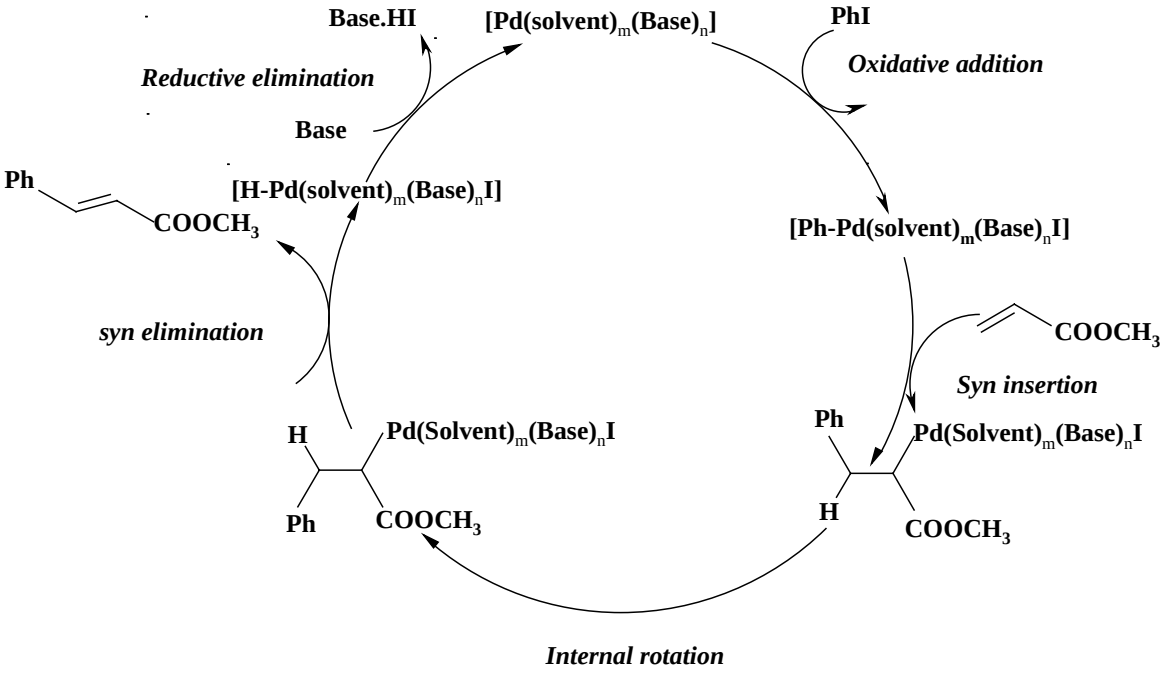

Scheme 6.3. Possible mechanism for Heck coupling reaction

6.7. Conclusions

Pd-SAPO-31 is a reusable and highly efficient catalyst for Heck reaction. Neutral or non-activated aryl halides like chlorobenzene are activated for the Heck reaction. Pd-SAPO-31 is more efficient than Pd-SAPO-11 and Pd-SAPO-41. In other words, support influences the catalytic activity. The activities of Ni and Cu catalysts are lower than that of the Pd catalyst. ^{1}H NMR spectra of some Heck reaction products are shown in Appendix 6.A

6.8. References

1. J. Tsuji, Palladium Reagents and Catalysts: Innovations in Organic Synthesis, Wiely, Chichister, 1995.

2 R. F. Heck, Palladium Reagents in Organic Synthesis, Academic Press, London, 1985.

3 (a) J.G. De Uries, Can. J. Chem. 79 (2001) 1086. (b) R.A. Sheldon, J. Mol. Catal. A: Chem. 107 (1996) 75.

4 A. F. Littke, G. C. Fu, Angew. Chem. Int. Ed. 41 (2002) 4176.

5 M. Wagner, K. Köhler, L. Djakovitch, S. Weinkauf, V. Hagen, M. Muhler, Topics in Catal. 13 (2000**)** 319.

6 C. M. Anderson, K. Korebelas, A. K. Awasti, J. Org. Chem. 50 (1985**)** 3891.

7 C. P. Mehnert, J. Y. Ying, Chem. Comm. (1997**)** 2215.

8 E. B. Mubofu, J. H. Clark, D. J. Macquarrie, Green Chem. 3 (2001**)** 23.

9 S. Iyer, V. Thakur, J. Mol. Catal. A: Chem. 157 (2000) 275.

10 B. Cornils, W. A. Hermann, Applied Homogeneous Catalysis with Organometallic Compounds, VCH. Wienheim, 1996.

11 A. Biffis, M. Zecca, M. Basato, J. Mol. Catal. A: Chem. 173 (2001) 249.

12 P. Mériaudeau, Vu A. Tuan, Vu T. Nghiem, G. Sapaly, C. Naccache, J. Catal. 185 (1999) 435.

13 M. Höchtl, A. Jentys, H. Vinek, J. Catal. 190 (2000) 419.

14 A. M. Prakash, S. V. V. Chilukuri, R. P. Bagwe, S. Ashtekar, D. K. Chakrabarty, Microporous Mater. 6 (1996) 89.

15 P. Mériaudeau, Vu A. Tuan, F. Lefebvre, Vu T. Nghiem, C. Naccache, Microporous Mesoporous Mater. 26 (1998) 161.

16 M. Julia, M. Duteil, Bull. Soc. Chim. Fr. (1973) 2790.

17 D. Savoia, C. Trombini, A. U. Ronchi, G. Verardo, J. Chem. Soc. Chem. Commun. (1981) 541.

18 K. Kaneda, M. Higuchi, T. Imanaka, J. Mol. Catal. A: Chem. 63 (1990) L33.

19 R. L. Augustine, S. T. O'leary, J. Mol. Catal. 72 (1992) 229.

20 A. J. Bird, D. T. Thomson, Catalysis, in: W.H. jones (Ed.) Organic Synthesis, Academic Press, New York, 1980, p 61.

21 F. Zhao, M. Shirai, Y. Ikushima, M. Arai, J. Mol. Catal. 180 (2002) 211.

22 G. Kumar, J.R. Blackburn, R.G. Albridge, W.E. Moddeman, M.M. Jones, Inorg. Chem. 11 (1972) 296.

Appendix-6.A

^{1}H NMR spectra of some Heck reaction products

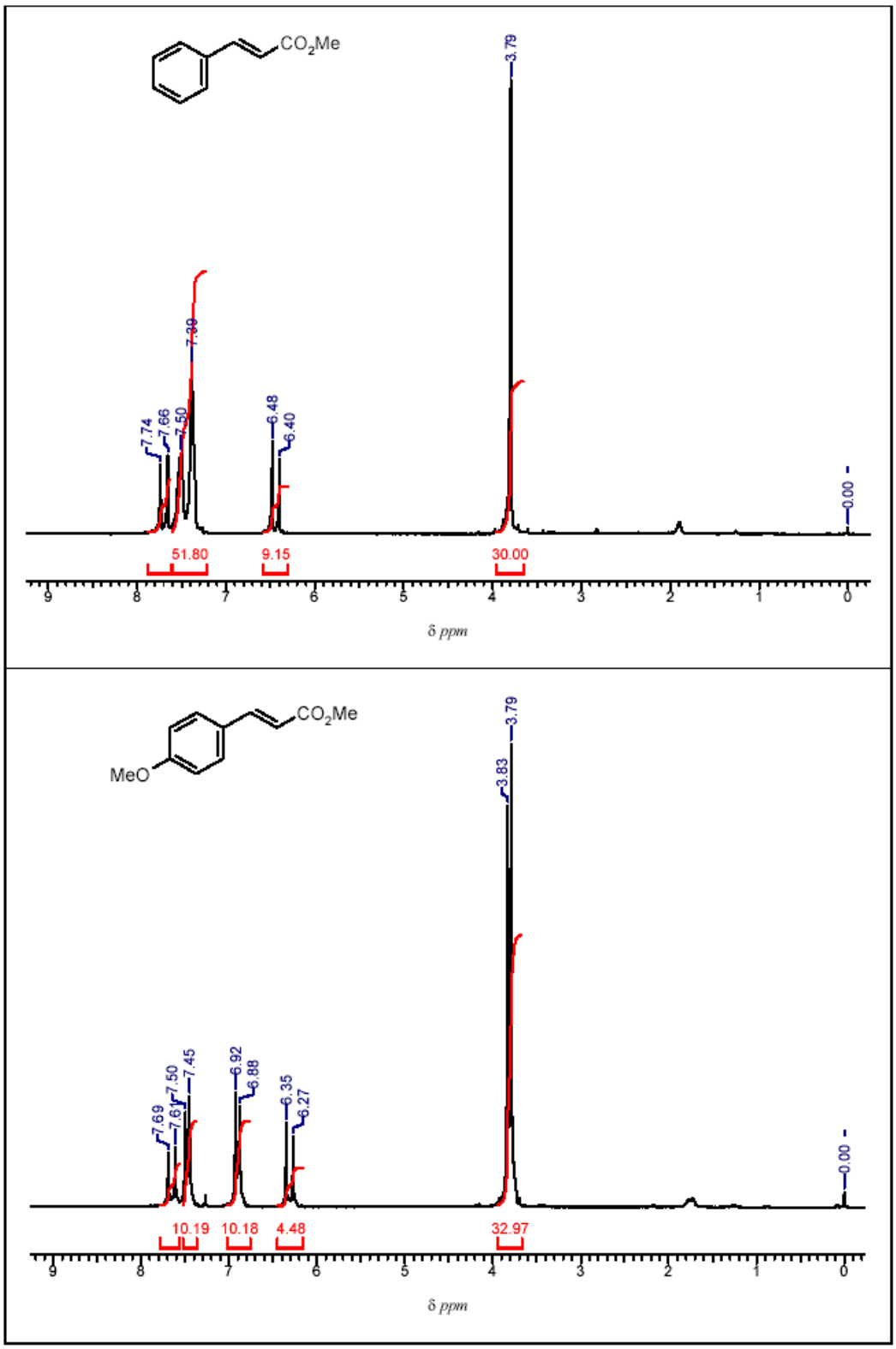

Chapter-7

Summary & Overall Conclusions

Activation and utilization of small molecules, in particular CO_2, for preparing value-added chemicals, by environmentally benign routes, using solid catalysts is an important and challenging area in catalysis research. The progressively increasing levels of CO_2 in the atmosphere are posing a great threat to the mankind. Hence, its activation and utilization in the synthesis of organic compounds is of considerable importance. CO_2 is an inexpensive reagent, environmentally benign, non-flammable and easily separable from the reaction mixture. However, due to inert nature of CO_2, its activation and incorporation into organic substrates still remains as a challenging task. The cycloaddition reaction of CO_2 and epoxide is a powerful method for CO_2 fixation to produce five-member-cyclic carbonates which can be used as polar aprotic solvents, precursor for polycarbonate materials and as intermediates in organic synthesis. Organic carbamates ($RNHCO_2R'$) are another important group of compounds widely used for a number of purposes including pharmaceutical preparation, production of agrochemicals such as pesticides and herbicides, and more generally, of intermediates of fine and commodity chemicals. These products are commonly synthesized by the aminolysis of chloroformate esters, obtained from phosgene and alcohol. This method of carbamates synthesis is hazardous because of the toxicity and corrosive properties of phosgene. To overcome this drawback many alternative routes have been developed. Most eco-friendly process is the coupling reaction of amines, CO_2 and alkyl halides. Good results were obtained using onium salts and base catalysts. Sterically hindered organic bases, crown ethers and cesium carbonate were reported to catalyze the carbamate synthesis through the anion route. Development of more efficient solid catalysts for this reaction is, however, needed. Activation and the mode of CO_2 coordination are the key steps for CO_2 utilization.

Organic carbonates such as dimethyl carbonate can be synthesized more efficiently by transesterification of cyclic carbonates with alcohol. Tranesterifiaction is an important organic reaction to prepare a variety of esters. Bio-fuel is fatty acid alkyl esters, which is conventionally prepared by transesterification of vegetable oils with alcohols in the presence of an alkali catalyst. At the end of the reaction the base catalyst is neutralized with mineral acid and separated by washing the products with water. During this process, saponified products are formed and complicate the bio-fuel recovery. Replacement of homogeneous catalyst by solid catalysts minimizes the processing costs. At the end of the reaction, the solid catalyst can be recovered by simple filtration from the product mixture and reused.

C-C bond formation (Heck) reaction is one of the versatile methods in modern organic chemistry. Recently, a few of the products are commercialized based on this reaction. To minimize the cost of production efforts are being made to replace Pd with less expensive Ni catalyst, replace aryl iodide and bromide with cheaper aryl chloride, eliminate the use of expensive phosphine ligands and utilize the heterogeneous, reusable catalysts in place of the present homogeneous catalysts.

To accomplish the above objective several catalyst systems have been investigated in the present work. They are (a) homogeneous copper complexes of acyclic and cyclic ligands (Cu-phenanthroline, Cu-bipyridine, Cu-salen, Cu-phthalocyanine, Cu-tetraphenylporphyrin), (b) zeolite-Y-encapsulated metal phthalocyanines (MPc-Y; M = Cu^{2+}, Ni^{2+}, Co^{2+} and Al^{3+}), (c) titanosilicate molecular sieves (microporous TS-1, mesoporous Ti-MCM-41 and Ti-SBA-15 and amorphous TiO_2-SiO_2), (d) organic-inorganic hybrids (as-synthesized zeolite-beta and Si-MCM-41), (e) organo-functionalized, ordered mesoporous materials (amine-, imidazole-, guanine- and adenine-functionalized (Ti/Al)-SBA-15), (f) Pd/Ni/Cu-loaded

silicoaluminophosphates (SAPO-31, SAPO-11 and SAPO-41), and (g) double metal cyanide catalysts of Fe and Zn. Chapter-2 described the synthesis and characterization (C, H & N and AAS analyses, XRD, TEM, nitrogen adsorption, thermal analysis, DRIFT-IR, DRUV-visible, EPR and NMR) of these materials.

Cyclic carbonates including chloropropene carbonate, propene carbonate, styrene carbonate and n-butene carbonate were synthesized at moderate reaction conditions by cycloaddition reaction of CO_2 with the oxirane ring of corresponding epoxides *viz.*, epichlorohydrin, propene oxide, styrene oxide and n-butene oxide, respectively (Chapter-3). Catalytic activities of copper complexes, zeolite-Y-encapsulated metal phthalocyanine complexes, titanosilicates, organo-inorganic hybrids and organo-functionalized mesoporous silica have been evaluated. Cyclic carbonate is the main product; diols and ethers formed as minor products. Pressure and temperature influenced the catalytic activity. The optimum reaction conditions for high yields of cyclic carbonates were found to be 6.9 bar and 393 K. The homogeneous metal complexes in combination with a co-catalyst/promoter (N,N-dimethylaminopyridine; DMAP) showed good activity but required additional efforts for their separation from the reaction mixture. Molecular structure and the nature of the ligand influenced the catalytic activity. Copper phthalocyanines and porphyrines exhibited higher activity than the Schiff base, cyclen, phenanthroline and bipyridine complexes. Titanosilicate molecular sieves and zeolite-Y-encapsulated metal phthalocyanine complexes were recyclable, but needed the co-catalyst/promoter. The use of co-catalysts/promoters was avoided when organo-inorganic hybrids and organo-functionalized mesoporous silica catalysts were used. These solid catalysts were reusable in several recycling experiments without significant loss in activity and cyclic carbonate selectivity. Activation and coordination of CO_2 and the mechanism of cyclic carbonate formation

were probed by DRIFT, TPD and other spectroscopic methods. The study revealed acidic Ti and Al in SBA-15 are the sites for epoxide activation. The organic functional groups (bases - amine, imidazole, guanine and adenine) are the sites for CO_2 activation. The type of the base amine (primary, secondary and tertiary) influenced the activation of CO_2. When both the acidic and basic sites are present in the catalyst system a synergic enhancement in catalytic activity was observed. Organo-fuctionalized mesoporous silica having both the acidic and basic active sites exhibited higher activity than the other catalysts investigated. Availability of epoxide and activation of CO_2 are the crucial factors for high carbonate yields. Using these novel mesoporous catalyst systems larger size cyclic carbonates, styrene carbonate, for example, could be synthesized in high yields. These catalysts are perhaps more efficient than the reported systems. In other words, more efficient solid catalysts are discovered for CO_2 activation for its further utilization as a replacement for toxic, phosgene in cyclic carbonate synthesis by cycloaddition reaction.

A “green”-route for the synthesis of alkyl and aryl carbamates utilizing CO_2 over solid catalysts has been developed (Chapter-4). A variety of carbamates were synthesized by coupling amines (butyl amine, hexylamine, octylamine, dodecyl amine, cyclohexyl amine, benzylamine, aniline, 2,4,6-trimethylaniline and cyclododecylamine), CO_2 and n-butyl halide. Catalytic activities of four different catalyst systems *viz.*, titanosilicates, encapsulated metal phthalocyanines, organo-inorganic hybrids and organo-functionalized mesoporous silica for this reaction have been studied (Chapter-4). Influence of reaction conditions (temperature, pressure, solvent, amount of catalyst, amine to bromide ratio etc.) on the catalytic activity was examined; 3.4 bar and 353 K were found to be the optimum conditions. The catalysts employed were highly active and reusable. In the case of titanosilicates and

encapsulated metal phthalocyanines high yields of carbamates were obtained only when the reaction was carried out in a solvent medium e.g., N,N-dimethylformamide (DMF). With organic-inorganic hybrids and organo-functionalized mesoporous silica, carbamates could be synthesized even without using DMF. Mechanism of carbamate synthesis was probed using DRIFT spectroscopy. Ti ions on SBA-15 activate amines. The activated CO_2 (at adenine base) participates in the reaction with activated amines forming the corresponding carbamates. The study revealed that the presence of Lewis acid Ti ions and basic adenine molecules are essential for high carbamate yields. These catalysts stabilized the carbamate anion and suppressed formation of N-alkylated side-product. CO_2 is used as a replacement for toxic phosgene/isocyanate in the synthesis of a variety of carbamates.

Novel solid catalysts for the synthesis of a variety of alkyl carbonates by transesterification reaction of cyclic carbonates with different alcohols have been studied (Chapter-5). Two types of solid catalysts *viz.*, titanosilicates and double metal cyanides (Fe and Zn based) were used. Double metal cyanide catalysts are known for their remarkably high catalytic activity in polymer synthesis. Their catalytic activity for transesterification reactions is examined for the first time, in this work. These catalysts were found superior to titanosilicates and other known catalysts in transesterification of cyclic carbonates with various alcohols. Competitive transesterification reactions in the presence of more than one alcohol were also studied. The method of preparation of double metal cyanide catalysts affected the catalytic activity. The catalysts prepared in the presence of tert.-butanol (complexing agent) and tri-block copolymer $EO_{20}PO_{70}EO_{20}$ (co-complexing agent) exhibited superior activity. The activity of double metal cyanide catalysts for transesterification of triglycerides of vegetable oils into fatty acid esters for bio-diesel and lubricant applications was also investigated

(Chapter-5). Vegetable oils such as coconut oil, sunflower oil, soyabean oil, margarine oil were transesterified with C1 to C8-alcohols. The study revealed that the process employing these solid catalysts is possibly more convenient than the conventional bio-diesel production using homogeneous alkali metal and mineral acid catalysts.

Activation of olefins and aryl halides for C-C coupling (Heck) reaction over Pd-loaded silicoaluminophosphates has been studied (Chapter-6). Three types of catalysts of varying pore dimensions and acidity *viz.*, Pd-SAPO-31, Pd-SAPO-11 and Pd-SAPO-41 were investigated. The performance of these catalysts in the preparation of a variety of C-C coupled products of industrial importance was studied. Most of the known catalysts systems are active only with aryl iodides. The unique feature of the present catalysts is that they can be used even for the deactivated aryl halides like chlorobenzene in C-C coupling reactions. During the reaction, metal ions leached out of the support. However, when the reaction was complete, the metal ions could not be detected in the liquid phase (AAS); all the leached Pd redeposited back onto the SAPO-31 support. These catalysts could be reused in recycling experiments with little loss in activity and selectivity. The Pd-containing catalysts are more efficient than the Ni and Cu-loaded catalysts. The SAPO catalysts exhibited high activity even with a small amount of Pd loading. A higher dispersion of zero-valent Pd is the cause for the superior activity.

By and large, the thesis reports efficient, reusable, novel, solid catalysts for activation of carbon dioxide, olefins and alkyl halides for their use in the benign synthesis of a variety of industrially important synthetic organic intermediates. The work contributes to the area of green chemistry and sustainable catalytic processes.

List of Research Publications

1. Pd-SAPO-31, an efficient, heterogeneous catalyst for Heck reactions of deactivated aryl chlorides
   Rajendra Srivastava, N. Venkatathri, D. Srinivas, Paul Ratnasamy
   Tetrahedron. Lett. 44 (No. 18) (2003) 3649 – 3651.

2. Synthesis of cyclic carbonates from olefins and CO_2 over zeolite-based catalysts
   Rajendra Srivastava, D. Srinivas, Paul Ratnasamy
   Catal. Lett. 89 (Nos. 1-2) (2003) 81 – 85.

3. Synthesis of polycarbonate precursors over titanosilicate molecular sieves
   Rajendra Srivastava, D. Srinivas and P. Ratnasamy
   Catal. Lett. 91 (Nos. 1-2) (2003) 133 – 139.

4. Synthesis of polycarbonate monomers by CO_2 insertion in epoxides over zeolite-based catalysts
   Rajendra Srivastava, D. Srinivas, P. Ratnasamy
   Recent Advances in the Science and Technology of Zeolites and Related Materials: Proceeding of the 14th International Zeolite Conference, Cape Town, South Africa (April 25 –30, 2004) Ed. by E.W.J. van Steen, L.H. Callanan, M. Claeys, C.T. O'Connor, Elsevier, Amsterdam, The Netherlands, 2703 - 2710 (2004).

5. Transesterifications over titanosilicate molecular sieves
   D. Srinivas, **R. Srivastava,** P. Ratnasamy
   Catal. Today 93 (No. 3) (2004) 127 – 133.

6. Phosgene-free synthesis of carbamates over zeolite-based catalysts
   R.Srivastava, Manju, M. D., D. Srinivas, P. Ratnasamy
   Catal. Lett. 97 (Nos. 1-2) (2004) 41 – 47.

7. Factors affecting activation and utilization of carbon dioxide in cyclic carbonate synthesis over Cu and Mn peraza macrocyclic complexes
   R. Srivastava, T. H. Bennur, D. Srinivas

J. Mol. Catal. A: Chemical 226 (No. 2) (2005) 199 – 205.

8. CO_2 activation and synthesis of cyclic carbonates and alkyl / aryl carbamates over adenine-modified Ti-SBA-15 solid catalysts
   R. Srivastava, D. Srinivas, Paul Ratnasamy
   J. Catal. 233 (2005) 1-15.

9. Zeolite-based organic-inorganic hybrid catalysts for phosgene-free and solvent-free synthesis of cyclic carbonates and carbamates at mild conditions utilizing CO_2
   Rajendra Srivastava, D. Srinivas, P. Ratnasamy
   Appl. Catal. A: General 289 (2005) 128.

10. Active sites for CO_2 activation over amine-functionalized mesoporous SBA-15 catalysts
    R. Srivastava, D. Srinivas, P. Ratnasamy
    Microporous Mesoporous Mater. (Communicated).

List of Patents Applied

1. An improved process for the preparation of cyclic carbonates
   Darbha Srinivas, **Rajendra Srivastava**
   Applied for Indian and US patents (Appl. No. 1179/DEL/2003, NF-292/2003; US Appln. No. 20050070724 A1 (March 31, 2005)).
2. A process for the production of cyclic carbonates
   Darbha Srinivas, **Rajendra Srivastava**, Paul Ratnasamy
   Applied for Indian and US patents (NF-423/03).
3. A process for the production of alkyl and aryl carbamates
   Darbha Srinivas, **Rajendra Srivastava**, Paul Ratnasamy
   Applied for Indian US patent (NCL-37/2004).
4. New adenine-modified catalyst for the production of cyclic carbonates
   Darbha Srinivas, **Rajendra Srivastava**, Paul Ratnasamy
   Applied for Indian and US patent (NCL-18/2005).
5. New adenine-modified catalyst for preparing carbamates

Darbha Srinvas, **Rajendra Srivastava**, Paul Ratnasamy

Applied for Indian and US Patents (NCL-19/2005).

6. Transesterification catalyst and a process for preparation thereof.

   Darbha Srinivas, **Rajendra Srivastava**, Paul Ratnasamy

   Applied for Indian and US Patents (NCL-20/2005).

7. Process for producing hydrocarbon fuel

   Darbha Srinivas, **Rajendra Srivastava**, Paul Ratnasamy

   Applied for Indian and US Patents (NCL-21/2005).

8. Process for producing lubricants

   Darbha Srinivas, **Rajendra Srivastava**, Paul Ratnasamy

   Applied for Indian and US Patents (NCL-22/2005).

9. Process for producing dialkyl carbonates

   Darbha Srinivas, **Rajendra Srivastava**, Paul Ratnasamy

   Applied for Indian and US Patents (NCL-23/2005).

List of Papers Presented in Conferences / Symposia

1. Studies on Heck Reactions over Pd/SAPO-31 Catalysts

   R. Srivastava, N. Venkatathri, D. Srinivas

   16th National Symposium & 1st Indo-German Conference on Catalysis, Hyderabad, India, February, 6-8, 2003.

2. Utilization of CO_2 in the Synthesis of Cyclic carbonates over Neat and zeolite-Y-Encapsulated Cu and Mn Complexes of 1,4,7,10-Tetraazacyclododecane (Cyclen): Structure and Catalytic Activity Studies

   T.H. Benuur, **Rajendra Srivastava**, Vedavati G. Puranik, D.Srinivas

   10th Symposium on Modern Trends in Inorganic Chemistry during 15-17 Dec 2003 held in IIT., Mumbai, India.

3. Synthesis of Polycarbonate Monomers by CO_2 Insertion in Epoxides over Zeolite-based Catalysts

   R. Srivastava, D. Srinivas, P. Ratnasamy

   14th International Zeolite Conference during April 25 –30, 2004 held at Cape

Town, South Africa.

4. Efficient Organic-Inorganic Hybrid Solid Catalysts for Organic Carbonates and Carbamates Synthesis Utilizing Carbon Dioxide
   R. Srivastava, D. Srinivas
   17th National Symposium on Catalysis held during January 18-20, 2005 at C.S.M.C.R.I., Bhavnagar, India.